Hippo Signalling in mammalian cortical development

Inauguraldissertation

zur

Erlangung der Würde eines Doktors der Philosophie

vorgelegt der

Philosophisch-Naturwissenschaftlichen Fakultät

der Universität Basel

von

Tanzila Mukhtar

Von Indien

Basel, 2019

Genehmigt von der Philosophisch-Naturwissenschaftlichen Fakultät
auf Antrag von

Prof. Dr. V. Taylor und Prof. Dr. W. Driever

_____

Basel, den 16. Oktober 2018

_____

Prof. Dr. Martin Spiess, Dekan

Acknowledgements

Since this is the only part of the thesis where my Kashmiri poeticism won't get deleted eventually, I would like to pour my heart out here. ☺

I started with Prof. Verdon Taylor in October 2010, for my Master's Dissertation in the Department of Biomedical science, University of Sheffield. Ever since that day, I have been fascinated by the complexity of neural stem cells. I recall when he explained Notch signalling to me the first time. Coming from a different education system back in India, and totally naïve to the complexity of the brain, I was taken by a huge surprise. The decision making for cells, how they communicate, how they know what to do when, was exciting! I stuck around to do my PhD with Prof. Verdon Taylor, because he valued my excitement about science even during my Master's. He was always accessible, took keen interest in my work and did every bit to groom me into an independent researcher. It is often said your first Boss makes the best impression on you and it is absolutely right in my case. Whoever I work with in future, will get compared to Prof. Verdon Taylor. I extend my deepest gratitude to him for understanding my potential and believing in me. He has always provided his support and guidance and he is extremely bright. Sometimes, in our meetings, I keep admiring him for being so brilliant! I want to say thank you for making me a part of NeuroStemX. I loved my projects. Though challenging, we did manage to do a great deal of good work as a consortium!

I am also grateful to Prof. Erik van Nimwegen and Prof. Wolfgang Driever, who have been on my thesis committee and seen my progress through the years, provided valuable comments and been as a strong source of encouragement.

I am grateful to all members of the Taylor group (old and new), for their stimulating discussions, journal clubs and lab meetings. I am grateful to all the members of NeuroStemX for their collective efforts. I want to thank Dr. Alice Grison, Dr. Runrui Zhang and Dr. Elena Parmagiani, for our many scientific discussions. I want to thank Mr. Frank Sager for his help with sectioning and helping me calm down many times.

I am grateful to my parents, Good Cop (my Mum) and Bad Cop (my Dad). Mum has mostly supported whatever I have wanted to do, while Dad has rarely supported me. I guess, both stimuli are needed in life, to prove one of them right and the other wrong! On a lighter note, I believe finally my Dad has realized, being a scientist isn't that bad, and may be as good as an 'Indian bureaucrat'.

I am grateful to all my friends who helped in maintaining my sanity throughout my PhD. A big thank you and a warm hug!!

Outline

Abstract

The cerebral cortex in humans is composed of billions of morphologically and functionally distinct neurons. Development of the neocortex requires an orchestrated succession of a series of processes, the appropriate generation, migration, and positioning of neurons, the acquisition of layer-specific transcriptional hallmarks, and the establishment of precise axonal projections. We have primarily focussed on elucidating the transcriptomic landscape of murine embryonic neural stem cells (NSCs), basal progenitors (BPs) and newborn neurons (NBNs) at the population level. I have focussed on one underexplored signalling pathway in the brain- the Hippo signalling pathway. Hippo signalling effectors are expressed dynamically during the course of development in NSCs and BPs at mRNA level. Hippo transcription factors (TFs), Tead1 and Tead3 show higher expression during gliogenesis while Tead2 is expressed at relatively higher levels during early phases of neural expansion. Known to be redundant in other biological systems, I explored different effects of three Tead TFs in NSCs using gain and loss of function. I observe reciprocal effects on neuronal migration and fate with Tead1, Tead3 and Tead2. We identified *ApoE*, *Cyr61* and *Dab2* as potential direct targets of Tead TFs in NSCs. ApoE gain of function partially recapitulates the gain of function of Tead2, reducing cell migration to the cortical plate (CP) and Dab2 gain of function recapitulates the gain of function of Tead1, an increased migration to CP. *ApoE* and *Dab2* are involved in Reelin signalling and hence we provide the first link between Hippo and Reelin signalling pathways controlling cortical development.

Chapter 1

Introduction

Our understanding of the complexity of the human brain has advanced quickly in the last 25 years. We have made major inroads into understanding how the brain transfers, stores and retrieves information. However, our understanding of the processes governing brain development has lagged behind to some degree. Developmental neurobiology has made advances including the discovery of neural stem cells (NSCs) and neural stem cell niches that remain into adulthood. Hence, it is now clear that diverse progenitor cell types give rise to all cell lineages of the brain. These advances in knowledge have benefited from novel approaches to lineage trace cell populations, advances in high resolution microscopy, increased cell specific markers and transgenic alleles, and genome-wide analysis of gene expression down to the cellular level. With the advent of cellular reprograming and programming of human induced pluripotent cells (iPS), we are now entering an age where functional human neurons can be generated and studied *in vitro* to obtain a greater understanding of gene function and dysfunction. These advances open up avenues that were previously not possible, where patient-derived iPS cells could potentially be used therapeutically for the treatment of neural degenerative diseases. As technologies and our understanding of neuron differentiation continue to advance, the field of neurobiology and its potential biomedical applications will expand greatly. This introduction aims to give a broad overview of neural development, neural stem cells (NSCs) and some of the key surface antigens used to identify specific cell populations.

Neurulation: formation of the central nervous system anlage

During early stages of post gastrulation embryonic development, the ectoderm differentiates to form the epidermis and the neural ectoderm, the primordium of the nervous system (for review see[1]). In vertebrates, the central nervous system (CNS) begins as the neural plate, an ectodermal-derived structure which folds dorsally to form the neural tube through a process called neurulation. Neurulation is divided into the sequential phases of primary and secondary neurulation initiated through a combination of growth factors and inhibitory signals secreted by the underlying axial mesoderm (notochord), dorsal ectoderm, and Spemann organizer, respectively (Figure 1'). The neural tube then differentiates rostrally into the future brain and caudally to form the spinal cord and most of the peripheral nervous system, which will not be covered here. The rostral part of the neural tube segregates into three

swellings, establishing the forebrain, midbrain and hindbrain. In parallel, the rostrocaudal tube segments into modules called neuromeres[2].

Neurulation and neural tube formation

The mammalian brain and most of the spinal cord are formed during the first phase of neurulation which is commonly divided into 4 phases. In mice, neurulation begins at around embryonic day (E) 8 with the induction of the neural plate when the inhibitory signals Chordin, Noggin and Follistatin are secreted by the Spemann organizer[3]. These factors block bone morphogenic protein 4 (Bmp4) signalling, inducing dorsal epiblast cells and allowing the anteroposterior midline of the ectoderm to adopt a neuroectodermal fate. These neuroectodermal cells undergo an apicobasal thickening and generate the neural plate along the dorsal midline of the embryo. Once committed, neuroectodermal cells no longer require inhibitory signals for neural plate formation to proceed (Figure 1')[2,4].

The neural plate undergoes a remodeling phase, whereby convergent-extension increases the length (rostrocaudally) while simultaneously narrowing the width (transversely). During these processes, the neural plate continues to thicken apicobasally generating cellular forces that begin to bend the neural plate and induce neural tube formation. As the lateral folds of the neural plate converge to the midline, the epidermal ectoderm delaminates from the neuroepithelium of the neural plate and fusion of both the ectoderm and dorsal neural tube proceeds[2,4]. The neural tube zips closed posteriorly from the hindbrain and anteriorly from the mid-hindbrain junction, while remaining open over the future 4th ventricle posterior to the cerebellum. By E9 in the mouse, fusion is complete and the neural tube is closed forming the primitive ventricles of the future brain regions[5].

Far less is known about secondary neurulation, which is the formation of the posterior region of the neural tube and caudal-most portion of the spinal cord. Secondary neurulation begins from a solid mass of cells forming from the tail bud. These cells form the medullary cord, which then cavitates to form multiple lumina. Finally, these lumina fuse into a single lumen continuing the central canal of the neural tube in the most rostral aspects. Contrary to primary neurulation, here the process is more a hollowing out of a mass of cells rather than tube formation from an ectodermal plate of cells [6].
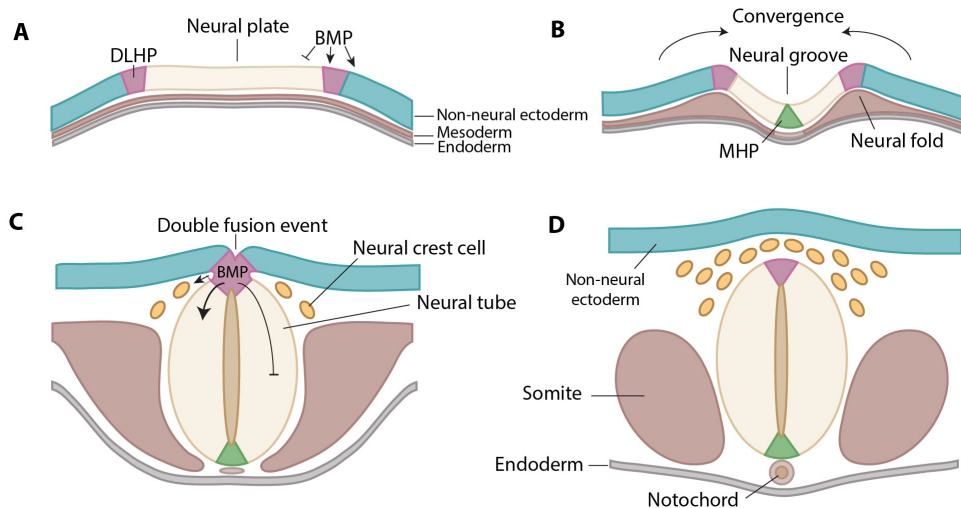
Figure 1'. Schemes of central nervous system development.

The brain and most of the spinal cord are formed during primary neurulation which is commonly divided into 4 phases. A. Epiblast cells are induced to a neuroectoderm fate, generating the neural plate. B. The remodeling phase where the neural plate undergoes convergent-extension and begins to fold along the median hinge point (MHP) and dorsolateral hinge points (DLHPs). C. The two neural folds converge at the midpoint and then proceed to fuse, leading to the dorsal closure of the neural tube. D. By embryonic day 9 in the mouse, fusion is complete. BMP – Bone morphogenic protein (Modified from Beattie and Mukhtar, 2015, adapted from[7-9]).

Regionalization of the mammalian neural tube

Molecular basis of regionalization

The neuroepithelium of the neural tube follows a sequential series of overlapping and competing patterning steps during brain development. Timing is critical, particularly in structures such as the cerebral cortex where even moderate changes in gene expression pattern can lead to serious developmental, motor, behavioral, psychological and cognitive disorders[10]. The best characterized morphogens and signalling pathways involved in regional identity include Sonic hedgehog (Shh), retinoic acid (RA), fibroblast growth factor (FGF), Wingless (Wnt), and BMP signalling (Figure 2')[11,12]. Shh is secreted by the notochord (axial mesoderm) beneath the floor plate of the neural tube and controls neuronal cell fate in a concentration-dependent manner[13]. RA is secreted from the mesoderm and defines the posterior CNS, including the hindbrain and spinal cord. RA contributes to segmentation of the hindbrain into eight distinct compartments called rhombomeres, which later give rise to the medulla, pons and cerebellum[14]. FGF activity along with RA and Wnts leads to the caudalization of the neural tissue[15,16]. Wnt signalling is crucial in development of the neural tube, particularly in establishing anteroposterior polarity. Several Wnt

antagonists including Cerberus, Dickkopf and Tlc are important in patterning the dorsal telencephalon[17-21]. Diffusion of BMPs and their antagonists along the neural plate creates a gradient of high BMP activity dorsally to low activity ventrally. This leads to the specification of distinct pools of progenitors in the dorsal spinal cord[7,12].

Additionally, the *Hox* gene family of homeodomain-containing transcription factors are highly conserved across vertebrates and play a key role in body patterning[22]. The majority of the 39 *Hox* genes found throughout vertebrates are expressed in the CNS where they play crucial roles in neuronal specification and selectivity. Hox genes are found as clusters (HoxA, HoxB, HoxC, and HoxD) on 4 different chromosomes and exhibit a 3'-5' gradient of sensitivity to RA[23]. *Hox1-Hox5* (like RA) are involved in hindbrain segmentation into rhombomeres. *Hox4-Hox11* are expressed in the spinal cord and lead to rostro-caudal positioning of neuronal subtypes (Figure 2)[23,24].
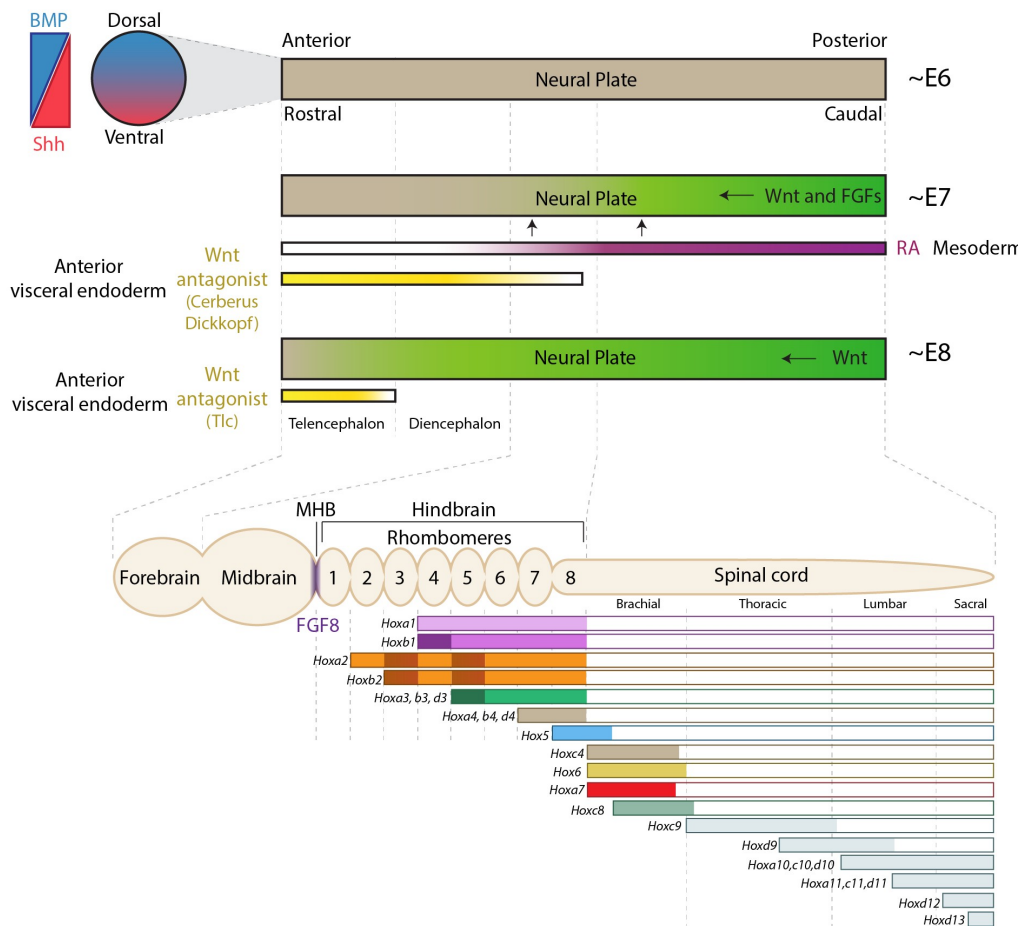
Figure 2'. Regionalization during neural tube formation is dependent on overlapping agonistic and antagonistic morphogen gradients.
Dorsoventral patterning of the neural tube is largely dependent on bone morphogenic protein (BMP) and Sonic hedgehog (Shh) signalling. Some of the key factors involved in patterning the anteroposterior axis include wingless (Wnt) and its antagonists (Cerberus, Dickkopf, Tlc), fibroblast growth factor (FGF), and retinoic acid (RA). Distribution of these factors leads to the eventual segmentation of the neural tube into the forebrain, midbrain, hindbrain and spinal cord. FGF8 expression delineates the

midbrain-hindbrain boundary (MHB). Additionally, the Hox family of genes, which are located on 4 different chromosomes (HoxA, HoxB, HoxC, and HoxD), are crucial in spatiotemporal patterning of the neural tube. *Hox1 - Hox5* are responsible for hindbrain segmentation, while *Hox4 - Hox11* are involved in patterning of the spinal cord ((Modified from Beattie and Mukhtar, 2015, adapted from[9,11,14,22-25]).

Structural organization of cellular compartments and boundaries in the developing neural tube

As the neural tube progressively becomes more regionalized, the organization of distinct structural domains arises. Segmentation of the neural tube in the mouse begins initially by assigning anterior-posterior identity along the neuraxis dividing into the forebrain, midbrain, hindbrain and spinal cord. The hindbrain (or rhombencephalon) is further divided into rhombomeres which give rise to the metencephalon (the pons and the cerebellum) as well as the myelencephalon (the medulla oblongata). The midbrain (or mesencephalon) is located caudal to the hindbrain and rostral to the forebrain. The forebrain (or prosencephalon) divides into the diencephalon (prethalamus, thalamus, hypothalamus, subthalamus, epithalamus, and pretectum) and the telencephalon (cerebrum) (Figure 2'). The cerebrum can be further divided into the cerebral cortex, the basal ganglia, and the limbic system (Figure 2').

Neuroepithelium to NSC transition and beyond

The process of neurulation induces formation of the neural tube, a pseudo-stratified epithelial sheet of neuroepithelial cells (NECs). It is the NECs that are the precursors of the central nervous system including cerebral cortex, which is formed over an extended period of development. Important biological questions remain about how the complex structure of the cerebral cortex, which is composed of diverse neuron subtypes, is generated from a simple epithelial sheet of cells to form the most complex tissue of the body. At embryonic day 9 (E9), the neuroepithelium gives rise to NSCs that line the luminal surface of the vesicles of the neural tube[26,27]. In mice, NSCs are located in the ventricular zone (VZ) and the ends of their basal processes remain in contact with the outer (pial) surface of the neural tube. This apical-basal polarity, which spans the thickness of the neural tube, requires the integrity of adherence junctions to segregate the apical and basolateral cell membrane and adhere neighboring NSCs to each other. The importance of adherence in NSC polarity is exemplified by the knockdown of the adherens-junction-associated protein Afadin

(Af6). Af6 depletion leads to a loss of adherens junctions and disturbed cell polarity [28].

At the onset of neurogenesis, the apical NSCs generate radial glial cells (RGCs) and short neural precursors[29,30]. The somata of these cells remain within the VZ but migrate radially along the apical-basal process through the zone during cell division in a process referred to as interkinetic nuclear migration (INM)[27,31-33]. The location of the soma within the VZ is cell-cycle dependent. During M-phase, the cell body is positioned apically at the luminal surface of the neural tube (Figure 3'). As the cell progresses through G1-phase of the cell cycle, the cell body moves radially to the VZ boundary with the overlying subventricular zone (SVZ) and forming cerebral cortex. S-phase and DNA replication occur at the basal boundary of the VZ followed by migration of the cell body back to the luminal surface of the neural tube during G2 to initiate mitosis[31,34,35]. Primary cilia in the apical membrane project into the vesicles and detect factors and signals in the fluid filling the neural tube and these support the apical-basal polarity. The orientated cell polarity is important for determining the structure of the cerebral cortex. Disruption of the small GTPase, ADP ribosylation Factor Like GTPase 13B (Arl13b), results in loss of cell polarity and the cortical wall is generated in an inverted fashion. M-phase of Arl13b-deficient RGLs is no longer restricted to the luminal surface but also occurs at the basal, pial surface and neurons migrate centripetally to the VZ[36].

During early phases of neurogenesis, embryonic day 10.5-11.5 (E10.5-11.5) in mice, NSCs undergo symmetric stem cell divisions, expanding the pool (Figure 3'). This is referred to as the 'neural expansion' phase of cortical development. Later, NSCs progressively undergo asymmetric cell divisions, allowing for both self-renewal as well as the generation of committed daughter cells (Figure 3'). The transition from symmetric stem cell to asymmetric neurogenic divisions during neurogenesis is associated with a lengthening of primarily G1-phase of the cell cycle. However, the S-phase of the NSCs in the symmetric dividing, expansion phase is longer than of those in the asymmetric dividing neurogenic phases[31,37]. Hence, although the precise function of INM and the changing in cell cycle phase length are not understood, it seems that they play an important role on the control of the sequential switching of NSCs from symmetric self-renewing modus to the asymmetric division mode that drives the production of neurons.

During the neurogenic phase of cortical development, the self-renewal and generation of committed daughter cells has to be tightly controlled. Loss of self-renewing NSC

daughter cells would purge the stem cell pool. Conversely, a failure to generate sufficient neuronal determined precursors would severely affect neuronal composition and cortical layering. During early stages of cortical development some asymmetric stem cell divisions generate one NSC daughter and a neuron directly. This is referred to as direct neurogenesis. However, as neurogenesis progresses the daughter cell that is committed to differentiate and leaves the stem cell pool becomes a basal progenitor (BP) and migrates to the forming SVZ (Figure 3')[31,37,38].
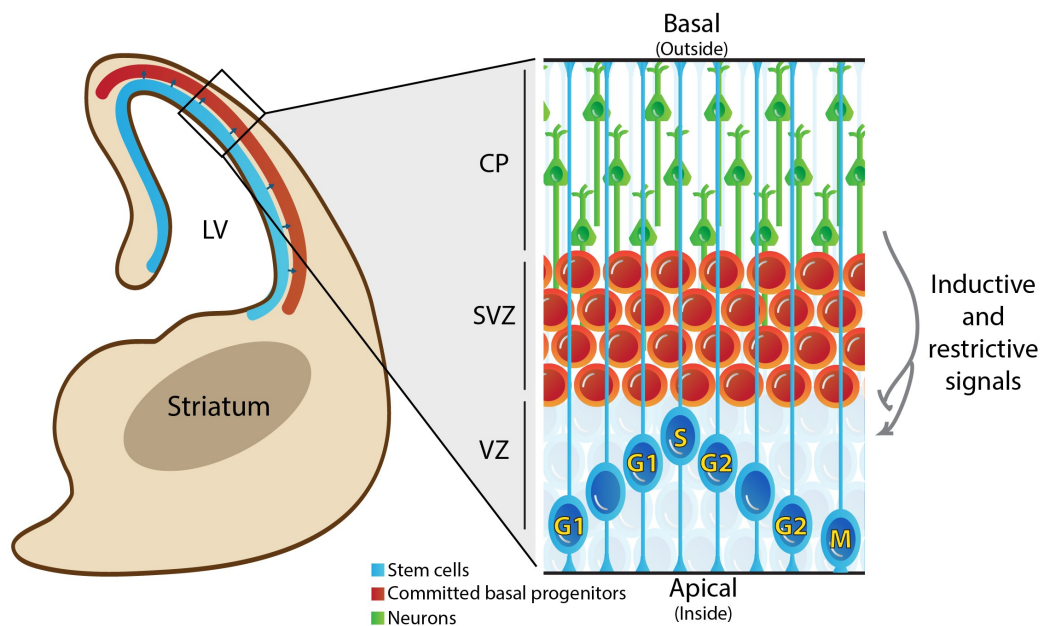
Figure 3'. Scheme of a coronal hemisection of the developing mouse telencephanlon and the stem and progenitor populations.
As neurogenesis continues, neural stem cells (NSCs) retain contact with the outside of the neural tube and their apical end feet line the tube resulting in long polarized processes. NSCs undergo interkinetic nuclear migration during cell cycle. DNA replication (S-phase) always takes place when the cell body reaches the ventricular (VZ)-subventricular zone (SVZ) boundary, mitosis (M) and karyokinesis take place at the luminal surface (apical) of the neural tube. Committed progeny of the NSCs, basal progenitors, migrate to the SVZ where they may divide before differentiating into immature neurons that migrate to the superficial layers of the forming cortical plate (CP) and future cerebral cortex. LV- lateral ventricle. (Modified from Beattie and Mukhtar, 2015)[9].

Distinct stem and progenitor populations contribute to cortical development

Throughout neurogenesis, another VZ population of dividing cells called the short neural precursors contributes to the progenitor pool. Short neural progenitors have either a short or no basal process at all but retain the apical process and contact to the lumen of the neural tube. These cells are morphologically, ultra-structurally and

molecularly different from the NSCs and have been observed to undergo direct neurogenesis, generating neurons without passing through a BP[29].

In higher mammals including, ferrets, primates and humans, additional intermediate progenitor populations have evolved, and although they also reside in the SVZ, they have different morphologies and larger cell fate potentials compared to the classic BPs in mice[30,39,40]. In fact, in primates, some of these intermediate progenitors display NSC potential and are even referred to as outer radial glial cells (oRGCs) [40]. oRGCs are morphologically distinct, unipolar, and retain only the basal process with no connection to the VZ and neural tube lumen[40-42]. They also do not express the apical membrane constituents associated with VZ NSCs and RGC including Prominin1 (CD133), Par3-family cell polarity regulator (Par3) or atypical Protein Kinase C λ (aPKCλ)[39]. They have a long basal phospho-Vimentin (pVim) positive process that extends towards the pia and retain the basal fiber throughout the duration of cell cycle[34]. Like VZ RGCs, the soma of oRGCs also moves during cell divisions but this movement is distinct to the INM of VZ NSCs. The soma of oRGCs moves basally and once translocation is complete, they divide mostly by self-renewing, asymmetric divisions and push the boundary of the outer subventricular zone (OSVZ) outwards expanding the SVZ [40,43]. Self-renewing oRGCs continue to proliferate while the daughter cells differentiate into neurons.

These SVZ progenitors in primates are the major source of expansion and neurogenesis in the cerebral cortex and are responsible for the massive evolutionary expansion of the cortical gray matter, neuron number and cortical surface. Indirectly, these SVZ progenitors are responsible for the increase in functional capacity of the cerebral cortex in primates[44]. The co-existence of oRGC cells and VZ RGCs NSCs demonstrates the distinct germinal zones in higher mammals, highlighting the mechanisms of increased neuron production, relevant for the formation of bigger brains. Here I will focus on cortical development in the mouse and refer to an excellent review focusing on primate and human cortical development[34].

BPs are intermediate, transient amplifying cells that undergo one or two divisions before giving rise to neurons (Figure 3'). The BPs are one of the main zones of amplification and neurogenesis in the developing mouse cortex. As neurogenesis reaches completion, the NSCs start to generate other cell lineages, oligodendrocytes, astrocytes and ependymal cells[45,46]. This is referred to as the 'gliogenesis phase' of

cortical development. The transition from neurogenesis to gliogenesis is associated with a down-regulation of the Golgi-derived apical trafficking and VZ NSCs lose tight junctions while keeping intact the adherence junctions[47,48]. This is followed by the gradual expression of the astroglial hallmarks including glial fibrillary acidic protein (Gfap) in the mouse[46,48-50]. Though the mechanisms of the neurogenic to gliogenic phase transition aren't clearly understood, Notch signalling and its downstream targets, the bHLH transcription factors including the Hes proteins, and the growth factor Fgf10 are necessary for this transition[51-53].

Since the generation of neurons from BPs results in the expansion of the neuronal progenitor pool enabling the production of many neurons from a restricted population of NSCs, their role is crucial in the expansion of the cortex[52,54,55]. In the mouse, BPs can undergo symmetric divisions and generate two neuronal daughter cells[55]. However, evidence suggests that some, if not all, may also undergo one or two rounds of self-renewing cell divisions[52,54,55]. BPs are defined based on their position in the SVZ, their lack of polarized morphology and expression of the transcription factors, Eomesodermin (Eomes or Tbr2), Btg antiproliferation factor 2 (also called Tis21), Cut like homeobox 1/2 (Cux1/Cux2) and Special AT-rich sequence binding protein (Satb2) and the non-coding RNA Svet1[56-60][61]. Since the different progenitor cell-types are localized to different niches and thus likely exposed to different combinations of cues from their microenvironment, it is imperative to study the role of their niche in controlling their proliferation and fate commitment. This cellular heterogeneity requires a deeper understanding of the cell fate identities and commitments[62].

Symmetric and asymmetric cell divisions

NSCs of the developing cerebral cortex display multiple modes of cell division. Initially, the major form of divisions are symmetric stem cell divisions, generating two daughter cells that retain stem cell potential and re-enter cell cycle. As development progresses, the stem cell divisions are slowly superseded by asymmetric neurogenic divisions where one daughter remains a stem cell and renters the cell cycle within the VZ whereas the other is committed to differentiate and will leave the VZ (Figure 4'). The third mode is the symmetric neurogenic division where both daughter cells will differentiate thereby depleting the stem cell pool. The balance between these different forms and outcomes of cell division are temporally and spatially regulated which is necessary to control correct cortical development.
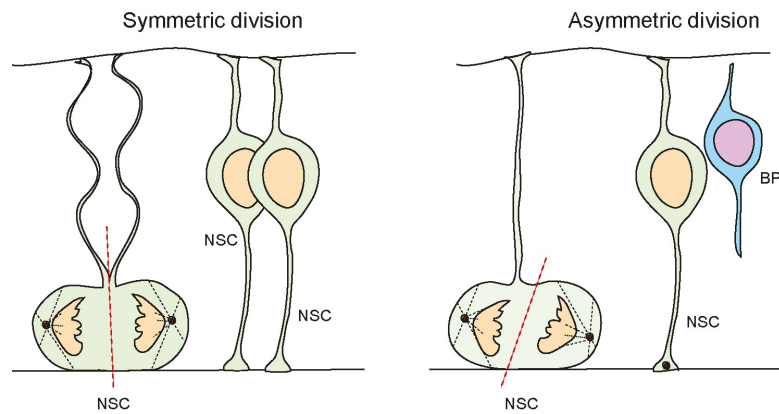
Figure 4': Types of NSC divisions in the ventricular zone are determined by spindle orientation and the inheritance of cell-fate determinants.
Symmetric divisions generate two NSCs while asymmetric division generates one NSC and one differentiating daughter cell. During neural expansion, most divisions are symmetric while during neurogenesis, most divisions are asymmetric. (Here adapted from Mukhtar, T and Taylor, V., 2018; previously adapted from Paridaen, J.T. and Huttner W.B., 2014)[27,63]. NSC - neural stem cell; BP - basal progenitor.

The molecular basis of symmetric and asymmetric divisions and the transition from self-renewing to differentiating modes of cell division are not understood. It has become clear that the orientation of the mitotic spindle plays an important role in the type of division and the fate of the respective daughter cells generated (Figure 4'). A cleavage plane bisecting the apical membrane of the NSCs, including inheritance of junctional complexes by both daughters, contributes heavily to maintenance of stem cell potential (Figure 4'). During symmetric divisions of NSCs, the cleavage plane is oriented perpendicular to the ventricular surface (Figure 4')[64]. This spatial organization of the mitotic spindle requires a proper centrosome assembly, duplication and a precise interaction between planar cell polarity components, G protein signalling modulator 2 (Lgn) and Inscuteable (Insc)[37,65-67]. The partition of cell components involved in cell polarity, including the Par3 family cell polarity regulator (Par3/Par6), proteins between daughter cells is critical for differential cell fate determination. In symmetric stem cell divisions, the basal process is equally split between the daughter cells (Figure 4')[68,69]. The transcription factor Empty spiracles homologue 2 (Emx2) is expressed by NSCs of the VZ and promotes perpendicular cleavage plane thereby promoting symmetric expansive cell divisions[70]. Forced Emx2 expression in NSCs during cortical development increases clonal expansion and symmetric cell divisions[70].

During asymmetric cell divisions, the cleavage plane is orientated parallel to the neural tube luminal surface (Figure 4'). This results in an unequal partition of Par3 into the two daughter cells and the sibling cell receiving less Par3 protein exits cell cycle

and differentiates[68,69]. In addition, asymmetric cell division is accompanied by an unequal distribution of fate determinants between the daughter cells. These components including mediators of Notch signalling, the Notch ligand Delta-like 1 (Dll1), Mindbomb, and Numb[71,72]. Segregation of Notch components including inhibitors of the pathway leads to differential Notch signalling between daughter cells. Notch signalling plays a critical role in NSC maintenance and differentiation by regulating cell proliferation and fate determination[71,73,74]. Notch activates the expression of *Hes* genes which encode basic helix loop helix transcriptional regulators. *Hes*-related proteins repress expression of the pro-neurogenic transcription factors including Neurogenins (Ngns) and Ascl1[75,76]. Thus, activation of Notch signalling inhibits differentiation of NSCs by suppressing transcription factors required for neurogenesis[74]. In addition, Notch signalling regulates cell cycle progression via regulation of Ascl1 expression. Ascl1 not only controls neurogenic differentiation but is also involved in entry of NSCs into cell cycle[77,78].

In addition to Notch, some cytoplasmic proteins show differential distribution upon asymmetric division. Staufen is a double stranded RNA binding protein which is pivotal in asymmetric cell fates in Drosophila neural development. Staufen is selectively segregated into the differentiating daughter cells upon asymmetric self- renewing cell division[79]. Staufen binds mRNAs that encode protein crucial in cell cycle exit and differentiation. Furthermore, the transcription factor Pax6 promotes asymmetric neurogenic cell division[80]. Pax6 mutant NSCs show a defective cell cycle exit and an increase in self-renewing capacity[80].

In addition to molecular segregation, the orientation of the mitotic spindle plays an important role in fate determination. In NSCs and RGCs, the mitotic spindle poles oscillate around their final positions before anaphase is initiated. This dynamic movement of the spindle seems to be important in determining the cleavage plane and then the segregation of intracellular components. Only subtle changes in spindle orientation can cause major shifts in the plane of cytokinesis and thereby the inheritance of membrane compartments and cell fate determinants[81]. Mutations in the Abnormal spindle-like microcephaly-associate (Aspm) gene severely affects cerebral cortical size and reduces the volume of the cerebral cortex in primates[82]. Aspm is important for spindle orientation and control symmetric versus asymmetric cells division modes.

Inheritance of the apical plasma membrane of NSCs has an influence on cell fate. During symmetric cell divisions both daughters acquire apical membrane and junctional components. When only one daughter cell inherits the apical plasma membrane, for example, when the cleavage plane is parallel to the neural tube luminal surface, that daughter remains as a NSC whereas the other sibling that does not receive apical membrane and adherence junctions from the mother cell will exit the VZ and commit to differentiation. The SNARE-mediated membrane fusion machinery controls NSC fate specification. A hypomorphic missense mutation in *a*-SNAP (*a*-soluble N-ethylmaleimide-sensitive fusion protein (NSF) attachment protein), causes NSCs to prematurely switch from symmetric proliferative to asymmetric neurogenic divisions[83]. This is primarily due to an impaired apical protein localization affecting the Golgi-derived membrane traffic necessary for NSC proliferation[84]. In addition, NSCs in these mice show distribution of apical *b*-catenin along the adherence junctions, and phenocopying conditional *b*-catenin null mutant mice. Hence, *b*-catenin also plays a role not only in the control of cell cycle but also in the choice between symmetric and asymmetric divisions[85,86].

Regulation and cell fate commitment

The stem and progenitor cells in the dorsal VZ of the anterior neural tube generate the multiple classes of projection neurons that make up the future cerebral cortex in sequential waves. In the dorsal cerebral cortex, neurogenesis commences around E10.5 in mice[49,50]. The earliest-born neurons segregate from the NSCs in the VZ and migrate radially to the pial surface forming the preplate. Later-born neurons migrate into the preplate, splitting it into the marginal zone (MZ) and the subplate (SP) (Figure 3). Throughout neurogenesis, newborn neurons migrate into the cortical plate (CP), through the preformed layers of earlier born neurons and as such the early-born neurons form the deep-layers and the later-born neurons form upper-layers. The detailed molecular cascade that determines neuronal cell fate commitment, an excitatory neuron subtype specification is largely unknown. Different models have been proposed to explain the temporal dynamics of neuronal specification in the dorsal cortex[87]. The 'common progenitor model' implies that a single type of NSC sequentially gives rise to the different neuron subtypes overtime during neurogenesis and that neuron fate is determined by time (Figure 5'a). According to the 'multiple progenitor model', multiple stem cell types coexist and are predetermined to generate specific neuron subtypes[88]. In the multiple progenitor model, the fate of the stem cell

and the type of neuron generated is determined by the NSC type (Figure 5'b). There is experimental evidence supporting both models[47,89].

The common progenitor model

McConnell and colleagues demonstrated that NSC fate becomes restricted overtime during development[90]. By performing elegant heterochronic transplantation experiments initially in ferrets, they demonstrated that early developmental stage progenitors have a greater potential, and can generate early and late neuronal subtypes when grafted into hosts. Conversely, late-stage progenitors have a more restricted potential and a reduced capacity to form early neuronal types in host embryos[90]. This implies that NSCs lose their potential to generate deep layer neurons with time[90-92]. In support of this model, clonal *in vitro* experiments showed the sequential generation of deep and upper layer neurons from NSCs supporting initial multipotency and subsequent fate restriction over time[90,93-95]. Finally, retroviral labeling and lineage tracing of individual NSCs supported progressive fate restriction *in vivo*[96]. More recently, genetic labeling in the developing mouse cerebral cortex following expression of the transcription factor Fezf2 (enriched in deep cortical layer V neurons), revealed that Fezf2 expressing NSCs generate deep, upper layer neurons and glial cells[89,97,98]. Instructive roles of factors such as Fezf2 in NSCs can have major implications in cell fate commitment during neurogenesis. Ectopic expression of Fezf2 can direct NSCs to differentiate into deep layer neurons and reverse late fate commitment[89,99].

The multiple progenitor model

An alternative model for fate specification proposes independent, fate-restricted lineages of NSC that generate specific neuronal subtypes and have limited potentials (Figure 5'b). Evidence suggests that many transcription factors expressed during cortical development instruct fate determination[98]. The onset of expression of these transcription factors was proposed to coincide with the developmental time point at which specific neuronal subtypes are determined, indicative of the presence of pre-determined NSC subtypes[88]. Analysis of transgenic mice revealed that Cux1 and Cux2 are expressed in VZ and SVZ as early as E10.5, primarily in specific and fate restricted NSCs. Genetic tracing of Cux1 positive progenitor cells mostly generated upper layer neurons[47,100]. During early development, Cux1, Cux2 positive NSCs undergo expansion and do not contribute to early layer neuronal differentiation[47,100]. These seem to be restricted in fate while they undergo neurogenesis and produce only upper layer neurons. Conversely, follow up experiments analyzing Cux2 positive

cells by lineage tracing elucidated their role in generating both deep and upper layer neurons as well as the interneurons from the ventral telencephalon[89,92].

Other experiments imply the co-existence of multipotent NSCs and their consequent fate restriction through the course of neurogenesis[47,101]. It is possible that cells can be more restricted in their potential and change to alternate fates when subjected to different extrinsic cues. This may explain the switch between multipotent to restricted NSC states. Since the precise structure of the lineage trees for specific neuronal subtypes remains largely unknown *in vivo*, single cell clonal analysis to identify markers of clusters of NSCs may contribute to this understanding of cell fate commitment. Both the 'common and multiple progenitor models" do not negate the possibility of the other, and future high-resolution experiments are needed at the single cell level to address NSC heterogeneity and dynamic potential.
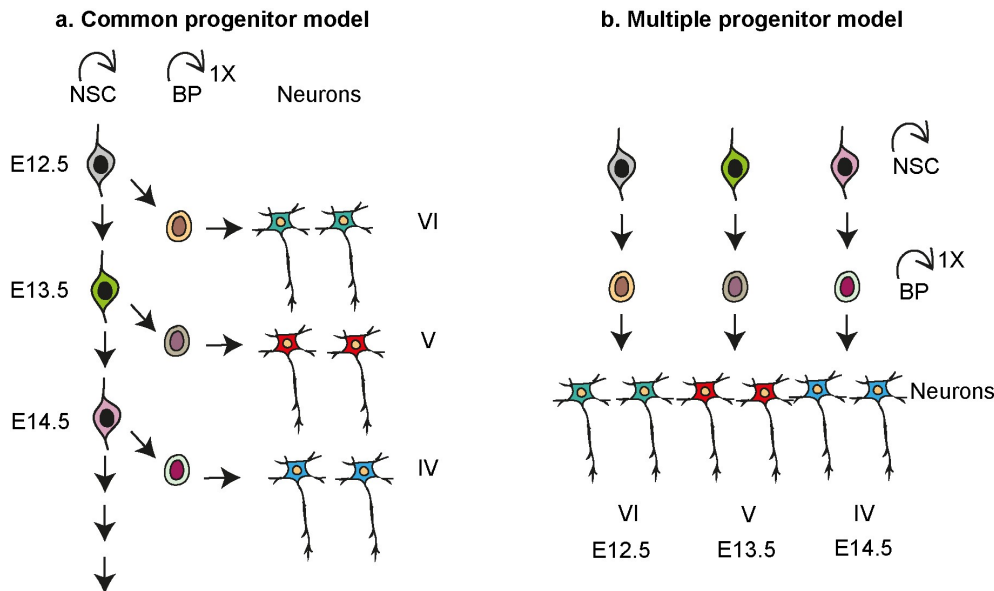
Figure 5': Different models of neuronal subtype specification in developing neocortex.
a) In the common progenitor model, a single type of multipotent NSC sequentially gives rise to all neuronal subtypes during the course of development. Overtime, the fate potential of this NSC becomes increasingly restricted. The fate of the neuron is specified based on its birth date. b) In the multiple progenitor model, multiple types of NSCs co-exist and are, to some degree, pre-determined to give rise to specific and restricted neuronal subtypes. The fate of the neuron is specified by the NSC type in this model. NSC - neural stem cell; BP - basal progenitor. (Here adapted from Mukhtar, T and Taylor, V., 2018)[63].

Interneuron generation

To this point, I have mainly discussed the generation of projecting neurons in the dorsal cerebral cortex. The VZ and NSCs of the dorsal cortical anlage only generate projecting and not inhibitory interneurons. However, inhibitory Gamma-AminoButyric

Acid-ergic (GABAergic) interneurons make up a major population in the cerebral cortex. Unlike the glutamatergic projecting neurons, interneurons are generated from the VZ of the ventral telencephalon, predominantly from the medial ganglionic eminence (MGE), caudal ganglionic eminence (CGE), the preoptic area (PoA) and the anterior entopeduncule (AEP) area of the subpallium (Figure 6'a). Cortical interneurons are produced predominantly between E11-E17. The ventral NSCs that generate interneurons express the Genomic screened homeobox-1/2 (Gsx1/Gsx2) and Oligodendrocyte transcription factor 2 (Olig2)[102]. These subpallial NSCs also expresses Distal-less homeobox 1 and 2 (Dlx1 and Dlx2) transcription factors, which are essential for interneuron production and migration[103]. The transcription factors Nk2 homeobox 1 (Nkx2.1) and SRY-box 6 (Sox6) are expressed by progenitors of the MGE and play a role in interneuron differentiation regulating the downstream transcriptional programs in the NSCs and post-mitotic neurons[104]. Retroviral labeling of NSCs in the MGE revealed that interneurons were generated from NSCs that undergo asymmetric cell divisions[98,99,102]. The ventral telencephalon contains an extensive SVZ and BPs undergo symmetric divisions to generate interneurons[104]. The dorsal cerebral cortex contains multiple interneuron subtypes with distinct neurochemical marker expression, firing patterns and synaptic connectivity[105]. Following dorsal migration from the subpallium to the pallium, the interneurons integrate into the cerebral cortex in a sequential and temporal fashion[102]. As embryonic development proceeds, the excitatory and inhibitory neurons mature and form synapses to establish a complex cortical neural network. Not much is known about the molecular cascade underlying the interneuron subtypes catering to the variety of their functions[105].
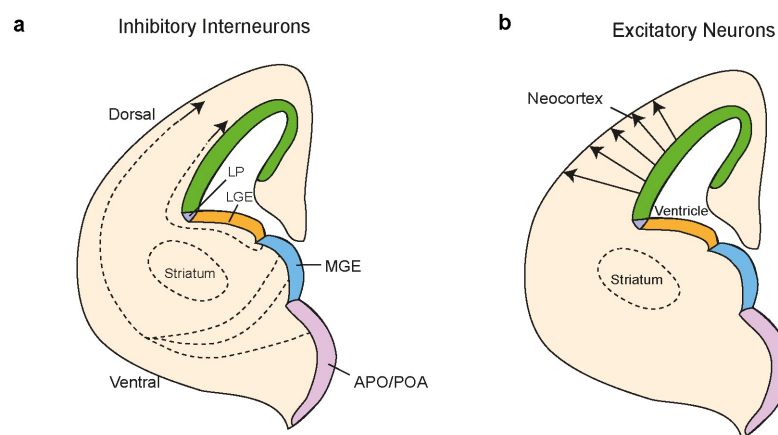
Figure 6': Inhibitory interneurons and excitatory projection neurons and of the cerebral cortex have different origins.
a) Inhibitory interneurons originate from the ventral telencephalon, especially from the MGE, AEP/POA. The immature interneurons migrate as neuroblasts tangentially and

dorsomedially towards the neocortex following two major routes (dotted arrows). The coloured zones depict the proliferative NSC zones in the dorsal and ventral telencephalon. b) Excitatory projection neurons originate from the ventricular zone of the dorsal telencephalon and migrate radially to the CP. LP, lateral pallium; MGE, medial ganglionic eminence, APO/POA, anterior entopeduncular area of the subpallium/ preoptic area. (Here adapted from Mukhtar, T and Taylor, V., 2018)[9,63].

Neuronal diversity and transcriptional dynamics in cortical layering

The cerebral cortex is an isocortex and composed of six clearly defined layers of neurons. The newborn excitatory neurons migrate out of the VZ along the radial processes of the NSCs (Figure 6'b). The immature neurons reach the CP by migrating through the layers formed by their earlier-born siblings. Upon reaching the pial surface, the immature neurons leave the RGC process and differentiate and form neurons of their specific cortical layer. Hence, the isocortex of the cerebrum is formed in an inside-out fashion, with early born neurons forming the deep layers while the later born neurons generate the upper layers (Figure 7'). The neuronal type and their location within the isocortex is critical for function.

The major types of cortical projection neurons can be defined by their connectivity and projection patterns depending whether they project through associative, commissural and corticofugal projection fibers. Associative projection neurons project their axons within a single cerebral hemisphere connecting local areas or proximal gyri. Commissural, callosal projection neurons are localized primarily in layers II/III, V and VI of the 6 layered isocortex. They extend their axons from one hemisphere to neurons in the contralateral hemisphere. The axons project either through the corpus callosum, the major commissural connection between the hemispheres, or through the anterior or posterior commissures. The commissural neurons are further subdivided based on the projection destinations[98]. Corticofugal neurons include the subcerebral neurons, which are the largest pyramidal neurons and extend projections to subcortical structures including the brainstem and spinal cord. The corticofugal projections include corticopontine, corticospinal and corticotectal neurons[106]. Another subtype of corticofugal neurons is the corticothalamic neurons, which populate the layer VI of the isocortex with a small population in layer V and extend their projections to different nuclei of the thalamus[98].

Hence, the regulation of neuron subtype formation and the temporospatial control of neurogenesis are critical for brain function. Numerous neocortical determinants   are

expressed along the dorsolateral wall of the cortex, upon the induction of neurogenesis. Key factors including Forkhead box G1 (FoxG1), LIM homeobox 2 (Lhx2), Emx2 and Pax6 which define and control the neocortical progenitor domains along the dorsal and ventral axis[48,98]. Ablation of the dorsal progenitor domain determinants Pax6 and Emx2 results in expansion of the ventral domains[107]. Pax6 and T-cell leukemia homeobox (Tlx) regulate the cell fate decisions in the VZ and the loss-of-function of these factors leads to a thicker superficial cortex. Hence, the NSCs and progenitors of the cerebral cortex are determined by their expression of axial specifying factors but these fates are not fixed or restricted as loss of these determinants results in alternate fate acquisition[98].

The transcription factors Tbr1, Ctip2, Sox5, Fezf2, Satb2, Cux1, Cux2, Brn1, Brn2 and others have been studied extensively and determined to be key determinants of neuronal specification[31,34,47,56,57,59,88,89,97,99]. These transcription factors are often used as markers of specific cortical neuron populations and layers and are expressed in waves during cortical development. Some of these markers are expressed in specific neuronal subtypes within a layer or, are expressed in more than one neuronal subtype and layer. For example, the Ets-related protein 81 (Er81/Etv1) is expressed in cortico-cortical and subcerebral projection neurons of layer V[108]. Conversely, LIM domain only 4 (Lmo4) is selectively expressed in callosal neurons of layers II/III.

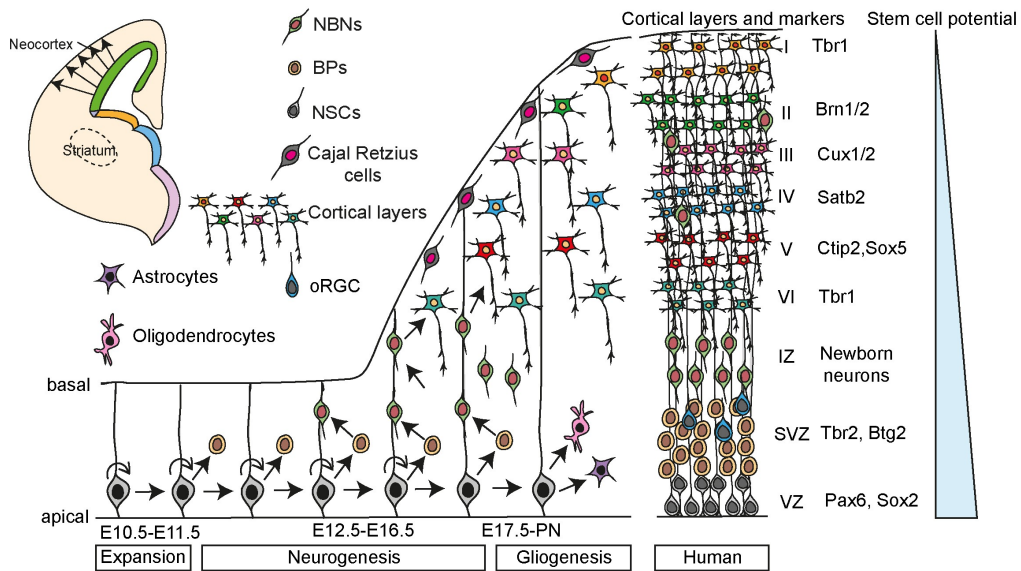***Figure 7': Systematic formation of isocortex layers in the dorsal telencephalon.***
During early stages of cerebral cortical development (embryonic day E10.5-E11.5), NSCs undergo predominantly symmetric cells divisions to expand the NSC pool. This phase is referred to as the Expansion phase. The first neurons to be formed are generated by direct neurogenesis of the NSCs. The Cajal Retzius cells populate layer

I of the isocortex and play important roles in establishing cortical architecture. During late embryogenesis (E12-E16.5), NSCs undergo increasingly more asymmetric divisions to generate one NSC (self-renewal) and one basal progenitor (BP). BPs generate the neurons. This is the Neurogenic phase. Neurons are generated in a sequential, inside-out fashion and are specified by different transcription factors, some of which are shown. At later stages of development, NSCs generate the other cell types of the brain including astrocytes, oligodendrocytes and ependymal cells (not shown). This is referred to as the Gliogenic phase. The potential of the NSC pool reduces over time during development. The formation of the human cerebral cortex follows a similar trajectory with the exception that additional progenitors, the outer radial glial cells (oRGC) expand the subventricular zone substantially to generate the increasing numbers of neurons needed in the human cerebral cortex. BPs - basal progenitors, IZ - intermediate zone, NBNs - newborn neurons, NSCs - neural stem cells, oRG - outer radial glia cells, SVZ - subventricular zone, VZ - ventricular zone. (Here adapted from Beattie, R and Mukhtar T, 2015)[9].

Some of these fate-determining and defining factors seem to be coexpressed initially and their expression becomes restricted and refined later in neuronal differentiation. For example, in mice, post-mitotic deep-layer neurons co-express Ctip2 and Satb2 at embryonic day 13.5[59,98,109]. As development progresses, these deep-layer neurons express either Ctip2 or Satb2 and become fate restricted to form subcerebral projection neurons or corticothalamic projection neurons, respectively[59,98,110,111]. Ngn1 and Ngn2 are two proneural transcription factors and induce neurogenesis, however, Tbr1 and Er81 expressing deep layer neurons are still generated in their absence[112,113]. It is likely that other proneural transcription factors are able to compensate for the loss of Ngns but the exact mechanism remains to be defined.

Epigenetic and epitranscriptomic interplay during neurogenesis

Not only is gene expression in NSCs regulated by transcription factors but also by epigenetic mechanisms. DNA methylation and Histone modifications are involved in spatial and temporal gene expression during neurogenesis and the switch from neuronal to glial fate[114-116]. New methods for genome-wide methylation mapping facilitates investigation of epigenetic landscapes that control lineage commitments and fate decisions during neuronal specification. Epigenetic regulation of critical transcription factors in NSCs play important roles in the regulation of cell fate and neurogenesis. The expression of epigenetic regulators including the High mobility group (HMG) proteins during early phases of cortical development regulate chromatin state and methyltransferase activity including Enhancer of zeste 2 polycomb repressive complex 2 subunit (Ezh2)[114-116]. This suggests that the chromatin in early NSCs is in a more "open" state than that of later NSCs[115]. The transcription factor Tbr2, which is critical for BP generation and differentiation, associates with the

Histone demethylase Jmjd3 (also called Kdm6b). Tbr2 directs Jmjd3-dependent chromatin remodeling to specific gene loci promoting the removal of H3K27me3 chromatin marks[117]. This emphasizes the additional level of control that Tbr2 has on neuronal specification by regulating the epigenetic marks at specific promoter and enhancer sites[117].

Hes5 is a pivotal mediator of Notch signalling and inducer of maintenance of NSCs by blocking proneural transcription factor expression. However, the expression of Hes5 also depends on Glial cell missing homolog (Gcm) and active DNA demethylation during neurogenesis[118]. Loss of Gcm prevents upregulation of Hes5 and the formation of definitive NSCs between E7.5 and E8.5[118]. Pax6 interacts with BAF155 and BAF170, components of the ATP-dependent multi-subunit mSWI/SNF nucleosome remodeling complexes in NSCs. At the onset of neurogenesis, BAF155 and BAF170 compete and modify euchromatin structure[119,120]. This leads to the recruitment of the Pax6/RE1 silencing transcription factor (REST)-corepressor complex to the Pax6 targets Transducin like enhancer of split 1 (Tle), Eomes and Cux2, and repressing their expression. This prevents the formation of BPs and late NSCs.

During the peak of neurogenesis, the chromatin remodeler Sucrose non-fermenting like protein 1 (Snf2l) represses expression of FoxG1, which leads to the de-repression of the cell cycle regulator p21 and promotes neuronal differentiation by inducing cell cycle exit[119,120]. During later stages of neurogenesis, the Polycomb proteins repress Ngn1 expression to trigger the NSC fate switch from neurogenesis to astrogliogenesis[114]. The NSC switch to gliogenesis is associated with the expression of the astrocytic protein GFAP. DNA methylation of the *Gfap* promoter prevents its premature activation. Notch signalling induces demethylation of the *Gfap* promoter through the transcription factor Nuclear Factor I (NFI), by dissociating associated DNA methyltransferases, and thereby supports generation of astrocytes[52,121,122]. Further analysis of the interplay between epigenetic and transcriptional dynamics during cortical development may contribute to a greater understanding of novel mechanisms and dysregulation during brain disorders.

The molecular machinery mediating m^6A mRNA methylation identifies novel physiological functions of this pathway in vivo. N^6-methyladenosine is installed by the Mettl3 and Mettl14 methyltransferase complex and is the most prevalent modification of mRNA. Recently a paper by Yoon *et al*, 2017, demonstrated the   role of Mettl14

and Mettl3 methyl transferases in neurogenesis and the conditional knockout of Mettl14 as a potential model to study the downstream effects of m[6]A mRNA methylation. They also replicated their studies in human induced pluripotent stem cell (iPSC)-derived forebrain organoids, elucidating the m[6]A modification landscapes in mouse and human NSCs[123]. These m[6]A mRNA modifications were mostly enriched in genes involved in neurogenesis, cell cycle and other fate determinants including Neurod1 and Neurod2 pivotal in the transition of NSCs to BPs[123]. These novel mechanisms highlight the differences and uniqueness of the targets between mice and humans, emphasizing the evolutionarily conserved and divergent genes. Further studies addressing the interplay between epigenetic and transcriptional dynamics during cortical development may contribute to a greater understanding of novel mechanisms and dysregulation during brain disorders.

Post-transcriptional regulation of gene expression

Recent screens have uncovered post-transcriptional regulation as an integral mechanism in cortical development[124]. An important post-transcriptional control on the neurogenic genes is through microRNAs. These are highly conserved non-coding RNAs of 18-24 nucleotides that bind to the 3'UTR of mRNAs, to downregulate their expression through degradation or by suppressing the translation. For example, MicroRNA-92 (miR-92) suppresses the transition of NSCs to BPs by downregulating Tbr2. This regulation may be by direct silencing or by indirectly forming regulatory loops. In case of Sry box-2 (Sox2), that controls LIN28 homolog through epigenetic modifications, which in turn regulates the biogenesis of let-7 miRNA, by controlling their maturation[125-127]. Because of this, LIN28 expression is suppressed by let-7 miRNA implicating the silencing of cell cycle regulators Cyclin D1 (Ccnd1), Cell division cycle 25A (Cdc25a) and proneural genes Ngn1 and Ascl1, affecting proliferation and differentiation[128]. Another mechanism studied is the regulation of neurogenesis by long non-coding RNAs (lncRNAs). These encode RNA transcripts of >200 nucleotides and modulate gene expression by alternative splicing. Studies in the midbrain implicate the lncRNA Rhabdomyosarcoma 2 Associated Transcript (Rmst), to co-transcriptionally interact with Sox2. These regulate many downstream genes involved in neurogenesis. Rmst acts as a transcriptional coregulator and mediates the binding of Sox2 to the promoters of its target genes[129-131]. Another example is of lncRNA Myocardial Infarction Associated Transcript (Miat), with selective regulation of proliferation over differentiation[129]. The transcriptional repressor REST is a potent master regulator of neurogenesis, and controls the

expression of many neurogenic genes. Alternative splicing of REST by Serine/Arginine Repetitive Matrix 4(nSR100) leads to derepression of proneural genes. Also, sequence specific RNA-binding proteins such as RNA binding protein Fox 1 homolog 3 (Rbfox3) mediate the alternative splicing of Numb, an important regulator of Notch signalling and promotes differentiation[132]. The expression of Rbfox3 is restricted to neurons. The molecular mechanisms of these splicing events are largely unknown. Additionally, non-canonical function of the RNase III Drosha and DGCR8 (also known as Pasha), key components of the microRNA (miRNA) microprocessor, is another mechanism to control the hypostable TFs during neurogenesis[133]. Drosha negatively regulates the expression of Ngn2 and Neural differentiation 1 (NeuroD1) by binding conserved hairpins in the mRNAs with similarities to pri-miRNAs and degrading them[133]. Thus, Drosha-mediated molecular inhibition of Ngn2 accumulation has implications on NSC maintenance and differentiation. Further insights into the modes of post-transcriptional regulation could help to explore the novel mechanisms controlling neuronal specification at the RNA level. An in depth post translational proteome analysis of NSCs to elucidate their temporal dynamics may be key to understand the various pallets of their regulation.

Signalling dynamics during neurogenesis

Various signalling pathways impinge on downstream effectors and regulate NSC fate decisions during neurogenesis. Among these pathways are Notch, Wnt, Shh, FGFs, TGF-*b*, Retinoic acid, and Hippo. How the crosstalk between these signalling pathways and the integration of their signals on target genes governs complex cell fate choices is unclear.

Notch signalling as a key regulator in maintenance of NSCs

In order to maintain neurogenesis from the developing embryo into adulthood, NSCs must be able to self-renew. One of the best-studied signalling pathways shown to be involved in NSC maintenance, proliferation, quiescence and survival is the Notch pathway [75,134-139]. Notch receptors are type-1 transmembrane proteins, which can be activated through extracellular protein-protein interactions with either Delta or Serrate (Delta-like and Jagged respectively in mammals) ligands on adjacent cells. Upon activation receptors undergo sequential proteolytic cleavage, first by a disintegrin and metalloprotease (ADAM) and then by a Presenilin containing γ-secretase, releasing the intracellular domain of Notch (NICD) [140,141]. Canonical-Notch signalling is mediated by the interaction of nuclear translocated NICD with the CSL transcriptional

complex (RBP-J in mice) (Figure 8'). This interaction disrupts the preformed repressor complex, and switches it to an activator by recruiting Mastermind and chromatin modifying agents (i.e. histone acetyl transferase) to induce target gene expression [142-147]. The best-studied targets of the Notch pathway in mammals are the orthologues of Hairy/Enhancer of Split (HES/HEY). The direct canonical Notch targets, *Hes1* and *Hes5* are two of these basic helix-loop-helix (bHLH) transcriptional regulators and are critical for neural development[148]. Hes1 and Hes5 directly repress transcription of proneural genes including *Ascl1*, *Atoh1* and *Neurog2* (Ngn2) thereby maintaining NSCs in a progenitor state[139,148]. Conversely, inactivation of Notch results in upregulation of the proneural genes and neural progenitor differentiation [73,75,149]. Manipulating the Notch signalling pathway using either γ-secretase inhibitors, by ablating *RBP-J*, knocking-out individual members of the Notch family or expressing an activated Notch intracellular domain (NICD) showed that Notch is key in modulating progenitor cell proliferation and neurogenesis during embryonic development[73,75,149].

The classic "lateral inhibition" model of Notch signalling in NSCs proposes that all early progenitors express similar levels of pro-neural genes and Notch ligands. Then through stochastic variations, the levels of receptors, ligands and pro-neural genes fluctuate between adjacent cells resulting in a "salt-and-pepper" pattern of Notch component gene expression[139]. Cells with slightly higher ligand levels of ligand activate receptors in neighboring cells causing an inhibition of pro-neural genes in those cells. The differences between neighboring cell gene expression levels continues to be exacerbated and eventually leads to the lineage commitment of the high pro-neural gene expressing cell. Real-time imaging in Hes reporter mice showed that negative feed-forward and feedback loops exist, resulting in oscillatory expression of downstream Notch signalling components and their targets over time [138,150,151]. Therefore, a cell with high proneural gene expression at one-time point may revert to a low proneural gene expression state shortly thereafter. These oscillations of Notch signalling in progenitors of the nervous system is analogous but not identical to the waves of Notch activity seen during somite formation[152]. Oscillations in Notch components may further alter the ability of NSCs to respond to external differentiation cues and be critical for regulating NSC potential [153]. Notch1 has been proposed to play a role in the maintenance of actively dividing NSCs in the adult neurogenic niche[154-158]. In the SVZ of the lateral ventricle wall and dentate gyrus (DG) of adult mice Notch activity promotes NSC survival, maintenance and stem cell self-renewal in the SVZ [154,155,157,159-161]. However, both the preservation and the transition from a quiescent NSC state to an activated state appears to be RBP-J dependent[75,156,158,160].

Great efforts have been made over the years to identify molecular markers that discriminate populations of niche astrocytes from quiescent and activated NSCs [162,163]. Epidermal growth factor receptors have been associated with active SVZ NSCs that maintain astrocytic (BLBP) and glial (GFAP) markers[158,162]. A horizontal, non-radial cell morphology identifies a population of actively dividing progenitors in the adult DG[161]. However, there is also a population of quiescent horizontal DG NSCs that currently cannot be discerned based on molecular marker alone[161,164]. New genetic tools will need to be generated and markers identified that allow for independent and simultaneous lineage tracing of these two NSC populations. For an in depth analysis of the role of Notch in quiescence and active NSC populations see Giachino and Taylor, 2014[165].

In the SVZ niche, NSCs receive inductive cues directing them to specific fates and restrictive signals, which limit their potential and prevent differentiation[166]. Some of these inductive cues most likely work in tandem with Notch[167]. Non-canonical activation of Notch through pigment epithelium–derived factor (PEDF) secreted by vascular endothelial cells within the adult lateral ventricle SVZ can bias cell fate towards RGC-like states. By activating NF-κB, PEDF exports nuclear receptor co-repressor (NCoR) which acts as a transcriptional inhibitor of the Notch target genes *Hes1* and of *Egfr*, allowing for NSCs to undergo asymmetric, self-renewing divisions [168]. Other inductive cues include hypoxia-inducible factor 1α (HIF1α), which under hypoxic conditions is stabilized and cooperates with Notch signalling to promote expression of target genes by NSCs[169,170].
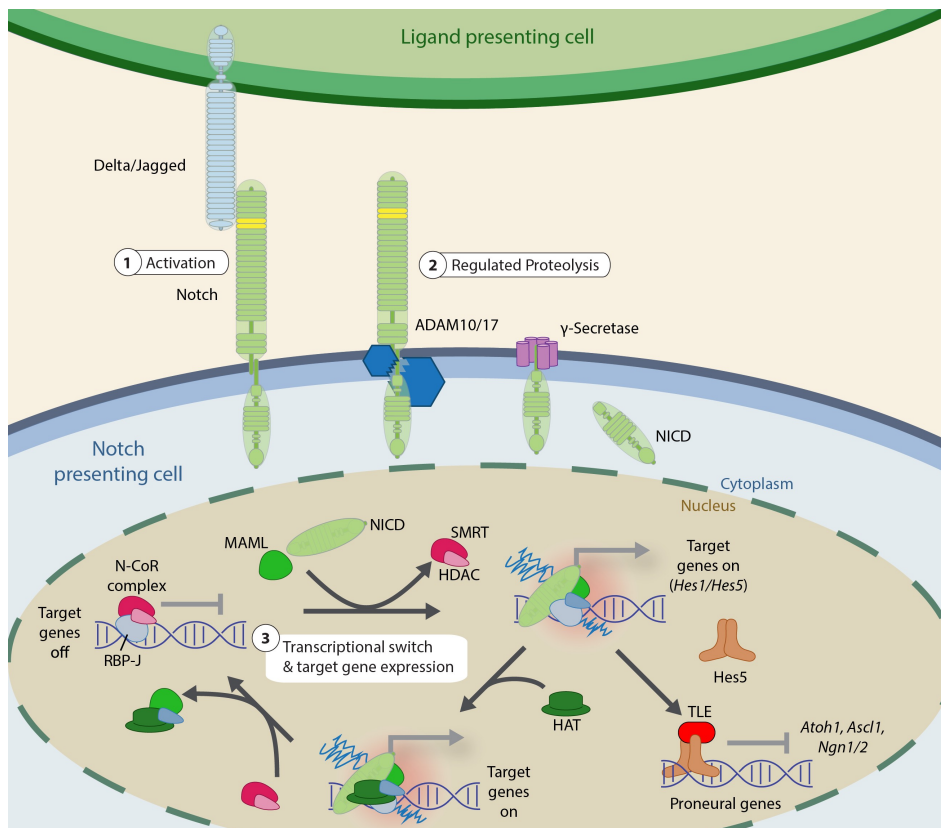
Figure 8'. Canonical Notch receptor signaling in the control of neurogenesis.
Notch receptors and their ligands are type 1 transmembrane proteins. Notch receptor activation is triggered when either Delta or Jagged presented by neighboring cells binds to the ectodomain resulting in regulated intramembrane proteolysis (RIP) in which first a disintegrin and metalloprotease (ADAM10 or 17), and then Presenilin containing gamma secretase cleave the receptor releasing a soluble intracellular domain (NICD). The NICD translocates to the nucleus where it interacts with the CSL (CBF1, Su(H), and Lag1 – RBP-J in mice) protein complex including the DNA binding protein recombining binding protein suppressor of hairless (RBP-J). The binding of NICD releases the nuclear receptor co-repressor complex (N-CoR), which includes silencing mediator of retinoid and thyroid receptors (SMRT) and histone deacetylases (HDACs). The NICD-bound CSL complex is a positive regulator of Notch target genes including *Hes1* and *Hes5*. Hes5 is a basic-helix-loop-helix (bHLH) transcription factor that, together with a zinc finger protein of the transducing-like enhancer of split (TLE) family, represses the proneural genes (*Atoh1*, *Ascl1* and *Ngn1/2*) in NSCs and thereby inhibits neuronal differentiation. The NICD complex also interacts with histone acetyltransferase (HATs) leading to epigenetic marking of target genes and transcriptional activation (Modified from Beattie and Mukhtar, 2015)[9].

Wnt signalling

Wnt signalling is involved in the patterning and development of many tissues including the nervous system[171,172]. Wnt1 and Wnt-3a are expressed by cells at the dorsal midline of the developing neural tube. In the absence of Wnt1, midbrain structures fail to form and Wnt3a mutant mice do not form a hippocampus likely due to the reduced proliferation of hippocampal precursors[173]. Wnt ligands bind the receptor complex

Frizzled/LRP5/6 leading to stabilization of cytoplasmic *b*-catenin. *b*-catenin translocates to the nucleus and binds to target genes via LEF/TCF factors and recruits Histone acetyltransferases[174]. Transgenic overexpression of *b*-catenin induces enhanced proliferation of cortical neural progenitors leading to an increase in cortical neurons and surface area[173]. During early neurogenesis, Wnts play an active role in symmetric divisions while later, during neurogenesis, Wnts are implicated in neuronal differentiation through expression of N-myc, which in turn represses the Notch signalling[172]. Wnt signalling can also induce the expression of Ngn1 and NeuroD1 thereby counteracting Notch signalling and promoting neuronal differentiation[114,172]. Thus, Wnt and Notch compete to regulate proneural gene expression and the maintenance and differentiation of NSCs. The differential dynamics of signalling pathways impinging on same or different downstream effectors could be cell-type or phase specific.

Fibroblast growth factor (Fgf) signalling

Fgf signalling has been long known to be involved in area specification in the brain[175]. Many Fgfs are expressed in the developing cerebral cortex. Fgf3, 8, 15, 17 and 18 are expressed along the rostral midline of the neocortex in the commissural plate between E9.5 and E12.5, suggesting the presence of a rostral, Fgf-secreting signalling center[176]. Fgf signals play important roles in anterior-posterior patterning of NSCs and promotes proliferation[177,178]. In addition, Fgf signalling can regulate *Hes1* transcription thereby synergizing with and promoting Notch signalling. Fgf18 is expressed in the cortical plate between E13.5-E16.5 although its role remains unclear[178]. Three of the classical receptor tyrosine kinase Fgf receptors (Fgfr1-3) are expressed by NSCs[177,179]. Fgfr1 is expressed higher by rostral NSCs than caudal NSCs, whereas Fgfr2 and Fgfr3 are expressed higher caudally than rostrally[180]. In mice, loss of Fgfr1 function results in the loss of rostral identity, indicating that Fgf1 acts as a secreted rostral morphogen. Conversely, Fgf2 is expressed higher in the dorsal forebrain than in the ventral, thus contributing to the dorsoventral patterning of the developing brain[178]. Loss-of-function of Fgf2 changes dorsal cortex specification[178]. Pea3-ETS transcription factors are downstream of the Fgf signalling pathway and ectopic expression of Fgf18 induces their expression with phenotypic changes in neuronal migration[179]. Pea3-ETS transcription factors are expressed in gradients high rostral to low caudally implying a role in axial patterning in the cerebral cortex[181].

Transforming growth factor-β (TGF-β)/Bone Morphogenetic protein (BMP) signaling

TGF-β/BMP are expressed in the dorsal cerebral cortex during embryonic neurogenesis and regulate proliferation, survival, differentiation and migration in the cerebral cortex[182]. BMP binds to the BMP receptor (BMPR1) on the cell surface and induces phosphorylation of Smad family transcription factors[183]. BMP signaling inhibits neuronal differentiation and promotes glial differentiation during corticogenesis[184]. BMP and Notch may converge on some cellular processes for example, they could impinge on some similar targets such as Hes3 and Inhibitor of DNA binding factor genes (Ids), as observed during adult neurogenesis[76].

Retinoic acid (RA)

RA is a derivative of Vitamin A, is involved in neuronal differentiation[185,186]. RA binds nuclear receptors of the Retinoic acid receptor family (RARs *a*, *b* and *g*) that regulate the expression of target genes that contain a retinoic acid response element[185]. RA interaction with the RAR bound as a repressor complex to target genes, releases co-repressor proteins and recruits Histone acetyltransferases[187]. However, RA can also induce rapid and transient activation of a cascade of kinases including the MAPK and Erk pathways which contribute to co-regulation of the RAR target genes by phosphorylation of cofactors and Histones[187,188]. Dietary depletion of Vitamin A in pregnant mothers' results in embryonic defects, including delayed development and reduced cortical hemispheres, with a reduction in Neuron specific class III *b* tubulin (*b*-TubulinIII) expression and lower levels of Harvey rat sarcoma viral oncogene (HRas) protein in the IZ and CP regions. The reduction in HRas levels is rescued by supplementing the embryos with RA indicating a stabilization of HRas by RA[189,190]. RA deficiency also affects neuronal migration to cortical layers V-III during development[191]. This impaired migration also results in neuronal fate switching to layer II neuron subtypes[191]. The RA pathway also cross-talks with Wnt signaling at the level of *b*-catenin[192]. The Wnt-RA axis is most prominent at the rostral end of the developing cerebral cortex, implying a potential role of RA in arealization of the forebrain[37].

Hippo signaling

Hippo signalling regulates size and homeostasis in many organs and tissues[193]. The Hippo signalling pathway is a cascade of kinases that converge onto the control of the transcriptional coregulators Yap and Taz[194]. The Hippo kinases and Yes-

associated protein/Transcriptional co-activator with PDZ-binding motif (Yap1/Taz) are regulated at different levels by different stimuli including G-protein coupled receptor signalling, cell adhesion, mechanical stress, and changes in cellular energy status[195]. The Hippo kinase cascade can be activated by activation of the Macrophage stimulating-1/2 (Mst1/2) and Large tumor suppressor-1/2 (Lats1/2) kinases. These serine/threonine kinases phosphorylate Yap1 and Taz. Phospho-Yap/Taz are targeted to degradation. If Lats1/2 are inactive, Yap/Taz are dephosphorylated and translocate to the nucleus where they interact with multiple transcriptional regulators[194]. Yap/Taz interact with *b*-catenin and Smads and thus co-regulate both the Wnt and TGF-*b* pathways to regulate gene expression[194]. The TEA domain transcription factors (Tead) are key targets and mediators of the Hippo pathway and critical effectors of Hippo regulated target gene expression[189,193]. In NSCs, the Hippo pathway plays a niche role and regulates the communication between neighboring cells. The expression of Fat tumor suppressor homologue (Fat4) and Dachsous (Dchs), the upstream receptor and ligand of the pathway, increases NSC proliferation and reduces differentiation[196]. However, the targets and the exact mechanism of the Hippo pathway in NSCs and cortical development remain unclear. Hence, future analysis of the Hippo pathway and its control of NSC maintenance, commitment and differentiation could uncover novel interactions and functions.

In summary, rather unsurprisingly, development of the brain and particularly the cerebral cortex incorporates many different signaling pathways. Due to the complexity of the cerebral cortex and the need for precise NSC proliferation, fate commitment and differentiation, the balance and interaction of these pathways will be critical. Hence, a deeper understanding of the signalling pathways and their underlying downstream mechanisms is required to develop a model of how NSCs integrate different signals to regulate development of the brain.

Chapter 2

Summary of Contributions for this part:

As part of my PhD, I focused on understanding the dynamics of Hippo signalling and its control in cortical development.

1. I performed all the *in vitro* and *in vivo* experiments for Hippo signalling project
2. I analyzed the data, for both *in vitro* and *in vivo* experiments.
3. I standardized the Chromatin Immunoprecipitation (ChIP) for Flag-tagged Tead1 and Tead2 in adherent NSCs.
4. I compiled the figures and wrote the manuscript.

Tead transcription factors differentially regulate cortical development through ApoE, Cyr61 and Dab2

Tanzila Mukhtar[1], Jeremie Breda[4], Zahra Karimadini[3], Marcelo Boareto[3], Pascal Grobecker[4], Alice Grison[1], Dagmar Iber[3], Christian Beisel[2], Erik van Nimwegen[4] and Verdon Taylor[1,5]

Affiliations:
[1] Department of Biomedicine, University of Basel, Mattenstrasse 28, CH-4058 Basel, Switzerland

[2] Quantitative Genomics Unit, D-BSSE, ETH Zürich, Mattenstrasse 26, CH-4058 Basel, Switzerland

[3] Computational Biology Group, D-BSSE, ETH Zürich, Mattenstrasse 26, CH-4058 Basel, Switzerland

[4] Biozentrum, University of Basel, Klingelbergstrasse 50-70, CH-4056 Basel, Switzerland

[5] Lead Contact

* Correspondence to: verdon.taylor@unibas.ch

Short Title: Hippo regulates brain development

Key Words: Brain development, neurogenesis, Hippo signalling

SUMMARY

The cerebral cortex of mammals is composed of billions of neurons with different morphologies and functions. Development of the cerebral cortex requires an orchestrated generation, migration, and positioning of specific neuron populations followed by gliogenesis. Through transcriptional profiling of neural stem cells (NSCs), progenitors and newborn neurons in the developing cerebral cortex, we identified developmental and cell-type specific dynamics in the expression of Hippo signalling components. We explored the functions of the transcriptional effectors of the Hippo pathway, the Tead transcription factors (TFs), in cortical stem and progenitor cells. Three of the four Tead TFs show distinct developmentally correlated expression patterns implying potential cell-type and stage specific functions. Tead2 expression is high during early phases of neural expansion whereas Tead1 and Tead3 are expressed highest during the gliogenesis phase. Although Teads have been reported to be functionally redundant in other systems, by gain- and loss-of-function, we found specific and reciprocal functions of the Teads in neuronal migration and fate determination in the developing cerebral cortex. Integrated System for Motif Activity Response Analysis (ISMARA) *in silico* and chromatin-immunoprecipitation (ChIP) revealed the *ApoE*, *Cyr61* and *Dab2* genes as direct targets of Teads in NSCs. We confirm Tead regulation of these targets *in vivo* and *in vitro*. We show that ApoE over expression partially recapitulates the Tead2 gain-of-function phenotype and that Dab2 over expression phenocopies Tead1 gain-of-function. *ApoE* and *Dab2* are key players in the Reelin signalling pathway which is known to control development of the cerebral cortex. Hence, our analysis provides a link between Hippo and Reelin signalling pathways in the control of mammalian cortical development.

INTRODUCTION

NSCs of the developing cerebral cortex form the ventricular zone (VZ) lining the lumen of the dorsal anterior neural tube[26,27,63]. These NSCs are the major source of the projecting neurons in the cerebral cortex[26,27,63]. The mechanisms controlling the patterning and cell fate specification of these stem cells during early brain development are not clearly understood. Various signalling pathways including Notch, Wnt, Shh, FGFs, TGF-*b*, Retinoic acid, Reelin and Hippo, impinge on and regulate NSC fate decisions to control proliferation, neurogenesis, and gliogenesis[26,27,63]. The crosstalk between the different signalling pathways and the integration of these signals on target genes governing complex cell fate choices is unclear.

Hippo signalling is evolutionarily conserved and a regulator of organ size control and tissue homeostasis (Supplementary Figure 1A)[193,194,197,198]. The pathway is regulated by numerous stimuli, including G-protein coupled receptor signalling, mechanical stress, cellular energy status, cell-cell contact, and cell-extra-cellular matrix interactions[193,194,197]. Hippo signalling employs a cascade of phosphorylation steps mediated by the kinases Mst1/2 and Lats1/2[197-199]. Lats1/2 phosphorylate the transcriptional coregulators Yap1 and Taz to promote cytoplasmic retention and subsequent degradation[193,194,197]. When Hippo signalling is inactive, Yap1/Taz translocate to the nucleus and form multiple complexes with different DNA binding partners including TEADs, SMADs, and Runx TFs[197-199]. The Tead transcription factors are major regulators of Hippo regulated target genes.

Fat4 and Dchs are receptor and ligand, respectively, of the Hippo pathway in embryonic NSCs. Activation of Fat4 results in increased proliferation in the developing nervous system and reduction of neuronal differentiation[196,200]. Mutations in *Fat4* and *Dchs* cause Van Maldergem syndrome in humans, an autosomal-recessive disorder characterized by intellectual disability, auditory, craniofacial, skeletal, limb and renal malformations[196]. In many cases Van Maldergem syndrome is associated with reduced cortical volume a partially penetrant periventricular neuronal heterotopias caused by mislocalized neurons in the periventricular area of the forebrain[200,201]. Therefore, Hippo signalling potentially plays a role in gyrification in higher vertebrates[201]. Manipulation of Fat4 and Dchs expression in the developing mouse cerebral cortex replicated some aspects of van Maldergem syndrome but the downstream molecular mechanisms are still not known[196].

Yap1^{-/-} mice developmentally arrest during mid-embryogenesis and die precluding analysis of Yap1 function in brain development[202,203]. Conditional gene ablation from the progenitors of the developing nervous system shows Yap1 to be necessary for

ependymal progenitor cell formation and *Yap1* conditional knockout mice develop hydrocephaly soon after birth[202,203]. Conversely, *Taz*^{-/-} mice are viable but develop renal cysts and lung defects[204]. Comparatively little is known about Taz functions in the developing brain. Gain-of-function experiments expressing Yap1 and Taz in NSCs implied that Tead2 is the mediator in their control of neural progenitor proliferation and neurogenesis[205]. *Tead1*^{-/-} and *Tead2*^{-/-} mice show severe growth retardation and morphological abnormalities including failure in dorsal neural tube closure as well as notochord and somite defects[206,207]. However, analysis also revealed partial redundancy in Tead1/2 functions during early development[206,207]. Although *Fat1*/*Fat4* double knockout mice show similar neural tube closure defects suggesting redundancy in these two Hippo pathway receptors, the downstream mechanisms causing these phenotypes are not understood[200].

In this study, we addressed the functions of the Hippo effectors, the Teads, in cortical development. We find that the expression of Hippo signalling components is highly dynamic during cortical development within the NSC, basal progenitor and neuronal lineage. Whereas in many systems Tead factors are redundant[206], they show specific temporal dynamics in their expression during cortical development. We show by gain and loss-of-function experiments that Tead1 and Tead3 are functionally similar but their effects on cortical development are opposite to that of Tead2. Using ISMARA, we predicted Tead targets and validated some of them as direct targets in NSCs by ChIP and expression analyses *in vivo*[208]. We show by gain-of-function that *ApoE*, *Cyr61* and *Dab2* convey some of the Tead-mediated mutant phenotypes we observed during cortical development. Thus, our data indicate multiple and specific roles of Hippo signalling effectors during cortical neurogenesis and provide a link between Hippo and the Reelin pathways.

RESULTS

Hippo signalling effectors are dynamically expressed during cortical development

Previously we addressed the changes in gene expression during formation of the dorsal cerebral cortex by next generation sequencing (Mukhtar *et al*. 2018). We isolated and FACSed NSCs, BPs and postmitotic newborn neurons from the dorsal cerebrum of *Hes5::GFP* and *Tbr2::GFP* embryos, at each day of development between embryonic day 10.5 (E10.5) and birth (PN) and performed RNA-seq analysis (Figure 1A) (Mukhtar *et al*. 2018)[138,209]. This time period covered the embryonic stages of cortex development from NSC expansion (E10.5- E11.5), through neurogenesis (E12.5- E16.5) to gliogenesis (E17.5-PN) (Figure 1B).

Analysis of the resulting transcriptomes revealed dynamic expression of Hippo signalling components during the three phases of corticogenesis (Figure 1C). The downstream effectors of Hippo signalling, the Tead TFs, showed distinct expression at the mRNA level indicative of potential specific functions. Tead1 and Tead2 expression were partially reciprocal in NSCs. While Tead1 expression increased from the expansion and neurogenic to the gliogenic phase, Tead2 expression was highest in expanding NSCs and reduced during late neurogenesis (Figure 1C). Tead3 expression remained relatively constant in NSCs during all phases from E10.5-PN and Tead4 mRNA was not detected at significant levels during cortical development (Figure 1C and not shown). In BPs, the expression of the Teads was also distinct. Tead1 and Tead3 were expressed at lower levels in BPs at early stages (E12.5 - E14.5) but increased dramatically in BPs of later stages (E15.5-PN). Conversely, Tead2 mRNA was expressed at high levels by BPs of all stages (Figure 1C). These findings suggest that Teads may have distinct temporal and cell-type specific functions during cortical development.

Similarly, the Tead coactivators Yap1 and Taz showed dynamic and partially reciprocal expression by cortical NSCs. Interestingly, Yap1 expression paralleled Tead2, reducing during late neurogenesis while Taz expression was more similar to that of Tead1, increasing during the gliogenic phase and in late stage BPs (Figure 1C). Thus, the expression profiles raised the interesting potential that Yap1 and Taz could use different Teads to transduce Hippo signals to target genes.

Hippo signalling can be activated by a variety of upstream receptors including Fat and Crb family members. NSCs expressed *Fat1* and *Crb2* with similar dynamics with lower expression during the neurogenic phase while *Fat2* and *Fat3* expression were higher

during the neurogenic compared to expansion and gliogenic phases (Figure 1C and Figure S1B). Hippo receptors also showed distinct dynamics in their expression in BPs and newborn neurons (Figure 1C and Figure S1C). *Fat1* was expressed highly by BPs and new neurons while *Crb2* was predominantly expressed by NSCs (Figure 1C and Figure S1B).

The Hippo ligands *Dchs1* and *CD44* also showed different dynamics in expression. *CD44* was expressed by NSCs but not BP or newborn neurons, conversely, *Dchs1* was expressed at high levels by all cell-types of the lineage (Figure 1C and Figure S1B). This indicated that Hippo signalling in the progenitors of the developing cortex is dynamic and may utilise different receptors and ligands to communicate between cells. Also, cells at different stages of the lineage and age of the mouse embryo could use different components to transduce Hippo signalling.

Yap1/Taz gain-of-function in NSCs affects cortical layering

In order to address the function of Hippo signalling in the generation of cortical neurons during development, we used *in utero* electroporation (IUE) of gain-of-function expression vectors to force expression of *Yap1* and *Taz* in NSCs *in vivo* (Figure 2A, B). Expression of Yap1 or Taz resulted in a cell-autonomous retention of the transfected cells (GFP$^+$) in the VZ compared to GFP expressing control cells (Figure S2A-C). The retention of cells in the VZ was associated with an increase in Pax6 expression by the transfected population in the VZ and SVZ (Figure S2B, C). In parallel, there was a reduction in the cells migrating to the cortical plate (CP) (Figure S2C).

We addressed whether the Yap1- and Taz-induced reduction in cells migrating to the CP was associated with a change in the expression of neuronal markers. Overexpression of Yap1 and Taz reduced the total number of deep layer Tbr1$^+$ neurons generated and their presence in the CP (12.3 ± 0.1% in the GFP control compared to 8.1 ± 1.7% in Yap1 and 8.3 ± 0.3% in Taz overexpressing animals (Figure 2C, D). Similarly, Yap1 and Taz overexpression reduced Ctip2$^+$ and Satb2$^+$ neurons in the CP. However, the total proportion of GFP$^+$ transfected cells that expressed Ctip2 was not changed, indicating a putative migration defect from the SVZ/IZ to the CP (Figure 2D, E). Interestingly, expression of Yap1 and Taz increased the proportion of transfected cells that expressed the upper layer neuronal marker Satb2 and their migration seemed also to be reduced due to accumulation in the SVZ/IZ (Figure S2E, F).

Together, these data suggest that Yap1 and Taz are involved in maintaining stem cell character and regulating differentiation. The reduction in lower layer neurons (Tbr1$^+$)

suggests that Yap1 and Taz can alter NSC fate choices. Our findings are similar to previous reports showing disruption of the migration of NSC progeny upon the overexpression of Yap1 and Taz[206,210,211].

Tead1, Tead2 and Tead3 TFs induce different effects on NSCs and cell migration

As Yap1 and Taz expression resulted in similar phenotypes, we addressed whether the Tead TFs are also functionally comparable. We performed IUE gain-of-function with Tead1, Tead2 and Tead3 expression vectors (Figure 3A). 48 hours after IUE at E13.5, *Tead1* and *Tead3* expression significantly increased retention of transfected cells in the VZ and reduced cells in the SVZ/IZ (Figure 3B-C). Tead1 and Tead3 overexpressing cells were proportionally increased in the CP compared to controls suggesting premature migration from the SVZ/IZ (24.4 ± 1.3% in Tead1 and 26.3 ± 0.75% in Tead3 overexpressing animals compared to 17.9 ± 0.6% in GFP control animals). Expression of *Tead2* also increase the number of transfected cells within the VZ but in contrast to *Tead1* and *Tead3* overexpression, Tead2 overexpression also increased the number of cells present in the SVZ/IZ (Figure 3B, C). *Tead2* overexpressing cells did not migrate to the CP. The differential distribution of cells in the gain-of-function experiments indicated that these three Tead TFs can convey unique functions and potentially mediate independent downstream mechanisms. Interestingly, only Tead3 overexpression had a significant effect on the expression of dorsal progenitor marker Pax6, increasing the total proportion of Pax6$^+$GFP$^+$ over total GFP$^+$ (41.2 ± 2.0%, over 30.6 ± 2.9% in GFP control) and increasing the number of Pax6$^+$ transfected cells in the VZ (Figure 3D).

Tead1, Tead2 and Tead3 TFs differentially affect neuronal fate

We analysed changes in the fate of the Tead overexpressing cells 48 hours after IUE. Tead1 and Tead3 expression significantly increased the total proportion of GFP$^+$ cells that differentiated into Tbr1$^+$ neurons (Figure S3A, B). This increase was significant in both the SVZ/IZ and CP (Figure S3A, B). However, Tead2 overexpression resulted in an almost complete block of Tbr1 neuron production (Figure S3A, B). Therefore, we analysed the expression of Ctip2, another deep layer neuronal marker, upon Tead overexpression. Although the total proportion of cells expressing Ctip2$^+$ was not changed, their proportion was significantly increased in the CP upon Tead1 and Tead3 expression (Figure S3C, D). Unlike the effects on Tbr1, Tead2 overexpression did not change differentiation to Ctip2$^+$ cells but there was a slight increase in the Ctip2$^+$ population in the SVZ/IZ and a dramatic reduction in the CP (Figure S3C, D).

In summary, Tead2 expression seemed to block Tbr1 fate acquisition but not Ctip2, but severely affected migration of all populations to the CP.

We addressed the expression of the upper layer neuronal marker Satb2. Overexpression of none of the Teads induce changes in the proportion of cells that adopted a Satb2 fate (Figure S3E, F). However, Tead2 overexpression resulted in a dramatic reduction in Satb2$^+$ cells in the CP, and like Tead1 and Tead3, Satb2$^+$ cells were increased in the SVZ/IZ (Figure S3E, F). Together, we observe that Tead1 and Tead3 overexpression show similar phenotypes while Tead2 induces reciprocal effects on cell distribution. The gain-of-function experimental results are summarized in Table 2. These observations highlight the array of phenotypes induced by Tead TF overexpression and indicate potentially different underlying molecular mechanisms. Interestingly, the Tead2 gain-of-function recapitulates the Yap1 overexpression phenotypes more closely than Tead1 or Tead3 and suggests a potential cooperation between Yap1 and Tead2 in cortical NSCs.

Dominant-negative DNA-binding mutant Tead TFs show reciprocal phenotypes in vivo

To further characterize and verify the potential different roles of Tead TFs in NSCs, we performed loss-of-function experiments by knockdown with 5 short hairpin RNA constructs against Tead1 and Tead2 mRNAs by IUE. We isolated the transfected cells from *in vivo* and performed RT-qPCR to test the efficiency of target knockdown. However, none of the constructs showed a significant knockdown in transfected cells (data not shown). To circumvent this and to still address the functions of the Teads, we generated dominant negative forms of Tead1, Tead2 and Tead3 by deletion of the DNA-binding domain as described previously[212,213]. Although these factors cannot bind DNA, they retain an intact Yap1/Taz binding domain (Figure 4A). We expressed the dominant-negative forms of the Teads in NSCs *in vivo* by IUE and examined the effects on cortical development 48 hours later. Tead1 and Tead3 dominant-negative (Tead1 DN and Tead3 DN) expressing cells failed to migrate to the CP (3.9 ± 0.9% in Tead1 DN, 8.8 ± 1.1% in Tead3 DN, compared to 17.9 ± 0.6% in GFP control: Figure 4B, C). This was accompanied by a significant increase in Tead1 DN and Tead3 DN expressing cells in the VZ (Figure 4B, C). In contrast, Tead2 DN expression increased cells in the CP (29.2 ± 1.7%) and in the VZ but resulted in a marked decrease in transfected cells in the SVZ/IZ (Figure 4B, C). The reciprocal phenotypes observed by overexpression of wild type and dominant-negative forms of the Teads strongly support the dominant negative strategy as a loss-of-function paradigm.

Tead DN TFs alter cell fate in vivo

We then examined the effects of the Tead DNs on cell fate. All of the Tead DNs induced an increase in the proportion of Pax6$^+$ cells compared to the GFP expressing controls (Figure 4B, D). These Pax6$^+$ cells were mainly in the VZ and, in the case of Tead2 DN, also in the SVZ/IZ (Figure 4B, D). Tead1 DN decreased the generation of Tbr1 cells (Supplementary figure 4A, B). Tead1 DN and Tead3 DN dramatically reduced the number of Tbr1$^+$ cells in the CP whereas the Tead2 DN increased both the total proportion of cells that expressed Tbr1 and their presence in the CP (Figure S4A, B). Interestingly, Tead3 DN slightly increased differentiation to Tbr1 expressing neurons but to a far lesser degree than Tead2 DN and many of these cells were retained in the SVZ/IZ (Figure S4B). Similarly, the effects of the Tead1 DN and Tead3 DN on Ctip2 expression were opposite to both their corresponding overexpression and Tead2 DN expression (Figure S4C, D compared to S3C, D). Tead1 DN and Tead3 DN induced a reduction in Ctip2 expressing cells in the CP (Figure S4C, D). Conversely, Tead2 DN increased Ctip2$^+$ cells in the CP with no change in the total proportion of cells adopting a Ctip2$^+$ fate (Supplementary figure 4C, D). A summary of the Tead DN data is shown in Table 3.

We then addressed potential effects of the Tead DNs on upper neuron fate. Tead1 DN and Tead3 DN expression decreased the number of Satb2$^+$ neurons in the CP without affecting the total proportion of cells that adopted a Satb2$^+$ cells (Figure S4E, F). This was accompanied by an increase in Satb2$^+$ cells in the SVZ/IZ suggesting that these cells had failed to migrate to the CP. Expression of Tead2 DN did not alter formation of Satb2$^+$ neurons (Figure S4E, F).

Transactive forms of Tead1 and Tead2 bind common targets

The gain and DN experiments indicated that Tead1 and Tead2 have distinct functions during cortical development. To address whether the different phenotypes induced by Tead1 and Tead2 manipulation is due to selectivity in their DNA-binding domains, we generated and tested transactive forms of Tead1 and Tead2. We expressed proteins where the DNA-binding domain of Tead1 or Tead2 was fused to the viral VP16 transactivation domain in neural progenitors by IUE at E13.5 (Figure 5A). These fusion proteins contain only the DNA-binding domain and not the other protein interaction domains of the Teads. Expression of Tead1 VP16 and Tead2 VP16 resulted in a reduction in cells migrating to the CP (7.7 ± 0.1% and 1.9 ± 0.6%, respectively) compared to the 17.9 ± 0.6% for the GFP control (Figure 5B, C). This was accompanied by a significant increase in total Pax6$^+$ cells in the Tead1 VP16 and Tead2 VP16 expressing embryos compared to controls (Figure 5B, D). The data are

summarised in Table 4. Thus, potential differences in the interaction of the Tead1 and Tead2 DNA-binding domains with target genes does not explain the differences in phenotype caused by Tead protein overexpression.

Tead1 and Tead2 TFs differentially regulate the same targets

ISMARA predicted the activity of the Tead binding motif in NSCs from E10.5 to PN (Figure 6A)[208,214]. Activity of the Tead motif is dynamic during cortical development being higher during the expansion phase of NSCs, reduced during neurogenesis, and increased during the gliogenesis phase. ISMARA predicted a number of genes that contribute majorly towards the Tead motive activity in NSCs during cortical development (Figure 6B). We validated some of the ISMARA-predicted Tead gene targets by chromatin immunoprecipitation (ChIP). We performed ChIP-PCR for Tead1 and Tead2 from adherent NSCs *in vitro*. In order to achieve comparable results, we expressed flag-tagged Tead1 or Tead2 in cortical NSCs and performed ChIP-PCR for the predicted target genes and Tead motifs (Figure 6C). *ApoE*, *Cyr61* and *Dab2* showed a significant enrichment in the Tead1 and Tead2 ChIP experiments (Figure 6D). Although expression of the Tead1-flag and Tead2-flag were comparable, *ApoE* promoter was twice as enriched in the Tead2 ChIP samples than in the Tead1. Together, *in silico* analysis predicted *ApoE*, *Cyr61* and *Dab2* as Tead TF targets and we could confirm that the promoters of these genes are bound by both Tead1 and Tead2.

In order to test the *in vivo* regulation of *ApoE*, *Cyr61* and *Dab2* by Tead1 and Tead2, we analysed regulation of their expression in NSCs *in vivo* following Tead1 and Tead2 expression. We expressed Tead1 or Tead2 by IUE and coexpressed GFP from the *Hes5* regulatory elements by co-transfection (Figure 6E). *Hes5::GFP* expression is restricted to VZ progenitors and inactive in BPs and neurons (Basak et al. 2007). 48 hours post IUE, we micro-dissected and sorted the *Hes5::GFP*+ cells by FACS, extracted RNA and performed qPCR for *ApoE*, *Cyr61* and *Dab2* (Figure 6E). Both Tead1 and Tead2 expression induced the expression of *ApoE*, *Cyr61* and *Dab2* in NSCs (Figure 6F). Interestingly, and in support of the ChIP data, Tead2 expression resulted in a greater induction in *ApoE* mRNA than Tead1.

ApoE, Cyr61 and Dab2 gain-of-function in NSCs partially recapitulate Tead gain-of-function phenotypes

We analyzed the expression profiles of *ApoE*, *Cyr61* and *Dab2* during cortical development (Figure 7A). *ApoE* is expressed predominantly by NSCs initially at lower levels during the expansion and neurogenesis periods and increases during

gliogenesis (Figure 7A). *Cyr61* is expressed by NSCs throughout cortical development (Figure 7A), whereas *Dab2* expression by NSCs reduces dramatically during neurogenesis and increases rapidly at the onset of gliogenesis at around E16.5 (Figure 7A). We analysed the effects of overexpression of ApoE, Cyr61 and Dab2 in NSCs by IUE during cortical development (Figure 7B). ApoE gain-of-function at E13.5 reduced cells migrating to the CP (12.3 ± 1.0%), compared to GFP control (17.9 ± 0.6%), with cells becoming trapped in the SVZ/IZ. These effects partially recapitulated the Tead2 gain-of-function phenotype we observed (Figure 7C). We did not observe phenotypic effects on the distribution of Cyr61 overexpressing cells except a slight decrease in cells in the SVZ/IZ (Figure 7C). Dab2 gain-of-function resulted in an increase in cells that had migrated to the CP (20.5 ± 0.4%), which partially recapitulated the gain-of-function of Tead1. Only ApoE overexpression resulted in a significant increase in Pax6$^+$ cells in the developing brain compared to the GFP controls (Supplementary 5A, B).

We addressed whether ApoE, Cyr61 or Dab2 overexpression changed the fate of NSCs during cortical development. Overexpression of Cyr61 and Dab2 resulted in an increase in Tbr1$^+$ neurons, particularly in the CP (Figure 7D, E). Conversely, ApoE overexpression did not change Tbr1 neuron production (Figure 7D, E). However, ApoE gain-of-function significantly increased Ctip2$^+$ cells in SVZ/IZ, as did Cyr61 and, to a lesser extent, Dab2 (Supplementary Figure 7C, D). Although ApoE, Cyr61 and Dab2 did not affect NSCs adopting a Satb2$^+$ fate, ApoE overexpression resulted in an increase in Satb2$^+$ cells in the CP and Dab2 in the SVZ/IZ, likely due to their effects on migration (Supplementary Figure 7E, F). Thus, ApoE gain-of-function partially recapitulated some of the Tead2 gain-of-function phenotypes and Dab2 gain-of-function recapitulated Tead1 induced phenotypic changes.

Tead2 preferentially binds the co-activator Yap1

In order to further characterize the potential molecular mechanism underlying the differential phenotypes of Tead1 and Tead2 gain-of-function, we tested potential differences in their binding to the co-activators Yap1 and Taz. Since Yap1 and Taz gain-of-function phenotypes were similar to Tead2 gain-of-function, we hypothesized that Yap1/Taz may function preferentially through Tead2. We transfected neuroblastoma cells (N2A) with flag-tagged Tead1 or Tead2 expression constructs together with either HA-tagged Yap1 or HA-tagged Taz expression constructs (Supplementary Figure 6A). Immunoprecipitation revealed Yap1 coprecipitated more efficiently with Tead2 than with Tead1 (Supplementary Figure 6B). Conversely, Taz was pulled-down equally well by both Tead1 and Tead2. These results suggest that

47

Yap1 preferentially binds Tead2 in a gain-of-function paradigm in N2As. This could explain the similarities in the effects seen in the Yap1 and Tead2 gain-of-function experiments *in vivo*.

DISCUSSION

Cerebral cortical development in mammals is a precisely controlled process. Although species-specific differences in the structure of the cerebral cortex are evident, the isocortex of the cerebral cortex is remarkably similar across mammals. Hence, we used mouse, taking advantage of the genetic tools and procedures, as a model to study and try to understand the mechanism controlling the formation of neurons that form the isocortex in the dorsal cerebral cortex. From comparative gene expression profiles study of temporal changes in mRNA expression by NSCs, BPs and NBNs, we identified dynamic expression of components of the Hippo signalling cascade.

Teads, Yap1 and Taz are key transcriptional effectors of the Hippo pathway. Tead TFs have extensively been explored during heart morphogenesis, vasculogenesis, muscle development, epithelial-to-mesenchymal transition, and in various cancers but little was known about their functions in the brain[193,212,213,215,216]. Here we show that Hippo effectors are major regulators of neurogenesis and play differential roles in the control of NSC differentiation during cerebral cortex formation. We demonstrate that Yap1 and Taz maintain stem cell characteristics in VZ progenitors and inhibit their differentiation when overexpressed. This is in line with previous observations examining gain-of Yap1 function in NSCs of the mouse neural tube showing that Yap1 expression induces Cyclin D1 (*Ccnd1*) expression, thus affecting cell proliferation[210,211]. We also show that Taz gain-of-function recapitulates the Yap1 phenotype indicating that Hippo co-activators may have similar downstream functions. Yap1 and Taz are known to interact with Tead TFs and the functions of the Teads as transcriptional regulators are regulated by their interactions with these co-activators[197,198,217,218].

Here we have shown that Tead TFs play differential roles in NSCs during corticogenesis, in gain and loss-of-function paradigms. In an attempt to understand how Tead TFs regulate cortical development, we identified novel targets of Tead TFs in NSCs which when expressed in cortical progenitors *in vivo* partially recapitulate aspects of the phenotypes observed following Tead TF expression. One key aspect of Hippo signalling is the regulation of migration of progenitors and immature neurons from the germinal zones of the VZ and SVZ to the   CP. One of the novel targets we

identified here, ApoE is a component of the Reelin signalling pathway, and is known as a critical regulator of migration of neuroblasts in the developing brain[219]. Though our manipulations focussed on one-time point between E13.5 and E15.5 which corresponds to the main period of neurogenesis, it is likely that Tead TFs may have additional roles or targets during other phases of expansion or gliogenesis.

Yap1, Tead2 gain recapitulates loss of Fat4 and Dchs1

In humans, bi-allelic mutations in Fat4 and Dchs1 cause Van Maldergem syndrome which is characterized by periventricular heterotopias. Fat4 and Dchs1 loss-of-function in mouse NSCs show some similarities to Van Maldergem syndrome[196,200]. These findings suggest that the function of Hippo signalling is conserved between mouse and human during brain development. We find that Yap1, Taz and Tead2 overexpression induce similar phenotypes to the loss of Fat4 and Dchs1. Yap1, Taz and Tead2 expression block migration of cells to the CP, and result in an increase in Pax6^{+} progenitors.

The receptors and ligands of the Hippo pathway Fat4 and Dchs1 negatively regulate the activity of downstream components and transcriptional activity of the pathway[197-199]. Hippo receptors regulate activity of the protein kinases *Mst1/2* and *Lats1/2*. These kinases are in complexes with regulatory proteins including *Sav1*, *Mob1a*, *Mob1b*, *Wwc1*, *Wwc2*, *Nf2*, *Ywhae*, *Cdc73*, *Amot*[220]. We find that these regulatory molecules also show dynamic expression in NSCs, BPs and NBNs throughout cortical development (Supplementary Figure 1).

When Hippo receptors are activated they promote Yap1 and Taz complex retention to the cytoplasm and degradation[197-199]. Conversely, when Hippo signalling is inactive, Yap1 and Taz escape degradation, stabilize and translocate to the nucleus where they interact with transcription factors including Teads. Hence, inactivation of Fat4 and Dchs1 inactivates Hippo signalling and results in stabilised Yap1 protein. This results in activation of downstream transcription pathway explaining the phenotypic similarities between gain of Yap1 and knockdown of Fat4 and Dchs1. Our results suggest that, during cortical development, Yap1 seems to preferentially work through Tead2 to regulate NSC maintenance and differentiation. It will be interesting in the future to address whether the Tead TF targets we identified by ISMARA in the developing cerebral cortex are miss-expressed in patients with Van Maldergem syndrome.

Differential expression of Hippo effectors in basal progenitors (BPs) and Newborn neurons (NBNs)

The Tead TFs are expressed at high levels in NSCs but also in other cell types in the embryonic neurogenic lineage including BPs and NBNs contributing and communicating with the NSC niche. Though the levels of their expression are higher in NSCs, we cannot rule out the possibility that the function of Tead genes in BPs and NBNs also contributes to the differential phenotypes we observe *in vivo* upon gain or loss-of-function. Considering the relatively lower levels of expression of the co-activators Yap1 and Taz in BPs and NBNs, these may be limiting factors in the transduction of the Hippo signal to the nucleus in these cells. This may also suggest that Teads, if active in BPs and NBNs, may not be active through the known and studied canonical Hippo signalling. It is interesting to speculate that in BPs and NBNs, Teads may function independent of Yap1 and Taz or may interact with other modulators and have other binding partners to control gene regulation. It would be interesting to explore the role of the Tead TFs in these other cell types and elucidate their interactomes and targets.

Teads target components of other signalling pathways

ApoE is expressed at lower levels during expansion and neurogenesis and increases during gliogenesis, which reaffirms its role in astrogliogenesis during later stages of corticogenesis[221]. *Dab2* is expressed at lower levels in NSCs throughout cortical development but increases when the stem cells enter the gliogenic phase. *ApoE* and *Dab2* are the components of Reelin signalling, which has long been studied to be critical for neuronal migration[222-225]. Based on the finding that Teads also have a migration phenotype and their regulation of Reelin effectors indicates a potential node of crosstalk between these two signalling pathways. Conversely, *Cyr61* is expressed relatively high throughout cortical development and its mRNA levels reduce slightly during neurogenesis. *Cyr61* is also a component of Integrin and canonical Wnt signalling, involved in neuronal migration[226]. It will be of interest in the future to address whether Hippo/Tead signalling act as a modulator and transistor to control the interface and outputs of different pathways (Reelin and Wnt and Integrin) to fine- tune cell fate during cortical development.

Future work will elucidate further mechanisms of these effectors in controlling cell plasticity during expansion and gliogenesis. In this paper, we report roles for canonical Hippo signalling intervention during corticogenesis. Components of the

pathway may be important in controlling brain size control and progenitor proliferation which has implications for targeting Hippo signalling in neurodegenerative disease.

STAR★METHODS

Detailed methods are provided in the online version of the paper and include the following:
- KEY RESOURCES TABLE
- CONTACT FOR REAGENTS AND RESOURCE SHARING
- EXPERIMENTAL MODELS AND SUBJECT DETAILS
  - Mice strain
- METHOD DETAILS
  - o Tissue preparation and fluorescence-assisted cell sorting (FACS)
  - o RNA isolation and RNA-sequencing
  - o In-utero electroporation for *in vivo* manipulation of NSCs and RNA isolation
  - o Tissue preparation and immunohistochemistry
  - o Adherent NSC culture and amaxa nucleofection *in vitro*
  - o Chromatin immunoprecipitation (ChIP)
  - o Neuroblastoma cell culture and immunoprecipitation (IP)
- QUANTIFICATION AND STATISTICAL ANALYSIS
- DATA AND SOFTWARE AVAILABILITY

STAR★METHODS

KEY RESOURCES TABLE

REAGENT OR RESOURCE		
Antibodies	**Source**	**Identifier**
Mouse anti-Beta-actin (1:2000)	Sigma	A5316 clone AC-74; RRID:AB_476743
Rat anti-Ctip2 (1:500)	Abcam	Cat# ab18465; RRID:AB_2064130
Rabbit anti-Flag (1:1000)	Sigma	Cat# F3165; RRID:AB_259529
Sheep anti-GFP (1:250)	AbD Serotec/Biorad	Cat# 4745-1051, RRID:AB_619712
Rabbit anti-HA tag (1:1000)	Cell Signalling	Cat# 3724, RRID:AB_1549585
Rabbit anti-Pax6 (1:500)	Covance	Cat# PRB-278P, RRID:AB_291612
Mouse anti-Satb2 (1:200)	Abcam	Cat# ab51502, RRID:AB_882455
Rabbit anti-Tbr1 (1:500)	Abcam	Cat# ab31940, RRID:AB_2200219

Donkey anti-Sheep, Alexa 488 (1:500)	Jackson ImmunoResearch Labs	Cat# 713-545-147, RRID:AB_2340745
Donkey anti-Rabbit, Cy3 (1:500)	Jackson ImmunoResearch Labs	Cat# 711-165-152, RRID:AB_2307443
Donkey anti-Mouse, Cy3 (1:500)	Jackson ImmunoResearch Labs	Cat# 715-165-151, RRID:AB_2315777
Continued		
Donkey anti-Rat, Cy3 (1:500)	Jackson ImmunoResearch Labs	Cat# 712-166-153, RRID:AB_2340669
Donkey anti-Mouse, HRP (1:10000)	Jackson ImmunoResearch Labs	Cat# 715-035-151, RRID:AB_2340771
Donkey anti-Rabbit, HRP (1:10000)	Jackson ImmunoResearch Labs	Cat# 711-035-152, RRID:AB_10015282
Chemicals	**Source**	**Identifier**
16% Formaldehyde Solution (w/v), methanol-free	Sigma	28908
DNase I, RNase-free	Sigma	04716728001
DNase I Grade II	Roche	10104159001
Glycine	Sigma	50046-1KG
L_Cysteine	Sigma	168149
Papain	Sigma	P3125-100MG
Trypsin inhibitor from Glycine max (soybean)	Sigma	T6522-5x100MG
L15 Medium	Invitrogen	31415029 (31415086)
PBS cell culture	Dulbecco	14080089 (14080048)
Transfectin	BioRad	1703351
cOmplete Proteinase inhibitor cocktail	Roche	11697498001
PMSF	Sigma	P7626 (78830)
SensiFast SYBR Kit	Bioline	BIO-02005
Trition X-100	Fisher	BPE151-500
TRIzol	Invitrogen	VX15596018
Dynabeads	Invitrogen	10765583
Glycoblue Co-precipitate	Life Technologies	D1417005
Bioscript, Reverse transcriptase	Bioline	BIO-27036-4
Transfectin Reagent	BioRad	1703352
Fastgreen	Sigma	F7252
P3 primary cell 4D-Nucleofector X kit 24 reactions	Lonza	LZ-V4XP-3024
Poly L- Lysine hydrobromide	Sigma	P9155-5MG
Laminin	Sigma	L2020-1MG
Phenol-chloroform isoamyl alcohol	Life Technologies	15593-031
B27 supplement+A26	Gibco	17504-044
Beta-mercaptoethanol	Sigma	M6250-100ML
DMEM/F12	Gibco	31966-047
DMEM (high glucose)	PAN Biotech	P04-04510
FBS	PAA	A15-101
Nitrocellulose membrane	Protan, GE	Z670995-1EA

Experimental models	Source	Identifier
Mouse: *Hes5::GFP*	Verdon Taylor (Basak *et al,* 2007)	N/A
Mouse: C57BL/6	Verdon Taylor	N/A
Neuroblastoma cells (N2A)	Verdon Taylor	N/A
Wt Neurospheres	Derived from C57Bl/6 embryos	N/A
Wt adherent neural stem cells	Derived from C57Bl/6 embryos	N/A
Recombinant DNA	**Source**	**Identifier**
pMYs-EGFP	Diepenbruck et al, 2014	N/A
pCMV-Flag-Tead1	This paper	N/A
pCMV-Flag-Tead2	Cat# RDB12171	RIKEN Bioresource
pCMV-Flag-Tead3	This paper	N/A
Continued		
pCMV-Flag-ApoE	This paper	N/A
pCMV-Flag-Cyr61	This paper	N/A
pCMV-Flag-Dab2	This paper	N/A
pMys-HA-Yap1-IRES-GFP	Diepenbruck et al, 2014	N/A
pMys-HA-Taz-IRES-GFP	Diepenbruck et al, 2014	N/A
pMYs-HA-Tead2FL-IRES-EGFP	Cat# RDB12173	RIKEN Bioresource
pMYs-HA-Tead1-VP16-IRES-EGFP	Cat# RDB12172	RIKEN Bioresource
pMYs-HA-Tead2-VP16-IRES-EGFP	Cat# RDB12174	RIKEN Bioresource
pCMV-Flag-Tead1-Dominant negative	This paper	(nucleotide 579-1800)
pCMV-Flag-Tead2-Dominant negative	This paper	(nucleotide 420-1421)
pCMV-Flag-Tead3-Dominant negative	This paper	(nucleotide 441-1571)
pBluescript-*Hes5::GFP*	Basak *et al*, 2007	N/A
Oligonucleotides	**Source**	**Identifier**
ApoE_Forward_5'-CTGACAGGATGCCTAGCCG-3'	https://pga.mgh.harvard.edu/primerbank/	N/A
ApoE_Reverse_5'-CGCAGGTAATCCCAGAAGC-3'	https://pga.mgh.harvard.edu/primerbank/	N/A
ApoE_Forward_5'-GAGTTCGCTATCTCGGCACC-3'	This paper	N/A
ApoE_Reverse_5'-TGGAAAGCAGGACTTAGCCG-3'	This paper	N/A
ApoE_Forward_5'-CGCTCTTCCCAAAGGTCTGT-3'	This paper	N/A
ApoE_Reverse_5'-TGGAAAGCAGGACTTAGCCG-3'	This paper	N/A
ApoE_Forward_5'-CGCTGCCAAAAATTCCAGCT-3'	This paper	N/A

ApoE_Forward_5'-GTACCACTTCGCAGGGATGG-3'	This paper	N/A
ApoE_Reverse_Xba1_5'-ATCTCTAGATCATTGATTCTCCTGGGCCAC-3'	This paper	N/A
Beta-actin_Forward_5'-AGGTGACAGCATTGCTTCTG-3'	This paper	N/A
Beta-actin_Reverse_5'-GGGAGACCAAAGCCTTCATA-3'	This paper	N/A
Cyr61_Forward_Not1_5'-TTCCGCGGCCGCATGAGCTCCAGCACCTTC-3	This paper	N/A
Cyr61_Reverse_Xba1_5'-CCCTCTAGATTAGTCCCTGAACTTGTGGAT-3'	This paper	N/A
Dab2_Forward_5'-CCCCTGAACGGTGATACTGAT-3'	This paper	N/A
Dab2_Reverse_5'-AAGTCCTGCTTTACGCCATTC-3'	This paper	N/A
Dab2_1_Forward_5'-TTGGAAGACTCGGCAGACAC-3'	This paper	N/A
Dab2_1_Reverse_5'-GGCCACTCCCGGTAGAGATA-3'	This paper	N/A
Dab2_2_Forward_5'-GGCGCTGGGGAAATCTTACA-3'	This paper	N/A
Dab2_2_Reverse_5'-CCTTGAGTCCGACCCCAAAG-3'	This paper	N/A
Dab2_Forward_Not1_5'-TCGGCGGCCGCATGTCTAACGAAGTAGAAA-3	This paper	N/A
Dab2_Reverse_Xba1_5'-CCATCTAGACTAGGCAAAAGGATTTCCGAA-3'	This paper	N/A
Gapdh_Forward_5'-CTCCCACTCTTCCACCTTCG-3'	This paper	N/A
Gapdh_Forward_5'-CCACCACCCTGTTGCTGTAG-3'	This paper	N/A
Tead1_Forward_5'-AAGCTGAAGGTAACAAGCATGG-3'	https://pga.mgh.harvard.edu/primerbank/	N/A
Tead1_Reverse_5'-GCTGACGTAGGCTCAAACCC-3'	https://pga.mgh.harvard.edu/primerbank/	N/A
Tead1_Forward_5'-CGCTCGCCAATGTGTGAATA-3'	https://pga.mgh.harvard.edu/primerbank/	N/A
Continued		
Tead1_Reverse_5'-AATACACAGGCCATGCAGAG-3'	https://pga.mgh.harvard.edu/primerbank/	N/A
Tead1_Forward_5'-TTCGAGAAATTCAAGCCGCC-3'	https://pga.mgh.harvard.edu/primerbank/	N/A
Tead1_Reverse_5'-GAGACGATCTGGGCTGATGA-3'	https://pga.mgh.harvard.edu/primerbank/	N/A
Tead1_Forward_5'-CCCTCAAAACGCCTTCTTCC-3'	https://pga.mgh.harvard.edu/primerbank/	N/A

Tead1_Reverse_5'-AACCTCGCATACTCCGTCTC-3'	https://pga.mgh.harvard.edu/primerbank/	N/A
Tead1_Forward_5'-GACATGCTTGGTTGAACTATCCT-3'	https://pga.mgh.harvard.edu/primerbank/	N/A
Tead1_Reverse-5'-GAGGGGTGATGTCTTCCTCC-3'	https://pga.mgh.harvard.edu/primerbank/	N/A
Tead2_Forward_5'-CCCTCCTTGCTCTTCTGGAA-3'	https://pga.mgh.harvard.edu/primerbank/	N/A
Tead2_Reverse_5'-CCACTTCACCCTACCCCAAG-3'	https://pga.mgh.harvard.edu/primerbank/	N/A
Tead2_Forward_5'-CCTGTCAGATGAGGGCAAGA-3'	https://pga.mgh.harvard.edu/primerbank/	N/A
Tead2_Reverse_5'-ACTTGGTCCTTCAGCTTGGA-3'	https://pga.mgh.harvard.edu/primerbank/	N/A
Tead2_Forward_5'-TCCACATCAGTCAGCAGTGT-3'	https://pga.mgh.harvard.edu/primerbank/	N/A
Tead2_Reverse_5'-ACTTGACGAGGAAGAAGGCA-3'	https://pga.mgh.harvard.edu/primerbank/	N/A
pCMV_Tead2_Forward_HindIII_5'-ACCCAAGCTTCCACCATGGAC-3'	This paper	N/A
pCMV_Tead2_Reverse_XbaI_5'-CGAGCATGCATCTAGAGGG-3'	This paper	N/A
pCMV_Tead2_Reverse_5'-ATCGTCTGGAAGGCCTTGTCCTTGGAGACTTGGTCC-3'	This paper	N/A
Tead2_DN_EcoRI_Forward_5'-TTCAGAATTCATGATTGCCCGTTACATCAA-3'	This paper	N/A
Tead2_DN XbaI_Reverse_5'-CCTGTCTAGACCTGAGTGTCCCTGTTTGT-3'	This paper	N/A
Tead2_DN_EcoRI_Forward_5'-TTCAGAATTCATGTCGAGAGAAATTCAGTCCAAG-3'	This paper	N/A
Tead1_DN_Not1_Forward_5'-TATTCACGCGGCCGCATGGAGCAGAGT-3'	This paper	N/A
Tead1_DN_Xba1_Reverse_5'-GCCGATTCTAGATGTAGATATGGTGCTGTG-3'	This paper	N/A
Tead1_Forward_5'-ACAAGGCCTTCCAGACGATG-3'	https://pga.mgh.harvard.edu/primerbank/	N/A
Tead1_Reverse_5'-TGTGAGAAGGGCTTCACGTC-3'	https://pga.mgh.harvard.edu/primerbank/	N/A
Tead1_transgene_Forward_5'-AAGCGGAGAATTCCACCAGG-3'	This paper	N/A
Continued		
Tead1_transgene_Reverse_5'-TCCTCACAAGACGTCAAGCC-3'	This paper	N/A

Tead2_transgene_Forward_5'-GCCTCTGACCTACCAGGGTA-3'	This paper	N/A
Tead2_transgene_Reverse_5'-TGCCTCTGGAACGAGTCAAC-3'	This paper	N/A
Tead3_Not1_Forward_5'-GATCGAGCGGCCGCCACTGTGCTGGAT-3'	This paper	N/A
Tead3_Xba1_Reverse-5'-TACATTTCTAGAGAGCTCGGATCCACT-3'	This paper	N/A
Tead3_DN_Not1_Forward_5'-TATCGAGCGGCCGCATGGCATCCATGTCG-3'	This paper	N/A
Yap1_Forward_5'-GCATGAGCAGCTACAGCATC-3'	https://pga.mgh.harvard.edu/primerbank/	
Yap1_Reverse_5'-CCAAGATTTCGGAACTCAGC-3'	https://pga.mgh.harvard.edu/primerbank/	
Yap1_Foward_5'-GGAGACACCATCAGCCAAAG 3'	https://pga.mgh.harvard.edu/primerbank/	
Yap1_Reverse_5'-ACTCCACGTCCAAGATTTCG 3'	https://pga.mgh.harvard.edu/primerbank/	
Resource	**Source**	**Identifier**
Fiji	Hosted by University of Wisconsin	https://imagej.net/Fiji Downloads
Photoshop	Adobe	N/A
Illustrator	Adobe	N/A
Prism 7	GraphPad Software, Inc	https://www.graphpad.com/scientific-software/prism/
R	R Core Team	https://www.r-project.org

CONTACT FOR REAGENT AND RESOURCE SHARING

Further information and requests for resources and reagents should be directed to and will be fulfilled by the Lead contact, Verdon Taylor (verdon.taylor@unibas.ch).

EXPERIMENTAL MODEL AND SUBJECT DETAILS

Wildtype (Wt) and *Hes::GFP (*Basak *et al,* 2007*)* transgenic line have been described previously. Mice were maintained on a 12-hr day-night cycle with free access to food and water under specific pathogen-free conditions and according to the Swiss federal regulations. All procedures were approved by the Basel Cantonal Veterinary Office (license number 2642).

METHOD DETAILS

Tissue preparation and fluorescence assisted cell sorting (FACS)

Dorsal cortices from embryonic day (E10.5) to postnatal day 1 (PN) were micro-dissected and dissociated into single cell suspensions using Papain and Ovo-mucoid mix (previously described by Giachino *et al*, 2009). Cells were washed with L15 medium and FAC-sorted for GFP positive NSCs using FACSarialII (BD Biosciences). For each time point, 3-4 biological replicates were generated.

RNA Isolation and RNA-sequencing

Total RNA was isolated from FAC-sorted GFP positive cells with *Hes5::GFP* transgenic line using TRIzol reagent. A time course was performed with neural stem cells isolated at each time point during development from E10.5 to postnatal day 1 (PN). Samples were submitted to Quantitative Genomics Facility, D-BSSE, ETH-Zurich analyzed for their integrity and concentration using Ribogreen assays and Fragment analyzer. cDNA libraries were prepared and samples were deep sequenced using the Biomark NGS platform.

In utero electroporation for *in vivo* manipulation of NSCs and RNA isolation

Pregnant C57Bl/6 mice at E13.5 were anaesthetized with isoflurane. Their uteri were exposed and DNA expression constructs were microinjected using Pneumatic Pico Pump, (WPI Rnage) and Borosilicate glass capillaries (Kwick-Fil; Hampton Research). The capillaries were pulled in a micropipette puller (Sutter Instrument Co.). The tips of the capillaries were sharpened using a capillary sharpener (Bachofer). The capillaries were loaded with $10 \propto l$ of the plasmid. Plasmid stocks were prepared using endotoxin-free conditions. Plasmids were dissolved in sterile water at high concentrations ($2\text{-}5 \propto g/\propto l$). A fast-green contrast dye was added to the plasmids, to visualize the area of injection in the lateral ventricle. The overexpression or dominant negative constructs were electroporated in a molecular ratio of 3:1, with transfection reporter vector (pMYs-IRES-GFP). Mice were secured on a heated pad to maintain a good body temperature, while being anaesthetized with 1-2% isoflurane (Baxter), along with a constant flow of O_2. A depilation cream was administered to remove the fur from the abdomen. Throughout the course of the procedure, the embryos and the peritoneal cavity was moistened with sterile HBSS to prevent drying. The uterine horn and the embryos were handled under sterile conditions, by hand and a cold light source was used to illuminate the developing embryos. We injected $1\text{-}2 \propto l$ of $2 \propto g/\propto l$ DNA solution, into the lateral

57

ventricles (LV) of each embryo. The embryos were electroporated (Electro Square Pavator, BTX, Harvard Apparatus) with five pulses of 50 V and a pulse length of 50ms at 950-ms intervals. The orientation of the electrodes directs the regions to be transfected. After the injections, the uteri are returned to the abdomen and the muscles, skin sutured. The females are allowed to recover under a heating lamp with constant observation. Postoperative analgesic (Temgesic) is administered. The animals were sacrificed after 48 hours by CO_2 inhalation. The embryos were isolated and brains dissected out. Positive brains were checked under Fluorescence microscope for GFP reporter and processed for tissue dissociation (as described above) and FACS or prepared for freezing and subsequent sectioning. Alternate positive samples were collected and dissociated as described above. Cells were sorted for GFP and RNA isolated from transfected cells. cDNA was prepared using Bioline Bioscript kit, followed by gene expression analysis using Bioline Sensifast SYBR.

Tissue preparation and immunohistochemistry

Positive brains isolated and fixed with 4% PFA in 0.1M phosphate buffer, then cryoprotected with 15% and 30% sucrose in phosphate buffer. Brains are embedded and frozen in OCT (TissueTEK) and sectioned 20∝m on slides (Superfrost glass slides, Thermo Scientific) by cryostat (Leica). Sections were dried at room temperature (RT) before antigen retrieval was performed with 1X Citrate buffer, at 80°C for 15 minutes. Sections were blocked with 5% Normal donkey serum with 0.01% Triton X-100 and 0.1M phosphate buffer for 2h at RT. Sections were incubated overnight at 4°C with primary antibody solutions made with blocking buffer. Sections were washed with phosphate buffer at RT and incubated with secondary antibody solutions with blocking buffer for 3h at RT. Sections were washed again as above and incubated with 1:1000 Dapi to stain the nuclei. The sections were rinsed once with phosphate buffer and dried at RT. Sections were mounted in mounting media containing diazabicyclo-octane (DABCO; Sigma) as an anti-fading agent and visualized using Zeiss Apotome 2 microscope.

Adherent NSC culture and amaxa nucleofection *in vitro*

Primary neural stem cells were isolated from E13.5 dorsal cortices and cultured in DMEM/F12 + Glutamax medium (with 2% B27 and 20 ng/∝l FGF2) as neurospheres (as described by Giachino *et al*, 2009). The tissue was dissociated as described above. On day 5 of culture, the neurospheres were plated on 100 ∝g/∝l Poly L-Lysine and 1 ∝g/∝l Laminin pre-coated sterile 6-well plates. The cue

was continued until confluency was reached and adherent NSCs were passaged and expanded.

Adherent NSCs were transfected with expression constructs following the Amaxa nucleofection kit instructions. Briefly NSCs were detached using trypsin for 5', followed by incubation with Ovo-mucoid mix. Cells were washed with sterile tissue culture grade phosphate buffer. We performed the nucleofections in 16-well strips and used phosphate buffer for transfections. Expression constructs: $7.5 \propto$g pCMV_Flag_Tead1; pCMV_Flag_Tead2 and pCMV_mCherry (control) were used for the nucleofections. The cells were kept in culture for 48h post transfection and collected for Chromatin Immunoprecipitation assays.

Chromatin immunoprecipitation (ChIP)

Transfected NSC were fixed with 1% PFA (Sigma) for 8' at RT. PFA is quenched with 125 mM Glycine and cells are washed with phosphate buffer with protease inhibitors and PMSF. Cells were lysed with cell lysis buffer and SDS-lysis buffer in two steps. Nuclei were sonicated using Diagenode Biorupter for 30s on and off cycles, 15 times. The supernatant was diluted with ChIP dilution buffer and used for IP using the $1 \propto$g of *a*-Flag antibody (Sigma, F3165). The ChIP protocol followed was the modified Millipore-Merck protocol. We used Protein-G dynabeads for the pulldown. Beads were washed with low salt, high salt, lithium chloride and TE buffer respectively. Fresh elution buffer was used to elute the DNA and reverse cross-linking overnight at 65°C in high salt conditions. The elutes were treated with proteinase K and RNase and purifies using phenol-chloroform iso-amyl alcohol (Invitrogen). From ISMARA, we obtained the putative binding sites of the Teads and we tested the IP elutes for pull-down, using primers directed against these sites. We tested the targets for few of the *in-silico* predicted Tead targets.

Neuroblastoma (N2A) cell culture and Immunoprecipitation (IP)

N2A cells were cultured in DMEM medium with high glucose, FBS and PenStrep. These cells were transfected with expression constructs at 60-70% confluency with Transfectin reagent (BioRad, 1703352).

Protein lysates were isolated after 48h and processed for IP using *a*-Flag antibody (Sigma, F3165). Dynabeads were used for the IP and proteins were eluted in Lämmli-buffer containing 2-mercaptoethanol, boiled for 10'. Protein samples were separated using 12% SDS-poly-acrylamide gels and transferred to Nitrocellulose membranes (Protan, GE). Primary antibody *a*-HA antibody (Cell Signalling, 3724) was incubated with the membrane overnight at 4°C. Secondary antibody *a*-Rabbit-

HRP (Jackson Immunoresearch Labs, 711-035-152) incubation was performed for 1h at RT. Detection was done by chemiluminescence (ECL, GE Healthcare).

QUANTIFICATION AND STATISTICAL ANALYSIS

Images taken by Zeiss Apotome 2 were processed with FIJI software. Contrast and image size of IF images were adjusted with Adobe photoshop. Expression profiles of genes of interest were produced in R. Bar graphs were generated by GraphPad Prism 7. All figures were made in Adobe Illustrator CS6.

Sample size is mentioned in the excel sheets for the quantifications. For FACS analysis, only the bright GFP positive cells were collected. For IF images, three fields of views were analyzed and quantified per sample. In IUE experiment analysis, the quantifications were also done over GFP positive cells, to analyze the cell autonomous effects. Unpaired t-tests were used for most studies. The cut-off value for statistical significance were indicated in corresponding figure legend.

DATA AND SOFTWARE AVAILABILITY

The RNA sequencing datasets have been deposited in Gene Expression Omnibus (GEO) with accession number GEO:
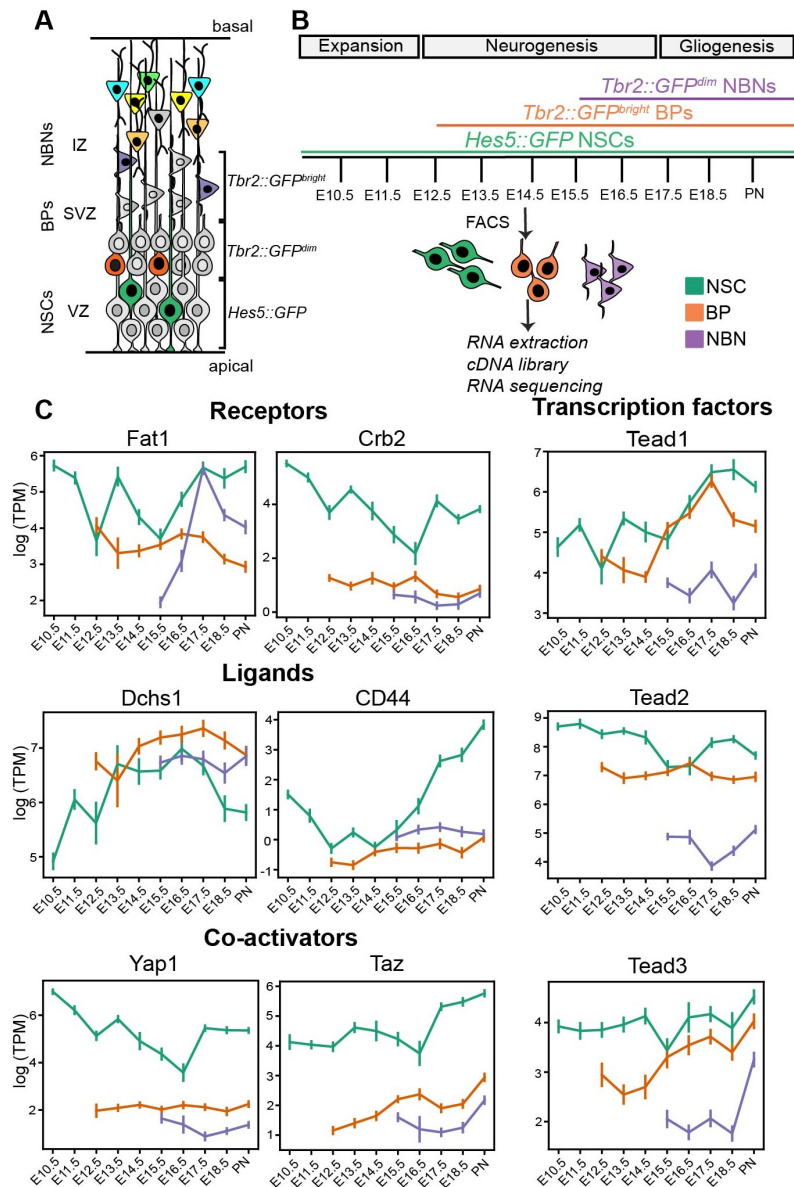
Figures:

Figure1: Transcriptional dynamics of Hippo effectors in NSCs, BPs, NBNs from RNA sequencing data.

A. Schematic representation of mouse developing cortex. NSCs reside in the VZ, with long processes extending from apical to basal surface. NSCs are labelled by *Hes5::GFP* transgenic line. BPs reside in the SVZ and are labelled by *Tbr2::GFP*dim population. NBNs are labelled by *Tbr2::GFP*bright population. B. Experimental paradigm used. 3-4 RNA samples extracted from FACSorted GFP+ NSCs, BPs and NBNs populations each day during development, from biological replicates, following the time-course (E10.5 to PN), through phases of expansion, neurogenesis and gliogenesis. cDNA libraries were prepared and Next-Generation RNA-sequencing performed. C. Expression profiles of Hippo signalling effectors; receptors Fat1 and Crb2, ligands Dchs1, CD44, co-activators Yap1, Taz, transcription factors Tead1, Tead2, Tead3 in NSCs, BPs and NBNs show dynamics during corticogenesis in these populations. Y-axis: mRNA level expressed as log2(Transcripts per million). NSCs-Neural stem cells, BPs- Basal progenitors, NBNs- Newborn neurons, VZ- Ventricular zone, SVZ- Subventricular zone, IZ- Intermediate zone, CP- Cortical plate.

Figure 2
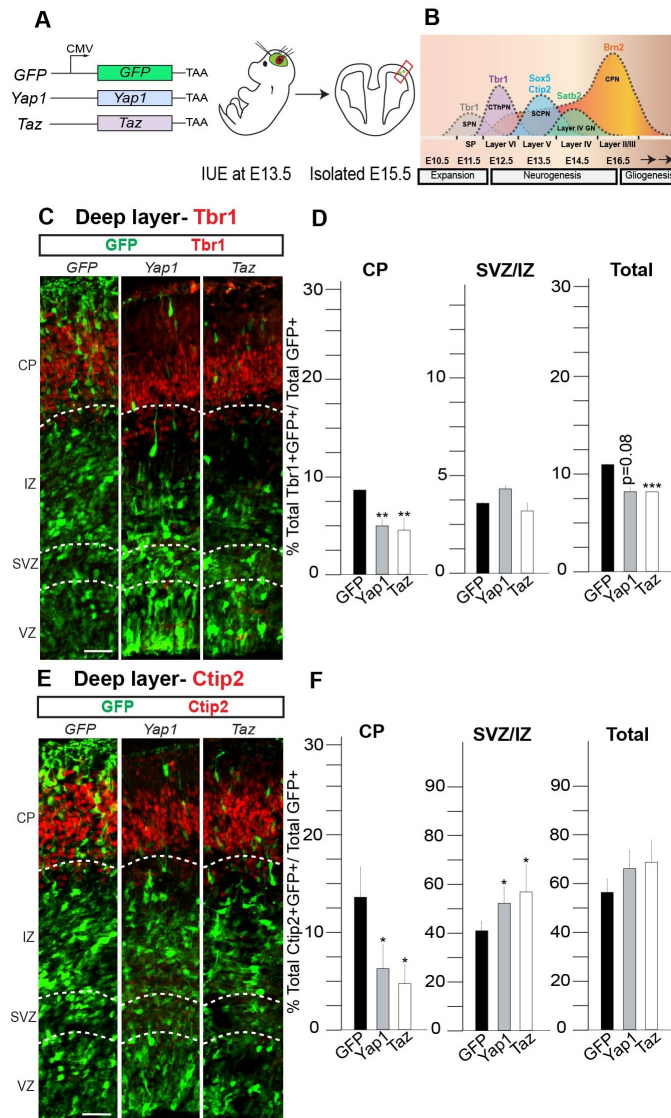**Yap1 and Taz gain of function affect cortical layering**

Figure 2: Gain-of-function of co-activators Yap1 and Taz affects cell fate, neuronal migration and cortical layering.

A. Experimental paradigm used to perform gain-of-function of Yap1 and Taz and empty GFP as a control. IUE were performed at E13.5 and brains isolated at E15.5, after 48h. B. Illustration to show the sequential generation of distinct types of cortical layers, specified by different TFs. The cortical development is divided in expansion, neurogenesis and gliogenesis. C. Coronal sections of transfected cortices immunostained for GFP and Tbr1, deep layer marker. D. Quantifications of Tbr1$^+$GFP$^+$ cells show a reduction upon gain-of-function of Yap1 and Taz, compared to GFP control in CP and total. E. Coronal sections of transfected cortices immunostained for GFP and Ctip2, deep layer marker. F. Quantifications of Ctip2$^+$GFP$^+$ cells show a reduction compared to GFP control in CP and no change in total, upon gain-of-function of Yap1 and Taz. SPN- Subplate neurons, CThPN- Corticothalamic projection neurons, SCPN- Subcerebral projection neurons, CPN- Callosal projection

neurons, IUE- in utero electroporations. Total- VZ+SVZ/IZ+CP. Scale bar = 50 ∝m. *p= 0.05, **p= 0.01, ***p=0.001, ****<p=0.0001. Summary for the quantifications are in Table 1 of the supplementary information.

62

Figure 3

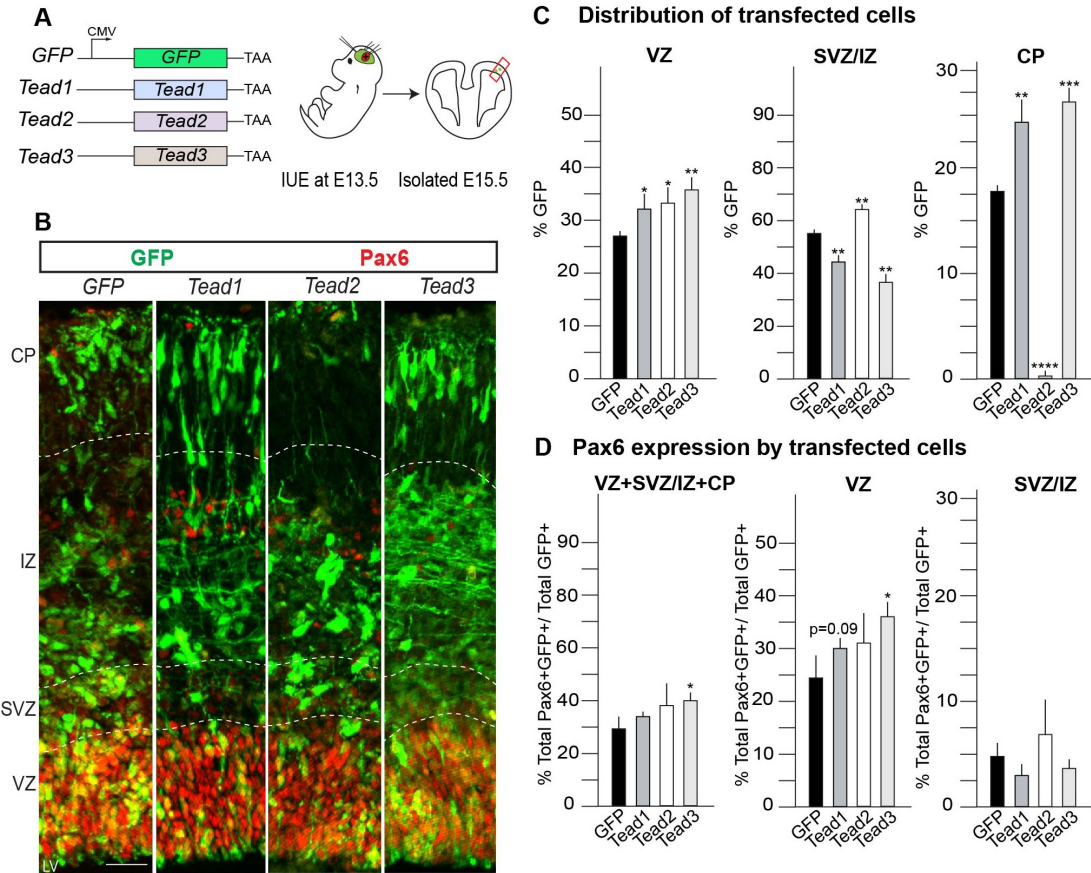## Gain of function of Tead1, Tead2, Tead3 affect cell fate and cortical layering

Figure 3: Gain-of-function of Tead1, Tead2, Tead3 affect cell fate, neuronal migration and cortical layering.

A. Experimental paradigm used to perform gain-of-function of Tead1, Tead2 and Tead3 and empty GFP as a control. IUE were performed at E13.5 and brains isolated at E15.5, after 48h. B. Coronal sections of transfected cortices immunostained for GFP and Pax6, NSC marker. C. Quantifications for distribution of GFP$^+$ transfected cells show Tead1 and Tead3 induce similar phenotypic changes in cell distribution while Tead2 gain-of-function shows an opposite phenotype. D. Quantifications for Pax6$^+$GFP$^+$ cells show an increase in total Pax6$^+$ cells upon gain-of-function of Tead3, compared to GFP control in VZ and total. Scale bar = 50 $\propto$m. *p= 0.05, **p= 0.01, ***p=0.001, ****<p=0.0001. Summary for the quantifications are in Table 2 of the supplementary information.

Figure 4

Dominant negative forms of Teads in NSCs show an opposite phenotype to the corresponding gain of function
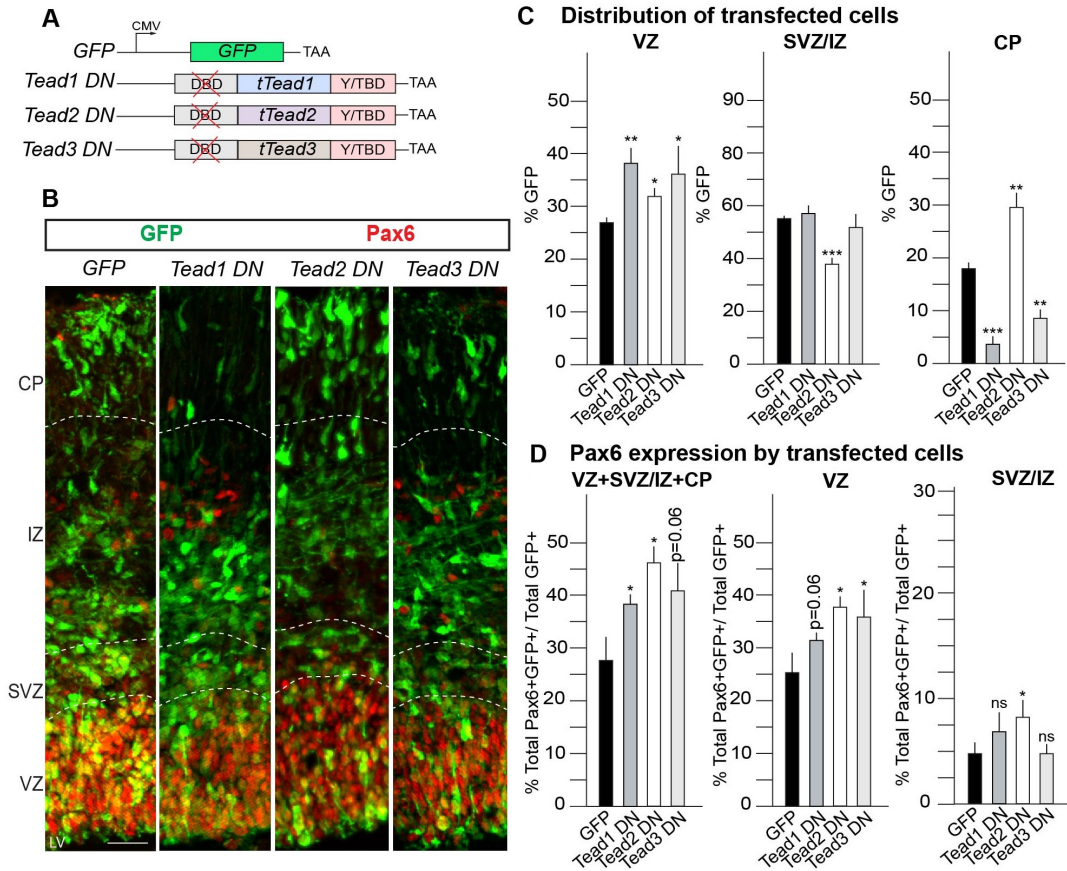

Figure 4: Dominant negative forms of Tead1, Tead2 and Tead3 show reciprocal phenotypes to their corresponding gain-of-function.

A. Experimental paradigm used to perform loss-of-function of Tead1, Tead2 and Tead3 and empty GFP as a control. DN constructs were cloned without the DNA-binding domains. IUE were performed at E13.5 and brains isolated at E15.5, after 48h. B. Coronal sections of transfected cortices immunostained for GFP and Pax6. C. Quantifications for distribution of GFP$^+$ transfected cells show Tead1 DN and Tead3 DN induce similar phenotypic changes in cell distribution while Tead2 DN shows an opposite phenotype. D. Quantifications for Pax6$^+$GFP$^+$ cells show an increase in total Pax6$^+$ upon Tead1 DN, Tead2 DN and Tead3 DN, compared to GFP control in VZ and total. DN- Dominant negative, tTead= Truncated Tead. Scale bar =

50 ∝m. *p= 0.05, **p= 0.01, ***p=0.001, ****<p=0.0001. Summary for the quantifications are in Table 3 of the supplementary information.

Figure 5

Transactive forms of Tead1 and Tead2 reduce differentiation
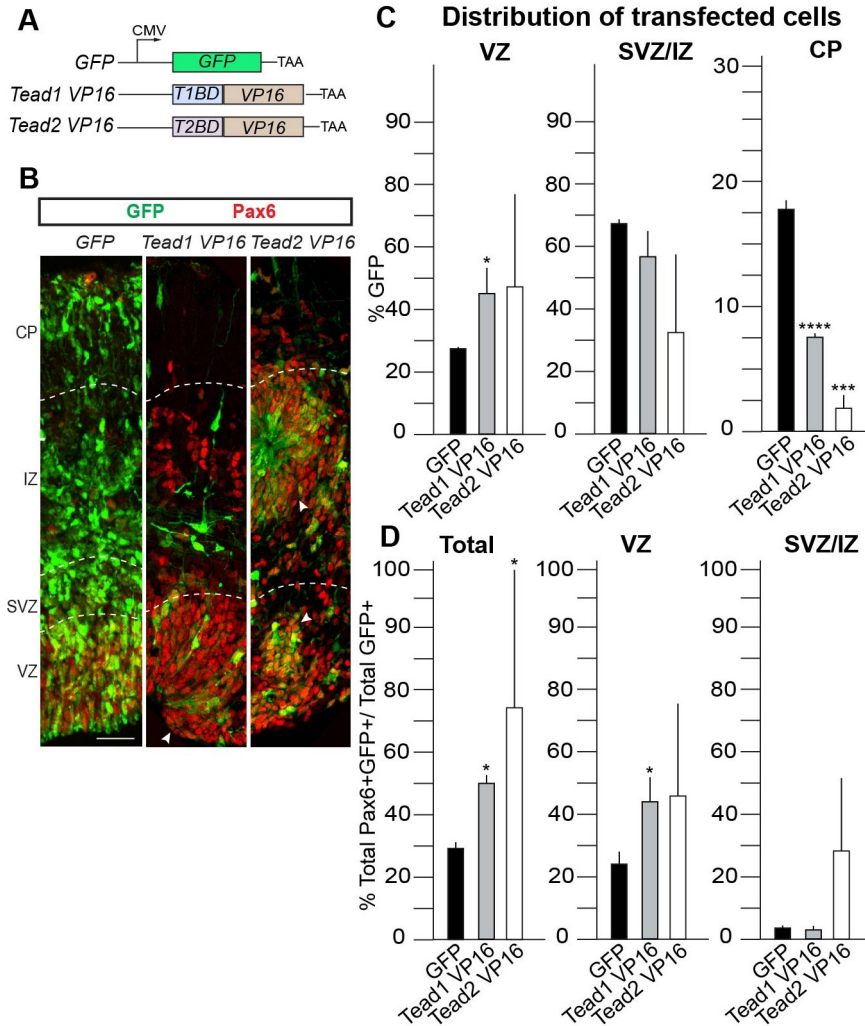
Figure 5: Transactive forms of Tead1 and Tead2 show similar phenotypic changes.
A. IUE with the transactive forms (with VP16 domain) of Tead1 and Tead2 were performed at E13.5 and brains isolated at E15.5, after 48h. B. Coronal sections of transfected cortices immunostained for GFP and Pax6. C. Quantifications for distribution of GFP+ transfected cells show Tead1 VP16 and Tead2 VP16 induce similar phenotypic changes in cell distribution. D. Quantifications for Pax6+GFP+ cells show an increase in total Pax6 positive cells upon Tead1 VP16, Tead2 VP16 compared to GFP control in all zones. Scale bar = 50 ∝m. *p= 0.05, **p= 0.01, ***p=0.001, ****<p=0.0001. Summary for the quantifications are in Table 4 of the supplementary information.

Figure 6

ISMARA in silico predicted Tead targets and their experimental validation
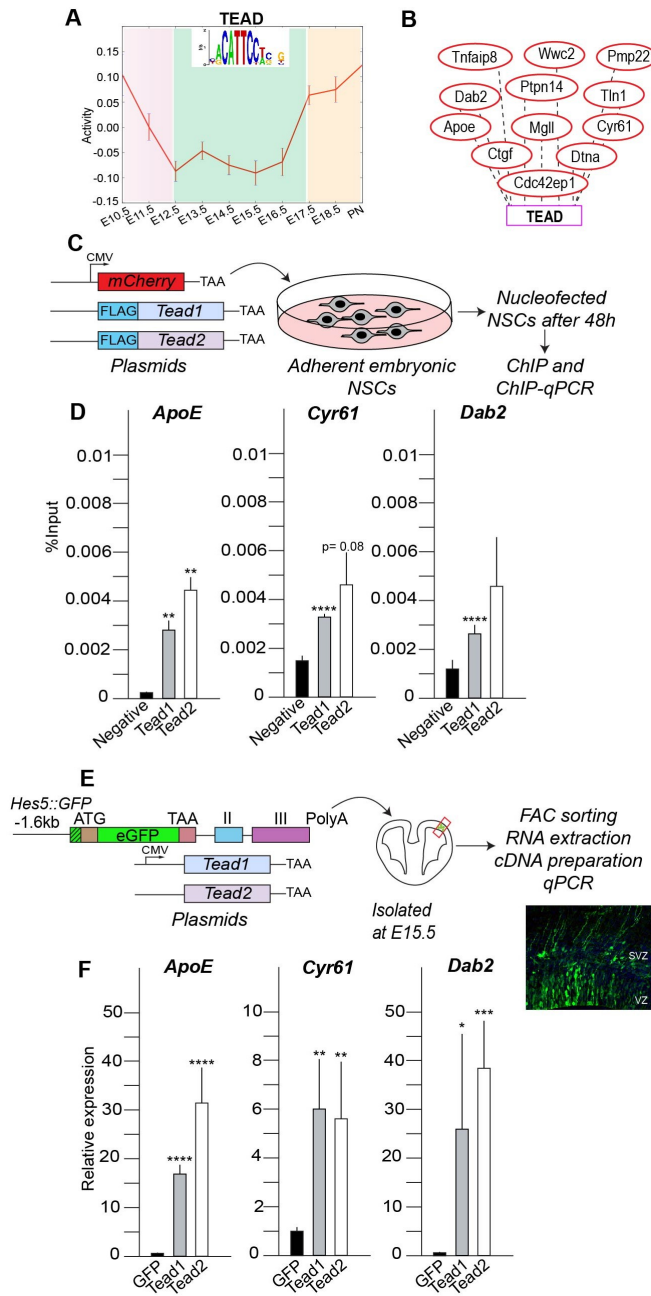
Figure 6: In silico predicted Tead targets by ISMARA and their experimental validation.
A. Activity of Tead binding motif in NSCs during expansion, neurogenesis and gliogenesis. B. Examples of *in silico* predicted targets of Tead. C. Chromatin Immunoprecipitation for flag tagged-Tead1 and Tead2, performed in adherent NSCs, 48h after nucleofection. D. ChIP-qPCR reproducibly pulls-down ApoE, Cyr61 and Dab2 with both Tead1 and Tead2. An empty mCherry vector was used as the negative control. E. IUE performed with co-transfection of *pBluescript-Hes5::GFP* plasmid, with Tead1 and Tead2 expression constructs, at E13.5. specifically expressed in NSCs in VZ and this approach allows to isolate only transfected NSCs after 48h. F. Relative expression of ApoE, Cyr61 and Dab2 show an induced expression upon gain-of-

66

function of both Tead1 and Tead2. Summary for the quantifications are in Table 5 of the supplementary information.

Figure 7

Tead targets recapitulate Tead gain of function phenotypes
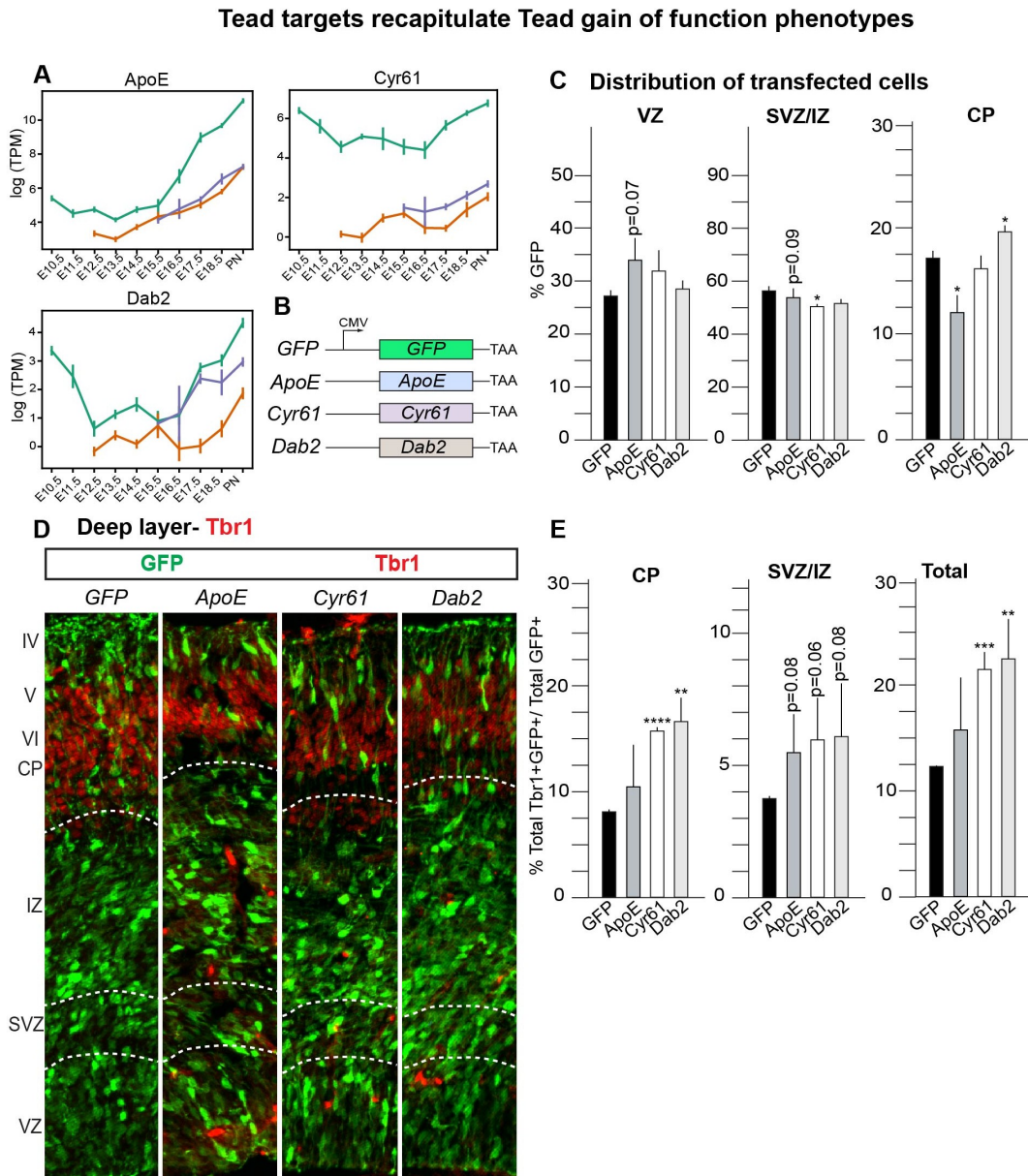
Figure 7: ApoE, Cyr61 and Dab2 gain-of-function recapitulate Tead gain-of-function phenotypic changes.
A. mRNA expression profiles of ApoE, Cyr61 and Dab2 in NSCs, BPs and NBNs. B. Expression constructs used for gain-of-function. C. Quantifications for distribution of GFP+ transfected cells show ApoE gain-of-function recapitulates Tead2 gain-of-function phenotype while Dab2 gain-of-function recapitulates Tead1 gain-of-function phenotype. D. Coronal sections of transfected cortices immunostained for GFP and Tbr1. D. Quantifications for Tbr1+GFP+ cells show an increase upon gain-of-function of Cyr61 and Dab2, compared to GFP control in CP and all zones. Scale bar = 50 ∝m. *p= 0.05, **p= 0.01, ***p=0.001, ****<p=0.0001. Summary for the quantifications are in Table 5 of the supplementary information.
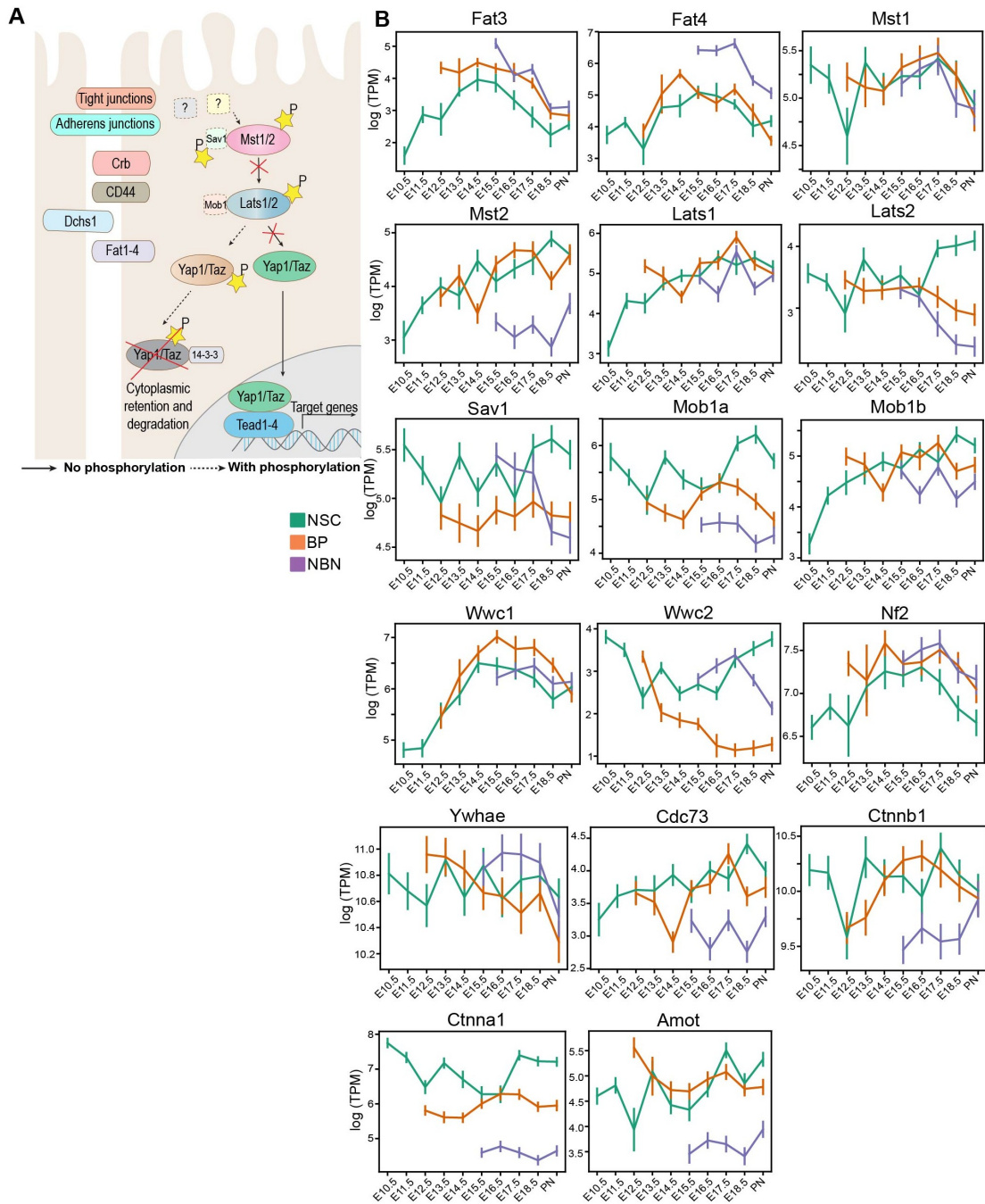
Supplementary Figure 1: Transcriptional Dynamics of additional Hippo signalling effectors in NSCs, BPs and NBNs from RNA sequencing.
A. Schematic representation of Hippo signalling cascade. Illustration depicts series of sequential phosphorylation steps for co-activators Yap1/Taz, mediated by Mst1/2 and Lats1/2 kinases. If Hippo signalling is on, Yap1/Taz is phosphorylated, retained in the cytoplasm and degraded. If Hippo signalling is off, Yap1/Taz escapes phosphorylation and translocates to the nucleus, where it binds its partner TFs, e.g. Teads, to regulate transcription. B. Expression profiles of intermediary effectors of Hippo signalling. Y-axis: mRNA level expressed as log2(Transcripts per million).
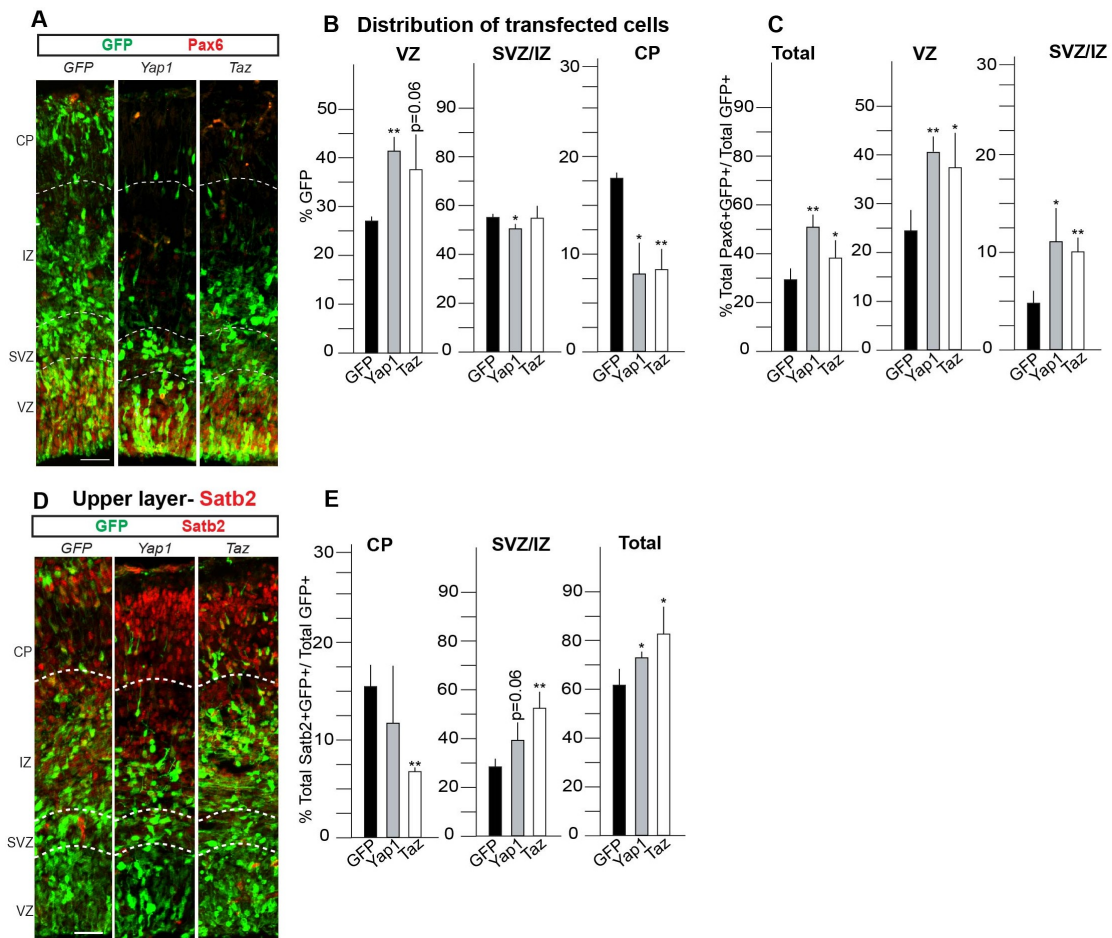
Supplementary Figure 2: Co-activators Yap1 and Taz gain-of-function increase percentage of NSCs and reduce differentiation.

A. Coronal sections of transfected cortices immunostained for GFP and Pax6. B. Quantifications for distribution of GFP$^+$ transfected cells show both Yap1 and Taz gain-of-function induce a similar phenotype. C. Quantifications for Pax6$^+$GFP$^+$ cells show an increase in total Pax6$^+$ cells upon Yap1 and Taz gain-of-function, compared to GFP control in VZ, SVZ and total. D. Coronal sections of transfected cortices immunostained for GFP and Satb2, shows an impaired migration of GFP$^+$ cells. E. Quantifications for distribution of GFP$^+$ transfected cells show both Yap1 and Taz gain-of-function increase total Satb2$^+$GFP$^+$ cells in all zones. Scale bar = 50 ∝m. *p= 0.05, **p= 0.01, ***p=0.001, ****<p=0.00001. Summary for the quantifications are in Table 3 of the supplementary information.
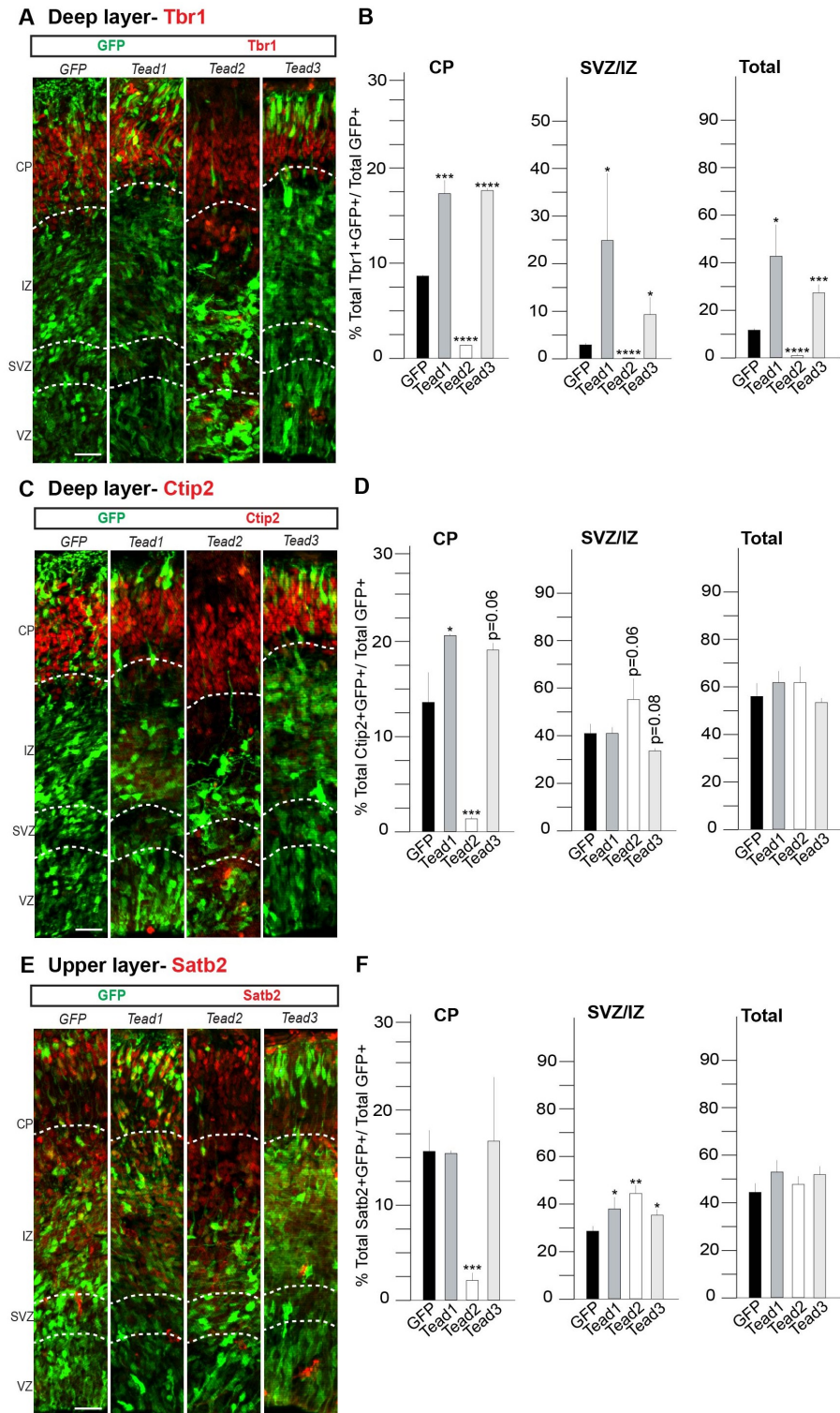
69

Supplementary Figure 3: Tead1, Tead2 and Tead3 gain-of-function affects cell fate and cortical layering

A. Coronal sections of transfected cortices immunostained for GFP and Tbr1. B. Quantifications for distribution of GFP$^+$ transfected cells show both Tead1 and Tead3 gain-of-function induce a similar phenotype, an increase of Tbr1$^+$GFP$^+$ cells in SVZ/IZ, CP and total. Tead2 gain-of-function shows an opposite phenotype to Tead1 and Tead3, with less Tbr1$^+$GFP$^+$ cells in 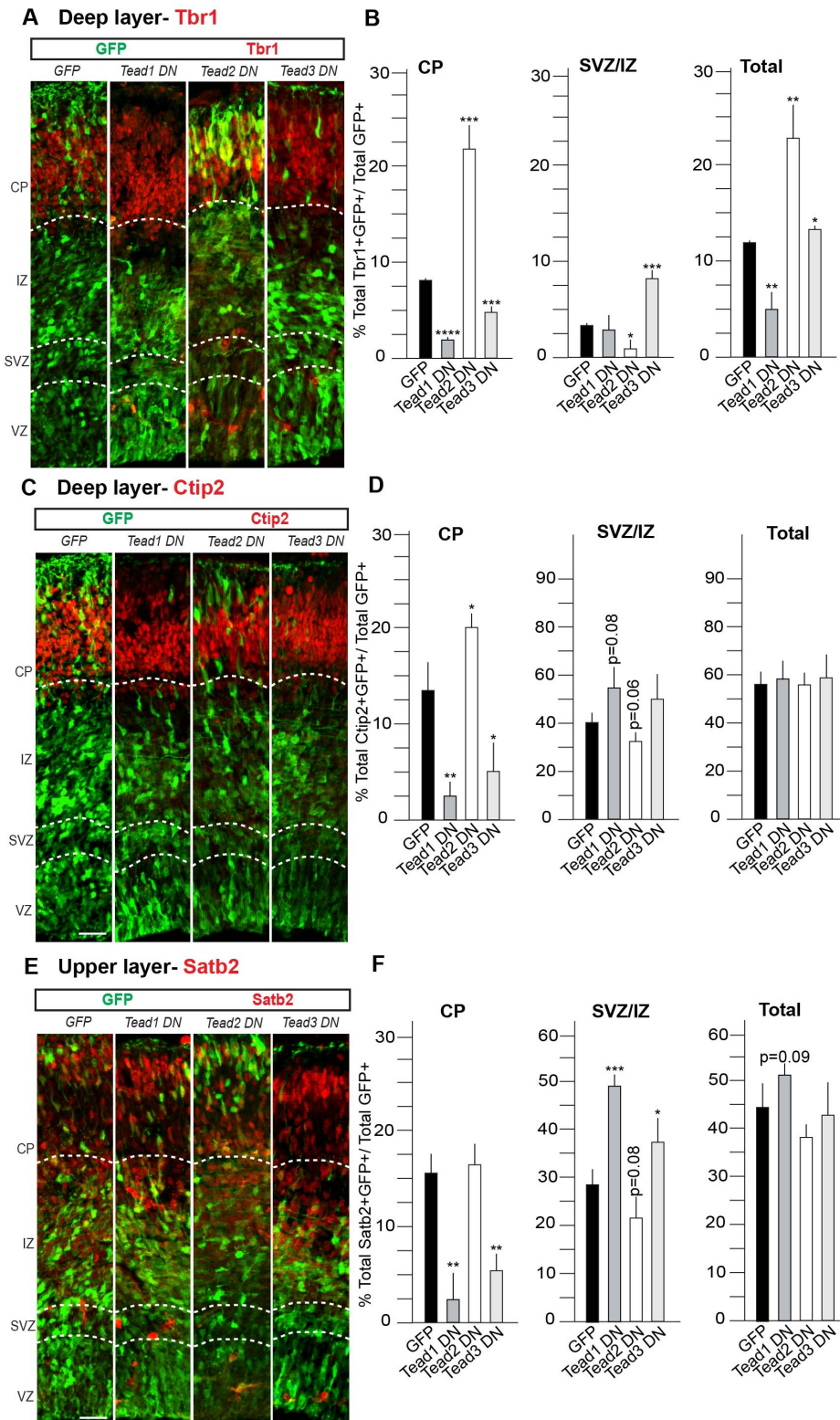the CP and also a significant decrease in total. C. Coronal sections of transfected cortices immunostained for GFP and Ctip2. D.

Quantifications for distribution of GFP$^+$ transfected cells show both Tead1 and Tead3 gain-of-function induce a similar phenotype, an increase of Ctip2$^+$GFP$^+$ cells in CP and no changes in total. E. Coronal sections of transfected cortices immunostained for GFP and Satb2. F. Quantifications for Satb2$^+$GFP$^+$ cells over total GFP$^+$ cells show a decrease in Satb2$^+$GFP$^+$ cells in CP upon Tead2 gain-of-function, compared to GFP control. Satb2$^+$GFP$^+$ cells remain unchanged upon gain-of-function of Tead1 and Tead3. Scale bar = 50 $\propto$m. *p= 0.05, **p= 0.01, ***p=0.001, ****<p=0.0001. Summary for the quantifications are in Table 3 of the supplementary information.

A Deep layer- Tbr1

B

C Deep layer- Ctip2

D

E Upper layer- Satb2

F

Supplementary Figure 4: Tead1 DN, Tead2 DN and Tead3 DN constructs affect cell fate and cortical layering

A. Coronal sections of transfected cortices immunostained for GFP and Tbr1. B. Quantifications for fate changes in deep layer Tbr1^{+} neurons, shows a decrease of Tbr1^{+}GFP^{+} cells in CP upon Tead1 DN and Tead3 DN transfection. This is opposite to the phenotype with Tead2 DN, with an increase of Tbr1^{+}GFP^{+} cells in CP. Similar changes are observed in total Tbr1^{+}GFP^{+} cells. C. Coronal sections of transfected

72

cortices immunostained for GFP and Ctip2. D. Quantifications for fate changes in deep layer Ctip2$^+$ neurons, shows a decrease of Ctip2$^+$GFP$^+$ cells in CP upon Tead1 DN and Tead3 DN transfection. This is opposite to the phenotype with Tead2 DN, with an increase of Ctip2$^+$GFP$^+$ cells in CP. The total cell numbers remain unchanged; hence the manipulations only affect the migration of Ctip2$^+$GFP$^+$ cells. E. Coronal sections of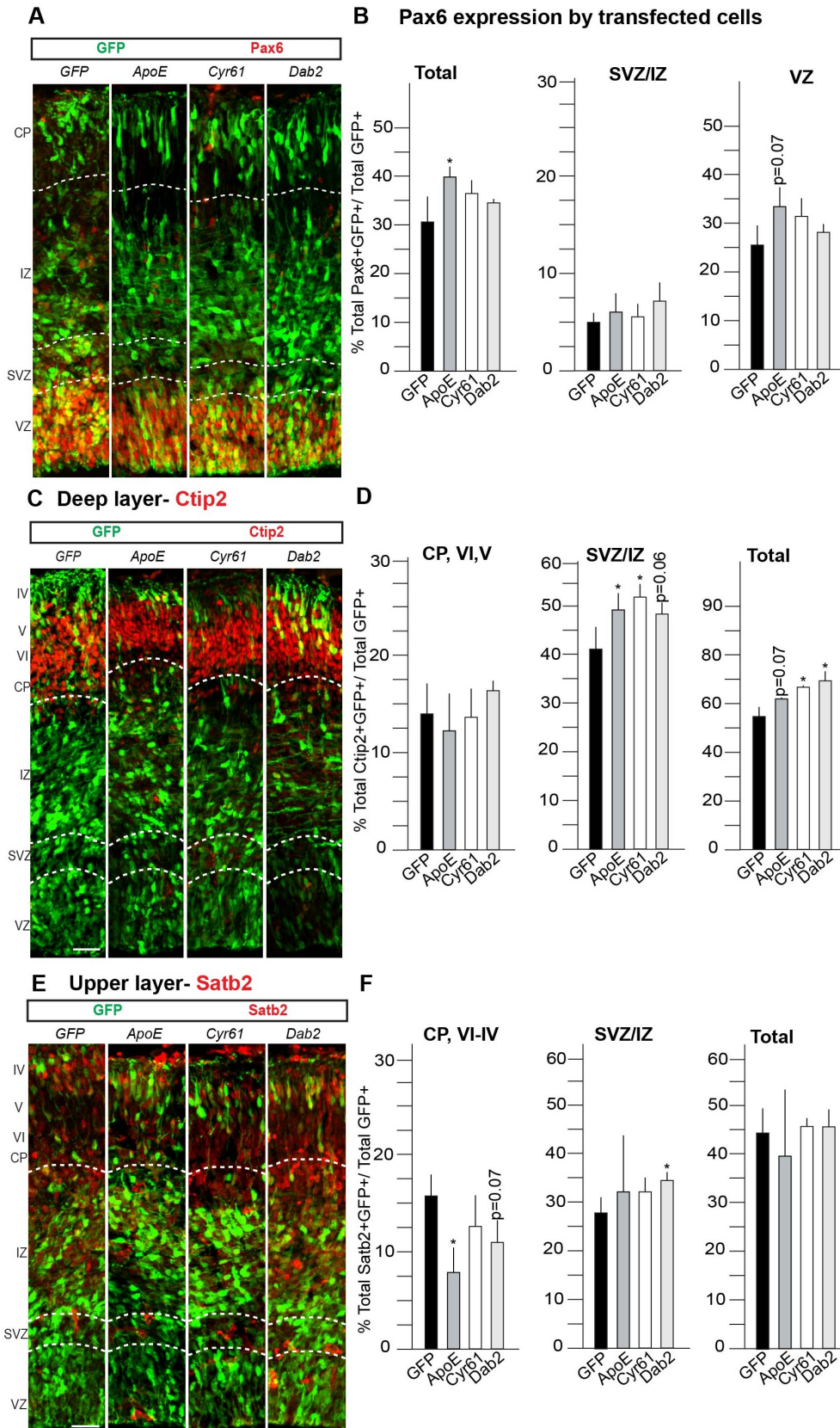 transfected cortices immunostained for GFP and Satb2. F. Quantifications for distribution of GFP$^+$ transfected cells show both Tead1 and Tead3 gain-of-function induce a similar phenotype, a decrease of Satb2$^+$GFP$^+$ cells in CP and no changes in total. Scale bar = 50 $\propto$m. *p= 0.05, **p= 0.01, ***p=0.001, ****<p=0.0001. Summary for the quantifications are in Table 4 of the supplementary information.

Supplementary Figure 5: Gain-of-function of ApoE, Cyr61 and Dab2 affects cell fate and cortical layering

A. Coronal sections of transfected cortices immunostained for GFP and Pax6. B. Quantifications for Pax6+GFP+ cells show an increase in total Pax6 positive cells upon ApoE gain-of-function. C. Coronal sections of transfected cortices immunostained for

GFP and Ctip2. D. Quantifications for fate changes in deep layer Ctip2$^+$ neurons, shows a slight increase of Ctip2$^+$GFP$^+$ cells in total upon Cyr61 and Dab2 gain-of-function. E. Coronal sections of transfected cortices immunostained for GFP and Satb2. F. Quantifications for distribution of GFP$^+$ transfected cells show ApoE gain-of-function decreased Satb2$^+$GFP$^+$ cells in CP and no changes in total. Dab2 gain-of-function increases the Satb2$^+$GFP$^+$ cells in SVZ/IZ. Scale bar = 50 $\propto$m. *p= 0.05, **p= 0.01, ***p=0.001, ****<p=0.0001. Summary for the quantifications are in Table 5 of the supplementary information.
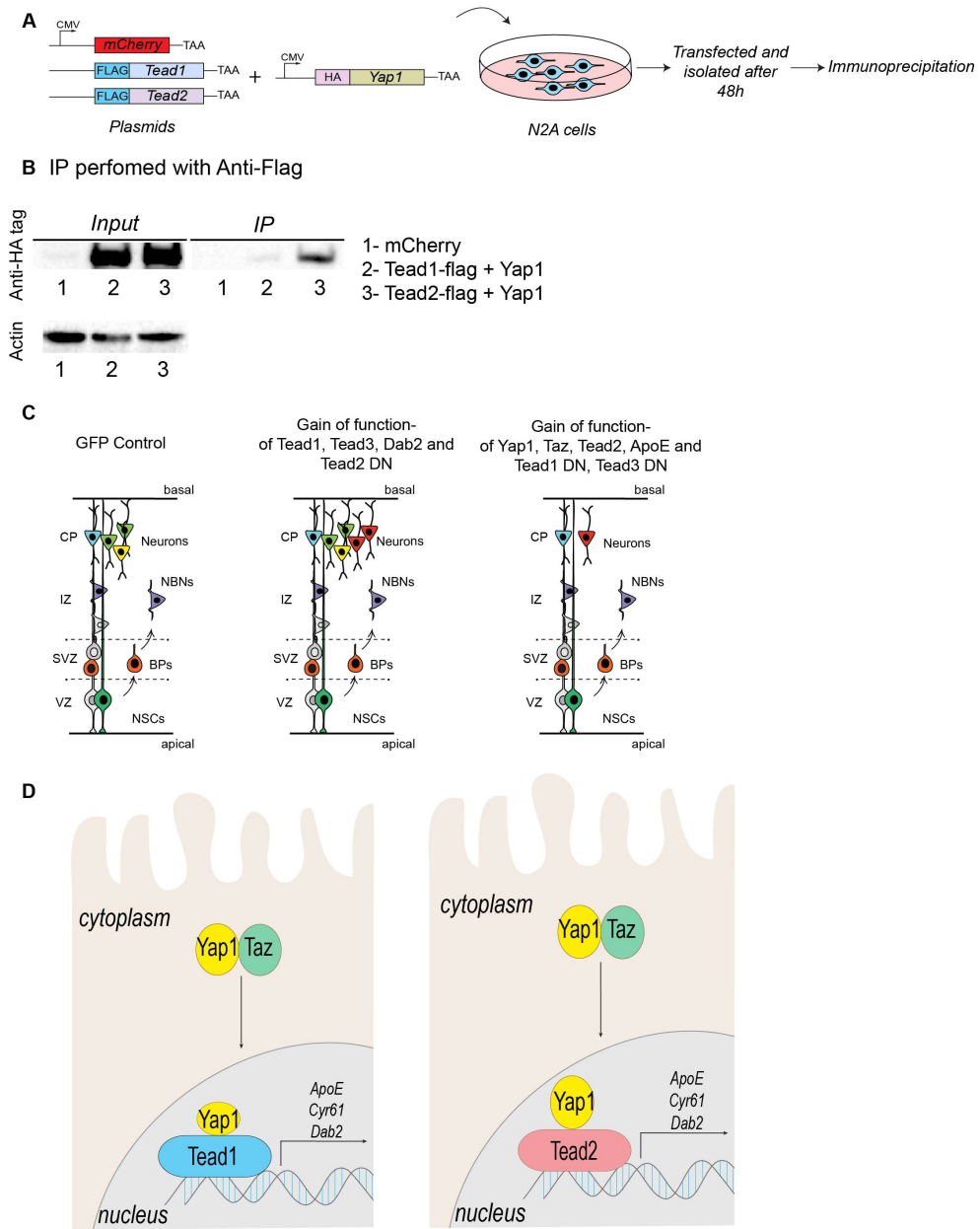
Supplementary Figure 6: Tead2 preferentially binds Yap1, in a gain-of-function paradigm.
A. N2A cells were transfected with flag tagged-Tead1 or Tead2 expression constructs; co-transfected with HA-tagged Yap1 expression construct. Cells were lysed after 48h and immunoprecipitation was performed using Anti-Flag antibody. B. Western blotting detection revealed that Yap1 preferentially binds Tead2 in N2A cells. C. Summarizing the phenotypic effects upon gain and loss-of-function of Hippo effectors and targets on neuronal migration in the CP. D. Model for the downstream molecular mechanism propose that Tead1 and Tead2 seem to regulate similar targets (*ApoE*, *Cyr61* and *Dab2*) and the differences in the regulation may exist at the binding partner level.

Supplementary Tables

TABLE 1

A

	Average ± SEM (GFP+ cells) E13.5-E15.5, 48h chase		
	VZ+	**SVZ/IZ+**	**CP+**
GFP Control	28.11 ± 0.4589 n=3	54.04 ± 0.9851, n=3	17.85 ± 0.5516, n=3
Yap1	52.45 ± 3.067, n=3	49.16 ± 1.406, n=3	8.346 ± 1.694, n=3
Taz	48.94 ± 4.646, n=3	53 ± 2.947, n=3	8.546 ± 1.308, n=3
P-Values (unpaired t-test)	0.0017 (**) 0.066 (*)	0.0466 (*) 0.7571 (ns)	0.0102 (*) 0.0049 (**)

B

	Average ± SEM (GFP+ Pax6+ cells)/Total GFP+ E13.5-E15.5, 48h chase		
	VZ+	**SVZ/IZ+**	**Total+**
GFP Control	25.71 ± 2.395, n=3	4.898 ± 0.6483, n=3	30.61 ± 2.87, n=3
Yap1	41.22 ± 1.569, n=3	11.24 ± 2.053, n=3	52.45 ± 3.067, n=3
Taz	38.45 ± 4.186, n=3	10.48 ± 0.8506, n=3	48.94 ± 4.646, n=3
P-Values (unpaired t-test)	0.0066 (**) 0.05 (*)	0.0299 (*) 0.006 (**)	0.0069 (**) 0.0283 (*)

C

	Average ± SEM (GFP+ Tbr1+ cells)/Total GFP+ E13.5-E15.5, 48h chase		
	SVZ/IZ+	**CP+**	**Total+**
GFP Control	3.66 ± 0.08, n=3	8.675 ± 0.06527, n=3	12.34 ± 0.0932, n=3
Yap1	2.875 ± 1.477, n=3	5.203 ± 0.3646, n=3	8.078 ± 1.698, n=3
Taz	3.44 ± 0.9135, n=3	4.835 ± 0.6975, n=3	8.275 ± 0.2526, n=3
P-Values (unpaired t-test)	0.2402 (ns) 0.7319 (ns)	0.011 (**) 0.0099 (**)	0.0838 (*) 0.0002 (***)

D

	Average ± SEM (GFP+ Ctip2+ cells)/Total GFP+ E13.5-E15.5, 48h chase			
	VZ+	**SVZ/IZ+**	**CP+**	**Total+**
GFP Control	1.866 ± 1.059, n=3	41.39 ± 2.465, n=3	13.98 ± 1.818, n=3	57.24 ± 3.024, n=3
Yap1	7.577 ± 2.9, n=3	53.4 ± 3.212, n=3	6.464 ± 1.356, n=3	67.44 ± 4.228, n=3
Taz	6.964 ± 1.682, n=3	56.21 ± 5.417, n=3	5.06 ± 1.095, n=3	70.32 ± 5.271, n=3
P-Values (unpaired t-test)	0.1082 (ns) 0.07 (ns)	0.041 (*) 0.05 (*)	0.0289 (*) 0.0126 (*)	0.1206 (ns) 0.1046 (ns)

E

	Average ± SEM (GFP+ Satb2+ cells)/Total GFP+ E13.5-E15.5, 48h chase		
	SVZ/IZ+	**CP+**	**Total+**
GFP Control	28.87 ± 1.81, n=3	15.89 ± 1.386, n=3	44.76 ± 2.784, n=3
Yap1	40.59 ± 4.446, n=3	12 ± 3.399, n=3	52.59 ± 1.048, n=3
Taz	53.15 ± 3.888, n=3	6.899 ± 0.3137, n=3	60.05 ± 4.199, n=3
P-Values (unpaired t-test)	0.6 (ns) 0.0047 (**)	0.3423 (ns) 0.0021 (**)	0.05 (*) 0.04 (*)

TABLE 2

A

	Average ± SEM (GFP+ cells) E13.5-E15.5, 48h chase		
	VZ+	**SVZ/IZ+**	**CP+**
GFP Control	28.11 ± 0.4589, n=3	54.04 ± 0.9851 n=3	17.85 ± 0.5516 n=3
Tead1	33.38 ± 1.866 n=3	43.99 ± 1.572 n=3	24.44 ± 1.325 n=3
Tead2	35.34 ± 1.544 n=3	64.08 ± 1.697 n=3	0.5864 ± 0.2152 n=3
Tead3	37.43 ± 1.622 n=3	36.33 ± 1.894 n=3	26.25 ± 0.7544 n=3
P-Values (unpaired t-test)	0.05 (*) 0.011 (*) 0.0048 (**)	0.0057 (**) 0.0072 (**) 0.0012 (**)	0.009 (***) <0.0001 (****) 0.0008 (***)

B

Average ± SEM (GFP+ Pax6+ cells)/Total GFP+
E13.5-E15.5, 48h chase

	VZ+	SVZ/IZ+	Total+
GFP Control	25.71 ± 2.395, n=3	4.898 ± 0.6483, n=3	30.61 ± 2.87, n=3
Tead1	31.74 ± 1.21, n=3	3.204 ± 0.6316, n=3	34.95 ± 1.484, n=3
Tead2	32.21 ± 3.485, n=3	7.057 ± 1.977, n=3	39.26 ± 5.459, n=3
Tead3	37.43 ± 1.622, n=3	3.727 ± 0.5711, n=3	41.15 ± 1.992, n=3
P-Values **(unpaired t-test)**	0.0927 (ns) 0.2016 (ns) 0.0173 (*)	0.1396 (ns) 0.4088 (ns) 0.2385 (ns)	0.2512 (ns) 0.2361 (ns) 0.0412 (*)

C

Average ± SEM (GFP+ Tbr1+ cells)/Total GFP+
E13.5-E15.5, 48h chase

	SVZ/IZ+	CP+	Total+
GFP Control	3.66 ± 0.08, n=3	8.675 ± 0.06527, n=3	12.34 ± 0.0932, n=3
Tead1	25.71 ± 8.387, n=3	17.53 ± 0.8791, n=3	43.24 ± 8.359, n=3
Tead2	0 ± 0, n=3	1.044 ± 0.5222, n=3	1.565 ± 0.0158, n=3
Tead3	10.22 ± 1.963, n=3	17.93 ± 0.2028, n=3	28.14 ± 2.096, n=3
P-Values **(unpaired t-test)**	0.0382 (*) <0.0001 (****) 0.0145 (*)	0.0003 (***) <0.0001 (****) <0.0001 (****)	0.014 (*) <0.0001 (****) 0.001 (***)

D

Average ± SEM (GFP+ Ctip2+ cells)/Total GFP+
E13.5-E15.5, 48h chase

	VZ+	SVZ/IZ+	CP+	Total+
GFP Control	1.866 ± 1.059, n=3	41.39 ± 2.465, n=3	13.98 ± 1.818, n=3	57.24 ± 3.024, n=3
Tead1	1.18 ± 1.18, n=3	27.91 ± 13.99, n=3	20.96 ± 0.06097, n=2	64.59 ± 3.4, n=2
Tead2	6.436 ± 1.416, n=3	56.21 ± 5.417, n=3	1.758 ± 0.2587, n=3	64.4 ± 4.226, n=3
Tead3	0.4444 ± 0.4444, n=3	35.33 ± 0.949, n=3	18.98 ± 0.4745, n=3	54.75 ± 1.034, n=3
P-Values **(unpaired t-test)**	0.6279 (ns) 0.7 (ns) 0.3258 (ns)	0.7329 (ns) 0.06 (ns) 0.08 (ns)	0.0255 (*) 0.001 (***) 0.06 (ns)	0.08 (ns) 0.2402 (ns) 0.479 (ns)

E

	Average ± SEM (GFP+ Satb2+ cells)/Total GFP+ E13.5-E15.5, 48h chase		
	SVZ/IZ+	**CP+**	**Total+**
GFP Control	28.87 ± 1.81, n=3	15.89 ± 1.386, n=3	44.76 ± 2.784, n=3
Tead1	37.24 ± 2.506, n=3	15.44 ± 0.1775, n=3	52.68 ± 2.683, n=3
Tead2	45.79 ± 2.312, n=3	2.185 ± 0.5617, n=3	47.97 ± 2.239, n=3
Tead3	35.53 ± 1.502, n=3	16.9 ± 3.858, n=3	52.43 ± 2.4, n=3
P-Values (unpaired t-test)	0.05 (*) 0.0045 (**) 0.047 (*)	0.7957 (ns) 0.0008 (***) 0.8589 (ns)	0.1097 (ns) 0.4181 (ns) 0.1051 (ns)

TABLE 3

A

	Average ± SEM (GFP+ cells) E13.5-E15.5, 48h chase		
	VZ+	**SVZ/IZ+**	**CP+**
GFP Control	28.11 ± 0.4589, n=3	54.04 ± 0.9851, n=3	17.85 ± 0.5516 n=3
Tead1 DN	38.59 ± 1.288, n=3	57.53 ± 1.928, n=3	3.888 ± 0.8776, n=3
Tead2 DN	32.36 ± 0.8977 n=3	38.46 ± 1.067, n=3	29.19 ± 1.682, n=3
Tead3 DN	36.59 ± 3.136, n=3	54.58 ± 3.102, n=3	8.832 ± 1.07, n=3
P-Values (unpaired t-test)	0.0014 (**) 0.013 (*) 0.05 (*)	0.1833 (ns) 0.0004 (***) 0.8746 (ns)	0.0006 (***) 0.0024 (**) 0.0028 (**)

B

	Average ± SEM (GFP+ Pax6+ cells)/Total GFP+ E13.5-E15.5, 48h chase		
	VZ+	**SVZ/IZ+**	**Total+**
GFP Control	25.71 ± 2.395, n=3	4.898 ± 0.6483, n=3	30.61 ± 2.87, n=3
Tead1 DN	32.36 ±0.8978, n=3	6.262 ± 0.7881, n=3	39.29 ± 1.234, n=3
Tead2 DN	38.58 ± 1.288, n=3	8.417 ± 1.052, n=3	47 ± 2.083, n=3
Tead3 DN	36.59 ± 3.136, n=3	5.059 ± 0.5592, n=3	41.65 ± 3.099, n=3
P-Values (unpaired t-test)	0.06 (*) 0.0107 (*) 0.05 (*)	0.1637 (ns) 0.0413 (*) 0.8484 (ns)	0.05 (*) 0.0108 (*) 0.06 (*)

C

	Average ± SEM (GFP+ Tbr1+ cells)/Total GFP+ E13.5-E15.5, 48h chase		
	SVZ/IZ+	**CP+**	**Total+**
GFP Control	3.66 ± 0.08, n=3	8.675 ± 0.06527, n=3	12.34 ± 0.0932, n=3
Tead1 DN	3.207 ± 1.005, n=3	2.216 ± 0.189, n=3	5.423 ± 1.014, n=3
Tead2 DN	1.037 ± 0.6296, n=3	22.44 ± 1.402, n=3	23.48 ± 2.002, n=3
Tead3 DN	8.533 ± 0.639, n=3	5.199 ± 0.2748, n=3	13.73 ± 0.38, n=3
P-Values (unpaired t-test)	0.6025 (ns) 0.041 (*) 0.0009 (***)	<0.0001 (****) 0.0003 (***) 0.0004 (***)	0.006 (**) 0.0036 (**) 0.224 (ns)

D

	Average ± SEM (GFP+ Ctip2+ cells)/Total GFP+ E13.5-E15.5, 48h chase			
	VZ+	**SVZ/IZ+**	**CP+**	**Total+**
GFP Control	1.866 ± 1.059, n=3	41.39 ± 2.465, n=3	13.98 ± 1.818, n=3	57.24 ± 3.024, n=3
Tead1 DN	3.446 ± 0.6887, n=3	54.43 ± 5.151, n=3	2.575 ± 0.8866, n=3	59.59 ± 4.985, n=3
Tead2 DN	0.998 ± 0.5064, n=3	33.09 ± 2.248, n=3	20.74 ± 0.8489, n=3	57.3 ± 2.656, n=3
Tead3 DN	2.844 ± 1.034, n=3	50.45 ± 5.999, n=3	5.224 ± 1.678, n=3	60.02 ± 5.137, n=3
P-Values (unpaired t-test)	0.2817 (ns) 0.6334 (ns) 0.5067 (ns)	0.08 (ns) 0.06 (ns) 0.2355 (ns)	0.0054 (**) 0.035 (*) 0.0285 (*)	0.7061 (ns) 0.9913 (ns) 0.6585 (ns)

E

	Average ± SEM (GFP+ Satb2+ cells)/Total GFP+ E13.5-E15.5, 48h chase		
	SVZ/IZ+	**CP+**	**Total+**
GFP Control	28.87 ± 1.81, n=3	15.89 ± 1.386, n=3	44.76 ± 2.784, n=3
Tead1 DN	49.14 ± 1.311, n=3	2.512 ± 1.559, n=3	51.65 ± 1.518, n=3
Tead2 DN	21.99 ± 2.322, n=3	16.75 ± 1.249, n=3	38.74 ± 1.552, n=3
Tead3 DN	37.68 ± 2.87, n=3	5.553 ± 1.036, n=3	43.24 ± 3.897, n=3
P-Values (unpaired t-test)	0.0066 (**) 0.08 (ns) 0.05 (*)	0.0299 (*) 0.6678 (ns) 0.04 (**)	0.095 (ns) 0.1312 (ns) 0.7638 (ns)

TABLE 4

A

	Average ± SEM (GFP+ cells) E13.5-E15.5, 48h chase		
	VZ+	**SVZ/IZ+**	**CP+**
GFP Control	28.11 ± 0.4589, n=3	54.04 ± 0.9851, n=3	17.85 ± 0.5516, n=3
Tead1 VP16	46.8 ± 4.553, n=3	45.36 ± 4.662, n=3	7.716 ± 0.08276, n=3
Tead2 VP16	48.34 ± 17.68, n=3	33.63 ± 13.64, n=3	1.891 ± 0.6124, n=3
P-Values (unpaired t-test)	0.0136 (*) 0.32 (ns)	0.1426 (*) 0.2091 (ns)	<0.0001 (****) 0.0002 (***)

B

	Average ± SEM (GFP+ Pax6+ cells)/Total GFP+ E13.5-E15.5, 48h chase		
	VZ+	**SVZ/IZ+**	**Total+**
GFP Control	25.71 ± 2.395, n=3	4.898 ± 0.6483, n=3	30.61 ± 2.87, n=3
Tead1 VP16	46.92 ± 4.588, n=3	4.194 ± 1.028, n=3	51.12 ± 3.595, n=3
Tead2 VP16	48.22 ± 17.76, n=3	29.13 ± 14.14, n=3	77.35 ± 15.58, n=3
P-Values (unpaired t-test)	0.0144 (*) 0.278 (ns)	0.5473 (ns) 0.1153 (ns)	0.0115 (*) 0.0476 (*)

TABLE 5

A

Chromatin Immunoprecipitation	Mean ± SEM (NSCs)		
	Negative	**Tead1-flag**	**Tead2-flag**
ApoE	0.0002373 ± 0, n=2	0.002739 ± 0.00019, n=2	0.004509 ± 0.000 n=2
p values (unpaired t-test)		0.0063	0.0048
Cyr61	0.001553 ± 2.55e-008, n=2	0.003421 ± 2.65e-007 n=2	0.004766 ± 0.0010 n=2
p values (unpaired t-test)		<0.0001	<0.0001
Dab2	0.0007925 ± 4.35e-008, n=2	0.00274 ± 4.4e-007, n=2	0.00335 ± 0.0013 n=2
p values (unpaired t-test)			
Relative Expression	**GFP control**	**Tead1**	**Tead2**
ApoE	1.113 ± 0.1097, n=4	16.67 ± 0.7039, n=3	31.43 ± 3.315, n=4
p values (unpaired t-test)		<0.0001	<0.0001
Cyr61	0.9887 ± 0.1157, n=4	5.991 ± 1.115, n=3	5.663 ± 1.143, n=4
p values (unpaired t-test)		0.0032	0.0066
Dab2	0.6497 ± 0.1639, n=4	26.8 ± 9.852, n=4	38.95 ± 4.797, n=4
p values (unpaired t-test)		0.0378	0.0002

TABLE 6

A

	Average ± SEM (GFP+ cells) E13.5-E15.5, 48h chase		
	VZ+	SVZ/IZ+	CP+
GFP Control	28.11 ± 0.4589, n=3	54.04 ± 0.9851, n=3	17.85 ± 0.5516 n=3
ApoE	33.85 ± 2.371, n=3	53.83 ± 1.395, n=3	12.32 ± 0.9937, n=3
Cyr61	31.44 ± 2.192, n=3	50.08 ± 0.3254, n=3	16.69 ± 0.7326, n=3
Dab2	28.35 ± 0.875 n=3	51.16 ± 0.9136, n=3	20.49 ± 0.4186, n=3
P-Values (unpaired t-test)	0.07 (*) 0.214 (ns) 0.82 (ns)	0.0906 (ns) 0.0189 (*) 0.0986 (ns)	0.0101 (*) 0.273 (ns) 0.0194 (*)

B

	Average ± SEM (GFP+ Pax6+ cells)/Total GFP+ E13.5-E15.5, 48h chase		
	VZ+	SVZ/IZ+	Total+
GFP Control	25.71 ± 2.395, n=3	4.898 ± 0.6483, n=3	30.61 ± 2.87, n=3
ApoE	33.85 ± 2.371, n=3	5.99 ± 1.188, n=3	39.84 ± 1.183, n=3
Cyr61	31.44 ± 2.192, n=3	5.554 ± 0.7901, n=3	36.99 ± 1.448, n=3
Dab2	28.35 ± 0.8754, n=3	7.042 ± 1.193, n=3	35.39 ± 0.602 n=3
P-Values (unpaired t-test)	0.07 (*) 0.1563 (ns) 0.3585 (ns)	0.5027 (ns) 0.5511 (ns) 0.195 (ns)	0.0441 (*) 0.1216 (ns) 0.1817 (ns)

C

	Average ± SEM (GFP+ Tbr1+ cells)/Total GFP+ E13.5-E15.5, 48h chase		
	SVZ/IZ+	CP+	Total+
GFP Control	3.66 ± 0.08, n=3	8.675 ± 0.06527, n=3	12.34 ± 0.0932, n=3
ApoE	5.492 ± 0.8049, n=3	10.53 ± 2.332, n=3	16.02 ± 3, n=3
Cyr61	5.997 ± 0.9568, n=3	15.91 ± 0.1428, n=3	21.9 ± 0.9068, n=3
Dab2	6.175 ± 1.129, n=3	16.66 ± 1.354, n=3	22.83 ± 2.011, n=3
P-Values (unpaired t-test)	0.08 (ns) 0.6 (ns) 0.08 (ns)	0.4972 (ns) <0.0001 (****) 0.0026 (**)	0.2927 (ns) 0.0003 (***) 0.0043 (**)

D

Average ± SEM (GFP+ Ctip2+ cells)/Total GFP+
E13.5-E15.5, 48h chase

	VZ+	SVZ/IZ+	CP+	Total+
GFP Control	1.866 ± 1.059, n=3	41.39 ± 2.465, n=3	13.98 ± 1.818, n=3	57.24 ± 3.024, n=3
ApoE	2.743 ± 0.366, n=3	50.29 ± 1.58, n=3	11.28 ± 1.83, n=3	64.31 ± 0.1158, n=3
Cyr61	2.779 ± 0.7738, n=3	52.22 ± 1.663, n=3	13.66 ± 1.674, n=3	68.66 ± 0.3716, n=3
Dab2	6.009 ± 1.509, n=3	48.51 ± 1.348, n=3	16.49 ± 0.5545, n=3	71.01 ± 2.582, n=3
P-Values **(unpaired t-test)**	0.5394 (ns) 0.4552 (ns) 0.09 (ns)	0.03 (*) 0.022 (*) 0.06 (ns)	0.03 (*) 0.9106 (ns) 0.2646 (ns)	0.078 (ns) 0.0189 (*) 0.0262 (*)

E

Average ± SEM (GFP+ Satb2+ cells)/Total GFP+
E13.5-E15.5, 48h chase

	SVZ/IZ+	CP+	Total+
GFP Control	28.87 ± 1.81, n=3	15.89 ± 1.386, n=3	44.76 ± 2.784, n=3
ApoE	32.79 ± 6.509, n=3	7.885 ± 1.575, n=3	40.68 ± 7.703, n=3
Cyr61	33.27 ± 1.764, n=3	12.87 ± 1.996, n=3	46.13 ± 0.4834, n=3
Dab2	35.09 ± 0.8777, n=3	11.2 ± 1.44, n=3	46.29 ± 2.129, n=3
P-Values **(unpaired t-test)**	0.6346 (ns) 0.1549 (ns) 0.0376 (*)	0.0208 (*) 0.2897 (ns) 0.7 (ns)	0.6831 (ns) 0.6491 (ns) 0.6831 (ns)

Discussion

We have shown that Hippo effectors play differential roles in NSCs during corticogenesis, using gain and loss of function paradigms. Although we focussed on time from E13.5-E15.5, it is likely, that the Tead TFs have additional roles or targets during other phases of expansion and gliogenesis. Though the Tead TFs have been extensively examined in other cell types, for example, during heart morphogenesis, vasculogenesis, muscle development, epithelial-to-mesenchymal transition and cancers, little is known about the molecular basis and their functions in the brain[193,212,213,215,216].

Knockdown of Yap1 leads to precocious exit of cells from the VZ and loss of neurons

In addition to being a partner of Teads, Yap1 is also known to bind Smads and p73[198,217]. Yap1 is expressed selectively in NSCs and astrocytes but is undetectable in neurons, making it a potential limiting binding factor[217]. The physiological role of Yap1 has also been explored in mouse neocortical NSCs and the results suggest a crosstalk with BMP signalling in the control of astrocytic differentiation[217]. Another effector Neurofibromin 2 (Nf2, also called as Merlin) suppresses Yap1 activity to promote cell differentiation in NSCs and prevents ectopic Slit2 expression during the formation of corpus callosum (CC)[227,228]. Deletion of Nf2 in the dorsal forebrain causes a significant expansion of NSCs resulting in dysgenesis of the CC and malformation of the hippocampus[227,228]. This finding identified a novel role for Hippo effectors in axon guidance through a potential crosstalk with Robo-Slit1 signalling[227,228]. In peripheral nervous system, knock-out of YAP/TAZ in Schwann cells results in reduced proliferation, impaired radial sorting and defective myelination[218].

To further test the role of Yap1 in NSCs, I performed knockdown (KD) of Yap1 using a published shRNA construct directed against the coding region of Yap1 mRNA[229]. I used an shRNA targeting Renilla Luciferase as a negative control. I performed IUE at E13.5 and isolated and analyzed the brains at E15.5 (Figure 9'). Upon Yap1 KD, the transfected cells precociously migrated out of the VZ and were retained in the SVZ/IZ. This was accompanied by a reduction in cells in the CP. In addition, the cells trapped in the SVZ/IZ underwent increased apoptosis (data not shown). This phenotype is opposite to the gain of function phenotype of Yap1 where we observe an increase in

Pax6+ cells and a reduction in CP neurons (Figure 9'). Data for this part is summarized in Table 1'.

TABLE 1'

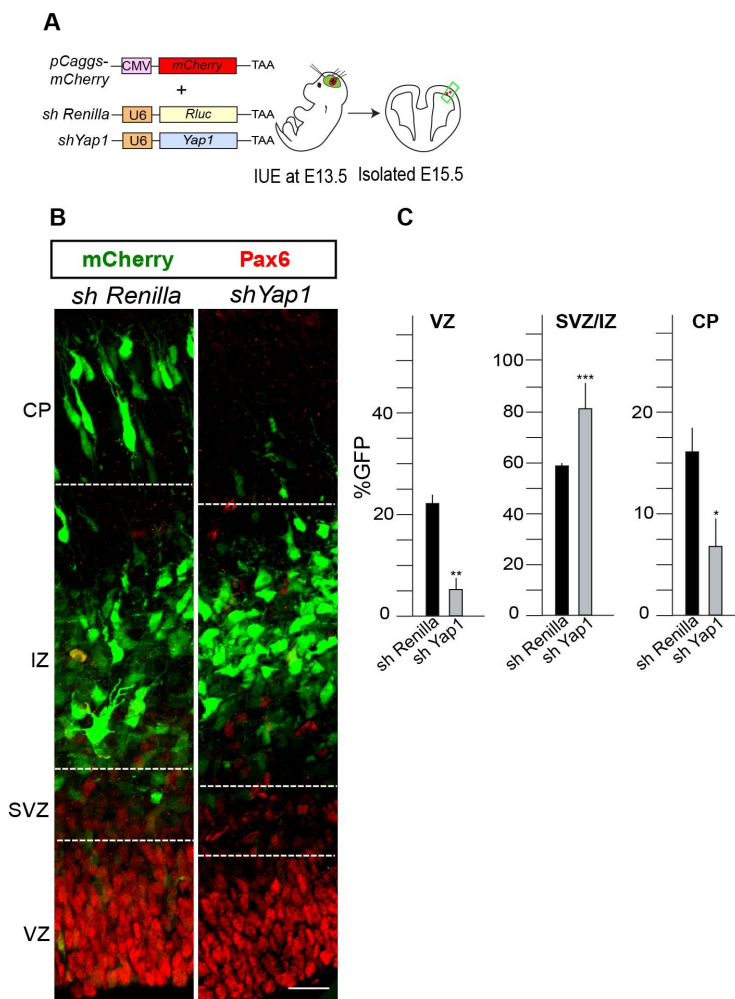|	Average ± SEM (mCherry+ cells) E13.5-E15.5, 48h chase		
	VZ+	SVZ/IZ+	CP+
shRenilla + mCherry	22.24 ± 1.242, n=2	61.36 ± 0.4653, n=2	16.4 ± 1.707, n=2
shYap1 + mCherry	5.134 ± 1.22, n=3	84.47 ± 5.684, n=3	6.893 ± 1.493, n=3
P-Values (unpaired t-test)	0.0026 (**)	0.0515 (*)	0.026 (*)

Figure 9': Knockdown (KD) of Yap1 demonstrates a phenotype similar to Tead2 EnR, reduction in NSCs in VZ and neurons in CP.
A. Experimental paradigm for knockdown of Yap1 with short-hairpin RNA directed against Yap1 coding sequence, sh Renilla luciferase is used as a control. The cells were co-transfected with pCaggs-mCherry, as a reporter. B. Upon KD of Yap1, transfected cells precociously leave the VZ, and are trapped in the SVZ/IZ and do not migrate to the CP. C. Quantifications for the cell distribution upon knockdown of Yap1,

compared to the control. Scale bar = 50µm. *p= 0.05, **p= 0.01, ***p=0.001, ****<p=0.00001.

Tead2-Engrailed- a dominant repressor form of TEAD2 reduces NSCs in VZ and neurons in the CP

We investigated the phenotypic changes of a dominant repressor form Tead2-engrailed (Tead2-EnR) in NSCs. Engrailed is a repressor of transcription; when the repressor domain is fused to any TF binding domain, it represses target expression. Here we used Tead2-EnR to confirm our Tead2 loss of function data in NSCs. We found, that Tead2-EnR expression in NSCs induced precocious exit from the VZ and trapping of the cells in the SVZ/IZ, with an associated reduction of transfected cells reaching the CP. These phenotypic changes partially oppose the gain of function of Tead2 phenotypes we observed (Figure 10'). Data for this part is summarized in Table 2'.

In addition, we found that Tead2-EnR expression in NSCs demonstrated a phenotype similar to knockdown of Yap1. These findings indicate that Yap1 could be a direct target of Tead2, or that Tead2 represses an activator of Yap1 in NSCs. *In silico* analyses of Tead binding motif revealed a weak putative Tead binding site in the promoter of the *Yap1* gene. Though this is yet to be validated experimentally, we hypothesize that the *Yap1* gene may indeed be a direct target of Tead2. Hence, Yap1 protein is not only upstream of Tead2 TF activation but the *Yap1* gene maybe a downstream target of Tead2. This again suggests a potential feedback loop in Hippo signalling.

TABLE 2'

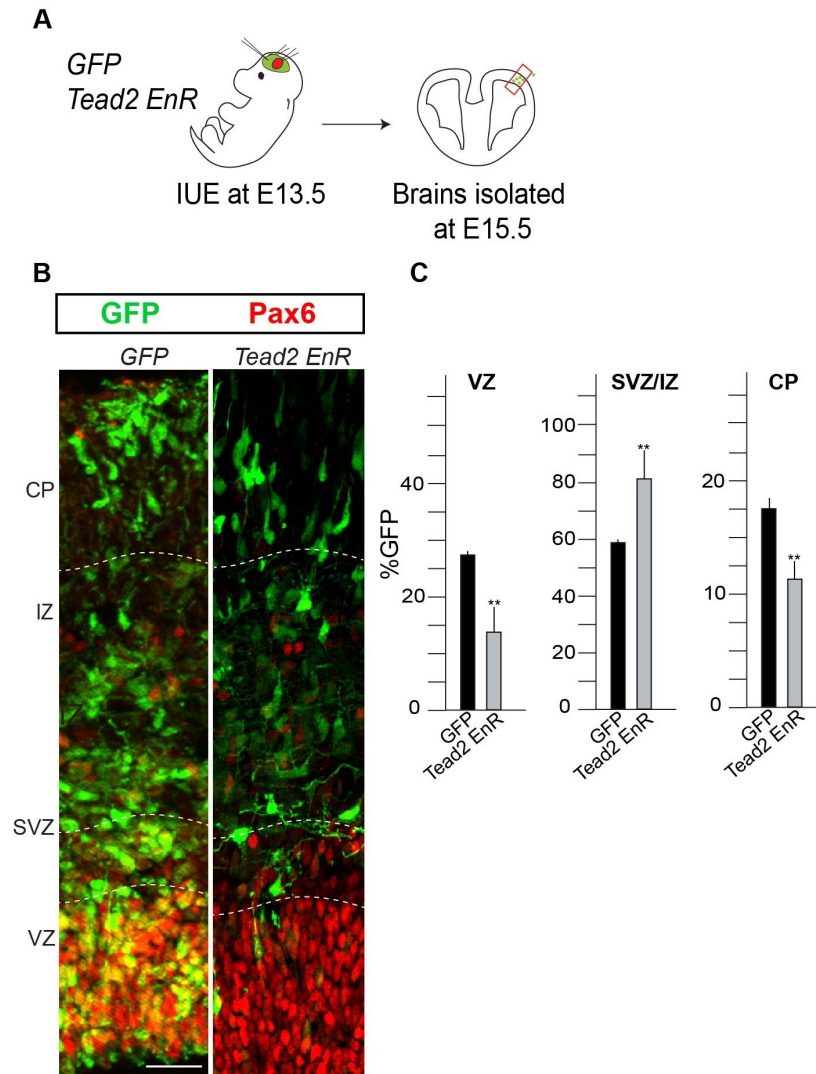|	Average ± SEM (GFP+ cells) E13.5-E15.5, 48h chase		
	VZ+	SVZ/IZ+	CP+
GFP control	28.11 ± 0.4589, n=3	54.04 ± 0.9851, n=3	17.85 ± 0.5516 n=3
Tead2-Engrailed	14.31 ± 2.493, n=3	74.1 ± 2.244, n=3	11.59 ± 0.8857, n=3
P-Values (unpaired t-test)	0.0055 (**)	0.0012 (**)	0.0039 (**)

Figure 10': Tead2-Engrailed (Tead2-EnR), dominant repressor form expression in NSCs reduces NSCs in VZ and neurons in CP

A. Experimental paradigm showing the in utero electroporations were done at E13.5 and transfected brains isolated at E15.5. B. Tead2 EnR expression in NSCs affects the distribution of GFP+ cells compared to the control. C. Quantifications for distribution of transfected cells in VZ, SVZ/IZ and CP. Scale bar = 50µm. *p= 0.05, **p= 0.01, ***p=0.001, ****<p=0.00001.

Tead2 as a potential downstream factor in periventricular heterotopia (PVH)

Periventricular heterotopia manifests as heterotopic localization of neurons along the lateral ventricle (Figure 11'A). From our current knowledge about the disease, 8 genes have been implicated in humans, accounting only 26% of the cases.[196,201,230,231] Though manipulation of Fat4 and Dchs1 in mouse embryos resulted in heterotopic neurons and resembled the disease manifestations, the downstream molecular mechanisms are still unclear[196].

We have elucidated that Tead2 gain and loss of functions affect neuronal migration. As a pilot study, we tested if these neurons, which remain in the SVZ/IZ, are able to recover and migrate at a later time to the correct layers in the cerebral cortex. This was to rule out the transient effect on neuronal migration caused by Tead2 manipulation. Therefore, I performed gain of function of Tead2 at E13.5 and isolated and analyzed the brains at E18.5, and compared the transfected cells and their progeny to GFP control animals (Figure 11'). We observe, a dramatic effect on the neuronal migration with many mispositioned neurons along the lateral ventricle (LV) in the VZ upon Tead2 gain of function. These phenotypic changes resemble the formation of PVH (Figure 11'B, C). Therefore, we propose that, Tead2 is a potential downstream factor in PVH. The model suggests that upon KD of Fat1 and/or Dchs1, Mst1/2 and Lats1/2 kinases' activity is reduced. This results in a decrease in Yap1 phosphorylation in the cytoplasm, translocation to be nucleus, to interact and activate Tead2. This model is supported by the similar phenotypic changes in fate and neuronal migration upon loss of Fat1, loss of Dchs1 and gain of Yap1 and Tead2 function.
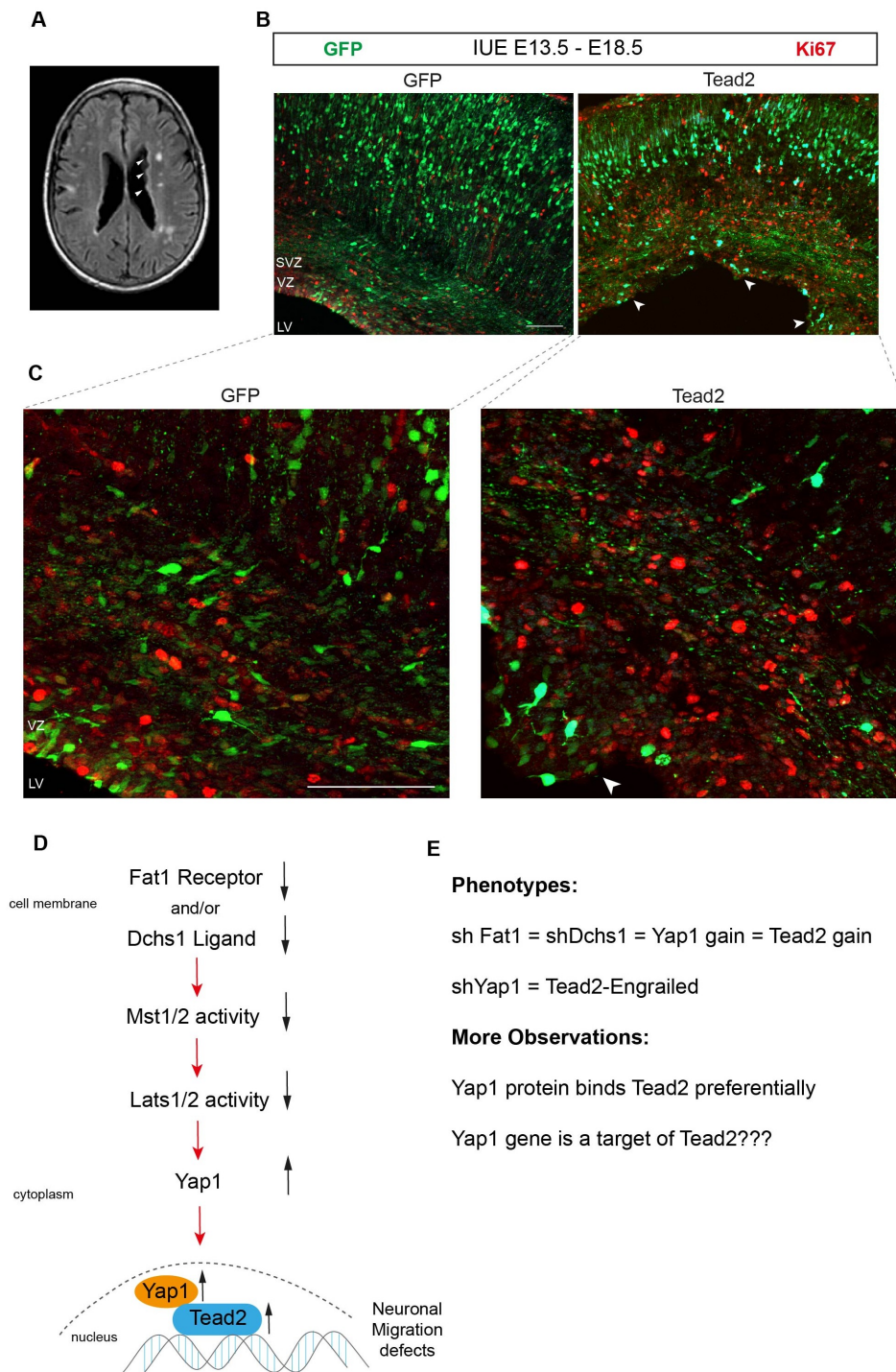
A

B

| GFP | IUE E13.5 - E18.5 | Ki67 |

GFP   Tead2

SVZ
VZ
LV

C

GFP   Tead2

VZ
LV

D

cell membrane

Fat1 Receptor
and/or
Dchs1 Ligand

Mst1/2 activity

Lats1/2 activity

cytoplasm   Yap1

Yap1
Tead2
nucleus

Neuronal
Migration
defects

E

Phenotypes:

sh Fat1 = shDchs1 = Yap1 gain = Tead2 gain

shYap1 = Tead2-Engrailed

More Observations:

Yap1 protein binds Tead2 preferentially

Yap1 gene is a target of Tead2???

Figure 11': Tead2 as potential downstream factor in periventricular heterotopia (PVH)

A. MRI scan of a human brain showing PVH along the LV, marked with arrowheads (*http://www.clinmedres.org/content/3/4/229/F1.expansion*). B-C. Coronal sections of transfected brains at E18.5, with GFP and Tead2 gain of function, arrowheads pointing to mispositioned neurons. D. Sequence of events, when Hippo signalling is downregulated. Directions of the arrows suggest gain (upwards) or loss of function (downwards). E. Summarizing the phenotypic observations, to demonstrate Yap1 and Tead2 to be downstream of PVH. Scale bar: 100µm.

Dominant negative Tead1 lacking Yap1/Taz binding domain recapitulates Tead1 gain of function phenotype

We show by our IP that Tead2 preferentially binds Yap1 over Taz. We also tested if Tead1 requires Yap1/Taz binding for its activity. We cloned dominant negative form of Tead1, which lacks the Yap1/Taz binding domain (data not shown). When IUEed into NSCs *in vivo*, we observe a phenotype similar to Tead1 gain of function, with more cells that migrated to the CP (Figure 12'A-C). This suggests that the Tead1 effect in the overexpression presumably does not require Yap1/Taz binding for its function *in vivo*. These observations emphasize the differential roles of Tead1 and Tead2, with preferential crosstalk with their binding partner-co-activators. In order to test this, we performed IP of Teads, to detect preferential binding with Taz in N2As upon overexpression (Figure 12' D, E). Interestingly, our preliminary results suggest that Tead2 binds Taz better than Tead1. We are yet to ascertain whether Tead1 requires other co-activators to function. Data for this part is summarized in Table 3'.

In conclusion, the downstream regulation of Hippo signalling may be either at the level of binding factors, co-activators and complexes the Tead TFs make. These putative differences in Tead1 and Tead2 complexes differentially regulate downstream targets. There are ample hypotheses possible and yet to be tested in the context of NSCs. It may also be that the Teads are in different complexes during different stages throughout the developmental time course. It would be interesting to explore the proteomic landscape of Tead TFs at different time points, or in different zones of expansion, neurogenesis and gliogenesis. In addition, ChIP-seq for the targets of Tead1 and Tead2 from these zones will provide further information about cell-type specific functions of the Teads or stage-specific regulations of gene sets. These data would further validate our different ISMARA analysis.

TABLE 3'

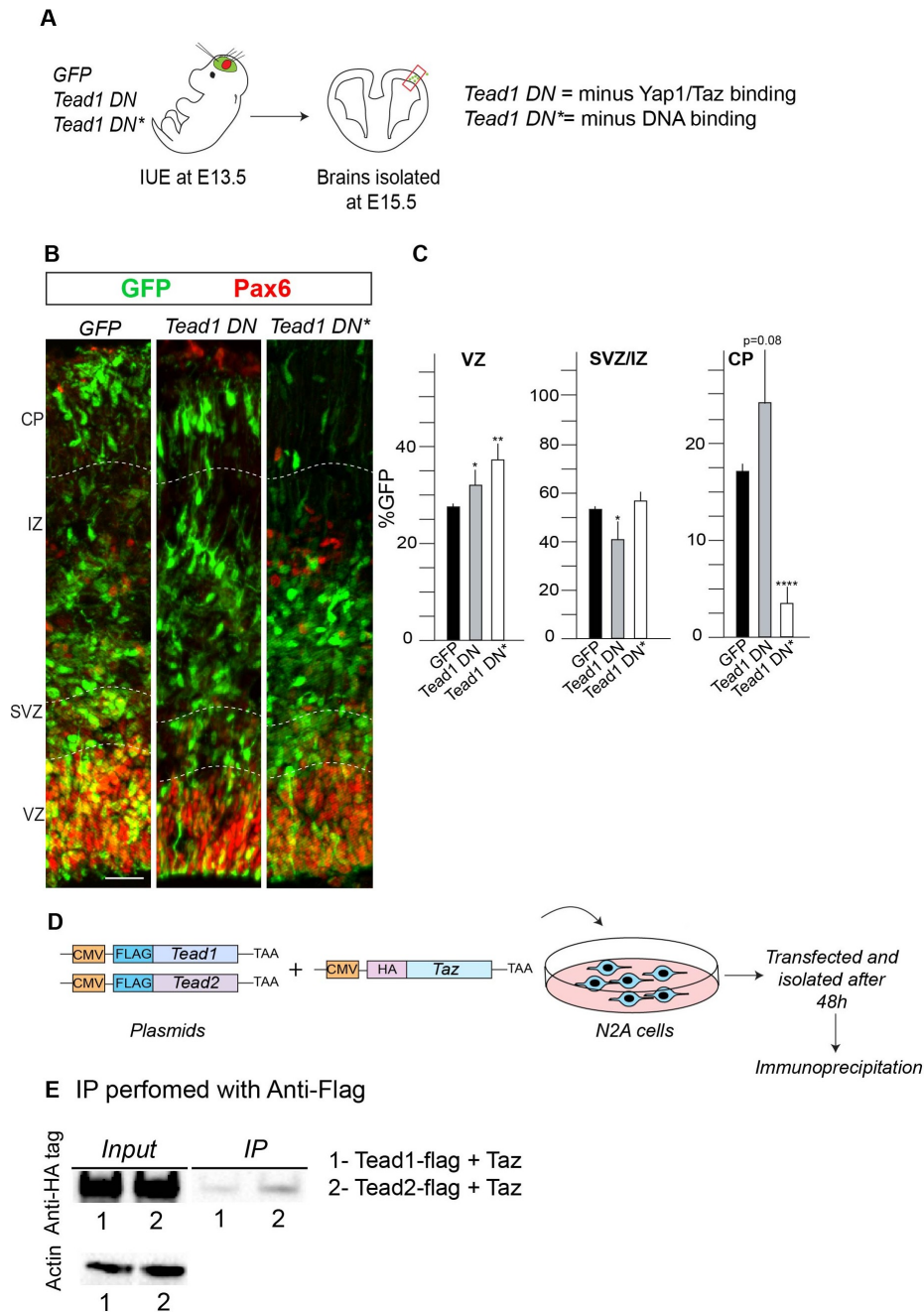|	Average ± SEM (GFP+ cells) E13.5-E15.5, 48h chase		
	VZ+	SVZ/IZ+	CP+
GFP control	28.11 ± 0.4589, n=3	54.04 ± 0.9851, n=3	17.85 ± 0.5516 n=3
Tead1 DN	33.36 ± 1.674, n=3	41.37 ± 4.269, n=3	25.27 ± 3.18, n=3
Tead1 DN*	38.61 ± 2.231, n=2	57.53 ± 1.928, n=3	3.888 ± 0.8776, n=3
P-Values (unpaired t-test)	0.0388 (*) 0.0095 (**)	0.0444 (*) 0.185 (ns)	0.0831 0.0002 (***)

A

GFP
Tead1 DN
*Tead1 DN**

IUE at E13.5 → Brains isolated at E15.5

Tead1 DN = minus Yap1/Taz binding
*Tead1 DN** = minus DNA binding

B

GFP | Pax6

GFP | *Tead1 DN* | *Tead1 DN**

CP
IZ
SVZ
VZ

C

VZ

SVZ/IZ

CP

D

CMV–FLAG–*Tead1*–TAA
CMV–FLAG–*Tead2*–TAA
+ CMV–HA–*Taz*–TAA

Plasmids

N2A cells

Transfected and isolated after 48h → Immunoprecipitation

E IP perfomed with Anti-Flag

Anti-HA tag

Input | *IP*

1- Tead1-flag + Taz
2- Tead2-flag + Taz

Actin

Figure 12': Tead1 DN (minus Yap1/Taz binding domain) phenotypically mimics Tead1 gain of function

A. Experimental paradigm using Tead1 DN (minus Yap1/Taz binding domain) and Tead1 DN* (minus DNA binding domain) and GFP as a control. B. Distribution of transfected cells is affected as observed in immunostained coronal sections of transfected cortices. C. Quantifications for the distribution of GFP+ cells in VZ, SVZ/IZ and CP. D. Experimental paradigm for *in vitro* overexpression of Flag tagged Tead1, Tead2; co-transfected with HA-tagged Taz in N2A cells and cell lysates tested by immunoprecipitation (IP). E. Western blot after IP suggests no significant differences in binding of Taz by Tead1 and Tead2. Scale bar = 50µm. *p= 0.05, **p= 0.01, ***p=0.001, ****<p=0.00001.

93

Co-expression of Tead1 or Tead3 with Tead2 rescues the individual phenotypic changes

Tead TFs are expressed dynamically during the course of corticogenesis by NSCs, BPs and NBNs. To test which of the Tead TFs would be dominant in a gain of function experimental paradigm, we performed double gain of function. Therefore, we co-expressed Tead1 and Tead2, Tead3 and Tead2 or Tead1 and Tead3 in NSCs *in vivo* by IUE. All combinations of the Teads gave a phenotype with cells normally migrating to the CP. When we co-expressed Tead1 and Tead2, transfected cells were no longer trapped in the SVZ/IZ CP. Tead1 co-transfection with Tead2 partially rescued the phenotypic migration defects (Figure 13'). We observed a similar rescue phenotype with Tead2 and Tead3 co-expression. Cell distribution through VZ, SVZ/IZ and CP was returned to normal. These findings suggest that a balance of Tead TFs is required for proper downstream regulation or that some targets are activated or repressed by the different Tead factors and in their presence, a homeostasis is reached. Data for this part is summarized in Table 4'.

TABLE 4'

D	Average ± SEM (GFP+ cells) E13.5-E15.5, 48h chase		
	VZ+	**SVZ/IZ+**	**CP+**
GFP control	28.11 ± 0.4589, n=3	54.04 ± 0.9851, n=3	17.85 ± 0.5516 n=3
Tead1, Tead2	33.94 ± 2.522, n=2	51.36 ± 1.58, n=2	14.7 ± 0.9415, n=2
Tead2, Tead3	37.27 ± 2.096, n=2	48.23 ± 0, n=2	14.01 ± 2.588, n=2
Tead1, Tead3	34.6 ± 1.125, n=2	48.7 ± 1.625, n=2	16.69 ± 2.751, n=2
P-Values (unpaired t-test)	0.05 (*) 0.0119 (*) 0.008 (**)	0.2196 (ns) 0.0197 (*) 0.0558 (*)	0.05 (*) 0.1581 (ns) 0.6305 (ns)

A

IUE at E13.5
Brains isolated at E15.5

Plasmids:
GFP
Tead1 wt; Tead2-GFP
Tead3 wt; Tead2-GFP
Tead1 wt; Tead3wt; GFP

C

GFP   Tead1

Tead1/Tead2

B Distribution of transfected cells

GFP   Pax6

GFP   *Tead1/Tead2*   *Tead3/Tead2*   *Tead1/Tead3*
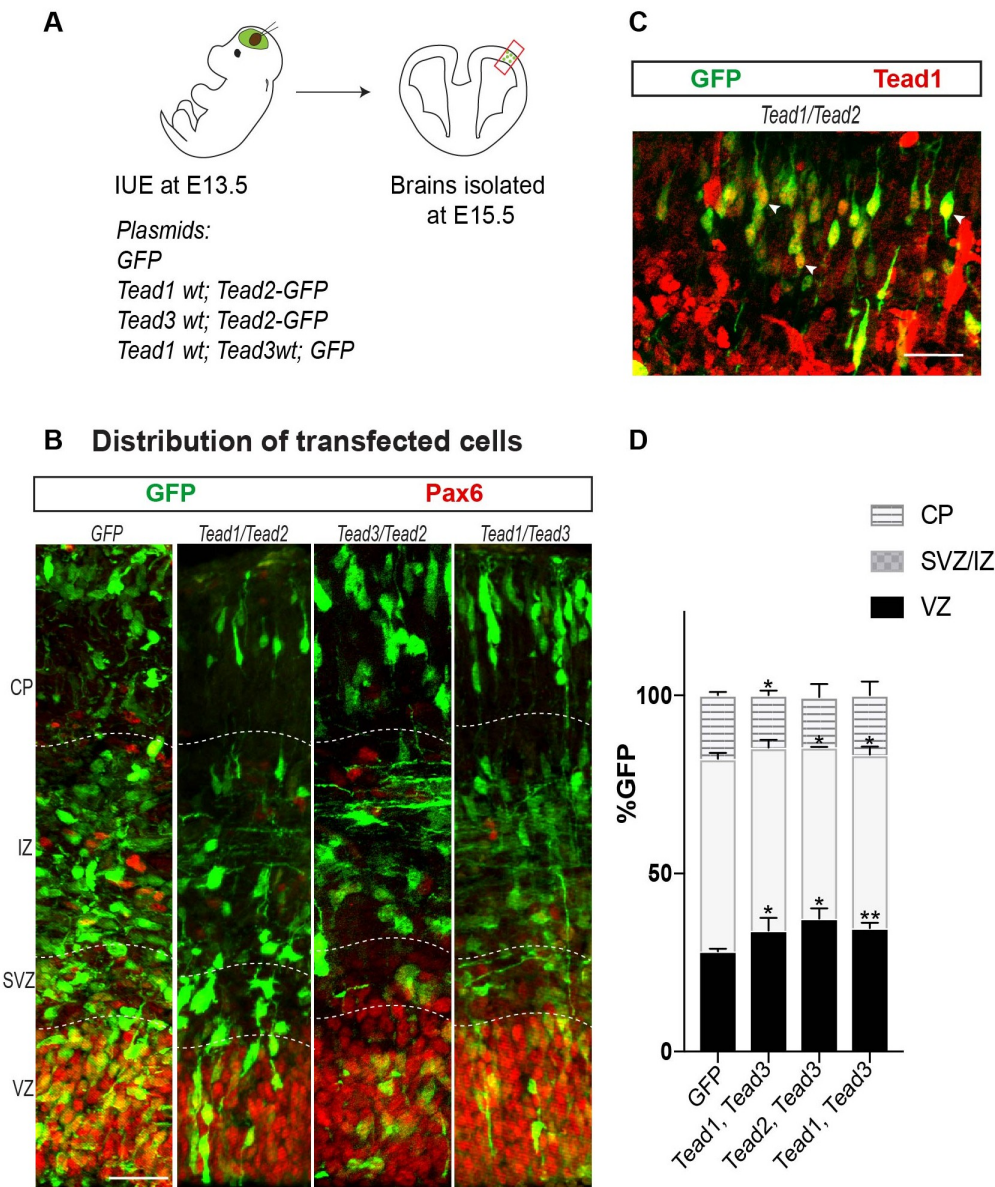
CP
IZ
SVZ
VZ

D

CP
SVZ/IZ
VZ

Figure 13': Tead1 and Tead3 double transfections with Tead2 rescue the phenotypes

A. Experimental paradigm showing the IUEs were done at E13.5 with wild-type forms of Tead1, Tead2 and Tead3. Tead2 has an IRES-GFP. An empty GFP plasmid was used as a control and also for co-transfection with Tead1 and Tead3. Brains were isolated 48h post transfection and analyzed using immunostaining. B. Distribution of transfected cells, post 48h showed that all the co-expressions rescued the phenotypes observed with single gain of function. C. Magnified image shows the expression of Tead1 in the CP, co-expressed with Tead2-GFP expressing cells. Tead1 or Tead3 co-transfection with Tead2 rescues the phenotypes and the cells migrate to the CP. D)Quantifications of the distribution of transfected cells show no significant phenotypes in the CP. Scale bar= 50µm.

Future Outlook

The role of Hippo signalling in corticogenesis is not clear but seems to be a new substantial node of regulation. Our current work has mostly focused on a short window of neurogenesis between E13.5 to E15.5. Since the mRNA expression of Tead genes is very dynamic throughout the developmental time course, it will be interesting to test the role of Teads in NSC expansion and gliogenesis. The current work has laid a strong foundation to the future analyses to be performed in understanding the molecular basis of our reciprocal phenotypes upon gain and loss of function.

Testing more predicted targets from in silico ISMARA analysis

We identified putative consensus Tead binding motifs in many genes in our NSC RNA-seq data. We explored the potential control of upstream effectors of Hippo signalling by the Tead TFs to understand any feedback mechanism in the signalling pathway. We found that *Lats2*, *Yap1, Fat1* have Tead binding motifs in their promoter regions. Though we did not validate Tead binding to these genes experimentally, we hypothesize that there could be some internal control and a feedback loop in Hippo signalling which maintains a homeostasis between different components of the pathways.

In this project, we tested only a few predicted targets experimentally during neurogenesis. Since the other predicted targets include important fate regulating genes such as *Olig2, Notch1, Lrp4, Hmgb2, Foxo4* and *Axl* (Appendix I), it will be important in the future to test the role of Teads in controlling the expression of these and other targets, in context of cortical fate specification.

Also, intracellular localization of Teads may control the shuttling of co-activators, in and out of the nucleus[193,232]. This is potentially a different level of control in Hippo signalling. It has been shown that nuclear localization of Teads also controls the Yap1/Taz retention in the nucleus. One of the known upstream cues for Hippo signalling activation is the cell/ tissue density. Under high density, the cytoplasmic retention and degradation of Yap1/Taz is observed[232]. This may also have consequential effects on the downstream cascade.

Mass spectroscopy to identify the binding partners of Tead TFs in vitro and in vivo

We identified a preferential binding of Yap1 with Tead2 in overexpression experimental paradigms in N2A cells. In addition, Tead1 DN experiments, using Tead1 protein lacking the Yap1/Taz binding suggested that Tead1 may not require Yap1/Taz for its function. These observations suggest that there could be potential differences in the binding partners of the Tead TFs and the complexes they form. Using mass spectroscopy of Tead1, Tead2 and Tead3 IP complexes, we can examine the interactome of individual Tead factors *in vitro* in our primary NSCs and *in vivo* NSCs, BPs or also whole dorsal cortices. This data will reveal molecular interactions that may be pivotal in controlling cell fate specification and migration in the developing forebrain.

Human Neocorticogenesis

From decades of work it is clear that transcription factors and signalling are key regulators of NSC generation of the cerebral cortex. However, there remains much to be learnt about how these pathways interact and converge to impose the precise regulation needed to form the complex structure of the cortical isocortex from a simple pseudostratified sheet of NECs. With the advent of high throughput single cell-omics and lineage tracing *in vivo*, the future looks demanding but bright and exciting for elucidating the mechanism of development of the cerebral cortex. Considering the high throughput datasets made available, it is an exciting new era to heavily translate our knowledge from mouse cortical development to human corticogenesis and disease.

The human cerebral cortex has expanded dramatically during phylogeny. Rodents have a smaller neocortex that lacks folding (lissencephalic) presenting limitations for studying the larger and highly folded (gyrencephalic) human neocortex[34]. Human corticogenesis is characterized by the appearance of an enlarged SVZ that is split into an inner SVZ (iSVZ) and an outer SVZ (oSVZ) by a thin fiber layer. The increased neocortical surface area and volume in humans is associated with an expanded pool of progenitor cells in the oSVZ[43].

In the human brain, an increase in the number of neurons is achieved through three stages of extensive cellular expansion. In humans, cortical neuron production begins by gestational week (GW) 6 subsequently the oSVZ develops after GW11 and expands dramatically to become the main germinal region of the neocortex[43]. Compared to the NSCs and BPs in the rodent telencephalon, humans have additional progenitor pools including outer radial glia (oRG) in the oSVZ (Figure 14'). oRG numbers increase as they undergo multiple cell divisions and add to the BP pool.

Experiments in ferrets, cats and humans also revealed that with an increase in brain gyrification, there are more proliferating cells associated with the oSVZ than there are in the VZ/iSVZ[34].

As great as our advances in understanding the molecular biology of the developing brain has been in recent decades, there is still much that must be addressed before NSCs and iPS cells can be considered for therapeutic intervention. A deeper understanding of population specific molecular markers, lineage relationships, and transcriptional profiles will certainly help. Recently, state-of-the-art technologies employing high throuput single cell DNA and RNA sequencing platforms have begun to provide a more complete understanding of activated gene networks at the single cell level in the developing brain, facilitating the extrapolation of intrinsic molecular architecture to function. For example, Pollen *et al*, 2015 demonstrated the molecular distinctions between vRG cells and oRG cells and suggested that oRG cells build a self-sustaining niche in the OSVZ[233]. They identified signalling mechanisms and processes active in these cells, such as the LIFR/STAT3 signalling pathway, inferring that the architecture and cellular interactions in the OSVZ niche play a pivotal role in cell fate and function[233]. Understanding how cellular heterogeneity arises within this niche requires a deeper grasp of the mechanisms that determine cell fate identity and commitment. Seminal work by Nowakowski *et al*, 2016 demonstrated the biological role of tRG cells[234]. Recently, Nowakowski *et al*, 2017 published an analyses of single cell transcriptomes in the developing human brain that revealed spatiotemporal gene expression patterns of cells from different brain regions, and outlined developmental trajectories during corticogenesis[235]. The data highlight a progression of modest transcriptional differences in RG cells that increases progressively through typological, temporal and topological hierarchies to maturing neurons, the successors of the RG cells. This signifies the control of spatiotemporal cues on gene expression with consequences on neocortical cell diversity[235].
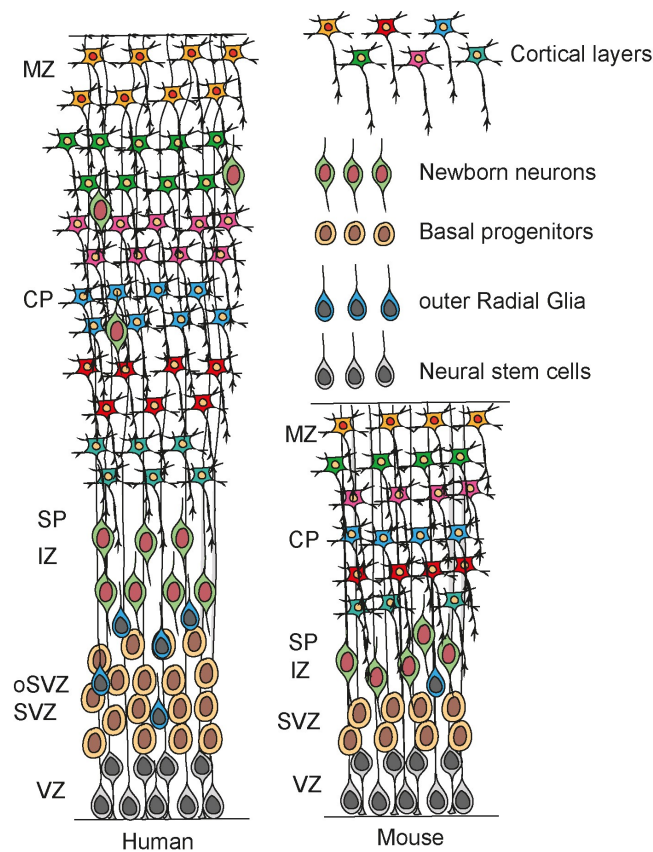
Figure 14': Scheme illustrating the composition and laminar organization of the developing human cortex, in comparison with mouse cortex.
The human cerebral cortex develops in a similar fashion to that of the mouse. One exception is the expansion of the subventricular zone (SVZ) to form the outer subventricular zone (oSVZ). The oSVZ in humans is the main zone of amplification. In addition to the neural stem cells (NSCs) and basal progenitors (BPs) of the developing mouse cerebral cortex, the human has addition progenitors, outer radial glial cells. CP - cortical plate, IZ - intermediate zone, MZ- marginal zone, SP – subplate, SVZ - subventricular zone, VZ - ventricular zone. (Adapted from Di Lullo, E. and A.R. Kriegstein, 2017).

Hippo signalling effectors in human brain

Interestingly, from the published single cell RNA-seq data-sets of human brain, OSVZ cells have an active epithelial to mesenchymal transition (EMT)[233]. Studies in breast cancers have elucidated the role of Teads and Yap in active EMT[215]. Hence, to investigate the relevance of Hippo signalling effectors in human brain, I extended my analyses to the published RNA seq data-set for single cells from different regions of human brain, (bit.ly/cortexSingleCell)[233,235]. Focussing primarily on the three radial glia cell types, human vRG cells, tRG cells and oRG cells in the germinal zones, I explored the dynamics of expression of Hippo effectors and Tead targets in these cells. Interestingly, many of the Hippo co-activators (YAP1), TFs TEADs (TEAD2, TEAD3), receptors (FAT1, FAT3, CRB2), ligands (CD44), and many predicted and   validated

Tead targets (CYR61, LRP4, PMP22, SPARC, ANXA2, DTNA, ZFP36L1, TRPS1, CTGF, APOE etc.) showed specific and higher expression in germinal zones of the human cortex[214]. Figure 15' illustrates the dynamics of Hippo pathway effectors in human vRG cells, tRG cells and oRG cells and also in intermediate progenitors (IPCs). I observed a vast heterogeneity in expression in RG cells undergoing division. Hence, it is interesting to study the molecular basis of the Hippo pathway in context of human brain, especially in terms of its role in germinal zone integrity, to infer its role in organ size and gyrification.

To test the role of Hippo signalling in context of human brain, organoids will serve as an important tool to manipulate and validate hypotheses concerning human cortical development. Another alternative to organoids would be the use of patient-derived 2D induced pluripotent cell (iPSC) cultures that are easier to manipulate and lineage-trace using viral transduction. The gain and loss of function of Hippo effectors in organoids, iPSCs and *in vivo* (in mice) can be performed by using lentiviral and CRISPR-Cas9 approaches as major experimental tools. The transduced cells upon gain or loss will be lineage-traced and consequent phenotypic studies, analyzing morphology, marker expression, transcriptomics etc. will be performed to test the effect and relevance of the manipulation. Cell cycle, differentiation, migration phenotypes will be tested using respective markers used in the field. Further validations will be performed by molecular and biochemical assays to micro-dissect the relevance of Hippo signalling in terms of human corticogenesis.
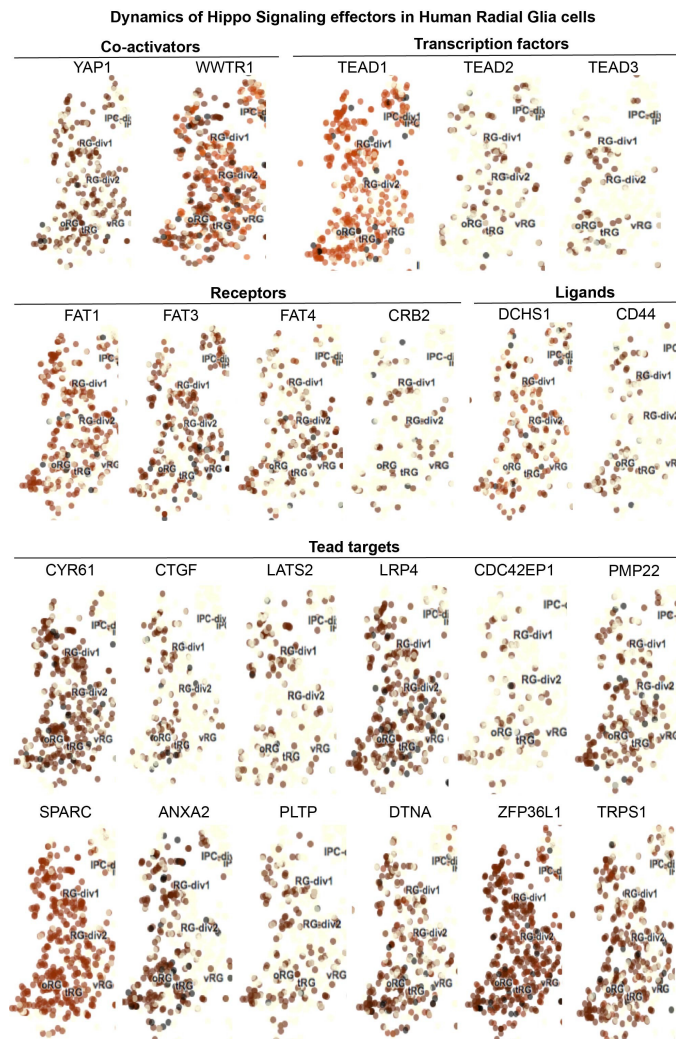
Figure 15': Dynamics of Hippo signalling effectors in human Radial Glia cells at single cell level.
Hippo effectors show massive heterogeneity in expression at single-cell level in vRG cells, oRG cells and tRG cells. Also, the predicted Tead targets from ISMARA show high expression in the germinal zones. For many effectors and targets, some heterogeneity is evident in IPCs and in different cell cycle zones as well.

In silico predicted Tead targets have interesting roles in Neurodegenerative diseases

Some of the predicted Hippo targets we describe are involved in a wide range of neuropathies. One of the top Tead targets, neuronal *Ctgf* (Connective tissue growth factor) regulates oligodendrogenesis and subsequent myelination[236]. The defects in Schwann cells are observed in Déjérine-Sottas neuropathy, which is associated with de novo PMP22 (Peripheral myelin protein 22) mutation, another strong predicted and validated Tead target[237]. Mutations in E4 allele of APOE (Apolipoprotein E), a target of Tead are associated with Alzheimer's disease[238]. Hippo signalling also interacts with many other signalling pathways. It opens an array of possibility to explore the

role of Hippo signalling effectors in neurodegenerative disease and tissue regeneration.

Graphical Abstract
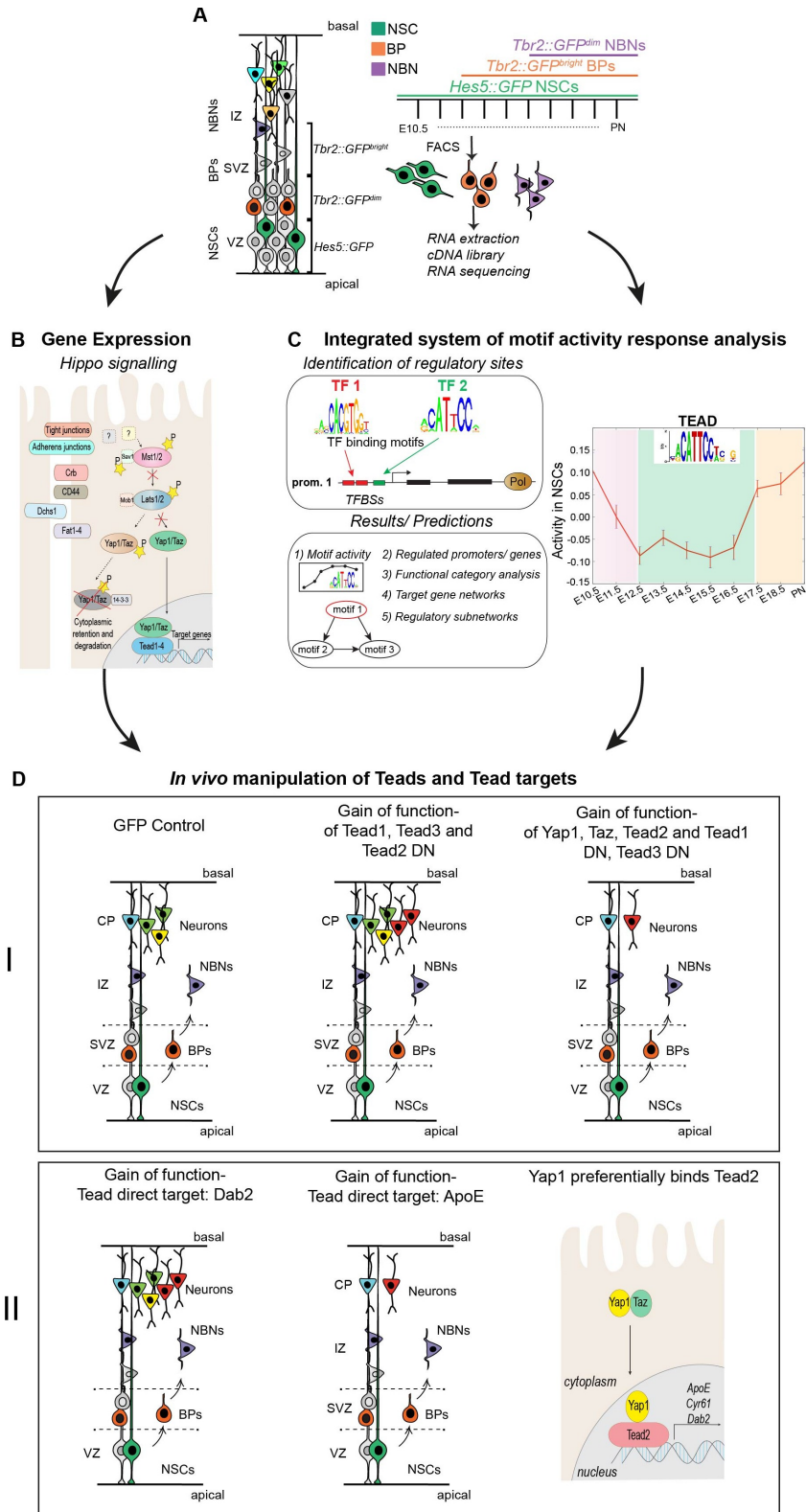
References

1. Tam PP, Loebel DA. Gene function in mouse embryogenesis: get set for gastrulation. *Nat Rev Genet.* 2007;8(5):368-381.
2. Copp AJ, Greene ND, Murdoch JN. The genetic basis of mammalian neurulation. *Nat Rev Genet.* 2003;4(10):784-793.
3. Smart IH. Proliferative characteristics of the ependymal layer during the early development of the mouse neocortex: a pilot study based on recording the number, location and plane of cleavage of mitotic figures. *J Anat.* 1973;116(Pt 1):67-91.
4. Copp AJ. Neurulation in the cranial region--normal and abnormal. *J Anat.* 2005;207(5):623-635.
5. Tong CK, Alvarez-Buylla A. SnapShot: Adult Neurogenesis in the V-SVZ. *Neuron.* 2014;81(1):220-220 e221.
6. Shimokita E, Takahashi Y. Secondary neurulation: Fate-mapping and gene manipulation of the neural tube in tail bud. *Dev Growth Differ.* 2011;53(3):401-410.
7. Liu A, Niswander LA. Bone morphogenetic protein signalling and vertebrate nervous system development. *Nat Rev Neurosci.* 2005;6(12):945-954.
8. Jessell TM, Sanes JR. *Principles of neural science: The Induction and Patterning of the Nervous System.* 4th ed. ed. New York: McGraw-Hill, Health Professions Division; 2000.
9. Beattie R, Mukhtar T, Taylor V. Fundamentals of Neurogenesis and Neural Stem Cell Development. *Neural Surface Antigens: From Basic Biology Towards Biomedical Applications.* 2015:13.
10. Geschwind DH, Rakic P. Cortical evolution: judge the brain by its cover. *Neuron.* 2013;80(3):633-647.
11. Rallu M, Corbin JG, Fishell G. Parsing the prosencephalon. *Nat Rev Neurosci.* 2002;3(12):943-951.
12. Lupo G, Harris WA, Lewis KE. Mechanisms of ventral patterning in the vertebrate nervous system. *Nat Rev Neurosci.* 2006;7(2):103-114.
13. Cohen M, Briscoe J, Blassberg R. Morphogen interpretation: the transcriptional logic of neural tube patterning. *Curr Opin Genet Dev.* 2013;23(4):423-428.
14. Maden M. Retinoic acid in the development, regeneration and maintenance of the nervous system. *Nat Rev Neurosci.* 2007;8(10):755-765.
15. Tiberi L, Vanderhaeghen P, van den Ameele J. Cortical neurogenesis and morphogens: diversity of cues, sources and functions. *Curr Opin Cell Biol.* 2012;24(2):269-276.
16. Sansom SN, Livesey FJ. Gradients in the brain: the control of the development of form and function in the cerebral cortex. *Cold Spring Harb Perspect Biol.* 2009;1(2):a002519.
17. Ciani L, Salinas PC. WNTS in the vertebrate nervous system: from patterning to neuronal connectivity. *Nat Rev Neurosci.* 2005;6(5):351-362.
18. Hebert JM, Fishell G. The genetics of early telencephalon patterning: some assembly required. *Nat Rev Neurosci.* 2008;9(9):678-685.
19. Houart C, Caneparo L, Heisenberg C-P, Barth KA, Take-Uchi M, Wilson SW. Establishment of the Telencephalon during Gastrulation by Local Antagonism of Wnt Signaling. *Neuron.* 2002;35(2):255-265.
20. Piccolo S, Agius E, Leyns L, et al. The head inducer Cerberus is a multifunctional antagonist of Nodal, BMP and Wnt signals. *Nature.* 1999;397(6721):707-710.
21. Bafico A, Liu G, Yaniv A, Gazit A, Aaronson SA. Novel mechanism of Wnt signalling inhibition mediated by Dickkopf-1 interaction with LRP6/Arrow. *Nature cell biology.* 2001;3(7):683-686.
22. Pearson JC, Lemons D, McGinnis W. Modulating Hox gene functions during animal body patterning. *Nat Rev Genet.* 2005;6(12):893-904.
23. Akin ZN, Nazarali AJ. Hox genes and their candidate downstream targets in the developing central nervous system. *Cell Mol Neurobiol.* 2005;25(3-4):697-741.
24. Philippidou P, Dasen JS. Hox genes: choreographers in neural development, architects of circuit organization. *Neuron.* 2013;80(1):12-34.
25. Kiecker C, Lumsden A. Compartments and their boundaries in vertebrate brain development. *Nat Rev Neurosci.* 2005;6(7):553-564.

26.   Lee HK, Lee HS, Moody SA. Neural transcription factors: from embryos to neural stem cells. *Mol Cells.* 2014;37(10):705-712.

27.   Paridaen JT, Huttner WB. Neurogenesis during development of the vertebrate central nervous system. *EMBO Rep.* 2014;15(4):351-364.

28.   Zhadanov AB, Provance DW, Jr., Speer CA, et al. Absence of the tight junctional protein AF-6 disrupts epithelial cell-cell junctions and cell polarity during mouse development. *Curr Biol.* 1999;9(16):880-888.

29.   Gal JS, Morozov YM, Ayoub AE, Chatterjee M, Rakic P, Haydar TF. Molecular and morphological heterogeneity of neural precursors in the mouse neocortical proliferative zones. *J Neurosci.* 2006;26(3):1045-1056.

30.   Stancik EK, Navarro-Quiroga I, Sellke R, Haydar TF. Heterogeneity in Ventricular Zone Neural Precursors Contributes to Neuronal Fate Diversity in the Postnatal Neocortex. *Journal of Neuroscience.* 2010;30(20):7028-7036.

31.   Tan X, Shi SH. Neocortical neurogenesis and neuronal migration. *Wiley Interdiscip Rev Dev Biol.* 2013;2(4):443-459.

32.   Kosodo Y, Suetsugu T, Suda M, et al. Regulation of interkinetic nuclear migration by cell cycle-coupled active and passive mechanisms in the developing brain. *EMBO J.* 2011;30(9):1690-1704.

33.   Taverna E, Huttner WB. Neural progenitor nuclei IN motion. *Neuron.* 2010;67(6):906-914.

34.   Lui JH, Hansen DV, Kriegstein AR. Development and evolution of the human neocortex. *Cell.* 2011;146(1):18-36.

35.   Takahashi T, Nowakowski RS, Caviness VS, Jr. Cell cycle parameters and patterns of nuclear movement in the neocortical proliferative zone of the fetal mouse. *J Neurosci.* 1993;13(2):820-833.

36.   Higginbotham H, Guo J, Yokota Y, et al. Arl13b-regulated cilia activities are essential for polarized radial glial scaffold formation. *Nat Neurosci.* 2013;16(8):1000-1007.

37.   Jiang X, Nardelli J. Cellular and molecular introduction to brain development. *Neurobiol Dis.* 2016;92(Pt A):3-17.

38.   Taverna E, Gotz M, Huttner WB. The cell biology of neurogenesis: toward an understanding of the development and evolution of the neocortex. *Annu Rev Cell Dev Biol.* 2014;30:465-502.

39.   Fietz SA, Kelava I, Vogt J, et al. OSVZ progenitors of human and ferret neocortex are epithelial-like and expand by integrin signaling. *Nat Neurosci.* 2010;13(6):690-699.

40.   Hansen DV, Lui JH, Parker PR, Kriegstein AR. Neurogenic radial glia in the outer subventricular zone of human neocortex. *Nature.* 2010;464(7288):554-561.

41.   Kelava I, Reillo I, Murayama AY, et al. Abundant occurrence of basal radial glia in the subventricular zone of embryonic neocortex of a lissencephalic primate, the common marmoset Callithrix jacchus. *Cereb Cortex.* 2012;22(2):469-481.

42.   Wang X, Tsai JW, LaMonica B, Kriegstein AR. A new subtype of progenitor cell in the mouse embryonic neocortex. *Nat Neurosci.* 2011;14(5):555-561.

43.   Hansen DV, Rubenstein JL, Kriegstein AR. Deriving excitatory neurons of the neocortex from pluripotent stem cells. *Neuron.* 2011;70(4):645-660.

44.   Shitamukai A, Konno D, Matsuzaki F. Oblique Radial Glial Divisions in the Developing Mouse Neocortex Induce Self-Renewing Progenitors outside the Germinal Zone That Resemble Primate Outer Subventricular Zone Progenitors. *Journal of Neuroscience.* 2011;31(10):3683-3695.

45.   Kriegstein AR, Gotz M. Radial glia diversity: a matter of cell fate. *Glia.* 2003;43(1):37-43.

46.   Malatesta P, Hartfuss E, Gotz M. Isolation of radial glial cells by fluorescent-activated cell sorting reveals a neuronal lineage. *Development.* 2000;127(24):5253-5263.

47.   Franco SJ, Muller U. Shaping Our Minds: Stem and Progenitor Cell Diversity in the Mammalian Neocortex. *Neuron.* 2013;77(1):19-34.

48.   Gotz M, Huttner WB. The cell biology of neurogenesis. *Nat Rev Mol Cell Biol.* 2005;6(10):777-788.

49.   Hartfuss E, Galli R, Heins N, Gotz M. Characterization of CNS precursor subtypes and radial glia. *Dev Biol.* 2001;229(1):15-30.

50.   Malatesta P, Hack MA, Hartfuss E, et al. Neuronal or glial progeny: regional differences in radial glia fate. *Neuron.* 2003;37(5):751-764.

51.	Bansod S, Kageyama R, Ohtsuka T. Hes5 regulates the transition timing of neurogenesis and gliogenesis in mammalian neocortical development. *Development.* 2017;144(17):3156-3167.

52.	Haubensak W, Attardo A, Denk W, Huttner WB. Neurons arise in the basal neuroepithelium of the early mammalian telencephalon: a major site of neurogenesis. *Proc Natl Acad Sci U S A.* 2004;101(9):3196-3201.

53.	Sahara S, O'Leary DD. Fgf10 regulates transition period of cortical stem cell differentiation to radial glia controlling generation of neurons and basal progenitors. *Neuron.* 2009;63(1):48-62.

54.	Miyata T, Kawaguchi A, Saito K, Kawano M, Muto T, Ogawa M. Asymmetric production of surface-dividing and non-surface-dividing cortical progenitor cells. *Development.* 2004;131(13):3133-3145.

55.	Noctor SC, V M-C, Ivic L, Kriegstein AR. Cortical neurons arise in symmetric and asymmetric division zones and migrate through specific phases. *Nature Neuroscience.* 2004;7(2):136-144.

56.	Cubelos B, Sebastian-Serrano A, Kim S, et al. Cux-2 controls the proliferation of neuronal intermediate precursors of the cortical subventricular zone. *Cereb Cortex.* 2008;18(8):1758-1770.

57.	Englund C, Fink A, Lau C, et al. Pax6, Tbr2, and Tbr1 are expressed sequentially by radial glia, intermediate progenitor cells, and postmitotic neurons in developing neocortex. *J Neurosci.* 2005;25(1):247-251.

58.	Nieto M, Monuki ES, Tang H, et al. Expression of Cux-1 and Cux-2 in the subventricular zone and upper layers II-IV of the cerebral cortex. *J Comp Neurol.* 2004;479(2):168-180.

59.	Britanova O, Akopov S, Lukyanov S, Gruss P, Tarabykin V. Novel transcription factor Satb2 interacts with matrix attachment region DNA elements in a tissue-specific manner and demonstrates cell-type-dependent expression in the developing mouse CNS. *Eur J Neurosci.* 2005;21(3):658-668.

60.	Zimmer C, Tiveron MC, Bodmer R, Cremer H. Dynamics of Cux2 expression suggests that an early pool of SVZ precursors is fated to become upper cortical layer neurons. *Cerebral Cortex.* 2004;14(12):1408-1420.

61.	Tarabykin V, Stoykova A, Usman N, Gruss P. Cortical upper layer neurons derive from the subventricular zone as indicated by Svet1 gene expression. *Development.* 2001;128(11):1983-1993.

62.	Stancik EK, Navarro-Quiroga I, Sellke R, Haydar TF. Heterogeneity in ventricular zone neural precursors contributes to neuronal fate diversity in the postnatal neocortex. *J Neurosci.* 2010;30(20):7028-7036.

63.	Mukhtar T, Taylor V. Untangling Cortical Complexity During Development. *J Exp Neurosci.* 2018;12:1179069518759332.

64.	Lancaster MA, Knoblich JA. Spindle orientation in mammalian cerebral cortical development. *Curr Opin Neurobiol.* 2012;22(5):737-746.

65.	Konno D, Shioi G, Shitamukai A, et al. Neuroepithelial progenitors undergo LGN-dependent planar divisions to maintain self-renewability during mammalian neurogenesis. *Nat Cell Biol.* 2008;10(1):93-101.

66.	Peyre E, Jaouen F, Saadaoui M, et al. A lateral belt of cortical LGN and NuMA guides mitotic spindle movements and planar division in neuroepithelial cells. *J Cell Biol.* 2011;193(1):141-154.

67.	Postiglione MP, Juschke C, Xie Y, Haas GA, Charalambous C, Knoblich JA. Mouse inscuteable induces apical-basal spindle orientation to facilitate intermediate progenitor generation in the developing neocortex. *Neuron.* 2011;72(2):269-284.

68.	Bultje RS, Castaneda-Castellanos DR, Jan LY, Jan YN, Kriegstein AR, Shi SH. Mammalian Par3 regulates progenitor cell asymmetric division via notch signaling in the developing neocortex. *Neuron.* 2009;63(2):189-202.

69.	Costa MR, Wen G, Lepier A, Schroeder T, Gotz M. Par-complex proteins promote proliferative progenitor divisions in the developing mouse cerebral cortex. *Development.* 2008;135(1):11-22.

70.	Heins N, Cremisi F, Malatesta P, et al. Emx2 promotes symmetric cell divisions and a multipotential fate in precursors from the cerebral cortex. *Mol Cell Neurosci.* 2001;18(5):485-502.

71. Gaiano N, Fishell G. The role of notch in promoting glial and neural stem cell fates. *Annu Rev Neurosci.* 2002;25:471-490.

72. Dong Z, Yang N, Yeo SY, Chitnis A, Guo S. Intralineage directional Notch signaling regulates self-renewal and differentiation of asymmetrically dividing radial glia. *Neuron.* 2012;74(1):65-78.

73. Gaiano N, Nye JS, Fishell G. Radial glial identity is promoted by Notch1 signaling in the murine forebrain. *Neuron.* 2000;26(2):395-404.

74. Lutolf S, Radtke F, Aguet M, Suter U, Taylor V. Notch1 is required for neuronal and glial differentiation in the cerebellum. *Development.* 2002;129(2):373-385.

75. Imayoshi I, Sakamoto M, Yamaguchi M, Mori K, Kageyama R. Essential roles of Notch signaling in maintenance of neural stem cells in developing and adult brains. *J Neurosci.* 2010;30(9):3489-3498.

76. Imayoshi I, Shimogori T, Ohtsuka T, Kageyama R. Hes genes and neurogenin regulate non-neural versus neural fate specification in the dorsal telencephalic midline. *Development.* 2008;135(15):2531-2541.

77. Alvarez-Rodriguez R, Pons S. Expression of the proneural gene encoding Mash1 suppresses MYCN mitotic activity. *J Cell Sci.* 2009;122(Pt 5):595-599.

78. Parras CM, Schuurmans C, Scardigli R, Kim J, Anderson DJ, Guillemot F. Divergent functions of the proneural genes Mash1 and Ngn2 in the specification of neuronal subtype identity. *Genes Dev.* 2002;16(3):324-338.

79. Vessey JP, Amadei G, Burns SE, Kiebler MA, Kaplan DR, Miller FD. An asymmetrically localized Staufen2-dependent RNA complex regulates maintenance of mammalian neural stem cells. *Cell Stem Cell.* 2012;11(4):517-528.

80. Heins N, Malatesta P, Cecconi F, et al. Glial cells generate neurons: the role of the transcription factor Pax6. *Nat Neurosci.* 2002;5(4):308-315.

81. Kosodo Y, Roper K, Haubensak W, Marzesco AM, Corbeil D, Huttner WB. Asymmetric distribution of the apical plasma membrane during neurogenic divisions of mammalian neuroepithelial cells. *EMBO J.* 2004;23(11):2314-2324.

82. Kouprina N, Pavlicek A, Mochida GH, et al. Accelerated evolution of the ASPM gene controlling brain size begins prior to human brain expansion. *Plos Biology.* 2004;2(5):653-663.

83. Chae TH, Kim S, Marz KE, Hanson PI, Walsh CA. The hyh mutation uncovers roles for alpha Snap in apical protein localization and control of neural cell fate. *Nat Genet.* 2004;36(3):264-270.

84. Sheen VL, Ganesh VS, Topcu M, et al. Mutations in ARFGEF2 implicate vesicle trafficking in neural progenitor proliferation and migration in the human cerebral cortex. *Nat Genet.* 2004;36(1):69-76.

85. Zechner D, Fujita Y, Hulsken J, et al. beta-catenin signals regulate cell growth and the balance between progenitor cell expansion and differentiation in the nervous system. *Developmental Biology.* 2003;258(2):406-418.

86. Chenn A, Walsh CA. Increased neuronal production, enlarged forebrains and cytoarchitectural distortions in beta-catenin overexpressing transgenic mice. *Cereb Cortex.* 2003;13(6):599-606.

87. Leone DP, Srinivasan K, Chen B, Alcamo E, McConnell SK. The determination of projection neuron identity in the developing cerebral cortex. *Curr Opin Neurobiol.* 2008;18(1):28-35.

88. Custo Greig LF, Woodworth MB, Galazo MJ, Padmanabhan H, Macklis JD. Molecular logic of neocortical projection neuron specification, development and diversity. *Nat Rev Neurosci.* 2013;14(11):755-769.

89. Guo C, Eckler MJ, McKenna WL, McKinsey GL, Rubenstein JL, Chen B. Fezf2 expression identifies a multipotent progenitor for neocortical projection neurons, astrocytes, and oligodendrocytes. *Neuron.* 2013;80(5):1167-1174.

90. McConnell SK. Fates of visual cortical neurons in the ferret after isochronic and heterochronic transplantation. *J Neurosci.* 1988;8(3):945-974.

91. Desai AR, McConnell SK. Progressive restriction in fate potential by neural progenitors during cerebral cortical development. *Development.* 2000;127(13):2863- 2872.

92. Han W, Sestan N. Cortical projection neurons: sprung from the same root. *Neuron.* 2013;80(5):1103-1105.

93. Eiraku M, Sasai Y. Mouse embryonic stem cell culture for generation of three-dimensional retinal and cortical tissues. *Nat Protoc.* 2011;7(1):69-79.

94. Gaspard N, Bouschet T, Hourez R, et al. An intrinsic mechanism of corticogenesis from embryonic stem cells. *Nature.* 2008;455(7211):351-357.

95. Shen Q, Wang Y, Dimos JT, et al. The timing of cortical neurogenesis is encoded within lineages of individual progenitor cells. *Nature Neuroscience.* 2006;9(6):743-751.

96. Tan SS, Breen S. Radial Mosaicism and Tangential Cell Dispersion Both Contribute to Mouse Neocortical Development. *Nature.* 1993;362(6421):638-640.

97. Chen B, Schaevitz LR, McConnell SK. Fezl regulates the differentiation and axon targeting of layer 5 subcortical projection neurons in cerebral cortex. *Proc Natl Acad Sci U S A.* 2005;102(47):17184-17189.

98. Molyneaux BJ, Arlotta P, Menezes JR, Macklis JD. Neuronal subtype specification in the cerebral cortex. *Nat Rev Neurosci.* 2007;8(6):427-437.

99. Kwan KY, Sestan N, Anton ES. Transcriptional co-regulation of neuronal migration and laminar identity in the neocortex. *Development.* 2012;139(9):1535-1546.

100. Franco SJ, Gil-Sanz C, Martinez-Garay I, et al. Fate-restricted neural progenitors in the mammalian cerebral cortex. *Science.* 2012;337(6095):746-749.

101. Gotz M, Williams BP, Bolz J, Price J. The specification of neuronal fate: a common precursor for neurotransmitter subtypes in the rat cerebral cortex in vitro. *Eur J Neurosci.* 1995;7(5):889-898.

102. Sultan KT, Brown KN, Shi SH. Production and organization of neocortical interneurons. *Front Cell Neurosci.* 2013;7:221.

103. Sultan KT, Brown KN, Shi SH. Production and organization of neocortical interneurons. *Front Cell Neurosci.* 2013;7.

104. Brown KN, Chen S, Han Z, et al. Clonal production and organization of inhibitory interneurons in the neocortex. *Science.* 2011;334(6055):480-486.

105. Marin O. Cellular and molecular mechanisms controlling the migration of neocortical interneurons. *European Journal of Neuroscience.* 2013;38(1):2019-2029.

106. Arlotta P, Molyneaux BJ, Chen J, Inoue J, Kominami R, Macklis JD. Neuronal subtype-specific genes that control corticospinal motor neuron development in vivo. *Neuron.* 2005;45(2):207-221.

107. Muzio L, DiBenedetto B, Stoykova A, Boncinelli E, Gruss P, Mallamaci A. Conversion of cerebral cortex into basal ganglia in Emx2(-/-) Pax6(Sey/Sey) double-mutant mice. *Nature Neuroscience.* 2002;5(8):737-745.

108. Hevner RF, Daza RA, Rubenstein JL, Stunnenberg H, Olavarria JF, Englund C. Beyond laminar fate: toward a molecular classification of cortical projection/pyramidal neurons. *Dev Neurosci.* 2003;25(2-4):139-151.

109. Di Lullo E, Kriegstein AR. The use of brain organoids to investigate neural development and disease. *Nat Rev Neurosci.* 2017;18(10):573-584.

110. Alcamo EA, Chirivella L, Dautzenberg M, et al. Satb2 regulates callosal projection neuron identity in the developing cerebral cortex. *Neuron.* 2008;57(3):364-377.

111. Srinivasan K, Leone DP, Bateson RK, et al. A network of genetic repression and derepression specifies projection fates in the developing neocortex. *Proc Natl Acad Sci U S A.* 2012;109(47):19071-19078.

112. Schuurmans C, Armant O, Nieto M, et al. Sequential phases of cortical specification involve Neurogenin-dependent and -independent pathways. *EMBO J.* 2004;23(14):2892-2902.

113. Fode C, Ma Q, Casarosa S, Ang SL, Anderson DJ, Guillemot F. A role for neural determination genes in specifying the dorsoventral identity of telencephalic neurons. *Genes Dev.* 2000;14(1):67-80.

114. Hirabayashi Y, Suzki N, Tsuboi M, et al. Polycomb limits the neurogenic competence of neural precursor cells to promote astrogenic fate transition. *Neuron.* 2009;63(5):600-613.

115. Kishi Y, Fujii Y, Hirabayashi Y, Gotoh Y. HMGA regulates the global chromatin state and neurogenic potential in neocortical precursor cells. *Nat Neurosci.* 2012;15(8):1127-1133.

116. Pereira JD, Sansom SN, Smith J, Dobenecker MW, Tarakhovsky A, Livesey FJ. Ezh2, the histone methyltransferase of PRC2, regulates the balance between self-renewal

and differentiation in the cerebral cortex. *Proceedings of the National Academy of Sciences of the United States of America.* 2010;107(36):15957-15962.

117.   Sessa A, Ciabatti E, Drechsel D, et al. The Tbr2 Molecular Network Controls Cortical Neuronal Differentiation Through Complementary Genetic and Epigenetic Pathways (vol 27, pg 3378, 2017). *Cerebral Cortex.* 2017;27(12):5715-5715.

118.   Hitoshi S, Ishino Y, Kumar A, et al. Mammalian Gcm genes induce Hes5 expression by active DNA demethylation and induce neural stem cells. *Nat Neurosci.* 2011;14(8):957-964.

119.   Tuoc TC, Boretius S, Sansom SN, et al. Chromatin regulation by BAF170 controls cerebral cortical size and thickness. *Dev Cell.* 2013;25(3):256-269.

120.   Yip DJ, Corcoran CP, Alvarez-Saavedra M, et al. Snf2l regulates Foxg1-dependent progenitor cell expansion in the developing brain. *Dev Cell.* 2012;22(4):871-878.

121.   Fan G, Martinowich K, Chin MH, et al. DNA methylation controls the timing of astrogliogenesis through regulation of JAK-STAT signaling. *Development.* 2005;132(15):3345-3356.

122.   Namihira M, Kohyama J, Semi K, et al. Committed neuronal precursors confer astrocytic potential on residual neural precursor cells. *Dev Cell.* 2009;16(2):245-255.

123.   Yoon KJ, Ringeling FR, Vissers C, et al. Temporal Control of Mammalian Cortical Neurogenesis by m(6)A Methylation. *Cell.* 2017;171(4):877-889 e817.

124.   Popovitchenko T, Rasin MR. Transcriptional and Post-Transcriptional Mechanisms of the Development of Neocortical Lamination. *Front Neuroanat.* 2017;11:102.

125.   Bian S, Hong J, Li Q, et al. MicroRNA cluster miR-17-92 regulates neural stem cell expansion and transition to intermediate progenitors in the developing mouse neocortex. *Cell Rep.* 2013;3(5):1398-1406.

126.   Bian S, Xu TL, Sun T. Tuning the cell fate of neurons and glia by microRNAs. *Curr Opin Neurobiol.* 2013;23(6):928-934.

127.   Nowakowski TJ, Fotaki V, Pollock A, Sun T, Pratt T, Price DJ. MicroRNA-92b regulates the development of intermediate cortical progenitors in embryonic mouse brain. *Proc Natl Acad Sci U S A.* 2013;110(17):7056-7061.

128.   Cimadamore F, Amador-Arjona A, Chen C, Huang CT, Terskikh AV. SOX2-LIN28/let-7 pathway regulates proliferation and neurogenesis in neural precursors. *Proc Natl Acad Sci U S A.* 2013;110(32):E3017-3026.

129.   Aprea J, Prenninger S, Dori M, et al. Transcriptome sequencing during mouse brain development identifies long non-coding RNAs functionally involved in neurogenic commitment. *EMBO J.* 2013;32(24):3145-3160.

130.   Fatica A, Bozzoni I. Long non-coding RNAs: new players in cell differentiation and development. *Nat Rev Genet.* 2014;15(1):7-21.

131.   Ng SY, Bogu GK, Soh BS, Stanton LW. The long noncoding RNA RMST interacts with SOX2 to regulate neurogenesis. *Mol Cell.* 2013;51(3):349-359.

132.   Kim KK, Nam J, Mukouyama YS, Kawamoto S. Rbfox3-regulated alternative splicing of Numb promotes neuronal differentiation during development. *J Cell Biol.* 2013;200(4):443-458.

133.   Knuckles P, Vogt MA, Lugert S, et al. Drosha regulates neurogenesis by controlling neurogenin 2 expression independent of microRNAs. *Nat Neurosci.* 2012;15(7):962-969.

134.   Androutsellis-Theotokis A, Leker RR, Soldner F, et al. Notch signalling regulates stem cell numbers in vitro and in vivo. *Nature.* 2006;442(7104):823-826.

135.   Mizutani K, Yoon K, Dang L, Tokunaga A, Gaiano N. Differential Notch signalling distinguishes neural stem cells from intermediate progenitors. *Nature.* 2007;449(7160):351-+.

136.   Ohtsuka T, Ishibashi M, Gradwohl G, Nakanishi S, Guillemot F, Kageyama R. Hes1 and Hes5 as Notch effectors in mammalian neuronal differentiation. *The EMBO Journal.* 1999;18(8):2196-2207.

137.   Hitoshi S, Alexson T, Tropepe V, et al. Notch pathway molecules are essential for the maintenance, but not the generation, of mammalian neural stem cells. *Genes Dev.* 2002;16(7):846-858.

138.   Basak O, Taylor V. Identification of self-replicating multipotent progenitors in the embryonic nervous system by high Notch activity and Hes5 expression. *Eur J Neurosci.* 2007;25(4):1006-1022.

139. Louvi A, Artavanis-Tsakonas S. Notch signalling in vertebrate neural development. *Nat Rev Neurosci.* 2006;7(2):93-102.

140. Brou C, Logeat F, Gupta N, et al. A novel proteolytic cleavage involved in Notch signaling: the role of the disintegrin-metalloprotease TACE. *Mol Cell.* 2000;5(2):207-216.

141. Mumm JS, Schroeter EH, Saxena MT, et al. A ligand-induced extracellular cleavage regulates gamma-secretase-like proteolytic activation of Notch1. *Mol Cell.* 2000;5(2):197-206.

142. Kurooka H, Kuroda K, Honjo T. Roles of the ankyrin repeats and C-terminal region of the mouse notch1 intracellular region. *Nucleic Acids Res.* 1998;26(23):5448-5455.

143. Tamura K, Taniguchi Y, Minoguchi S, et al. Physical interaction between a novel domain of the receptor Notch and the transcription factor RBP-J kappa/Su(H). *Curr Biol.* 1995;5(12):1416-1423.

144. Kato H, Taniguchi Y, Kurooka H, et al. Involvement of RBP-J in biological functions of mouse Notch1 and its derivatives. *Development.* 1997;124(20):4133-4141.

145. Hsieh JJ, Hayward SD. Masking of the CBF1/RBPJ kappa transcriptional repression domain by Epstein-Barr virus EBNA2. *Science.* 1995;268(5210):560-563.

146. Dou S, Zeng X, Cortes P, et al. The recombination signal sequence-binding protein RBP-2N functions as a transcriptional repressor. *Mol Cell Biol.* 1994;14(5):3310-3319.

147. Fiuza UM, Arias AM. Cell and molecular biology of Notch. *J Endocrinol.* 2007;194(3):459-474.

148. Hatakeyama J, Bessho Y, Katoh K, et al. Hes genes regulate size, shape and histogenesis of the nervous system by control of the timing of neural stem cell differentiation. *Development.* 2004;131(22):5539-5550.

149. Lütolf S, Radtke F, Aguet M, Suter U, Taylor V. Notch1 is required for neuronal and glial differentiation in the cerebellum. *Development.* 2002;129(2):373-385.

150. Kageyama R, Ohtsuka T, Kobayashi T. The Hes gene family: repressors and oscillators that orchestrate embryogenesis. *Development.* 2007;134(7):1243-1251.

151. Shimojo H, Ohtsuka T, Kageyama R. Oscillations in Notch Signaling Regulate Maintenance of Neural Progenitors. *Neuron.* 58(1):52-64.

152. Dequéant M-L, Glynn E, Gaudenz K, et al. A Complex Oscillating Network of Signaling Genes Underlies the Mouse Segmentation Clock. *Science.* 2006;314(5805):1595-1598.

153. Kageyama R, Ohtsuka T, Shimojo H, Imayoshi I. Dynamic Notch signaling in neural progenitor cells and a revised view of lateral inhibition. *Nature neuroscience.* 2008;11(11):1247-1251.

154. Ables JL, Decarolis NA, Johnson MA, et al. Notch1 is required for maintenance of the reservoir of adult hippocampal stem cells. *J Neurosci.* 2010;30(31):10484-10492.

155. Aguirre A, Rubio ME, Gallo V. Notch and EGFR pathway interaction regulates neural stem cell number and self-renewal. *Nature.* 2010;467(7313):323-327.

156. Basak O, Giachino C, Fiorini E, Macdonald HR, Taylor V. Neurogenic subventricular zone stem/progenitor cells are Notch1-dependent in their active but not quiescent state. *J Neurosci.* 2012;32(16):5654-5666.

157. Nyfeler Y, Kirch RD, Mantei N, et al. Jagged1 signals in the postnatal subventricular zone are required for neural stem cell self-renewal. *The EMBO Journal.* 2005;24(19):3504.

158. Giachino C, Basak O, Lugert S, et al. Molecular diversity subdivides the adult forebrain neural stem cell population. *Stem Cells.* 2014;32(1):70-84.

159. Basak O, Taylor V. Stem cells of the adult mammalian brain and their niche. *Cell Mol Life Sci.* 2009;66(6):1057-1072.

160. Ehm O, Goritz C, Covic M, et al. RBPJkappa-dependent signaling is essential for long-term maintenance of neural stem cells in the adult hippocampus. *J Neurosci.* 2010;30(41):13794-13807.

161. Lugert S, Basak O, Knuckles P, et al. Quiescent and active hippocampal neural stem cells with distinct morphologies respond selectively to physiological and pathological stimuli and aging. *Cell Stem Cell.* 2010;6(5):445-456.

162. Pastrana E, Cheng LC, Doetsch F. Simultaneous prospective purification of adult subventricular zone neural stem cells and their progeny. *Proc Natl Acad Sci U S A.* 2009;106(15):6387-6392.

163. Beckervordersandforth R, Tripathi P, Ninkovic J, et al. In vivo fate mapping and expression analysis reveals molecular hallmarks of prospectively isolated adult neural stem cells. *Cell Stem Cell.* 2010;7(6):744-758.

164. Suh H, Consiglio A, Ray J, Sawai T, D'Amour KA, Gage FH. In vivo fate analysis reveals the multipotent and self-renewal capacities of Sox2+ neural stem cells in the adult hippocampus. *Cell Stem Cell.* 2007;1(5):515-528.

165. Giachino C, Taylor V. Notching up neural stem cell homogeneity in homeostasis and disease. *Front Neurosci.* 2014;8:32.

166. Doetsch F. A niche for adult neural stem cells. *Current opinion in genetics & development.* 2003;13(5):543-550.

167. Shen Q, Goderie SK, Jin L, et al. Endothelial cells stimulate self-renewal and expand neurogenesis of neural stem cells. *Science.* 2004;304(5675):1338-1340.

168. Andreu-Agulló C, Morante-Redolat JM, Delgado AC, Fariñas I. Vascular niche factor PEDF modulates Notch-dependent stemness in the adult subependymal zone. *Nature neuroscience.* 2009;12(12):1514-1523.

169. Bar EE, Lin A, Mahairaki V, Matsui W, Eberhart CG. Hypoxia increases the expression of stem-cell markers and promotes clonogenicity in glioblastoma neurospheres. *The American journal of pathology.* 2010;177(3):1491-1502.

170. Gustafsson MV, Zheng X, Pereira T, et al. Hypoxia requires notch signaling to maintain the undifferentiated cell state. *Developmental cell.* 2005;9(5):617-628.

171. Harrison-Uy SJ, Pleasure SJ. Wnt signaling and forebrain development. *Cold Spring Harb Perspect Biol.* 2012;4(7):a008094.

172. Kuwahara A, Hirabayashi Y, Knoepfler PS, et al. Wnt signaling and its downstream target N-myc regulate basal progenitors in the developing neocortex. *Development.* 2010;137(7):1035-1044.

173. Inestrosa NC, Varela-Nallar L. Wnt signalling in neuronal differentiation and development. *Cell Tissue Res.* 2015;359(1):215-223.

174. Wrobel CN, Mutch CA, Swaminathan S, Taketo MM, Chenn A. Persistent expression of stabilized beta-catenin delays maturation of radial glial cells into intermediate progenitors. *Developmental Biology.* 2007;309(2):285-297.

175. Fukuchi-Shimogori T, Grove EA. Neocortex patterning by the secreted signaling molecule FGF8. *Science.* 2001;294(5544):1071-1074.

176. Bachler M, Neubuser A. Expression of members of the Fgf family and their receptors during midfacial development. *Mechanisms of Development.* 2001;100(2):313-316.

177. Itoh N, Ornitz DM. Evolution of the Fgf and Fgfr gene families. *Trends Genet.* 2004;20(11):563-569.

178. Rash BG, Lim HD, Breunig JJ, Vaccarino FM. FGF signaling expands embryonic cortical surface area by regulating Notch-dependent neurogenesis. *J Neurosci.* 2011;31(43):15604-15617.

179. Iwata T, Hevner RF. Fibroblast growth factor signaling in development of the cerebral cortex. *Dev Growth Differ.* 2009;51(3):299-323.

180. Sansom SN, Livesey FJ. Gradients in the Brain: The Control of the Development of Form and Function in the Cerebral Cortex. *Csh Perspect Biol.* 2009;1(2).

181. Hasegawa H, Ashigaki S, Takamatsu M, et al. Laminar patterning in the developing neocortex by temporally coordinated fibroblast growth factor signaling. *J Neurosci.* 2004;24(40):8711-8719.

182. Rodriguez-Martinez G, Velasco I. Activin and TGF-beta effects on brain development and neural stem cells. *CNS Neurol Disord Drug Targets.* 2012;11(7):844-855.

183. Ebendal T, Bengtsson H, Soderstrom S. Bone morphogenetic proteins and their receptors: Potential functions in the brain. *Journal of Neuroscience Research.* 1998;51(2):139-146.

184. Gomes FC, Sousa Vde O, Romao L. Emerging roles for TGF-beta1 in nervous system development. *Int J Dev Neurosci.* 2005;23(5):413-424.

185. Gudas LJ, Wagner JA. Retinoids regulate stem cell differentiation. *J Cell Physiol.* 2011;226(2):322-330.

186. Duester G. Retinoic acid synthesis and signaling during early organogenesis. *Cell.* 2008;134(6):921-931.

187. Perissi V, Jepsen K, Glass CK, Rosenfeld MG. Deconstructing repression: evolving models of co-repressor action. *Nat Rev Genet.* 2010;11(2):109-123.

188. Rochette-Egly C. Retinoic acid signaling and mouse embryonic stem cell differentiation: Cross talk between genomic and non-genomic effects of RA. *Biochimica Et Biophysica Acta-Molecular and Cell Biology of Lipids.* 2015;1851(1):66-75.

189. Park R, Moon UY, Park JY, et al. Yap is required for ependymal integrity and is suppressed in LPA-induced hydrocephalus. *Nature Communications.* 2016;7.

190. Chuang JH, Tung LC, Lin Y. Neural differentiation from embryonic stem cells in vitro: An overview of the signaling pathways. *World J Stem Cells.* 2015;7(2):437-447.

191. Easwaran V, Pishvaian M, Salimuddin, Byers S. Cross-regulation of beta-catenin-LEF/TCF and retinoid signaling pathways. *Curr Biol.* 1999;9(23):1415-1418.

192. Haushalter C, Asselin L, Fraulob V, Dolle P, Rhinn M. Retinoic acid controls early neurogenesis in the developing mouse cerebral cortex. *Dev Biol.* 2017;430(1):129-141.

193. Lin KC, Park HW, Guan KL. Regulation of the Hippo Pathway Transcription Factor TEAD. *Trends Biochem Sci.* 2017;42(11):862-872.

194. Panciera T, Azzolin L, Cordenonsi M, Piccolo S. Mechanobiology of YAP and TAZ in physiology and disease. *Nat Rev Mol Cell Biol.* 2017;18(12):758-770.

195. Zeng Q, Hong W. The emerging role of the hippo pathway in cell contact inhibition, organ size control, and cancer development in mammals. *Cancer Cell.* 2008;13(3):188-192.

196. Cappello S, Gray MJ, Badouel C, et al. Mutations in genes encoding the cadherin receptor-ligand pair DCHS1 and FAT4 disrupt cerebral cortical development. *Nat Genet.* 2013;45(11):1300-1308.

197. Zhao B, Tumaneng K, Guan KL. The Hippo pathway in organ size control, tissue regeneration and stem cell self-renewal. *Nat Cell Biol.* 2011;13(8):877-883.

198. Badouel C, McNeill H. SnapShot: The hippo signaling pathway. *Cell.* 2011;145(3):484-484 e481.

199. Wang Y, Yu A, Yu FX. The Hippo pathway in tissue homeostasis and regeneration. *Protein Cell.* 2017;8(5):349-359.

200. Badouel C, Zander MA, Liscio N, et al. Fat1 interacts with Fat4 to regulate neural tube closure, neural progenitor proliferation and apical constriction during mouse brain development. *Development.* 2015;142(16):2781-2791.

201. Matsumoto N, Hoshiba Y, Morita K, et al. Pathophysiological analyses of periventricular nodular heterotopia using gyrencephalic mammals. *Hum Mol Genet.* 2017;26(6):1173-1181.

202. Morin-Kensicki EM, Boone BN, Howell M, et al. Defects in yolk sac vasculogenesis, chorioallantoic fusion, and embryonic axis elongation in mice with targeted disruption of Yap65. *Mol Cell Biol.* 2006;26(1):77-87.

203. Park R, Moon UY, Park JY, et al. Yap is required for ependymal integrity and is suppressed in LPA-induced hydrocephalus. *Nat Commun.* 2016;7:10329.

204. Makita R, Uchijima Y, Nishiyama K, et al. Multiple renal cysts, urinary concentration defects, and pulmonary emphysematous changes in mice lacking TAZ. *Am J Physiol Renal Physiol.* 2008;294(3):F542-553.

205. Han D, Byun SH, Park S, et al. YAP/TAZ enhance mammalian embryonic neural stem cell characteristics in a Tead-dependent manner. *Biochem Biophys Res Commun.* 2015;458(1):110-116.

206. Sawada A, Kiyonari H, Ukita K, Nishioka N, Imuta Y, Sasaki H. Redundant roles of Tead1 and Tead2 in notochord development and the regulation of cell proliferation and survival. *Mol Cell Biol.* 2008;28(10):3177-3189.

207. Kaneko KJ, Kohn MJ, Liu C, DePamphilis ML. Transcription factor TEAD2 is involved in neural tube closure. *Genesis.* 2007;45(9):577-587.

208. Artimo P, Duvaud S, Pachkov M, Ioannidis V, van Nimwegen E, Stockinger H. The ISMARA client. *F1000Res.* 2016;5.

209. Arnold SJ, Sugnaseelan J, Groszer M, Srinivas S, Robertson EJ. Generation and analysis of a mouse line harboring GFP in the Eomes/Tbr2 locus. *Genesis.* 2009;47(11):775-781.

210. Cao X, Pfaff SL, Gage FH. YAP regulates neural progenitor cell number via the TEA domain transcription factor. *Genes Dev.* 2008;22(23):3320-3334.

211. Saito K, Kawasoe R, Sasaki H, Kawaguchi A, Miyata T. Neural Progenitor Cells Undergoing Yap/Tead-Mediated Enhanced Self-Renewal Form Heterotopias More

Easily in the Diencephalon than in the Telencephalon. *Neurochem Res.* 2018;43(1):171-180.

212. Zhao B, Ye X, Yu J, et al. TEAD mediates YAP-dependent gene induction and growth control. *Genes Dev.* 2008;22(14):1962-1971.

213. Liu-Chittenden Y, Huang B, Shim JS, et al. Genetic and pharmacological disruption of the TEAD-YAP complex suppresses the oncogenic activity of YAP. *Genes Dev.* 2012;26(12):1300-1305.

214. Balwierz PJ, Pachkov M, Arnold P, Gruber AJ, Zavolan M, van Nimwegen E. ISMARA: automated modeling of genomic signals as a democracy of regulatory motifs. *Genome Res.* 2014;24(5):869-884.

215. Diepenbruck M, Waldmeier L, Ivanek R, et al. Tead2 expression levels control the subcellular distribution of Yap and Taz, zyxin expression and epithelial-mesenchymal transition. *J Cell Sci.* 2014;127(Pt 7):1523-1536.

216. Zhou Y, Huang T, Cheng AS, Yu J, Kang W, To KF. The TEAD Family and Its Oncogenic Role in Promoting Tumorigenesis. *Int J Mol Sci.* 2016;17(1).

217. Huang Z, Hu J, Pan J, et al. YAP stabilizes SMAD1 and promotes BMP2-induced neocortical astrocytic differentiation. *Development.* 2016;143(13):2398-2409.

218. Poitelon Y, Lopez-Anido C, Catignas K, et al. YAP and TAZ control peripheral myelination and the expression of laminin receptors in Schwann cells. *Nat Neurosci.* 2016;19(7):879-887.

219. Cheng L, Tian Z, Sun R, et al. ApoER2 and VLDLR in the developing human telencephalon. *Eur J Paediatr Neurol.* 2011;15(4):361-367.

220. Totaro A, Panciera T, Piccolo S. YAP/TAZ upstream signals and downstream responses. *Nat Cell Biol.* 2018;20(8):888-899.

221. Yang CP, Gilley JA, Zhang G, Kernie SG. ApoE is required for maintenance of the dentate gyrus neural progenitor pool. *Development.* 2011;138(20):4351-4362.

222. Huang Z. Molecular regulation of neuronal migration during neocortical development. *Mol Cell Neurosci.* 2009;42(1):11-22.

223. Stouffer MA, Golden JA, Francis F. Neuronal migration disorders: Focus on the cytoskeleton and epilepsy. *Neurobiol Dis.* 2016;92(Pt A):18-45.

224. Myant NB. Reelin and apolipoprotein E receptor 2 in the embryonic and mature brain: effects of an evolutionary change in the apoER2 gene. *Proc Biol Sci.* 2010;277(1680):345-351.

225. Luque JM. Integrin and the Reelin-Dab1 pathway: a sticky affair? *Brain Res Dev Brain Res.* 2004;152(2):269-271.

226. Si W, Kang Q, Luu HH, et al. CCN1/Cyr61 is regulated by the canonical Wnt signal and plays an important role in Wnt3A-induced osteoblast differentiation of mesenchymal stem cells. *Mol Cell Biol.* 2006;26(8):2955-2964.

227. Lavado A, He Y, Pare J, et al. Tumor suppressor Nf2 limits expansion of the neural progenitor pool by inhibiting Yap/Taz transcriptional coactivators. *Development.* 2013;140(16):3323-3334.

228. Lavado A, Ware M, Pare J, Cao X. The tumor suppressor Nf2 regulates corpus callosum development by inhibiting the transcriptional coactivator Yap. *Development.* 2014;141(21):4182-4193.

229. Tamm C, Bower N, Anneren C. Regulation of mouse embryonic stem cell self-renewal by a Yes-YAP-TEAD2 signaling pathway downstream of LIF. *J Cell Sci.* 2011;124(Pt 7):1136-1144.

230. O'Neill AC, Kyrousi C, Einsiedler M, et al. Mob2 Insufficiency Disrupts Neuronal Migration in the Developing Cortex. *Front Cell Neurosci.* 2018;12:57.

231. Sheen VL, Ganesh VS, Topcu M, et al. Mutations in ARFGEF2 implicate vesicle trafficking in neural progenitor proliferation and migration in the human cerebral cortex. *Nat Genet.* 2004;36(1):69-76.

232. Lin KC, Moroishi T, Meng Z, et al. Regulation of Hippo pathway transcription factor TEAD by p38 MAPK-induced cytoplasmic translocation. *Nat Cell Biol.* 2017;19(8):996-1002.

233. Pollen AA, Nowakowski TJ, Chen J, et al. Molecular identity of human outer radial glia during cortical development. *Cell.* 2015;163(1):55-67.

234. Nowakowski TJ, Pollen AA, Sandoval-Espinosa C, Kriegstein AR. Transformation of the Radial Glia Scaffold Demarcates Two Stages of Human Cerebral Cortex Development. *Neuron.* 2016;91(6):1219-1227.

235. Nowakowski TJ, Bhaduri A, Pollen AA, et al. Spatiotemporal gene expression trajectories reveal developmental hierarchies of the human cortex. *Science.* 2017;358(6368):1318-1323.

236. Ercan E, Han JM, Di Nardo A, et al. Neuronal CTGF/CCN2 negatively regulates myelination in a mouse model of tuberous sclerosis complex. *J Exp Med.* 2017;214(3):681-697.

237. Valentijn LJ, Ouvrier RA, van den Bosch NH, Bolhuis PA, Baas F, Nicholson GA. Dejerine-Sottas neuropathy is associated with a de novo PMP22 mutation. *Hum Mutat.* 1995;5(1):76-80.

238. Corder EH, Saunders AM, Strittmatter WJ, et al. Gene dose of apolipoprotein E type 4 allele and the risk of Alzheimer's disease in late onset families. *Science.* 1993;261(5123):921-923.

Appendices

Appendix I

TEAD targets from ISMARA

Promoter	Score	RefSeq	Gene Symbol	Gene Name
chr7 - 20284370	34.096		Apoe	apolipoprotein E
chr8 - 49075884	26.423	NM_133791	Wwc2	WW, C2 and coiled-coil domain containing 2
chr10 + 24315247	24.27	NM_010217	Ctgf	connective tissue growth factor
chr15 + 6336747	22.745	NM_001037905 NM_001102400 NM_023118	Dab2	disabled homolog 2 (Drosophila)
chr15 + 78673024	20.682	NM_027219	Cdc42ep1	CDC42 effector protein (Rho GTPase binding) 1
chr14 - 49282546	20.502	NM_144841	Otx2	orthodenticle homolog 2 (Drosophila)
chr11 + 62944973	19.295	NM_008885	Pmp22	peripheral myelin protein 22
chr11 - 32122259	18.147	NM_010117	Rhbdf1	rhomboid family 1 (Drosophila)
chr3 - 145312928	17.005	NM_010516	Cyr61	cysteine rich protein 61
chr11 - 55233339	15.485		Sparc	secreted acidic cysteine rich glycoprotein
chr11 - 55233366	15.457		Sparc	secreted acidic cysteine rich glycoprotein
chr16 + 91225794	15.297	NM_016967	Olig2	oligodendrocyte transcription factor 2
chr8 - 108489925	14.383	NM_009195	Slc12a4	solute carrier family 12, member 4
chr11 - 32122236	14.318		Rhbdf1	rhomboid family 1 (Drosophila)
chr18 + 50212935	14.224	NM_134131	Tnfaip8	tumor necrosis factor, alpha-induced protein 8
chr2 + 91297678	14.018	NM_001145857 NM_172668	Lrp4	low density lipoprotein receptor-related protein 4
chr10 - 86956393	12.593	NM_008553	Ascl1	achaete-scute complex homolog 1 (Drosophila)
chr2 + 156601175	12.579	NM_172118	Myl9	myosin, light polypeptide 9, regulatory
chr6 - 37391993	11.467	NM_178661	Creb3l2	cAMP responsive element binding protein 3-like 2
chr11 - 55233354	11.371		Sparc	secreted acidic cysteine rich glycoprotein
chr2 + 156601150	11.191		Myl9	myosin, light polypeptide 9, regulatory
chr11 - 55233581	11.005	NM_009242	Sparc	secreted acidic cysteine rich glycoprotein
chr6 + 90424727	10.813		Klf15	Kruppel-like factor 15
chr9 + 37175190	10.403	NM_175189	Hepacam	hepatocyte cell adhesion molecule
chr11 + 61890494	10.374	NM_001029936	Specc1	sperm antigen with calponin homology and coiled-coil domains 1
chr9 + 69301471	10.371	NM_007585	Anxa2	annexin A2
chr2 - 164683125	10.298	NM_011125	Pltp	phospholipid transfer protein
chr17 + 47730384	9.788	NM_007632	Ccnd3	cyclin D3
chr18 + 23573977	9.591		Dtna	dystrobrevin alpha
chr1 + 74438416	9.569		Ctdsp1	CTD (carboxy-terminal domain, RNA polymerase II, polypeptide A) small phosphatase 1
chr2 + 51893618	9.407	NM_009398	Tnfaip6	tumor necrosis factor alpha induced protein 6
chr1 + 74438416	9.304	NM_153088	Ctdsp1	CTD (carboxy-terminal domain, RNA polymerase II, polypeptide A) small phosphatase 1
chr5 - 77380189	9.125		Ppat	phosphoribosyl pyrophosphate amidotransferase
chr11 - 109472695	9.082	NM_145940	Wipi1	WD repeat domain, phosphoinositide interacting 1
chr7 - 20283542	8.967		Apoe	apolipoprotein E
chr13 + 113254277	8.778	NM_010560	Il6st	interleukin 6 signal transducer
chrX + 98449866	8.599	NM_018789	Foxo4	forkhead box O4
chr15 - 50721552	8.33	NM_032000	Trps1	trichorhinophalangeal syndrome I (human)
chr10 + 93103715	8.316	NM_021320	Ntn4	netrin 4
chr8 + 23868194	8.294	NM_008872	Plat	plasminogen activator, tissue
chr18 + 23573908	8.22	NM_010087 NM_207650	Dtna	dystrobrevin alpha
chr10 - 86955909	8.175		Ascl1	achaete-scute complex homolog 1 (Drosophila)
chr9 - 79566271	8.159	NM_007730	Col12a1	collagen, type XII, alpha 1
chr5 + 77380332	7.876	NM_025939	Paics	phosphoribosylaminoimidazole carboxylase, phosphoribosylaminoribosylaminoimidazole, succinocarboxami
chr10 + 93103936	7.768		Ntn4	netrin 4
chr8 + 14911653	7.656	NM_001037736 NM_172751	Arhgef10	Rho guanine nucleotide exchange factor (GEF) 10
chrX + 137909951	7.6	NM_001163155 NM_007736	Col4a5	collagen, type IV, alpha 5
chr7 - 104566013	7.55	NM_009381	Thrsp	thyroid hormone responsive SPOT14 homolog (Rattus)
chr9 - 66896961	7.536		Tpm1	tropomyosin 1, alpha
chr8 + 74676812	7.448			
chr9 - 66897015	7.447	NM_001164248 NM_001164249 NM_001164250 NM_001164251 NM_001164255 NM_024427	Tpm1	tropomyosin 1, alpha
chr1 + 74438139	7.433		Ctdsp1	CTD (carboxy-terminal domain, RNA polymerase II, polypeptide A) small phosphatase 1

Position	Value	Accession	Gene	Description
		NM_001170433		
chr6 + 146837012	7.113	NM_026221	Ppfibp1	PTPRF interacting protein, binding protein 1 (liprin beta 1)
chr8 + 59990639	7.071	NM_008252	Hmgb2	high mobility group box 2
chr2 - 26314921	7.065		Notch1	Notch gene homolog 1 (Drosophila)
chr2 - 25325248	7.052	NM_008963	Ptgds	prostaglandin D2 synthase (brain)
chr5 - 77380226	6.956		Ppat	phosphoribosyl pyrophosphate amidotransferase
chr4 - 133574655	6.92	NM_145833	Lin28a	lin-28 homolog A (C. elegans)
chr11 - 72951771	6.861	NM_010353	Gsg2	germ cell-specific gene 2
chr2 - 25324650	6.728		Ptgds	prostaglandin D2 synthase (brain)
chr2 - 25325196	6.633		Ptgds	prostaglandin D2 synthase (brain)
chr10 + 126415772	6.389	NM_001113470	Ctdsp2	CTD (carboxy-terminal domain, RNA polymerase II, polypeptide A) small phosphatase 2
		NM_001171147		
chr9 - 8004559	6.277	NM_009534	Yap1	yes-associated protein 1
chr2 - 90420626	6.251	NM_008982	Ptprj	protein tyrosine phosphatase, receptor type, J
chr8 + 131248283	6.219		Itgb1	integrin beta 1 (fibronectin receptor beta)
chrX - 73120485	6.157	NM_001166453	Pls3	plastin 3 (T-isoform)
chr3 - 141645214	6.012	NM_007560	Bmpr1b	bone morphogenetic protein receptor, type 1B
chr6 - 128093543	5.955	NM_175414	Tspan9	tetraspanin 9
chr11 - 8911119	5.923	NM_008316	Hus1	Hus1 homolog (S. pombe)
chr11 + 100437204	5.821	NM_001146318	Cnp	2',3'-cyclic nucleotide 3' phosphodiesterase
chr4 + 88783273	5.674	NM_024433	Mtap	methylthioadenosine phosphorylase
chr7 - 110991602	5.669	NM_008219	Hbb-bh1	hemoglobin Z, beta-like embryonic chain
chr6 - 17256383	5.393		Cav1	caveolin 1, caveolae protein
chr11 + 70514004	5.317	NM_153103	Kif1c	kinesin family member 1C
chr10 + 79457716	5.237		Cnn2	calponin 2
chr1 - 174128558	5.225		Pea15a	phosphoprotein enriched in astrocytes 15A
chr16 + 77013880	5.185	NM_013918	Usp25	ubiquitin specific peptidase 25
chr3 + 90341208	4.961		S100a16	S100 calcium binding protein A16
chr9 - 8004450	4.953		Yap1	yes-associated protein 1
chr6 + 121586190	4.833	NM_175628	A2m	alpha-2-macroglobulin
		NM_025838		
chr11 + 68884268	4.803	NM_028336	Tmem107	transmembrane protein 107
chr3 - 30894668	4.738	NM_008857	Prkci	protein kinase C, iota
chr4 + 99382314	4.66	NM_001081264	Alg6	asparagine-linked glycosylation 6 homolog (yeast, alpha-1,3,-glucosyltransferase)
		NM_001042673		
chr13 - 63532777	4.562	NM_007985	Fancc	Fanconi anemia, complementation group C
chr5 - 37221812	4.497	NM_008550	Man2b2	mannosidase 2, alpha B2
chr17 - 49703661	4.428	NM_001008231	Daam2	dishevelled associated activator of morphogenesis 2
chr8 + 88364729	4.373	NM_199446	Phkb	phosphorylase kinase beta
chr14 - 69903072	4.34	NM_026331	Slc25a37	solute carrier family 25, member 37
chr11 - 115674905	4.248	NM_080643	Caskin2	CASK-interacting protein 2
chr5 - 48374328	4.075	NM_178804	Slit2	slit homolog 2 (Drosophila)
chr11 - 55223449	4.066		Sparc	secreted acidic cysteine rich glycoprotein
chr3 - 60305108	4.042	NM_020007	Mbnl1	muscleblind-like 1 (Drosophila)
chr15 - 42508294	4.015	NM_009640	Angpt1	angiopoietin 1
chr10 + 126415973	4.008		Ctdsp2	CTD (carboxy-terminal domain, RNA polymerase II, polypeptide A) small phosphatase 2
chr2 + 153171730	4.008	NM_001039939	Asxl1	additional sex combs like 1 (Drosophila)
chr3 - 154259975	3.942	NM_009968	Cryz	crystallin, zeta
chr8 - 74676404	3.927		Tpm4	tropomyosin 4
chr4 + 15885062	3.908	NM_013752	Nbn	nibrin
chr6 - 17256415	3.901		Cav1	caveolin 1, caveolae protein
chr3 + 88004544	3.825		AW047730	expressed sequence AW047730
		NM_027733		
chr18 - 35821788	3.78	NM_029485	Spata24	spermatogenesis associated 24
chr9 - 61970402	3.726		Glce	glucuronyl C5-epimerase
chr17 - 10512094	3.694		Qk	quaking
chr6 + 5340417	3.68		Asb4	ankyrin repeat and SOCS box-containing 4
chr15 + 38908403	3.635	NM_026778	Cthrc1	collagen triple helix repeat containing 1
chr6 + 82984190	3.604	NM_013586	Loxl3	lysyl oxidase-like 3
chr12 + 85328810	3.506	NM_134188	Acot2	acyl-CoA thioesterase 2
		NM_001110266		
		NM_001110267		
chr17 - 46162111	3.504	NM_001110268	Vegfa	vascular endothelial growth factor A
chr2 + 156665812	3.493	NM_173396	Tgif2	TGFB-induced factor homeobox 2
chr9 + 65434966	3.454	NM_172453	Pif1	PIF1 5'-to-3' DNA helicase homolog (S. cerevisiae)
chr8 + 73905282	3.428		Nr2f6	nuclear receptor subfamily 2, group F, member 6
chr17 - 71351523	3.363		2900073G15	RIKEN cDNA 2900073G15 gene
chr4 - 35104577	3.309	NM_178061	Mobkl2b	MOB1, Mps One Binder kinase activator-like 2B (yeast)
chr15 - 99481964	3.273	NM_012025	Racgap1	Rac GTPase-activating protein 1
chr1 - 137662648	3.2	NM_013750	Phlda3	pleckstrin homology-like domain, family A, member 3
		NM_001025613		
chr3 + 95908422	3.135	NM_001025614	Otud7b	OTU domain containing 7B
chr3 - 37538897	3.095		Spry1	sprouty homolog 1 (Drosophila)
chr11 + 70467599	3.09		Pfn1	profilin 1
chr9 - 70055127	3.02	NM_181072	Myo1e	myosin IE
chr4 - 19497166	2.958	NM_027769	Cpne3	copine III

Position	Value	Accession	Gene	Description
chr9 + 13553629	2.953		Mtmr2	myotubularin related protein 2
chr1 - 155179844	2.931	NM_010683	Lamc1	laminin, gamma 1
chr3 - 107474108	2.916		Ahcyl1	S-adenosylhomocysteine hydrolase-like 1
chr17 - 71351465	2.845		2900073G15	RIKEN cDNA 2900073G15 gene
chr11 - 85048564	2.843	NM_025825	Appbp2	amyloid beta precursor protein (cytoplasmic tail) binding protein 2
chr17 + 56442759	2.815	NM_001111079 NM_010931	Uhrf1	ubiquitin-like, containing PHD and RING finger domains, 1
chr17 - 28487544	2.813	NM_001098226 NM_011566	Tead3	TEA domain family member 3
chr7 + 4085699	2.779		Ttyh1	tweety homolog 1 (Drosophila)
chr6 - 134516799	2.758		Lrp6	low density lipoprotein receptor-related protein 6
chr3 - 90417072	2.755		S100a6	S100 calcium binding protein A6 (calcyclin)
chr9 - 103207488	2.755	NM_176979	Topbp1	topoisomerase (DNA) II binding protein 1
chr6 - 72386442	2.748		Mat2a	methionine adenosyltransferase II, alpha
chr1 - 55135054	2.746		Hspd1	heat shock protein 1 (chaperonin)
chr2 + 31615444	2.679	NM_009594	Abl1	c-abl oncogene 1, non-receptor tyrosine kinase
chr16 + 37777075	2.675	NM_008047	Fstl1	follistatin-like 1
chr9 + 108199200	2.665	NM_001013814	Amt	aminomethyltransferase
chr9 - 13553574	2.657	NM_023858	Mtmr2	myotubularin related protein 2
chr6 - 90378423	2.649	NM_173775	Ccdc37	coiled-coil domain containing 37
chr4 - 109337891	2.645	NM_007671	Cdkn2c	cyclin-dependent kinase inhibitor 2C (p18, inhibits CDK4)
chr12 + 53604952	2.635		Arhgap5	Rho GTPase activating protein 5
chr8 + 131209787	2.63		Itgb1	integrin beta 1 (fibronectin receptor beta)
chr1 + 12708582	2.629	NM_172294	Sulf1	sulfatase 1
chr8 + 131209614	2.629		Itgb1	integrin beta 1 (fibronectin receptor beta)
chr2 - 105234998	2.627		Rcn1	reticulocalbin 1
chr17 - 10512217	2.572	NM_001159516 NM_001159517 NM_021881	Qk	quaking
chr6 + 13019758	2.57	NM_027992	Tmem106b	transmembrane protein 106B
chr11 - 8368505	2.559		Tns3	tensin 3
chr7 - 30290470	2.537	NM_001081028	Sipa1l3	signal-induced proliferation-associated 1 like 3
chr18 + 56559977	2.525		Gramd3	GRAM domain containing 3
chr18 + 78033276	2.524	NM_013831	Pstpip2	proline-serine-threonine phosphatase-interacting protein 2
chr1 + 106665395	2.501	NM_011800	Cdh20	cadherin 20
chr14 + 70009282	2.498	NM_033325	Loxl2	lysyl oxidase-like 2
chrX - 138740740	2.489	NM_021487	Kcne1l	potassium voltage-gated channel, Isk-related family, member 1-like, pseudogene
chr11 + 79153388	2.488	NM_010897	Nf1	neurofibromatosis 1
chr3 - 157686385	2.48	NM_026989	Srsf11	serine/arginine-rich splicing factor 11
chr8 + 131209680	2.449		Itgb1	integrin beta 1 (fibronectin receptor beta)
chr11 + 98273797	2.389	NM_001003817	Erbb2	v-erb-b2 erythroblastic leukemia viral oncogene homolog 2, neuro/glioblastoma derived oncogene homolog
chr6 + 90412566	2.38	NM_023184	Klf15	Kruppel-like factor 15
chr4 + 46485096	2.361			
chrX - 138740574	2.359		Kcne1l	potassium voltage-gated channel, Isk-related family, member 1-like, pseudogene
chr6 + 29685629	2.332		Smo	smoothened homolog (Drosophila)
chr2 - 120229789	2.328	NM_001110496 NM_001110497 NM_173734	Tmem87a	transmembrane protein 87A
chr11 + 117061031	2.326		Sep.09	septin 9
chr5 + 104888468	2.283	NM_008861	Pkd2	polycystic kidney disease 2
chr10 + 4541138	2.276		Fbxo5	F-box protein 5
chr12 + 79962662	2.25		Eif2s1	eukaryotic translation initiation factor 2, subunit 1 alpha
chr19 - 9210047	2.232	NM_025610	Asrgl1	asparaginase like 1
chr10 + 110182506	2.223	NM_178609	E2f7	E2F transcription factor 7
chr6 - 90666474	2.223	NM_001134383	Iqsec1	IQ motif and Sec7 domain 1
chr2 - 129094163	2.21		Ckap2l	cytoskeleton associated protein 2-like
chr14 + 63741339	2.208		Ctsb	cathepsin B
chr9 + 108997946	2.202	NM_172775	Plxnb1	plexin B1
chr7 - 29747201	2.199		Actn4	actinin alpha 4
chr9 + 13553750	2.194		Mtmr2	myotubularin related protein 2
chr12 + 8980697	2.193	NM_001159527 NM_172470	Wdr35	WD repeat domain 35
chr1 - 137268058	2.187		Shisa4	shisa homolog 4 (Xenopus laevis)
chr9 + 123428782	2.181		Limd1	LIM domains containing 1
chr8 - 67171805	2.17	NM_013494	Cpe	carboxypeptidase E
chr1 + 183081066	2.15		Cnih4	cornichon homolog 4 (Drosophila)
chr15 + 3224767	2.148		Sepp1	selenoprotein P, plasma, 1
chr8 - 13494457	2.102	NM_019521	Gas6	growth arrest specific 6
chr18 + 44540137	2.092	NM_027490	Dcp2	DCP2 decapping enzyme homolog (S. cerevisiae)
chr10 + 4541075	2.079	NM_025995	Fbxo5	F-box protein 5

chr15 - 13103346	2.079	NM_007666	Cdh6	cadherin 6	
chr5 - 116872852	2.079	NM_030704	Hspb8	heat shock protein 8	
chr11 + 117060974	2.07	NM_001113486	Sep.09	septin 9	
chr14 + 70008874	2.064		Loxl2	lysyl oxidase-like 2	
chr1 - 187941133	2.054	NM_146106	Lyplal1	lysophospholipase-like 1	
chr1 + 183081112	2.053		Cnih4	cornichon homolog 4 (Drosophila)	
chr3 + 94641626	2.05		Pogz	pogo transposable element with ZNF domain	
chr1 - 176431933	2.046	NM_019445	Fmn2	formin 2	
chrX + 160707362	2.042	NM_027153	Pir	pirin	
chr7 - 26573483	2.038	NM_001190974 NM_001190975 NM_009465	Axl	AXL receptor tyrosine kinase	
chr5 + 76569257	2.025	NM_020611	Srd5a3	steroid 5 alpha-reductase 3	
chr12 + 113883038	2.011	NM_001161737 NM_013929	Siva1	SIVA1, apoptosis-inducing factor	
chr13 + 49282844	2.011	NM_013610	Ninj1	ninjurin 1	
chr9 + 108998083	1.988		Plxnb1	plexin B1	
chr2 - 153171562	1.979		Asxl1	additional sex combs like 1 (Drosophila)	
chr3 - 51364525	1.934	NM_080793	Setd7	SET domain containing (lysine methyltransferase) 7	
chr13 - 64471609	1.93	NM_009984	Ctsl	cathepsin L	

GO categories for Tead motif
GO:0022610:biological adhesion:(39)
GO:0007155:cell adhesion:(37)
GO:0048731:system development:(89)
GO:0051239:regulation of multicellular organismal process:(63)
GO:0010001:glial cell differentiation:(12)
GO:0007399:nervous system development:(52)
GO:0022008:neurogenesis:(41)
GO:0048856:anatomical structure development:(93)
GO:0048869:cellular developmental process:(74)
GO:0042063:gliogenesis:(12)
GO:0007275:multicellular organismal development:(98)
GO:0065008:regulation of biological quality:(67)
GO:0042552:myelination:(9)
GO:0007272:ensheathment of neurons:(9)
GO:0008366:axon ensheathment:(9)
GO:0048699:generation of neurons:(37)
GO:0032502:developmental process:(103)
GO:0032879:regulation of localization:(44)
GO:0048878:chemical homeostasis:(31)
GO:0007154:cell communication:(32)
GO:0030154:cell differentiation:(69)
GO:0048518:positive regulation of biological process:(90)
GO:0021529:spinal cord oligodendrocyte cell differentiation:(3)
GO:0021530:spinal cord oligodendrocyte cell fate specification:(3)
GO:0009653:anatomical structure morphogenesis:(51)
GO:0019228:regulation of action potential in   neuron:(9)
GO:0007167:enzyme linked receptor protein signaling pathway:(21)

Appendix II

1) NeuroStemX main paper

2) Book chapter

3) Review

4) Paper in Science Advances

5) Curriculum Vitae

Dynamic and sequential transcriptional changes in cortical neurogenic lineage over time
Or
Temporal and sequentional transcriptional dynamics during murine corticogenesis

Abstract

The murine cerebral cortex is composed of millions of morphologically and functionally distinct neurons. Development of the neocortex requires an orchestrated succession of a series of processes; the appropriate generation, migration, and positioning of neurons, the acquisition of layer-specific transcriptional hallmarks, and the establishment of precise axonal projections. We have focused on elucidating the transcriptomic landscape of murine embryonic neural stem cells (NSCs), basal progenitors (BPs) and newborn neurons (NBNs) at the population and single cell level. Using unprecedented population and single cell RNA-Seq approaches, unbiased computational modeling, we have deciphered the signaling and transcriptional networks that regulate cerebral cortical NSC expansion, neurogenesis and gliogenesis. Our data indicate that NSCs, rather than being homogeneous, are a heterogeneous population, which dynamically shift in transcriptional space over time. Using unbiased computational approaches, we have identified a continuous path for NSCs at the population level and observed that single NSCs follow a similar path and divide in distinct clusters overtime. We have identified signature hallmarks of these clusters, and performed similar analyses for BPs and NBNs. Using predicted active transcriptional nodes and networks that contribute to neuronal cell fate determination, we have identified some novel key players regulating corticogenesis. Further, to elucidate the dynamics of signaling pathways controlling neuron production, we have characterized highly expressed receptors, ligands and downstream components, during cortical development. In particular, we have examined the interplay among bHLH factors during corticogenesis.

Introduction

The detailed understanding of the mechanisms that lead to the formation of multiple neuronal subtypes from NSCs and BPs are largely unknown. Temporal expansion and differentiation during cortical development can be defined by multiple hypotheses (Hevner et al., 2003; Lodato and Arlotta, 2015; Molyneaux et al., 2007; Woodworth et al., 2012). In one, NSCs switch their fate in coherence with the time points of neurogenesis and generate successive neuronal layers of the cortex and glial cells temporally (Guo et al., 2013). Alternately, NSCs are a multipotent cell pool, wherein each cell would be guided by its intrinsic and extrinsic signals to generate a specific neuronal subtype or glial cells in a sequential manner (Franco et al., 2012; Gil-Sanz et al., 2015). Novel experimental

paradigms have been followed to understand the lineage relationships of different neocortical projection neurons (Nowakowski et al., 2017; Telley et al., 2019; Telley et al., 2016). An elaborate list of biomarkers has been identified to play critical roles in cortical layering and projection neuron development (Arlotta et al., 2005; Franco and Muller, 2013). Several factors and morphogens play key roles during neurogenesis, speculated to regulate the cell fate decisions of the NSCs in the ventricular zone (VZ) (Arlotta et al., 2005; Franco and Muller, 2013). Although, much progress has been made to identify the major players that determine the neocortical progenitors, there is a distinct lack of markers to distinguish stem cell populations (Englund et al., 2005). Subtype identities of neurons are progressively specified during neurogenesis and the expression of many factors become restricted during development. Several inductive and repressive cues which regulate the regimental corticogenesis influence the factors expressed throughout development (Arlotta et al., 2005; Chuang et al., 2015; Custo Greig et al., 2013; Desai and McConnell, 2000; Fode et al., 2000; Gotz and Huttner, 2005; Han and Sestan, 2013; Haubensak et al., 2004; Hevner et al., 2003; Lodato and Arlotta, 2015; Lui et al., 2011; Molyneaux et al., 2007; Mukhtar and Taylor, 2018; Paridaen and Huttner, 2014; Pollen et al., 2015).

Information about stage and cell type-specific gene expression from RNA profiling and analyses during formation of the brain and genetic manipulation experiments has increased massively over the last decade (Ecker et al., 2017; Johnson and Walsh, 2017; Liu et al., 2016; Nowakowski et al., 2017; Rosenberg et al., 2018; Stancik et al., 2010; Telley et al., 2016; Zhang et al., 2019). The maintenance of NSC potential and fate commitment are regulated through the integration of dynamic signaling organized in space and time, with elaborate interplay of downstream transcriptional networks. Although the neuronal diversity of adult neocortex is well defined and understood, the understanding of transcriptional programs during embryogenesis and cortical patterning is rather limited. This has been primarily due to the technical limitations and the poor identification of clean populations of NSCs and their lineage. To circumvent this, we have employed our genetic tools and isolated NSCs, BPs and NBNs at daily intervals during cortical development, from embryonic day 10.5 (E10.5) to postnatal day 1 (PN1).

Bulk RNA sequencing provides prospects to elucidate the transcriptional landscape of NSCs, BPs and neuronal subtypes and follow the temporal dynamics systematically. In order to analyze the underlying heterogeneity at the single-cell level and identify similar cell pools within the population, single-cell RNA sequencing provides a great opportunity. We have elucidated the transcriptional landscapes of three different cell types, determined the differential gene expression during stages of corticogenesis, identified novel transcriptional nodes and networks regulating cell fate commitment in the dorsal cortex. Using the same transgenic tools and unbiased computational approaches, we have identified clusters of single-cells in NSCs, BPs and NBNs and further elucidated the signature genes for each cluster. We have elucidated the dynamics of known biomarkers rendering cortical waves during neuronal specification, and exposed their heterogeneity in expression at single-cell level. We

have further evaluated the signaling pathways active during phases of NSC expansion, neurogenesis and gliogenesis and identified unique dynamics of expression in highly expressing receptors, ligands and downstream signaling components during these phases. As an example, we have focused on the dynamics of bHLH factors at the population and single-cell level to highlight the heterogeneity of expression in the NSC pool to show the potential of this resource. These in-depth analyses provide a versatile and comprehensive resource for the field to dig deeper and overlay known and novel aspects of cortical patterning and fate changes in neuronal lineage.

Results

Overview and validation of the biological system and preliminary transcriptional analyses

In order to address the changes in gene expression during formation of the mouse dorsal cerebral cortex by next generation sequencing, we isolated and FACSed NSCs, BPs and postmitotic NBNs from the dorsal cortices of *Hes5::GFP* and *Tbr2::GFP* embryos, at each day of development between embryonic day 10.5 (E10.5) and birth (PN) and performed RNA-seq analysis (Figures 1A and S1A) (Arnold et al., 2008; Bansod et al., 2017; Basak and Taylor, 2007; Sessa et al., 2017; Zhang et al., 2019). This time period covered the embryonic stages of cortical development from NSC expansion (E10.5-E11.5), through neurogenesis (E12.5-E16.5) to gliogenesis (E17.5-PN). *Hes5::GFP* and *Tbr2::GFP* uniquely label NSCs and BPs, NBNs, respectively, validated by *in vitro* and *in vivo* methods (Figures S1B-F). Further gene expression analyses showed that *Hes5* is specifically highly expressed in NSCs, and at low levels in BPs and NBNs (Figure 1B). *Eomes* (*Tbr2*) and *Btg2* are markers of BPs, are also expressed in NSCs at relatively high levels, with no detectable protein (Figures 1B and S1B, D-F). *Tbr2* and *Btg2* are expressed at much lower levels in NBNs, compared to BPs (Figure 1B). The prevalence of their RNA in NSCs and no detectable protein is in line with previous observations (Pollen et al., 2015).

In order to further validate our RNA-seq data, we analyzed the gene expression dynamics of known NSC, BP and NBN markers (Figures 1C and S1G). We observed that known NSC markers such as, *Fabp7, Pax6, Vim* and *Nestin* are highly expressed with characteristic temporal dynamics in NSC populations (Gotz and Huttner, 2005; Molyneaux et al., 2007; Mukhtar and Taylor, 2018; Ohtsuka et al., 2011; Pollen et al., 2015). Known BP markers such as *Nfib, Ngn2, Tcf4, Neurod1* are highly expressed throughout in BPs. Astrocytic markers such as, *S100b, ApoE, Gfap, Aldoc* are expressed highly in late NSCs corresponding to onset of gliogenesis (Liddelow and Barres, 2015; Molofsky et al., 2012; Zhang and Barres, 2010). Similarly, key markers for oligodendrocytes such as *Pdgfd, Sox10, Cspg4, Sox9* are expressed higher in late stages in NSCs, corresponding to the last wave of oligodendrogenesis, originating in the VZ of the dorsal cortex (Ono et al., 2008; Takebayashi and Ikenaka, 2015; Zhang and Barres, 2010). Interestingly, from our data, the known mature neuronal markers such as *Grin2a, Chat, Bdnf, Igf1* are expressed at low levels in our NSC, BP or NBN samples,

thus validating the specificity and purity of our transgenic lines and experimental set-up (Figures 1C and S1G) (Sarnat, 2013).

After considerable examination of our data with the known markers, we employed unbiased computational analyses to determine the transcriptional dynamics of different cell types. The principal component analysis (PCA), capturing more than 40% of the total variance in the PC1 and 20% in PC2 revealed that all samples separated based on their cell types and time points. Strikingly, the projection of the BPs and NBNs on the first two components suggest that their state of gene expression is closer to the NSCs at the neurogenic phase than the NSCs at the two other phases, with BPs projecting in between the NSCs and the NBNs (Figures 1D and S1H). NSCs displayed maximum variations in gene expression across time on the first two principal components, with clear separation in phases of expansion, neurogenesis and gliogenesis. Following this, we performed pairwise differentially expressed gene analyses (DEG) of different cell types (Figures 1E and S1J-O). We identified novel markers for NSCs, BPs and NBNs using two independent methods- DEGs and Z-score log2 (TPM) expression values (Table S1). Genes such as *Sp9, Cyr61, Yap1, Hes1, Lfng, Notch3* are expressed highly in NSCs. Identification of these signature genes using an unbiased approach is counterintuitive as the function of some has been studied in NSCs. The Hippo co-activator *Yap1*, Notch effectors *Hes1*, *Lfng* are involved in NSC proliferation and maintenance (Bray, 2006; Pourquie, 2003; Takebayashi and Ikenaka, 2015). Genes such as *Gucy1b3, Nhlh1, Serping1* are highly expressed in BPs with not much known about their function (Lipkowitz et al., 1992). *Ntm, Nrip1* are uniquely expressed higher in NBNs than in BPs or NSCs (Gil et al., 1998). Interestingly, DEG analyses revealed that the majority of highly expressed genes are downregulated in BPs and are further down in NBNs compared to NSCs.

Temporal dynamics in transcriptional landscapes of NSCs, BPs and NBNs based on gene expression

From our previous observations, NSCs displayed maximum variance over time and therefore mostly determine the first two principal components. To further understand the transcriptional dynamics of only NSC population, we performed PCA on NSC samples over time. The first two PCs covered almost 70% of the total variance, demonstrating a dynamic transcriptional path among phases of expansion, neurogenesis and gliogenesis (Figures 2A and S2A). Intriguingly, even when the NSCs were isolated using the same transgene, *Hes5*, we observed striking dynamics in their transcriptional space. NSCs follow a continuous path from expansion to neurogenesis and then gliogenesis, consistent with the common origin model of cell specification in a sequential order over time. We observed that genes such as *Hbb-bh1, Hba-x* and *Hbb-y* distinguish the NSC in expansion phase, along PC1 negative axis. *Neurod6, Cntn2*, *Slc14a1* and *Nfix* separated the NSCs in the neurogenic phase along PC2 negative axis. *Pdgfra, Olig1, Gpr17, Tnc* and *Bcan* have the highest contribution along PC2 positive axis to separate NSCs in the gliogenic phase (Figure 2B-D). It is interesting using

an entirely unbiased computational approach, we could identify some of the known genes already studied in NSCs, along with the novel markers (Pollen et al., 2015; Telley et al., 2019; Telley et al., 2016). In order to validate the novel signature genes from PC separations, we performed RT-qPCR on independent biological replicates (Figures 2B and S2B, C; Table S2). We randomly selected and validated signature genes, differentially expressed during expansion, neurogenic and gliogenic phases. *Ccnd1, Crabp2, Hbb-bh1* are highly expressed in expansion; *Bcl11b, Cntn2, Id2, Satb2* as examples of genes highly expressed during neurogenic phase, while *ApoE, Aqp4, Sparcl1, Tril* are some highly expressed in gliogenic phase by NSCs (Figure S2C and Table S2). We clustered the transcriptional dynamics of genes as upregulation, down regulation, transient upregulation and transient down regulation (Figure S2D-G).

In order to address the transcriptional changes among the cell types, we excluded the variance induced by first two PCs of NSCs by computing principal components of all the samples orthogonal to the first two principal components of the NSCs. After performing PCA on the remaining expression values, we observed that all NSCs now cluster together, opposite to Figure 1D. This suggests that considering only the part of all data orthogonal to the first PCs of NSCs successfully discards the variations on NSCs while keeping the differences between cell types. This increases the separation of BPs and NBNs on the first two PCs, with BPs displaying clear separation between early (E12.5-E14.5) and late (E15.5-PN) time points (Figures 2E, F and S2H). NBNs show less transcriptional dynamics over time. In order to identify the maximum contributing genes in PC1 and PC2, we performed pairwise DEG analyses. Genes such as *Dlx1, Dlx5* and *Dlx2* separate NSCs while *Tbr2, Nhlh1* represent the highest loading along PC1 negative axis. *Crym, Pf4* and *Crlf4* separate BPs and NBNs along the PC1 positive axis (Figures 2F-H, Table S2).

In order to investigate the gene expression changes in BPs and NBNs, we performed PCAs on BPs and NBNs separately. Despite their being selected using the same transgene *Tbr2*, the PCA plots displayed continuous dynamics over time in these populations. However, only the first PC was sufficient to separate BPs over time (Figures 2I-L and S3A). We identified genes such as, *Fezf1, Samd3, Robo3* to be highest in early BPs while genes such as *Tac2, Dhrs3, Sh3rf3* show their expression increased in late BPs. Similarly, the first PC was sufficient to separate NBNs over the course of development (Figures 2M-P, S3B). In order to validate the novel signature genes separating BPs and NBNs, we performed RT-qPCR on independent biological replicates (Figure S3C, D and Table S2). We randomly selected and validated signature genes, differentially expressed between early BPs, late BPs and their corresponding NBNs. *Cckar, Kif2c, Uncx, Robo3* are highly expressed in early BPs while *Loxl1, Unc5d, Ezr* are highly expressed in late BPs. On the contrary, NBNs displayed high expression of genes such as *Mef2c, Usp43, Lrfn5, Ntsr1* and *Gucy1a3* (Figure S2D). A more comprehensive list of these DEGs is available in Table 2. Similar dynamics of upregulation and down regulation were evident in BPs, as observed in NSCs (Figure S3E, F). From our preliminary analyses of gene expression, we demonstrate dynamics in NSCs, BPs and NBNs and also have

identified novel signature genes which are binary and unique for these populations.

Temporal dynamics in transcriptional landscapes of NSCs, BPs and NBNs based on transcriptional nodes and networks

In order to characterize the transcriptional states of NSCs, BPs and NBNs at subsequent stages and in particular map the activities of transcription factors (TFs) throughout the time course, we employed Integrated System Motif Activity Response Analysis (ISMARA) (Artimo et al., 2016; Balwierz et al., 2014). This method aims to explain the expression of a gene as linear combination of the activities of the transcription factors that have some binding sites in the promoter region of that gene. This model allows to infer the regulatory state of samples as *'motif activities'* (Figure 3A). A preliminary PCA on the motif activities of all samples revealed that the maximum variance was dominated by NSCs, in coherence with the observations from gene expression. To circumvent this, we split the data into two subsets, first to analyze the NSCs from all time points and second to analyze NSCs from neurogenic phase, compared to BPs and NBNs.

The PCA analysis for NSCs showed 80% variance captured on the first two components, dividing the NSC samples in expansion, neurogenic and gliogenic phases, similar to gene expression analyses (Figure 3B). This means that NSCs, also based of TF binding motif activities show strong dynamics and a continuous path as observed with gene expression. We next identified the top 20 TF binding motifs with the highest contribution to the variance in the PC1 and PC2, displayed as motif projections on the same subspace of gene expression (Figures 3C, S4A). We observe that the samples follow a fairly circular trajectory through time and can be defined in a two-dimensional space so that every motif can be mapped to a position on that circle. We represent expansion phase in red, neurogenesis in green and gliogenesis in blue. Each motif is predicted to impinge on target genes and as examples, E2f1 targets *Hmga2*, Neurod1 targets *Neurod6* and Nfic_Nfib target *Gfap* (Figure 3D). Upon in-depth analyses of the target genes, we observed a stark coherence with the genes identified in Figure 2B-D, thus increasing our confidence in the inferred motif activity.

Another important aspect of ISMARA is that it can predict the interactive regulatory networks of TFs in all cell types. Each edge of the network is characterized by the likelihood of the interaction and we selected the top motif-motif interactions to draw a simplified yet representative regulatory network of NSCs in the three phases (Figure 3E). Each rectangular node of the network is a motif containing its activity plot across time. An elliptical node represents top GO categories. Each arrow represents an activation while a blunt end represents repression. The dotted lines represent the main GO categories associated with the predicted targets of the connected motifs. The colors define the relative motif activity in the three phases, as shown in the key. A large proportion of motifs project in neurogenesis

and the genes regulated are known to be involved in cortical development. For example, Scrt1 and Scrt2 are known to be active in NSC expansion, while Hoxb7, Sox5 are active during neurogenesis and Nfix, Nfia are involved in glial cell proliferation (Bel-Vialar et al., 2002; Lai et al., 2008; Paul et al., 2014; Zhou et al., 2015). From our predicted networks, the set motifs active in neurogenesis seem to be repressing the motifs from expansion and towards the end of neurogenesis, the activities of these motifs reduce and they in turn activate the motifs responsible for the transition to gliogenesis.

Next, we analyzed the dynamics of all cell types together, while removing the PC1 and PC2 of NSCs and identified the top TF motifs determining the separation on the PCA (Figure S4B, C). Additionally, in coherence with our gene expression analyses, we performed parallel analyses for BPs and NBNs based on TF motif activities and found similarities in separation, identifying top selective nodes active in these cell types. These are represented both as projections on the same subspace and as profiles of activities as determined from ISMARA (Figure S4D-I). To further understand the relationship between the different cell types, we observed the dynamics of *neurogenic* NSC-BP-NBN over time. The PC1 separates them in three clusters, with early NSCs on the left, NBNs on the right and late NSCs and late BPs in the center of the plot. The PC2 seems to capture the direction of time which is surprisingly shared by the 3 cell types (Figure 3F). Indeed, we have identified novel set of genes that define the time evolution of the three cell types (Figure G, H). Noting that the first two components seem to separately capture the differences in cell types (PC1) and the time evolution (PC2), we associated the motifs with a color gradient depending on their contribution with those two axes. A projection solely on the first axis is represented in magenta and a projection solely on the second is represented as cyan. As every gene can contribute to both axes, we define the continuous spectrum of colors between magenta and cyan in order to include the relative contribution of each motif to both components. We identified the main interactions within this subset as shown in Figure 3I, with two poorly connected subgraphs. On the right we see a dense subnetwork of E2f family of motifs, involved in DNA replication, methylation and cell cycle. Although, these motifs characterize differences between cell types, they remain relatively constant in time. Towards the middle, we observe motifs that have similar activity in all cell types but increase along time. Foxd1, Stat2 are examples of motifs regulating neural and glial development. On the extreme left, we observe motifs that are both different across cell types and vary along time. In Figures 3E and I, we observe that interactions generally come from motifs that are highly active in NSCs during neurogenesis and towards motifs that are highly active in other cell types and phases of NSCs. This directionality seems to naturally arise from the graphs indicating strong intrinsic properties of neurogenic NSCs.

Single-cell RNA sequencing reveals underlying heterogeneity in NSCs, BPs and NBNs

In order to classify NSCs, BPs and NBNs at the single-cell level, based on their transcriptional landscapes, we employed similar experimental paradigm and isolated and sequenced single NSCs, BPs and NBNs over time (Figure S5A). Preliminary analyses of single-cell transcriptomes by PCA of

highly variable genes (HVGs) revealed a low heterogeneity within the NSCs during expansion and gliogenesis, in comparison with the NSCs at neurogenesis (Figure 4A). To compare our single-cell and population RNA-sequencing data, we calculated the average of single-cell transcriptomes and projected them on the matrices of population samples. Strikingly, the average single-cell data superimposed on the biological replicates at population level, despite their heterogeneity (Figure 4B), hence confirming that average of the single-cell pool actually corresponds to the respective population time point. The projection of average samples also displayed similar developmental path as the population samples across time. This clearly indicates that single-cell samples are proper representatives of population samples despite constituting of fewer cells.

Further, using K-means clustering, we divided NSCs in five clusters and identified differentially regulated genes in each of these clusters (Figures 4C, S5C-F and Table 4), also visualized by t-SNE in Figure 4D. NSCs from the neurogenic phase cluster in more groups compared to NSCs from expansion or gliogenesis. The markers identified for the clusters from expansion and gliogenesis are distinct, for example, *Crabp2* and *Tnc* are markers for clusters 1 and 5, respectively while *Tubb3* and *Dcx* are expressed in a more expanded domain across the clusters (Figure 4D). The heatmap shows a more comprehensive list of distinct signature genes for the five clusters (Figure S5F and Table 4). (GO ANALYSIS FOR CLUSTERS- Table 5)

Next, in order to analyze the heterogeneity in BPs, we plotted the single BPs on PCA using most HVGs, identified from BPs at the population level. Single BPs from the same time point show less heterogeneity compared to NSCs (Figure 4E). Strikingly, the average single-cell data superimposed on the biological replicates at population level (Figure 4F), hence confirming that average of the single-cell pool actually corresponds to the respective population time point. We clustered BPs in three distinct clusters, bifurcating the early BPs and late BPs (Figures 4G, S5G-I and Table 4), also visualized by t-SNE in Figure 4H. Signature genes for the clusters, for example, *Lrfng* for cluster 1 and *Sema3c* for cluster 3 are more uniquely expressed. Cluster 2 comprises of BPs from intermediary time point E16.5, but does show heterogeneity with single cells from early and later BPs. *Grin2a* is a signature gene for Cluster 2, less uniquely upregulated or down regulated by these BPs (Figures 4G, H and S5J). We performed similar analyses for NBNs and identified two clusters, of early and late NBNs (Figure 4I-L; S5K-M and Table 4. Compared to NSCs and BPs, NBNs displayed relatively less heterogeneity. *Plk2* and *Tcf7l1* are examples of signature genes for the respective clusters of NBNs (Figure 4K, L; S5N and Table 4). Altogether, from our data, we demonstrate heterogeneity in NSCs, BPs and NBNs at the single-cell level and have further identified signature genes for each cluster of NSCs, BPs and NBNs.

Neuronal specification markers show sequential waves in gene expression at population level and massive heterogeneity at single-cell level

During cortical development, morphologically and physiologically unique classes of neurons are

formed systematically. The NSCs are known to give rise to cortical neurons in sequential waves throughout neurogenesis (Custo Greig et al., 2013; Molyneaux et al., 2007; Telley et al., 2016) (Figure 5A). Several TFs and genes have been identified over the years specifying the distinct classes of projection neurons (Custo Greig et al., 2013; Molyneaux et al., 2007). In order to analyze the dynamics in expression of known neuronal specification factors, we selected and curated an extensive list of these genes from the literature. We identified sequential waves of expression in NSCs at the population level while these markers were heterogeneously expressed at the single-cell level (Figures 5B, S6A). We highlight some factors as examples and show the dynamics of their expression in NSCs, BPs, and NBNs at the population level and heterogeneity at the single-cell level. *Tbr1* and *Ctip2* are deep layer markers (Layers V and VI), and are highly expressed during early phases of neurogenesis and their expression reduces in late NSCs, BPs and NBNs over time. On the contrary, upper layer markers (Layers IV and II/III) such as *Satb2* and *Cux2* show a transient down regulation initially with the highest expression during later time points (Figure 5C). The peaks of their expression correspond to the time points when these neurons start to form (Molyneaux et al., 2007). We were intrigued to see the presence of neuronal specification factors in NSCs at the RNA level, as not many are expressed at the detectable protein level. We plated the freshly FACsorted GFP positive cells, derived from the *Hes5::GFP* and *Tbr2::GFP* (bright) cortices on Poly L-lysine and performed immunocytochemistry for some of the cortical layering factors. We detected no protein in these cells, while they expressed high levels of these factors at the RNA level. We performed similar computational analyses and identified strong sequential waves also in BPs, with high levels of neuronal specifiers at the RNA level, yet no detectable protein (Figures 5C, E, F and S6B). Considering NBNs, we identified similar dynamics of expression in these markers, and a large heterogeneity at the single-cell level (Figures 5G, S6C). We plated the freshly FACsorted dim GFP-positive cells, derived from the *Tbr2::GFP* cortices on Poly L-lysine and performed immunocytochemistry for some of the cortical layering factors. We detected protein in these cells, validating our experiments (Figures 5H).

This strikingly is a strong proof that the neuronal specification program starts much before in NSCs and BPs and continues in NBNs. At the single-cell level, NSCs express high levels of deep layer neuronal markers (at E10.5) while later they express both deep and upper-layer neuronal markers (Figure S6D). In comparison, majority of BPs and NBNs express high levels of both deep and upper layer cortical layering markers throughout development at the single-cell level (Figure S6E, F).

Signaling pathway effectors show dynamic expression in the neurogenic lineage

Signaling pathways impinge on downstream effectors and regulate NSC fate decisions during neurogenesis. The crosstalk between the signaling pathways and the integration of their targets governs stem cell maintenance and fate. In order to evaluate the expression dynamics of the signaling pathways in the neurogenic lineage, we selected the genes that are known to be signaling receptors

from the top 10,000 most variable genes. A total of 440 receptors were selected. We observed that the expression profiles of these genes can be divided into three groups (Figure 6A, B). In the first group, most receptors are highly expressed in the NSCs during most of the developmental process. These receptors are part of signaling pathways that are involved in stem cell maintenance, such as Wnt (*Fzd5, 7, 9*), Notch (*Notch1, 2, 3*), Fgf (*Fgfr2, Fgfr3*) and Shh signaling (*Smo, Ptch1*) (Blaschuk and ffrench-Constant, 1998; Bray, 2006; Fukuchi-Shimogori and Grove, 2001; Gaiano and Fishell, 2002; Imayoshi et al., 2010; Itoh and Ornitz, 2004; Iwata and Hevner, 2009; Louvi and Artavanis-Tsakonas, 2006; Rash et al., 2011; Sahara and O'Leary, 2009; Shimojo et al., 2008, 2011; Wang et al., 2011). In the second group, most receptors are highly expressed during neurogenesis in the NSCs and in the newborn neurons. This includes receptors from signaling pathways related to cell migration such as Ephrin receptors (Ephb2, Epha3) (Gerstmann et al., 2015) . Lastly, in the third group, most receptors are highly expressed only at later stages of development in the NSCs. This includes receptors from known signaling pathways that have been liked to gliogenesis, such as Tgf-beta/BMP signaling (*Tgfbr2, Bmpr1a, Bmpr1b*) and Il6/Lif signaling (*Lifr, Il6st*) (Ebendal et al., 1998; Gomes et al., 2005; Pollen et al., 2015; Rodriguez-Martinez and Velasco, 2012).

We further evaluated the expression profile of known ligands from the highlighted signaling pathways (Figure 5C). Similarly, to the expression profile of the receptors, the expression of the ligands can also be divided into three clusters. We observed that most Wnt ligands are expressed by NSCs, which the exception of *Wnt7b*, which is mostly expressed in NBNs. In contrast, many Fgf ligands are expressed by NBNs, although the receptors are mostly expressed in the NSCs (Figure 5A, C).

Lastly, we evaluated selected modulators and key target genes of the mostly known signaling pathways. We observed that Bmp, Wnt, Notch and Shh signaling activity is similar to the expression profile of their receptors (Figure 6D).

bHLH factors are dynamically and heterogeneously expressed in NSCs

We next evaluated the expression profile of genes from the bHLH family of transcription factors. Interestingly, we also observed three main expression profiles, similar to what we previously observed for signaling receptors. We observed that bHLH factors related to maintenance of NSCs, such as *Hes1, Hey1* and *Id4*, are highly expressed in the NSCs, mainly during early stages of brain development (Figure 7A, B). In contrast, proneural differentiation genes such as *Neurog2, Neurod2* and *Neurod6*, are highly expressed in the NSCs during neurogenesis and in BPs and only a few remain their expression in NBN (Figure 7A, C). Lastly, we also observed bHLH genes that are highly expressed mostly at later stages and have been associated with gliogenesis. This includes bHLH factors such as *Olig1, 2* and *Id1* (Figure 7A, D).

We further evaluated the expression of bHLH factors in the single-cell level. We observed that the expression of these factors in the NSCs is highly heterogeneous, even at the same embryonic time point (Figure 7E). We observed that at E10.5, most NSCs express high stemness markers (*Hes1,*

Hey1, Id4). As neurogenesis starts, more cells start to express neurogenic markers (*Neurog2, Neurod2, Neurod6*). It is interesting to note that two populations are observed at E13.5, one expressing high stemness markers and low neurogenic markers, and other expressing low stemness markers and high neurogenic markers. Moreover, these populations are not segregated, but rather a continuous path is observed. This is likely to be a result of the oscillatory expression of stemness factors such as *Hes1, Hes5* and their neurogenic targets such as *Neurog2*.

As neurogenesis advances, more cells are observed expressing low levels of stemness markers and high levels of neurogenic markers. At the end of embryonic development (PN), we observe a large heterogeneity in the expression of bHLH markers, with many cells expressing gliogenic markers (*Olig1, Olig2, Id1*) (Figure 7E).

Discussion

A precise understanding and prediction of the regulatory nodes and signaling networks controlling cell fate commitment and corticogenesis, has important implications for patients with congenital brain defects and neurological disorders. In this paper, we have created an extensive resource for the field of cortical development, with more than 100 transcriptomes of NSC, BP and NBN populations, which is available via an interactive browser ([Figure S7; http://neurostemx.ethz.ch/)](http://neurostemx.ethz.ch/). We have analyzed the gene expression of this neuronal lineage over time, focussing on phases of expansion, neurogenesis and gliogenesis. The development of the cerebral cortex is a dynamic process and involves series of transcriptional and signalling networks, which converge to impose precise regulation. Notch signalling pathway is long known to regulate NSC fate and maintenance and harnessing *Hes5*, the downstream effector and pivotal mediator of Notch signalling, we can isolate clean populations of NSCs, at each time point of development (Basak and Taylor, 2007; Blaschuk and ffrench-Constant, 1998; Bray, 2006; Imayoshi et al., 2010; Louvi and Artavanis-Tsakonas, 2006; Zhang et al., 2018). This is already a milestone, as until now, due to the lack of available transgenic tools, it has been a challenge to sequentially profiles clean populations NSCs temporally. Upon asymmetric divisions, NSCs give rise to BPs and they divide once or twice and differentiate into neurons. Using our transgenic mouse line *Tbr2::GFP*, we have isolated clean populations of BPs and their progeny NBNs throughout development (Arnold et al., 2008; Arnold et al., 2009). It is interesting to visualize and follow the dynamic transcriptional landscapes of these populations and identify their novel marker genes, speculate their gene regulatory networks and elucidate the downstream targets.

From our data, using unbiased computational pipelines, we have identified signature genes of NSCs in expansion, neurogenic and gliogenic phases. As all the known genes depicted the dynamics of expression as expected, we believe, we provide more extensive lists of novel signature genes, which could be used to identify NSCs in different phases. It is more like a 'scorecard' for the NSC population undergoing corticogenesis, some of which we have validated experimentally as well (Figure S2M, N). Similar analyses for BPs and NBNs have yielded key signature markers, which hold promise for

further biological exploration. It is rather crucial to differentiate between early and late BPs, or different NBN populations across time, in order to consolidate our knowledge about their downstream fate and function. The up and down regulations of genes could be presumptive of active or inactive downstream programs in these cells and their progeny. The exciting conjunction of gene expression dynamics and predicted transcriptional networks from ISMARA, though counterintuitive, present a strong validation for the system. We have identified active TFs in NSCs, BPs and NBNs. We can separate these cell populations based on the activities of TFs, and hence determine the gene regulatory networks active in these cells, at any given time point. ISMARA predicts more than 800 TFs and their targets in all cell types. This as well encompasses a broad data-set and resource to explore and extrapolate the known regulatory networks to the missing novel nodes. The dynamic changes in the TFs in NSCs for example, reflects the sequential changes these cells undergo during corticogenesis. Our analyses about determining the relationship among the neuronal lineage demonstrate a naturally occurring directionality, indicating strong intrinsic control. Moreover, NSCs among all the cell types seem to be most dynamic, be it at gene expression level, or the transcriptional networks. The NSCs follow a continuous path, through the three phases, supporting the neuronal origin from 'common progenitors', sequentially changing in transcriptional space.

To further resolve the conundrum about 'common versus multiple' progenitor models, we employed the state-of-art technologies, the high-throughput single-cell sequencing platform. We have generated more than 1200 single-cell transcriptomes for NSCs, BPs and NBNs, with the sequencing depth of upto 2 million reads per cell. The resolution at the single-cell level provides a more comprehensive understanding of the heterogeneity among these cell populations. To draw parallels between the population and single-cell data, we focused on HVGs from the population samples and superimposed the single cells on the same matrices. The average single-cells matched the dynamics with corresponding population samples validating the data-set and we have identified clusters of cells in NSCs population which change their composition over time. These clusters express several unique genes, which could be followed to label single-NSCs. With the advent of lineage-labelling and tracing approaches, it is interesting to investigate the biological meaning of these clusters, to identify their individual fate trajectories. For example, the expression and heterogeneity of neuronal markers in NSCs and BPs suggests of the start of the neuronal program much before the formation of the respective layer. The programs start in NSCs and BPs and the peaks of expression for neuronal markers such as *Bcl11b, Satb2, Pou3f2* corresponds to premeditated formation of their neuronal layers. At the single-cell level, it seems that the cells with markers for deep layers reduce in numbers across time, while the ones expressing upper layer markers are always in the NSC pool. The co-expression of deep and upper layer neuronal markers by majority of single cells also suggests that the cells could be multi-potent but get restricted over time due to various intrinsic or extrinsic cues.

The microenvironment of the cells plays critical roles in regulating cell fate choices. NSCs and BPs are localized in different niches, share different combination of cues. It requires a rather deeper

understanding of the signaling cues these cells are subject to at each time point to determine their fate. From our data, we have identified series of receptors and ligands that are differentially expressed during different phases and cell types, suggesting the roles the signaling pathways may be playing in cell fate determination. To identify the sources of ligands is challenging, for example, we have identified the Fgf ligands expressed in NBNs, but the receptors are expressed by NSCs. Observations like this are suggestive of cell interactions within the niche. Focusing on the heterogeneity and dynamics of bHLH factors, we elucidate the most intriguing expression profiles. The strong switches between expansion to neurogenesis and then gliogenesis in a continuous path illustrate the precision with which these factors control cell fate.

Together with the recent developments in the field, we provide a consolidated resource with systematic characterization of major progenitor pools in cortical development. Further biological validations of our predicted signaling and transcriptional nodes will provide more promise towards the deeper exploration of mechanisms controlling corticogenesis.

Figures

Graphical abstract
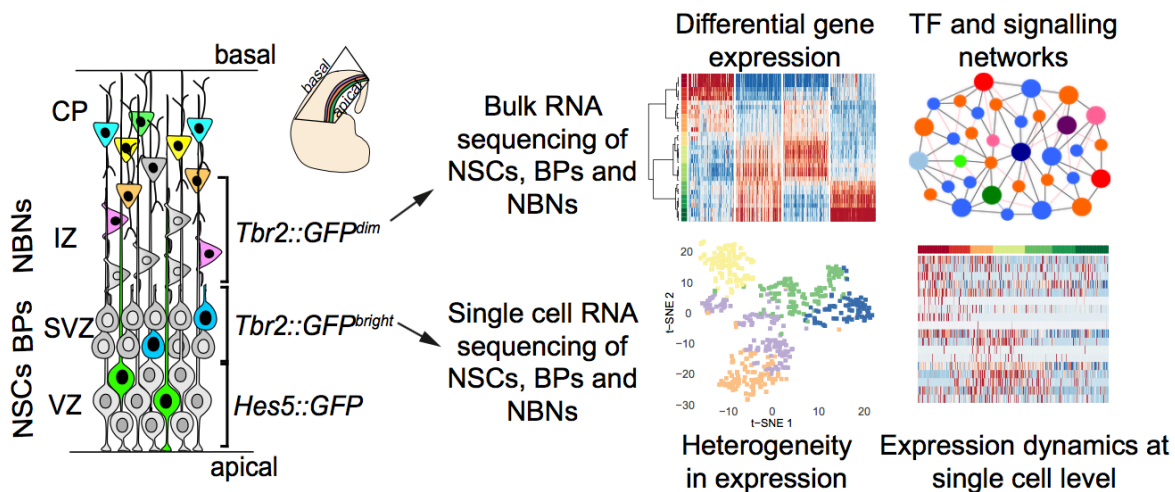
Figure 1
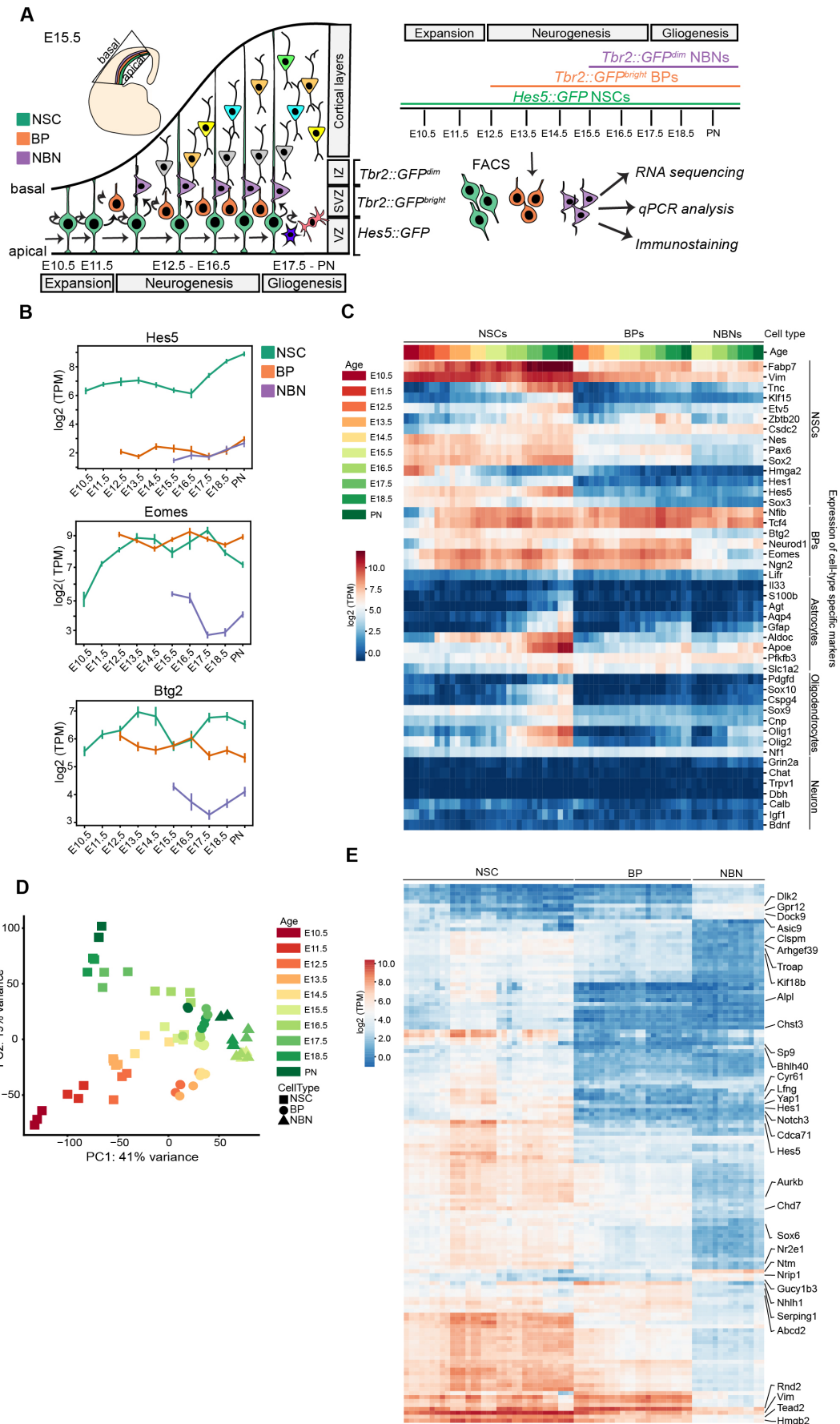
Figure 2
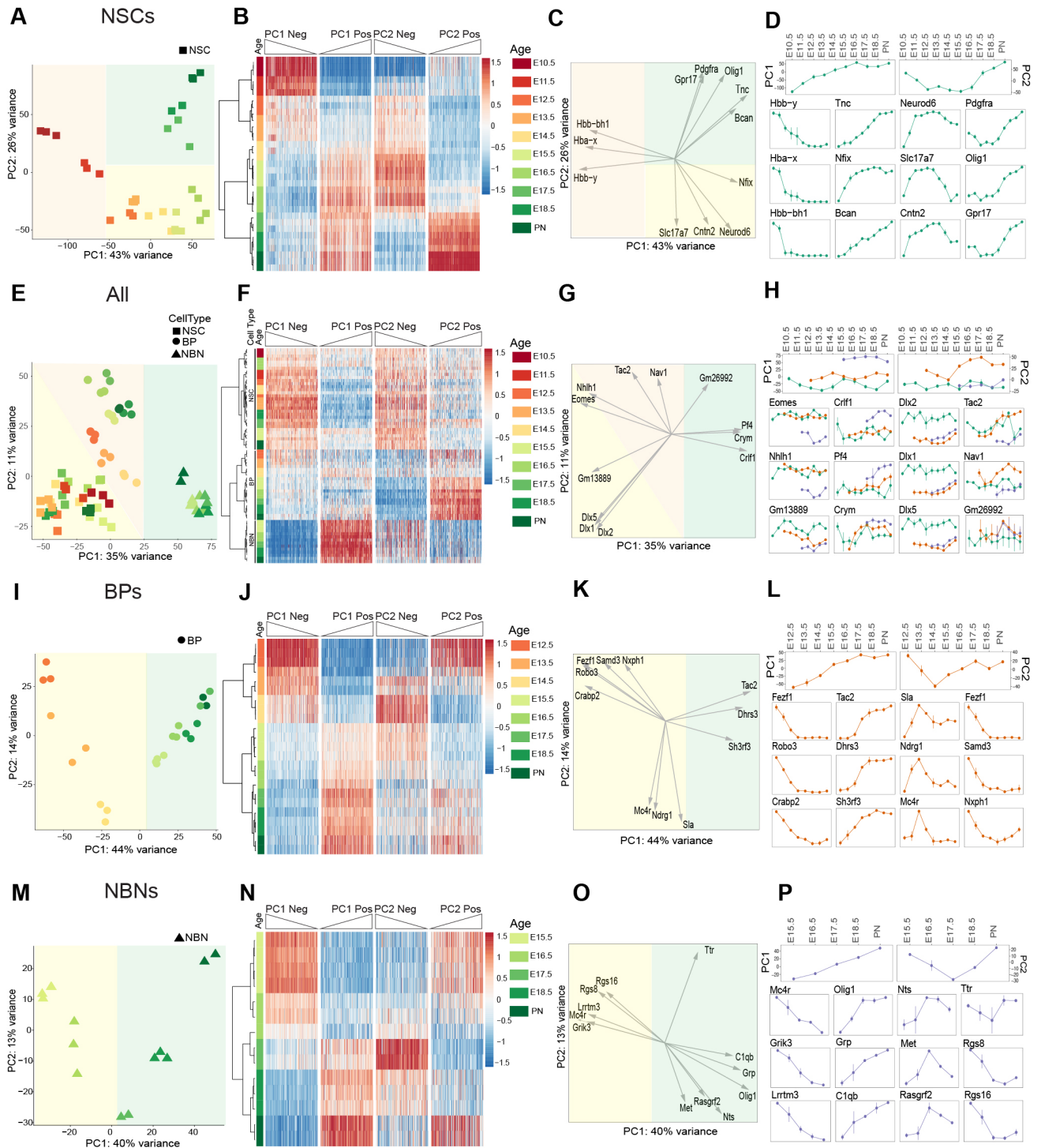
Figure 3

Figure 4

Figure 5

A — Cortical Layer marker expression

Expansion — Neurogenesis — Gliogenesis

E10.5 E11.5 E12.5 E13.5 E14.5 E16.5

B — NSCs

C — expression profiles in bulk / expression profiles in single cells

Tbr1 — Layer V

Ctip2 — Layer V

Satb2 — Layer IV

Cux2 — Layer II/III

D — E13.5 Hes5::GFP NSCs

E — BPs

F — E16.5 Tbr2::GFP BPs

G — NBNs

H — E16.5 Tbr2::GFP NBNs

Figure 6

A

Stem cell maintenance   Neurogenic   Gliogenic

B

C

Ligands

D

BMP signaling

WNT signaling

SHH signaling

Notch signaling

137

Figure 7

Figure S1

Figure S2

A Variance Plots
NSCs

B

C

Expansion — Neurogenesis

Ccnd1 *Crabp2* *Hbb-bh1* — *Bcl11b* *Bhlhe22* *Cabp1* *Cntn2*

Neurogenesis — Gliogenesis

Id2 *Satb2* *Tubb3* *Fezf2* — *ApoE* *Aqp4* *Cspg4*

D NSC — Upregulation — Cspg4

E Downregulation — Shh

F Transient Downregulation — Jag1

G Transient Upregulation — Neurog2

Gliogenesis

Hmgb2 *Olig1* *Pdgfra* *Sparcl1* *Tril*

H Orthogonal

140
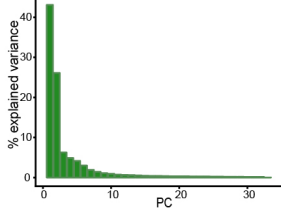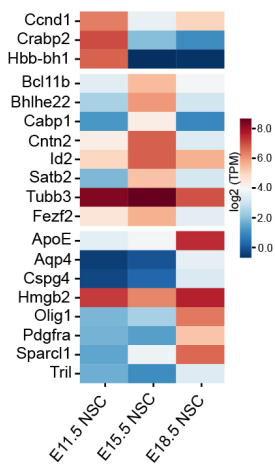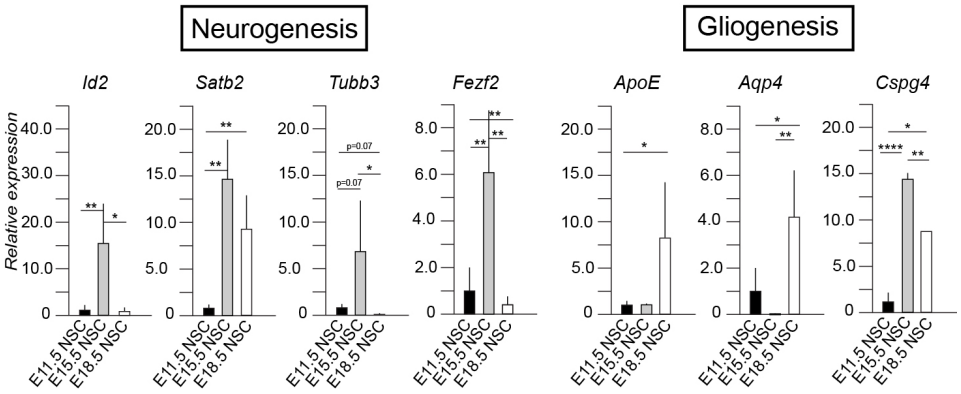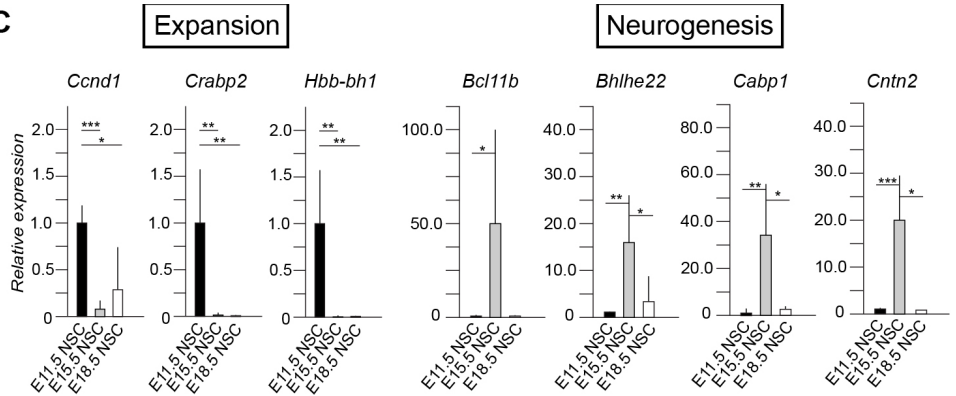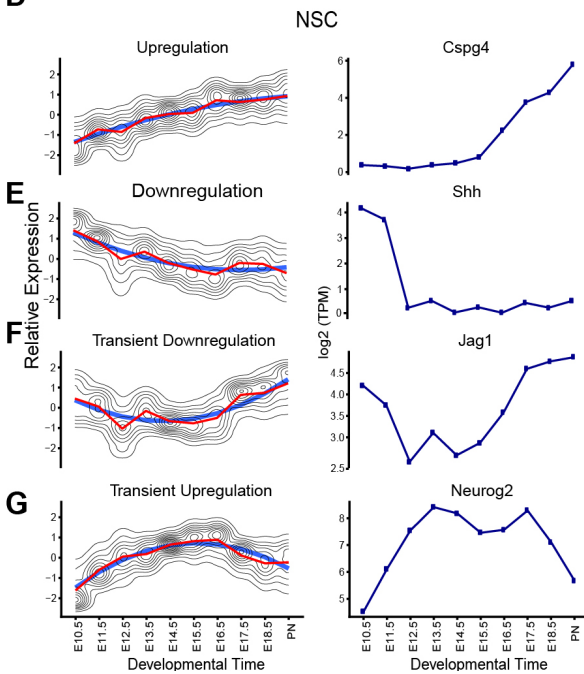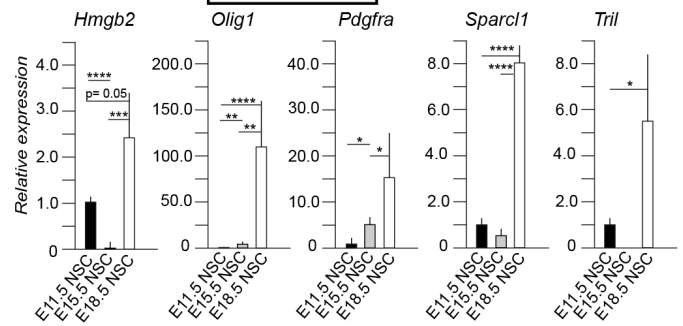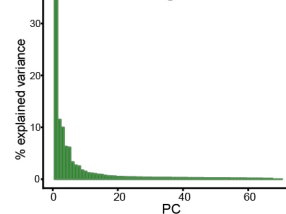
Figure S3

Figure S4

142
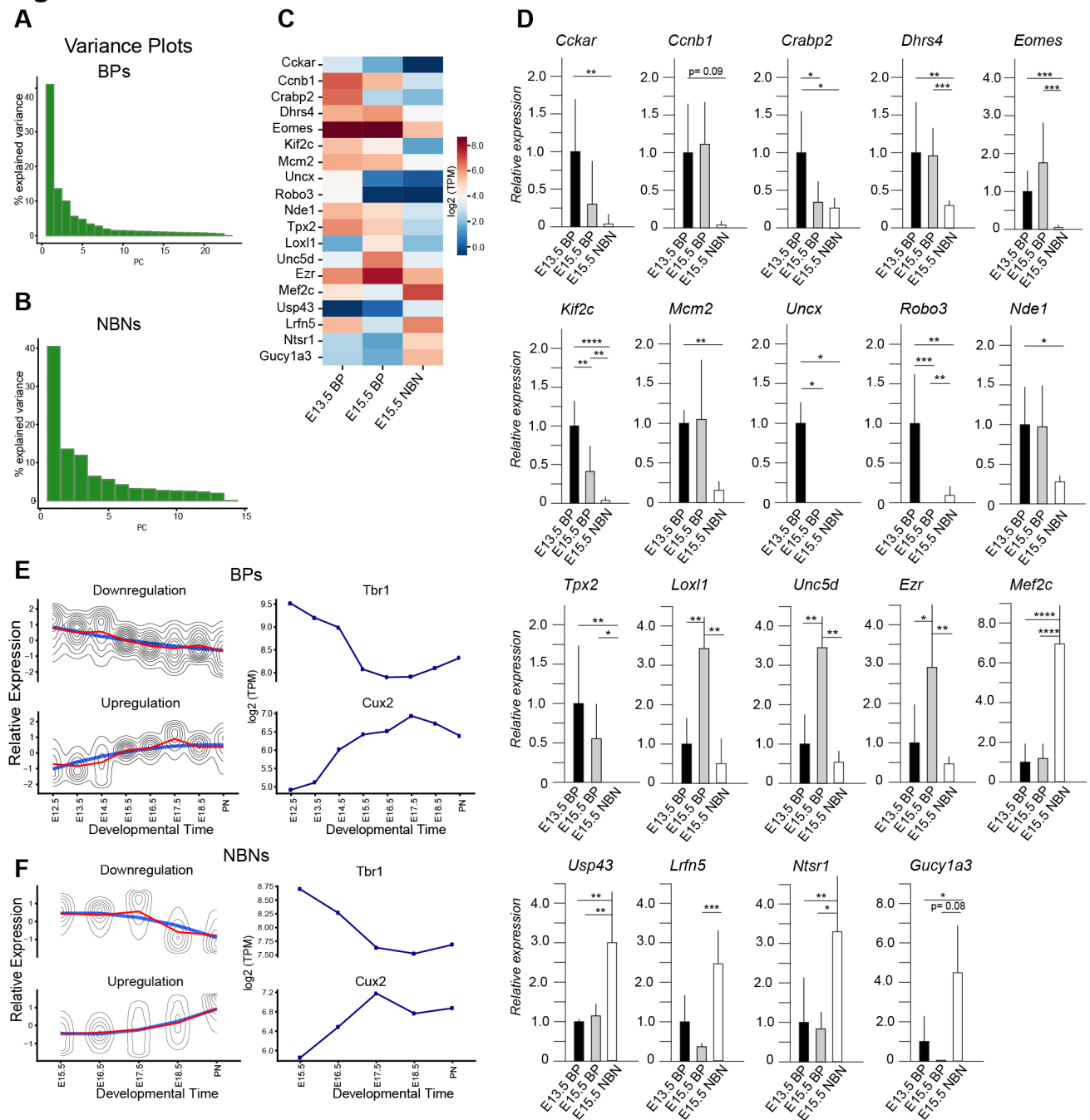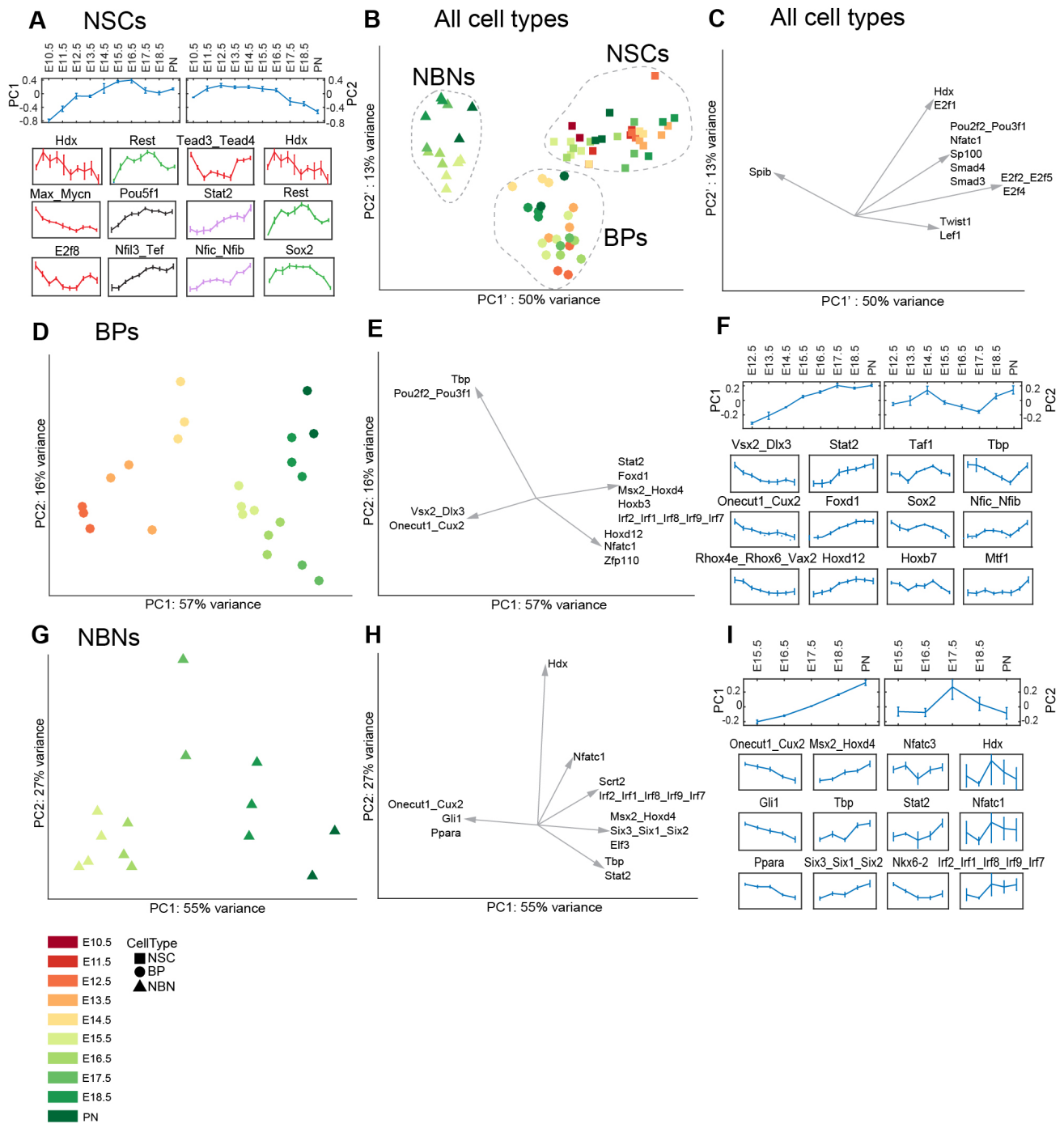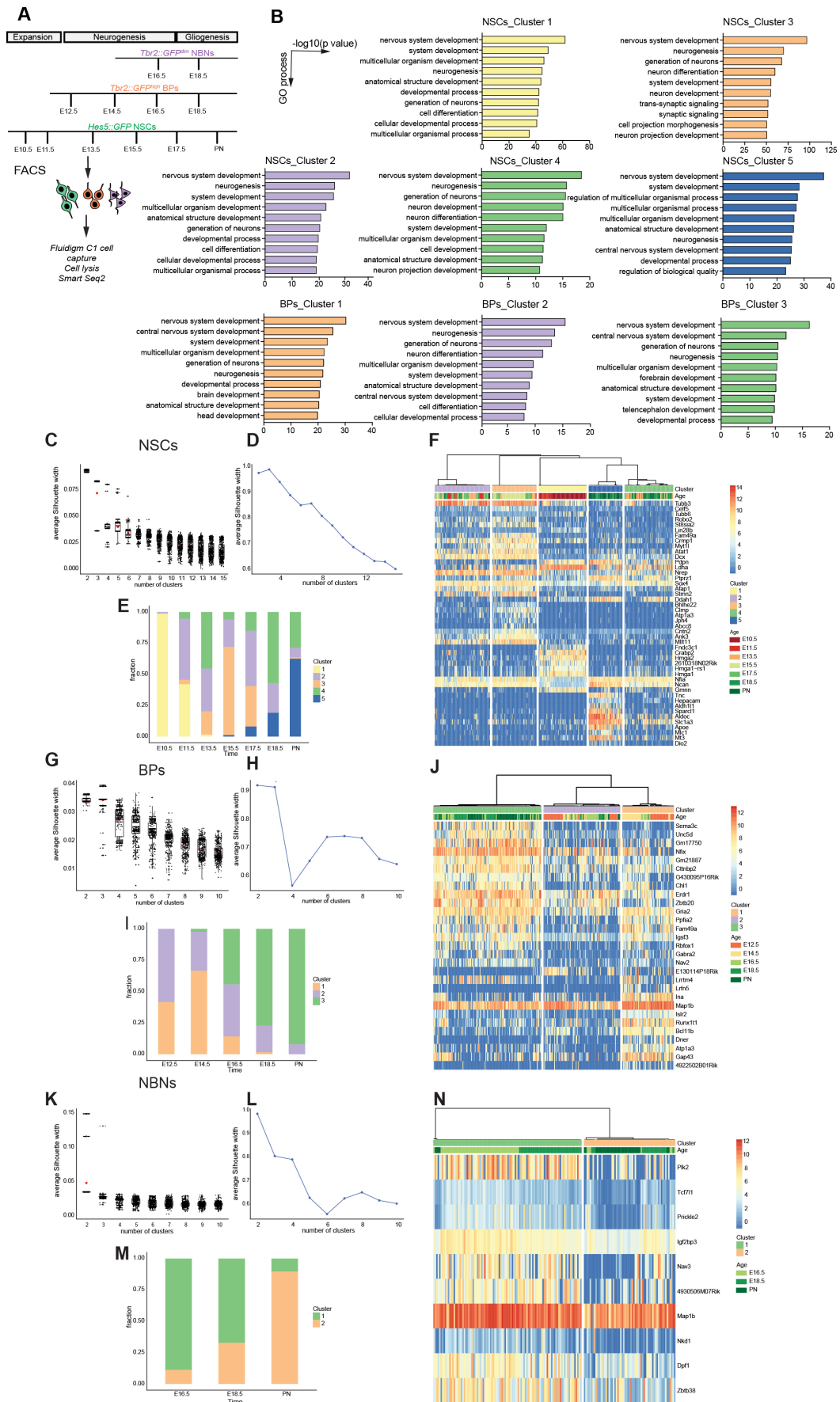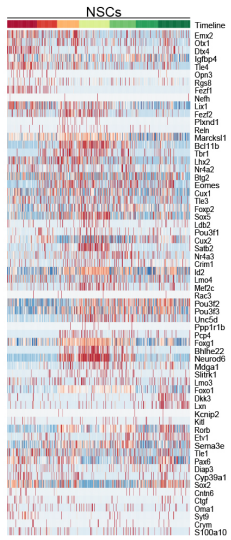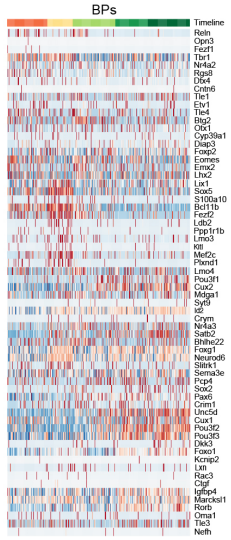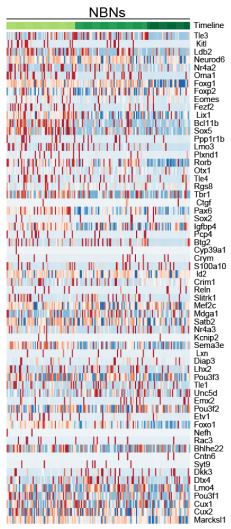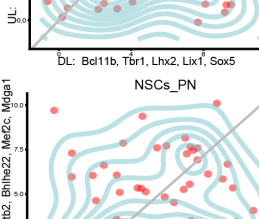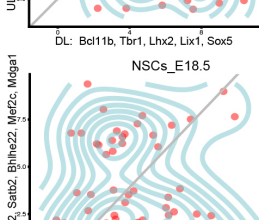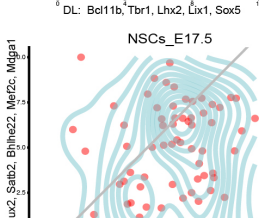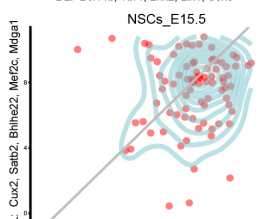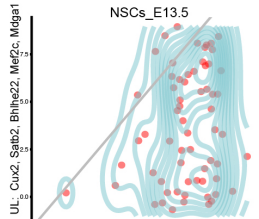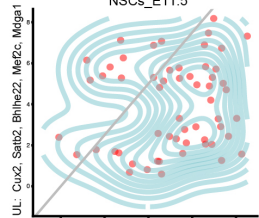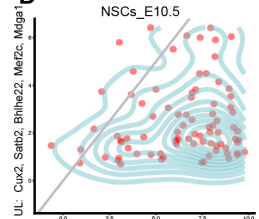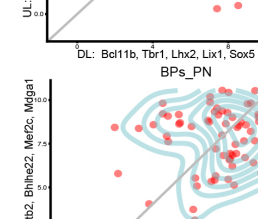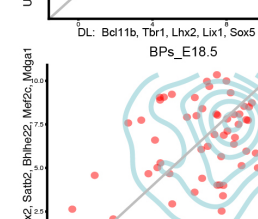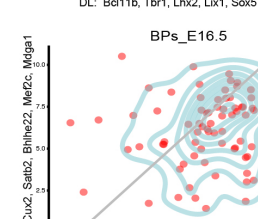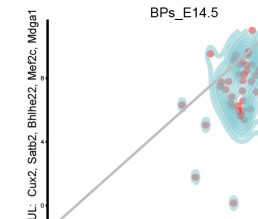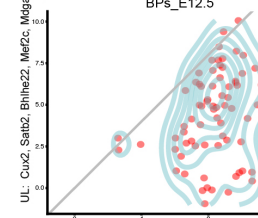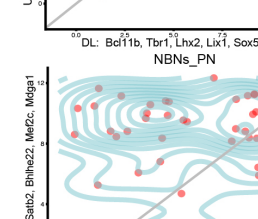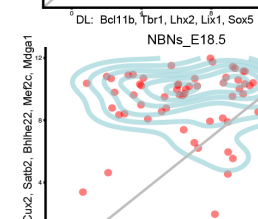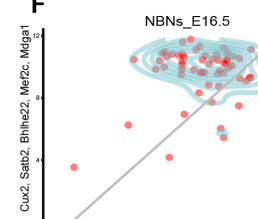
Figure S5

Figure S6

Figure S7

A
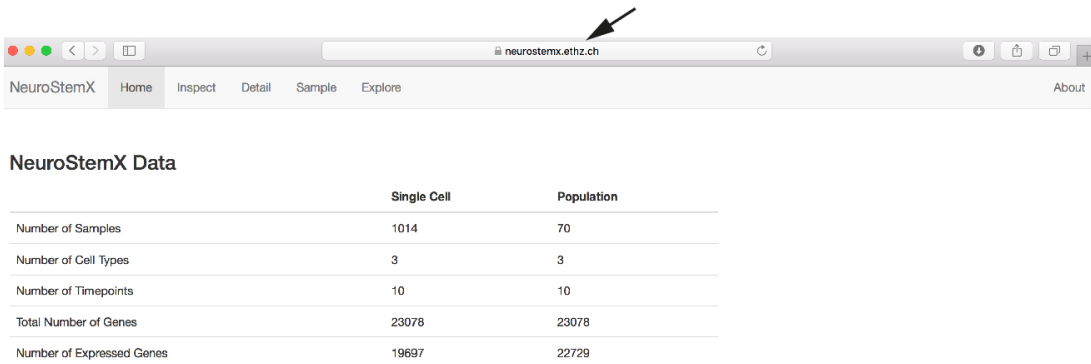
B

C
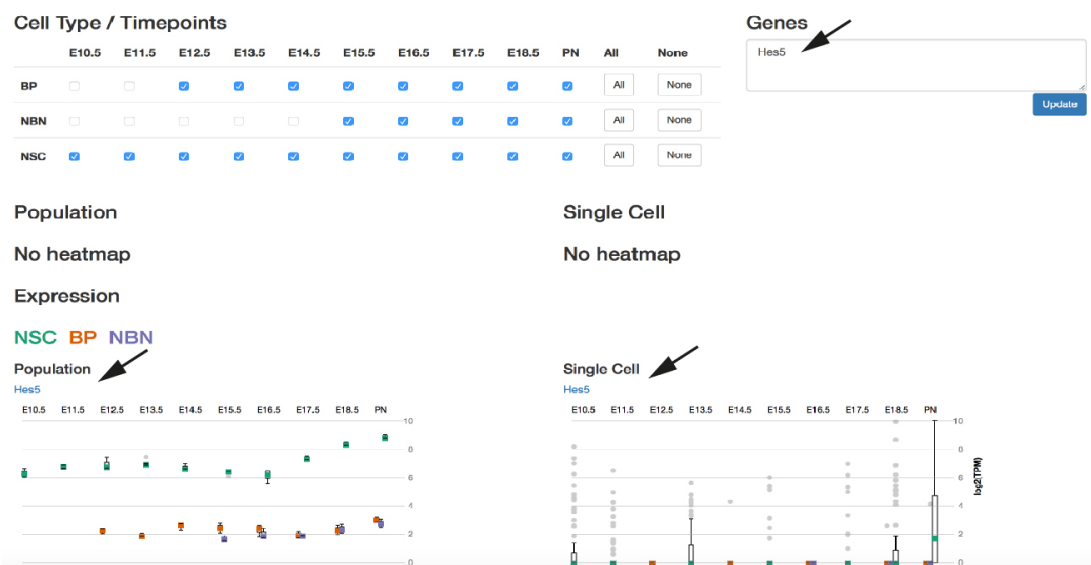
Figure legends

Figure 1: Overview and validation of the transcriptional analyses.

(A) Overview of the biological system with experimental paradigm, illustrating NSCs, BPs and NBNs were isolated at each day during development from E10.5 to PN.

(B) Notch signaling effector *Hes5* is expressed high in NSCs while *Eomes (Tbr2)* and *Btg2* are expressed high in both NSCs and BPs at the mRNA level.

(C) Heatmap validating the known cell-type specific marker gene expression from RNA sequencing data.

(D) Principal Component Analysis (PCA) for all samples of NSCs, BPs and NBNs throughout development, covering maximum variance.

(E) Heatmap illustrating the novel marker genes identified from the RNA sequencing data, as signature genes for NSCs, BPs and NBNs. NSCs- Neural stem cells, BPs-Basal progenitors, NBNs- Newborn neurons, E-Embryonic day, PN-Post natal, VZ-Ventrical zone, SVZ- Subventrical zone, IZ-Intermediate Zone. Expression values on the heatmaps are log2(transcripts per million).

Figure 2: Dynamics of transcriptional profile changes in different populations over time.

(A) PCA of NSCs from E10.5 to PN showing their transcriptional dynamics.

(B) Heatmap of genes that have the highest contribution to the PC1 and PC2 for NSCs, sorted by their weights (250 genes from each side).

(C) PCA plots with projected genes shown as vectors illustrating their contribution.

(D) Illustrating the trends (top), based on the position of samples along PC1 and PC2, and the gene expression profiles of top three genes from each side of PC1 and PC2 for NSCs (bottom).

(E) PCA of all samples removing the first two principle components of NSCs from E10.5 to PN showing their transcriptional dynamics.

(F) Heatmap of genes that have the highest contribution to the PC1 and PC2, sorted by their weights (250 genes from each side).

(G) PCA plots with projected genes shown as vectors illustrating their contribution.

(H) Illustrating the trends (top), based on the position of samples along PC1 and PC2, and the gene expression profiles of top three genes from each side of PC1 and PC2 (bottom).

(I) PCA of BPs from E12.5 to PN showing their transcriptional dynamics.

(J) Heatmap of genes that have the highest contribution to the PC1 and PC2 for BPs, sorted by their weights (250 genes from each side).

(K) PCA plots with projected genes shown as vectors illustrating their contribution.

(L) Illustrating the trends (top), based on the position of samples along PC1 and PC2, and the gene expression profiles of top three genes from each side of PC1 and PC2 for BPs (bottom).

(M) PCA of NBNs from E15.5 to PN showing their transcriptional dynamics.

(N) Heatmap of genes that have the highest contribution to the PC1 and PC2 for NBNs, sorted by their weights (250 genes from each side).

(O) PCA plots with projected genes shown as vectors illustrating their contribution.

(P) Illustrating the trends (top), based on the position of samples along PC1 and PC2 and the gene expression profiles of top three genes from each side of PC1 and PC2 for NBNs (bottom).

In D, H, L and P (bottom), the x-axis is embryonic days and the y-axis is log2(TPM).

Figure 3: Dynamics of transcriptional network changes with ISMARA in different populations over time.

(A) The ISMARA model's promoter expression as a linear combination of the TF binding motifs activity that are present in the promoter region.

(B) PCA on motif activity for NSCs for all time points, on the first two components, representing 80% of the total variance. The background colour represents the three phases expansion (red, E10.5-E11.5), neurogenesis (green, E12.5-E15.5) and gliogenesis (purple, E16.5-PN).

(C) Top 20 motifs contributing the most to the first two PCs, projected on the first two PCs.

(D) Examples of motifs (one per phase) regulating the genes identified from gene expression analyses, contributing highest to the PC1 and PC2 (figure 2 for NSCs).

(E) Directed graphical representations of the main motif-motif interactions and the gene ontology and biological functions of the target genes. Each motif is shown with the colour defining the zones of expansion, neurogenesis and gliogenesis along with plots of its activity.

(F) PCA on motif activity for NSCs only from the neurogenesis phase,
BPs and NBNs, representing 69% of the total variance.

(G) Top motifs contributing the most to the first two principal components, projected on the first two principal components from (F).

(H) Examples of motifs (one per cell type, NSCs- green, BPs- orange and NBNs- purple) regulating the genes identified from gene expression analyses, contributing highest to the PC1 and PC2.

(I) Directed graphical representations of the main motif-motif interactions and the gene ontology and biological functions of the target genes. Each motif is shown with the colour defining the cell types NSCs (green), BPs (orange) and NBNs (purple) along with plots of its activity.

Figure 4: Heterogeneity of NSCs, BPs and NBNs at single cell level.
(A) PCA of NSC single cells, using the top 2000 highly variable genes obtained from bulk NSCs.

(B) Projection of average single cells of NSCs at each time point on the first two PCs of bulk NSCs using the top 2000 highly variable genes obtained from bulk NSCs.

(C) Clustering of assignment matrix of NSC single cells using k-means and hierarchical clustering.

(D) Marker genes that are up/down regulated in each cluster of NSCs.

(E) PCA of BP single cells, using the top 2000 highly variable genes obtained from bulk BPs.

(F) Projection of average BP single cells on the first two PCs of bulk BPs using the top 2000 highly variable genes obtained from bulk BPs.

(G) Clustering of assignment matrix of NBN single cells using k-means and hierarchical clustering.

(H) Marker genes that are up/down regulated in each cluster of NBNs.

(I) PCA of NBN single cells, using the top 2000 highly variable genes obtained from bulk NBNs.

(J) Projection of average single cells of NBNs on the first two PCs of bulk NBNs using the top 2000 highly variable genes obtained from bulk NBNs.

(K) Clustering of assignment matrix of NBN single cells using k-means and hierarchical clustering.

In C, G and K, heatmaps represent the hierarchal clustering of assignment matrix of single cells after 500 times applying k-means clustering. The optimal number of clusters is selected based on the Silhouette coefficient. It is "1" (red) when two cells are always clustered together, "0" (blue) when two cells never fall in the same cluster. Pie charts represent the percentage of single cells at each time point in each cluster.

Figure 5: Dynamic expression of neuronal specification factors in NSCs, BPs and NBNs.
(A) Illustration of distinct projection neurons born sequentially during the course of neurogenesis.

(B) Heatmap illustrating the dynamics of expression of cortical layering markers in NSCs at population level.

(C) Examples of expression dynamics of deep layer markers Tbr1, Ctip2 and upper layer markers Satb2, Cux2 in NSCs, BPs and NBNs, profiles at population level (left) and single cell level (right).

(D) Experimental validation of NSCs isolated at E13.5 using *Hes5::GFP* transgenic embryos, showing no detectable protein for Tbr1, Ctip2 and Satb2. NSCs do express Brn2(Pou3f2) *in vitro* and *in vivo* at protein level.

(E) Heatmap illustrating the dynamics of expression of cortical layering markers in BPs at population level.

(F) Experimental validation of BPs isolated at E16.5 using *Tbr2::GFP* transgenic embryos, showing no detectable protein for Tbr1, Ctip2 and Satb2.

(G) Heatmap illustrating the dynamics of expression of cortical layering markers in NBNs at population level.

(H) Experimental validation of NBNs isolated at E16.5 using *Tbr2::GFP* transgenic embryos, showing protein expression for Tbr1, Ctip2, Satb2 and Brn2(Pou3f2).

In B, E and F, heatmaps are based on z-score of log2(TPM) expression values.

Figure 6: Dynamic expression profile of signalling receptors during corticogenesis.

(A) Heatmaps representing the expression profile of signalling receptors that can be divided into three main groups based on k-means clustering of z-scored log2(TPM) expression values: stem cell maintenance (121 receptors), neurogenic (180 receptors) and gliogenic (139 receptors). Names of selected receptors are displayed. For the complete list please see Supplementary Information. Expression profiles are represented by their z-score.

(B) Average expression profile of each cluster for NSCs (green), BP (orange) and NBN (purple). Solid line represents the average z-score, while the area represents the standard deviation estimated from different biological samples.

(C) Heatmap representing the expression profile of ligands from selected signalling pathways, based on the z-scored log2(TPM) expression values.

(D) Expression profile of selected target or modulator of key signalling pathways: BMP, Wnt, Shh and Notch signaling.

Figure 7: Dynamic and heterogenic expression profile of bHLH factors during forebrain development.

(A) Heatmaps representing the expression profile of bHLH factors. Three main groups are observed based on k-means clustering of z-scored log2(TPM) of expression value: stem cell maintenance (high expression in the NSCs at early embryonic times and low in BPs and NBNs), neurogenic (high expression in the NSCs during neurogenesis and high expression in BPs and NBNs) and gliogenic (high expression in the NSCs at late embryonic times and low in BPs and NBNs). Expression profiles are represented by their z-score.

(B) Expression profile of selected stem cell maintenance markers Hes1, Hey1 and Id4. (C) Expression profile of selected neurogenic markers Neurog2, Neurod2, and Neurod6.

(D) Expression profile of selected gliogenic markers Olig1, Olig2 and Id1.

(E) Expression of stem cell markers (Hes1, Hey1 and Id4), neurogenic markers (Neurog2, Neurod2, and Neurod6) and gliogenic markers (Olig1,2 and Id1) in NSCs during different embryonic time points in the single-cell levels. Each point represents the expression value of one single cell in log2(TPM).

Supplementary figure 1:

(A) *Hes5::GFP* and *Tbr2::GFP* transgenic mice used for cell isolation.

(B) Expression of *Hes5::GFP* and *Tbr2::GFP* embryonic cortices at E17.5. Scale bar = 100μm.

(C) Examples of FACS plots for GFP positive cell sorting at E14.5 *Hes5::GFP* and E15.5 *Tbr2::GFP.*

(D-F) Expression validation of *Hes5::GFP* and *Tbr2::GFP* positive cells after FAC sorting *in vitro*. Scale bar = 20μm

(G) Expression plots of some known markers of NSCs.

(H) Bar plot representing the proportion of variance covered by each PC in PCA of all cell types.

(I) Heatmap showing differentially expressed genes in three cell populations illustrating NSCs, BPs and NBNs vary in expression, based on z-scored log2(TPM) expression values.

(J, L, N) Volcano plots for DEG analysis for NSCs versus BPs, NSCs versus NBNs and BPs versus NBNs, respectively. Significantly DEGs are coloured as grey and top 100 DEGs are coloured by red.

(K, M, O) Top ten DEGs for NSCs versus BPs, NSCs versus NBNs and BPs versus NBNs, respectively.

(J-O) are related to analysis of Figure 1E.

The range of p-values is very different: NSC (0.01%-0.4%), BP (1.6% – 4.9%), NBN (0.06%-0.2%). There are no good marker genes for BPs as their gene expression tends to be similar to either NSC or NBN.

Supplementary figure 2:

(A) Bar plot representing the variance coverage by PC corresponding to PCA plot in Figure 2 (A).

(B) Heatmap illustrating the expression changes in signature genes in time points corresponding to expansion, neurogenesis and gliogenesis.

(C) qPCR validation of signature genes in three zones. Each time point has samples varying from N =3 to N= 7.

(D-G) K-means clustering of z-scored log2 (TPM) gene expression profiles over developmental time course in NSCs with genes showing upregulation, e.g. Cspg4, downregulation, e.g. Shh, transient downregulation, e.g. Jag1, transient upregulation, e.g. Neurog2.

(H) Bar plot representing the variance coverage by PC corresponding to PCA plot in Figure 2 (E).

Supplementary figure 3:

(A, B) Bar plots representing the variance coverage by PCs corresponding to PCA plot in Figure 2 (I, M).

(C) Heatmap illustrating the expression changes in signature genes in time points corresponding to early BPs, mid-BPs and NBNs.

(D) qPCR validation of signature genes for three sample types. Each time point has samples varying from N =3 to N= 7.

(E) K-means clustering of z-scored log2(TPM) gene expression profiles over developmental time course in BPs with genes showing downregulation, e.g. Tbr1 and upregulation, e.g. Cux2.

(F) K-means clustering of z-scored log2(TPM) gene expression profiles over developmental time course in NBNs with genes showing downregulation, e.g. Tbr1 and upregulation e.g. Cux2.

Supplementary figure 4:

(A) Examples of dynamic motifs based on the PCA of NSCs (Figure 3B). Plots show the replicate average of samples across the sampling time for the first two principal components separately, and for the three motifs contributing the most to the first and second principal component, positively and negatively, separately.

(B) PCA plot for all cell types (NSCs, BPs and NBNs) after removing the first two components of NSC variance (from Figure 3B).

(C) Plot showing the projections of each cell type sample on the replicate average of motif activity, representing 63% of the total variance.

(D) PCA analysis on motif activity for BPs for all time points, on the first two components, representing 73% of the total variance.

(E) Top 12 motifs contributing the most to the first two principal components, projected on the first two principal components.

(F) Examples of dynamic motifs based on the PCA of BPs. Plots show the replicate average of samples across the sampling time for the first two principal components separately, and for the three motifs contributing the most to the first and second principal component, positively and negatively, separately.

(G) PCA on motif activity for NBNs for all time points, on the first two components, representing 82% of the total variance.

(H) Plot showing the projections of each cell type sample on the replicate average of motif activity, representing 82% of the total variance.

(I) Examples of dynamic motifs based on the PCA of NBNs. Plots show the replicate average of samples across the sampling time for the first two principal components separately, and for the three motifs contributing the most to the first and second principal component, positively and negatively, separately.

In A, F and I bottom, the y-axis is the embryonic day and x-axis is log2(TPM) expression values.

Supplementary figure 5:

(A) Schematic representation of the experimental approach used for single cell collection used to isolate *Hes5::GFP* and *Tbr2::GFP* cells for single cell sequencing using Fluidigm C1 platform.

(B) Gene Ontology (GO) analysis of the biological process in different clusters of NSC` and BP single cells. Metacore Software was used, -log10(p value) is indicated. The analyses were performed only on the clusters which are composed by 50 or more genes.

(C) Silhouette analysis where points represent the average Silhouette width of k-means clusters of NSC single cells for each k for a random initial number. For each k, 500 k-means clustering applied with different initial values.

(D) Silhouette coefficient of hierarchal clustering of the assignment matrix of NSC single cells for different k.

(E) Bar plot shows the fractions of NSC cells at each cluster at different time points.

(F) Signature genes identified for each NSC single cell cluster.

(G) Silhouette analysis where points represent the average Silhouette width of k-means clusters of NSC single cells for each k for a random initial number. For each k, 500 k-means clustering applied with different initial values.

(H) Silhouette coefficient of hierarchal clustering of the assignment matrix of BP single cells for different k.

 (I) Bar plot shows the fractions of BP cells at each cluster at different time points.

(L) Signature genes identified for each BP single cell cluster.

(M) Silhouette analysis where points represent the average Silhouette width of k-means clusters of NSC single cells for each k for a random initial number. For each k, 500 k-means clustering applied with different initial values.

(N) Silhouette coefficient of hierarchal clustering of the assignment matrix of BP single cells for different k.

(O) Bar plot shows the fractions of NBN cells at each cluster at different time points.

(P) Signature genes identified for each NBN single cells cluster.

Supplementary figure 6:

(A) Heatmap of cortical layer markers in NSC single cells, based on z-scored log2(TPM) expression values.

(B) Heatmap of cortical layer markers in BP single cells, based on z-scored log2(TPM) expression values.

(C) Heatmap of cortical layer markers in NBN single cells, based on z-scored log2(TPM) expression values.

(D) Temporal distribution of NSC single cells along the deep or upper layer markers.

(E) Temporal distribution of BP single cells along the deep or upper layer markers.

(F) Temporal distribution of NBN single cells along the deep or upper layer markers.

In D-F, X axis: deep layer markers- Bcl11b, Tbr1, Lhx2, Lix1, Sox5 and Y axis- Cux2, Satb2, Bhlhe22, Mef2c, Mdga1.

Supplementary figure 7:
(A) The online browser (http://neurostemx.ethz.ch/) directs to detailed population and single-cell RNA sequencing analyses for NSCs, BPs and NBNs.
(B) Going through the Inspect tab, one can select the time points or genes one is interested in and click on Update. The website in real-time processes the request and displays the desired heatmaps.
(C) Example showing a query for a single gene, here, Hes5, yields two types of plots- population and single-cell for all cell types.
(The data are in log2(TPM), colour code as mentioned in the key).

Table legends

Table 1: This table corresponds to Figures 1 and S1.
Tab1- List of highly variable signature genes from PCA in Figure 1D.
Tab2- List of genes in heatmap of Figure 1E.
Tab3- List of DEGs between NSCs and BPs
Tab4: List of DEGs between BPs and NBNs
Tab5: List of DEGs between NSCs and NBNs
Tab6: Signature genes NSCs versus BPs and NBNs
Tab7: Signature genes BPs versus NSCs and NBNs
Tab8: Signature genes NBNs versus NSCs and BPs

Table2: This table corresponds to Figures 2, S2 and S3.
Tab1- List of highly variable signature genes from PCA in Figures 2B and S2B, C.
Tab2- List of highly variable signature genes from PCA in Figures 2F.
Tab3- List of highly variable signature genes from PCA in Figures 2J and S3C, D.
Tab4- List of highly variable signature genes from PCA in Figure 2N and S3C, D.
Tab5: List of genes in NSCs clustered as upregulation, downregulation, transient upregulation and transient downregulation in Figures S2D-G.
Tab6: List of genes in BPs clustered as downregulation and upregulation in Figure S3E.
Tab7: List of genes in NBNs clustered as downregulation and upregulation in Figure S3F.

Table 3: This table corresponds to Figure 3.
Tab1: Motif activity scores for PCA in Figure 3B.
Tab2: List of motifs with fraction of total variance captured by each motif on the first 2 principal components, from Figure 3C.
Tab3: List of predicted motif interaction with interaction likelihood scores in Figure 3D, E.
Tab4: Motif activity scores for PCA in Figure 3F.
Tab5: List of motifs with fraction of total variance captured by each motif on the first 2 principal components, from Figure 3G.
Tab6: List of predicted motif interaction with interaction likelihood scores in Figure 3H, I.

Table 4: This table corresponds to Figures 4 and S5.
Tab1-6: Signature genes and summary from 5 NSC clusters identified in Figures 4D and S5F.
Tab7-10: Signature genes and summary from 3 BP clusters identified in Figures 4H and S5J.
Tab11-12: Signature genes and summary from 2 NBN clusters identified in Figures 4L and S5N.

Table 5: This table corresponds to Figures 4 and S5.
Tab1-5: Gene Ontology analyses for 50 enriched categories in 5 NSC clusters identified in Figures 4D and S5F.

Tab6-8: Gene Ontology analyses for 50 enriched categories in 3 BP clusters identified in Figures 4H and S5J.

Table 6: This table corresponds to Figures 6.

Tab1: List of genes considered as markers of stemness, gliogenic and neurogenic phases of NSCs, in Figure 6A-C.

STAR★METHODS

Detailed methods are provided in the online version of the paper and include the following:

- KEY RESOURCES TABLE

- CONTACT FOR REAGENTS AND RESOURCE SHARING

- EXPERIMENTAL MODELS AND SUBJECT DETAILS

    - Mice strain

- METHOD DETAILS

    o Tissue preparation and fluorescence-assisted cell sorting

    o RNA isolation and RNA-sequencing

    o Tissue preparation, immunocytochemistry and immunohistochemistry

- QUANTIFICATION AND STATISTICAL ANALYSIS

- DATA AND SOFTWARE AVAILABILITY

STAR★METHODS

KEY RESOURCES TABLE

REAGENT OR RESOURCE		
Antibodies	**Source**	**Identifier**
Chick anti-GFP (1:300)	Millipore	Cat# 06-896, RRID:AB_11214044
Rat anti-Ctip2 (1:500)	Abcam	Cat# ab18465; RRID:AB_2064130
Goat anti-Brn2 (1:250)	Santa Cruz	Cat# sc-6029 RRID:AB_2167385
Sheep anti-GFP (1:250)	AbD Serotec/Biorad	Cat# 4745-1051, RRID:AB_619712
Rabbit anti-Tbr2 (1:500)	Abcam	Cat# ab23345, RRID:AB_778267
Rabbit anti-Pax6 (1:500)	Covance	Cat# PRB-278P, RRID:AB_291612
Mouse anti-Satb2 (1:200)	Abcam	Cat# ab51502, RRID:AB_882455
Rabbit anti-Tbr1 (1:500)	Abcam	Cat# ab31940, RRID:AB_2200219
Donkey anti-Sheep, Alexa 488 (1:500)	Jackson ImmunoResearch Labs	Cat# 713-545-147, RRID:AB_2340
Donkey anti-Rabbit, Cy3 (1:500)	Jackson ImmunoResearch Labs	Cat# 711-165-152, RRID:AB_2307
Donkey anti-Mouse, Cy3 (1:500)	Jackson ImmunoResearch Labs	Cat# 715-165-151, RRID:AB_2315
Donkey anti-Rat, Cy3 (1:500)	Jackson ImmunoResearch Labs	Cat# 712-166-153, RRID:AB_2340
Donkey anti-Goat, Cy3 (1:500)	Jackson ImmunoResearch Labs	Cat# 705-165-147, RRID:AB_2307
Donkey anti-Chicken, Alex488 (1:500)	Jackson ImmunoResearch Labs	Cat# 703-545-155, RRID:AB_2340
Chemicals	**Source**	**Identifier**
Formaldehyde Solution (w/v)	Sigma	47608(47673/33220)
DNase I, RNase-free	Sigma	04716728001
DNase I Grade II	Roche	10104159001
L_Cysteine	Sigma	168149

Papain	Sigma	P3125-100MG
Trypsin inhibitor from Glycine max (soybean)	Sigma	T6522-5x100MG
L15 Medium	Invitrogen	31415029 (31415086)
PBS cell culture	Dulbecco	14080089 (14080048)
Trition X-100	Fisher	BPE151-500
TRIzol	Invitrogen	VX15596018
Glycoblue Co-precipitate	Life Technologies	D1417005
Poly L- Lysine hydrobromide	Sigma	P9155-5MG
B27 supplement+A26	Gibco	17504-044
DMEM/F12	Gibco	31966-047
Chloroform	Sigma	288306
Normal Donkey Serum	Jackson ImmunoResearch Labs	017-000-121
Agarose	Fisher Scientific	BPE1356-100
RNAse free water	Ambion	AM9906
TE buffer	Invitrogen by Thermo Fisher Scientific	AM9849
NaOH	Roth	6785.1
Chamber slides	Lab-Tek	177402
Critical Commercial Assays	**Source**	**Identifier**
2x Assay Loading Reagent	Fluidigm	85000736
20x DNA Binding Dye Sample Loading Reagent	Fluidigm	100-3738
20x GE Sample Loading Reagent	Fluidigm	85000746
Sso Fast EvaGreen SuperMix with low Lox	BioRad	172-5211
Dynamic Array 48.48	Fluidigm	BMK-M-48.48
Dynamic Array 96.96	Fluidigm	BMK-M-96.96
PreAmp and Reverse Transcription Master Mix	Fluidigm	100-6300
Human Brain Reference RNA	Life Technologies	AM6050
Exonuclease I	New England Biolabs	M0293L
C1 Single Cell Auto Prep Array for mRNA Seq Multipack - contains: - Module 1 Single Cell Auto Prep Kit - Module 2 mRNA Seq - C1 Single Cell Auto Prep Array for mRNA Seq (5-10µm)	Fluidigm	100-6041 100-5518 100-6209 100-5757
SMARTer Ultra Low RNA Kit for Illumina Sequencing	Clontech/Takara	634936
Advantage 2 PCR Kit	Clontech/Takara	639206
Nextera XT DNA Library Preparation Kit	Illumina	FC-131-1096
Nextera XT Index Kit v2 Set A	Illumina	FC-131-2001
Nextera XT Index Kit v2 Set B	Illumina	FC-131-2002
Nextera XT Index Kit v2 Set C	Illumina	FC-131-2003
Nextera XT Index Kit v2 Set D	Illumina	FC-131-2004
Agencourt AMPure XP	Beckman Coulter	A63882
DNA Suspension Buffer, pH 8.0	Teknova	T0221

HS NGS Fragment 35-6000bp.mthds	Labgene Scientific SA	DNF-486-0500
HS NGS Fragment 1-6000bp.mthds	Labgene Scientific SA	DNF-474-0500
SS NGS Fragment 35-6000bp.mthds	Labgene Scientific SA	DNF-479-0500
SS NGS Fragment 1-6000bp.mth	Labgene Scientific SA	DNF-473-0500
RNA 6000 Pico Complete Kit	Agilent Technologies	5067-1513
Agilent RNA 6000 Nano Kit	Agilent Technologies	5067-1511
Quant-IT RiboGreen® RNA Assay Kit	Life Technologies	R11490
Quant-iT PicoGreen® dsDNA Assay Kit	Life Technologies	P11496
GREINER-384-Well plate, black	Greiner	784076
TruSeq RNA Library Preparation Kit v2, Set A	Illumina	RS-122-2001
TruSeq RNA Library Preparation Kit v2, Set B	Illumina	RS-122-2002
Superscript II Reverse Transcriptase	Life Technologies	18064-014
twin.tec PCR Plate 96, semi-skirted	Vaudaux-Eppendorf AG	0030 128.575
Ethanol absolut Honeywell 1L	Honeywell	02860-1L
10mM TRIS-HCl with 0.1% TWEEN-20, pH 8.5	TEKNOVA	T7724
Experimental models	**Source**	**Identifier**
Mouse: *Hes5::GFP*	Verdon Taylor (Basak *et al*, 2007)	N/A
Mouse: *Tbr2::GFP*	Arnold *et al*, 2009	N/A
Oligonucleotides	**Source**	**Identifier**
Ccnd1_Forward_5'-TGCCGAGAAGTTGTGCATCTA-3'	This paper	N/A
Ccnd1_Reverse_5'-TGTTCACCAGAAGCAGTTCCA-3'	This paper	N/A
Crabp2_Forward_5'-ATGCCTAACTTTTCTGGCAACT-3'	https://pga.mgh.harvard.edu/primerbank/	N/A
Crabp2_Reverse_5'-GCACAGTGGTGGAGGTTTTGA-3'	https://pga.mgh.harvard.edu/primerbank/	N/A
Hbb-bh1_Forward_5'-GAAACCCCCGGATTAGAGCC-3'	https://pga.mgh.harvard.edu/primerbank/	N/A
Hbb-bh1_Reverse_5'-GAGCAAAGGTCTCCTTGAGGT-3'	https://pga.mgh.harvard.edu/primerbank/	N/A
Bcl11b_Forward_5'-CCCGACCCTGATCTACTCAC-3'	https://pga.mgh.harvard.edu/primerbank/	N/A
Bcl11b_Reverse_5'-CTCCTGCTTGGACAGATGCC-3'	https://pga.mgh.harvard.edu/primerbank/	N/A
Bhlhe22_Forward_5'-AAGCGCATCAAGGTGGAGAA-3'	This paper	N/A
Bhlhe22_Reverse_5'-CTTGGTTGAGGTAGGCGACTAA-3'	This paper	N/A
Cabp1_Forward_5'-GAGCTGTCTCAGCAGATCAAC-3'	https://pga.mgh.harvard.edu/primerbank/	N/A
Cabp1_Reverse_5'-TTTAGGGCCCATCAGTTCCA-3'	https://pga.mgh.harvard.edu/primerbank/	N/A
Cntn2_Forward_5'-GCTGATGCCATGACCATGAA-3'	This paper	N/A
Cntn2_Reverse_5'-ACTTAAGGCTGAGGCTGGAA-3'	This paper	N/A
Id2_Forward_5'-ACCCTGAACACGGACATCA-3'	This paper	N/A

Id2_Reverse_5'-TCGACATAAGCTCAGAAGGGAA-3'	This paper	N/A
Satb2_Forward_5'-GCCGTGGGAGGTTTGATGATT-3'	https://pga.mgh.harvard.edu/primerbank/	N/A
Satb2_Reverse_5'-ACCAAGACGAACTCAGCGTG-3'	https://pga.mgh.harvard.edu/primerbank/	N/A
Tubb3_Forward_5'-GCGCATCAGCGTATACTACA-3'	This paper	N/A
Tubb3_Reverse_5'-AGGTTCCAAGTCCACCAGAA-3'	This paper	N/A
Fezf2_Forward_5'-GTCACCGGCCACTTCTAAAAC-3'	https://pga.mgh.harvard.edu/primerbank/	N/A
Fezf2_Reverse_5'-GTCTGCCTCTAACGCAGCA-3'	https://pga.mgh.harvard.edu/primerbank/	N/A
ApoE_Forward_5'-CTGACAGGATGCCTAGCCG-3'	https://pga.mgh.harvard.edu/primerbank/	N/A
ApoE_Reverse_5'-CGCAGGTAATCCCAGAAGC-3'	https://pga.mgh.harvard.edu/primerbank/	N/A
Aqp4_Forward_5'-CTTTCTGGAAGGCAGTCTCAG-3'	https://pga.mgh.harvard.edu/primerbank/	N/A
Aqp4_Reverse_5'-CCACACCGAGCAAAACAAAGAT-3'	https://pga.mgh.harvard.edu/primerbank/	N/A
Cspg4_Forward_5'-GGGCTGTGCTGTCTGTTGA-3'	https://pga.mgh.harvard.edu/primerbank/	N/A
Cspg_Reverse_5'-TGATTCCCTTCAGGTAAGGCA-3'	https://pga.mgh.harvard.edu/primerbank/	N/A
Hmgb2_Forward_5'-GTGGCAGGTACATGCAATCC-3'	This paper	N/A
Hmgb2_Reverse_5'-GTACTTTGGTGGTGGTGTCCTA-3'	This paper	N/A
Olig1_Forward_5'-CTGTATGAGCTGGTGGGTTACA-3'	This paper	N/A
Olig1_Reverse_5'-GAGAAGGGATGCGGTGGAA-3'	This paper	N/A
Pdgfra_Forward_5'-AGAGTTACACGTTTGAGCTGTC-3'	https://pga.mgh.harvard.edu/primerbank/	N/A
Pdgfra_Reverse_5'-GTCCCTCCACGGTACTCCT-3'	https://pga.mgh.harvard.edu/primerbank/	N/A
Sparcl1_Forward_5'-GGCAATCCCGACAAGTACAAG-3'	https://pga.mgh.harvard.edu/primerbank/	N/A
Sparcl1_Reverse_5'-TGGTTTTCTATGTCTGCTGTAGC-3'	https://pga.mgh.harvard.edu/primerbank/	N/A
Tril_Forward_5'-CTATGTATGCCGTTGGGGTAGG-3'	https://pga.mgh.harvard.edu/primerbank/	N/A
Tril_Reverse_5'-AGCTTTTCACTTATTTCGCCCAT-3'	https://pga.mgh.harvard.edu/primerbank/	N/A
Cckar_Forward_5'-CTTTTCTGCCTGGATCAACCT-3'	https://pga.mgh.harvard.edu/primerbank/	N/A
Cckar_Reverse_5'-ACCGTGATAACCAGCGTGTTC-3'	https://pga.mgh.harvard.edu/primerbank/	N/A
Ccnb1_Forward_5'-AAGGTGCCTGTGTGTGAACC-3'	https://pga.mgh.harvard.edu/primerbank/	N/A
Ccnb1_Reverse_5'-GTCAGCCCCATCATCTGCG-3'	https://pga.mgh.harvard.edu/primerbank/	N/A
Dhrs4_Forward_5'-CCTGTCGCTCCTTCCATCCTA-3'	https://pga.mgh.harvard.edu/primerbank/	N/A
Dhrs4_Reverse_5'-	https://pga.mgh.harvard.edu/primerbank/	N/A

GCAAGGTGTCTCTTTTGTGGGA-3'		
Tbr2_Forward_5'- GCGCATGTTTCCTTTCTTGAG-3'	https://pga.mgh.harvard.edu/primerbank/	N/A
Tbr2_Reverse_5'- GGTCGGCCAGAACCACTTC-3'	https://pga.mgh.harvard.edu/primerbank/	N/A
Kif2c_Forward_5'- ATGGAGTCGCTTCACGCAC-3'	https://pga.mgh.harvard.edu/primerbank/	N/A
Kif2c_Reverse_5'- CCACCGAAACACAGGATTTCTC-3'	https://pga.mgh.harvard.edu/primerbank/	N/A
Mcm2_Forward_5'- ATCCACCACCGCTTCAAGAAC-3'	https://pga.mgh.harvard.edu/primerbank/	N/A
Mcm2_Reverse_5'- TACCACCAAACTCTCACGGTT-3'	https://pga.mgh.harvard.edu/primerbank/	N/A
Uncx_Forward_5'- ACCCGCACCAACTTTACCG-3'	https://pga.mgh.harvard.edu/primerbank/	N/A
Uncx_Reverse_5'- TGAACTCGGGACTCGACCA-3'	https://pga.mgh.harvard.edu/primerbank/	N/A
Robo3_Forward_5'- AGATGAACTTGTTCGCGGACT-3'	https://pga.mgh.harvard.edu/primerbank/	N/A
Robo3_Reverse_5'- GGAAGCAGACTAGGGTTGAGC-3'	https://pga.mgh.harvard.edu/primerbank/	N/A
Nde1_Forward_5'- ATGGAGGACTCGGGAAAGACC-3'	https://pga.mgh.harvard.edu/primerbank/	N/A
Nde1_Reverse_5'- TCAGCTTCGTATTCTCGGCTT-3'	https://pga.mgh.harvard.edu/primerbank/	N/A
Tpx2_Forward_5'- GATGCCCCCACCGACTTTATC-3'	https://pga.mgh.harvard.edu/primerbank/	N/A
Tpx2_Reverse_5'- CTTGTTCTCCAAGTTGGCCTT-3'	https://pga.mgh.harvard.edu/primerbank/	N/A
Loxl1_Forward_5'- GAGTGCTATTGCGCTTCCC-3'	https://pga.mgh.harvard.edu/primerbank/	N/A
Loxl1_Reverse_5'- GGTTGCCGAAGTCACAGGT-3'	https://pga.mgh.harvard.edu/primerbank/	N/A
Unc5d_Forward_5'- TGGCTAGGACTCTTTTTCTGGG-3'	https://pga.mgh.harvard.edu/primerbank/	N/A
Unc5d_Reverse_5'- GCTCCTCGATGAAATGAGGCA-3'	https://pga.mgh.harvard.edu/primerbank/	N/A
Ezr_Forward_5'- CAATCAACGTCCGGGTGAC-3'	https://pga.mgh.harvard.edu/primerbank/	N/A
Ezr_Reverse_5'- GCCAATCGTCTTTACCACCTGA-3'	https://pga.mgh.harvard.edu/primerbank/	N/A
Mef2c_Forward_5'- GTCAGTTGGGAGCTTGCACTA-3'	https://pga.mgh.harvard.edu/primerbank/	N/A
Mef2c_Reverse_5'- CGGTCTCTAGGAGGAGAAACA-3'	https://pga.mgh.harvard.edu/primerbank/	N/A
Usp43_Forward_5'- AGCTCACGGGCTGGTATCT-3'	https://pga.mgh.harvard.edu/primerbank/	N/A
Usp43_Reverse_5'- AAGACCTGTACTGTGCTTGAAAG-3'	https://pga.mgh.harvard.edu/primerbank/	N/A
Lrfn5_Forward_5'- TGTTTCTCATTGGCATAGCTGT-3'	https://pga.mgh.harvard.edu/primerbank/	N/A
Lrfn5_Reverse_5'- TGGTGGAACAAATAGAAGCCCT-3'	https://pga.mgh.harvard.edu/primerbank/	N/A
Ntsr1_Forward_5'- CAGTTCGGACTGGAGACGATG-3'	https://pga.mgh.harvard.edu/primerbank/	N/A
Ntsr1_Reverse_5'- ACCAGCACCTTGGAATAAATGTC-3'	https://pga.mgh.harvard.edu/primerbank/	N/A
Gucy1a3_Forward_5'- CCCCTGGTCAGGTTCCTAAG-3'	https://pga.mgh.harvard.edu/primerbank/	N/A

Gucy1a3_Reverse_5'-GGAGACTCCCTTCTGCATTCT-3'	https://pga.mgh.harvard.edu/primerbank/	N/A
β-actin_Forward_5'-AGGTGACAGCATTGCTTCTG-3'	https://pga.mgh.harvard.edu/primerbank/	N/A
β-actin_Reverse_5'-GGGAGACCAAAGCCTTCATA-3'	https://pga.mgh.harvard.edu/primerbank/	N/A
Ubb_Forward_5'-TCTGAGGGGTGGCTATTAA-3'	https://pga.mgh.harvard.edu/primerbank/	N/A
Ubb_Reverse_5'-TGCTTACCATGCAACAAAAC-3'	https://pga.mgh.harvard.edu/primerbank/	N/A
Topp_Forward_5'-GGCTGTACAGAGACTAGAAGAGCA-3'	https://pga.mgh.harvard.edu/primerbank/	N/A
Topp_Reverse_5'-CCTCTCGATCTGTGGCTTG-3'	https://pga.mgh.harvard.edu/primerbank/	N/A
Gapdh_Forward_5'-CTCCCACTCTTCCACCTTCG-3'	https://pga.mgh.harvard.edu/primerbank/	N/A
Gapdh_Reverse_5'-CCACCACCCTGTTGCTGTAG-3'	https://pga.mgh.harvard.edu/primerbank/	N/A
Resource	**Source**	**Identifier**
Fiji	Hosted by University of Wisconsin	https://imagej.net/Fiji/Downloads
Photoshop	Adobe	N/A
Illustrator	Adobe	N/A
Prism 7	GraphPad Software, Inc	https://www.graphpad.com/scientifi software/prism/
R	R Core Team	https://www.r-project.org
MATLAB R2016a 9.0.0.341360	MathWorks	mathworks.com/products/matlab
Python 2.7.11	Python Software Foundation	www.python.org
Python 3.6	Python Software Foundation	www.python.org
goatools		https://github.com/tanghaibao/ goatools
InCHLib		https://openscreen.cz/software/inch /home/
MGI_Gene_Model_Coord.rpt		http://www.informatics.jax.org/dow reports/index.html
fastcluster		http://www.danifold.net/ fastcluster.html
Inkscape	The Inkscape Project	inkscape.org

CONTACT FOR REAGENT AND RESOURCE SHARING

Further information and requests for resources and reagents should be directed to and will be fulfilled by the Lead contact, Verdon Taylor (verdon.taylor@unibas.ch).

EXPERIMENTAL MODEL AND SUBJECT DETAILS

*Hes::GFP (*Basak *et al,* 2007*)* and *Tbr2::GFP (*Arnold *et al,* 2009*)* transgenic lines have been described previously. Mice were maintained on a 12-hr day-night cycle with free access to food and water under specific pathogen-free conditions and according to the Swiss federal regulations. All procedures were approved by the Basel Cantonal Veterinary Office (license number ZH_Tay).

METHOD DETAILS

Tissue preparation and fluorescence assisted cell sorting (FACS)

Dorsal cortices from embryonic day (E10.5) to postnatal day 1 (PN) were micro-dissected and dissociated into single cell suspensions using Papain and Ovo-mucoid mix (previously described by Giachino *et al*, 2009). Cells were washed with L15 medium and FAC-sorted for GFP positive NSCs using FACSariaIII (BD Biosciences) derived from *Hes5::GFP* transgenic embryos for NSCs and *Tbr2::GFP* transgenic embryos for BPs and NBNs. For each time point, 3-4 biological replicates were generated.

RNA Isolation and RNA-sequencing

Total RNA was isolated from FAC-sorted GFP positive cells from *Hes5::GFP* and *Tbr2::GFP* transgenic lines using TRIzol reagent. A time course was performed with NSCs, BPs and NBNs isolated at each time point during development from E10.5 to postnatal day 1 (PN), or as specified in the figure 1A. Samples were analyzed for their integrity and concentration using Agilent 2100 Bioanalyzer and Quant-IT RiboGreen RNA Assay Kit . Sequencing libraries were prepared with the Illumina TruSeq RNA Library Prep Kit v2 according to Illumina's instructions. After quality control (Fragment Analyzer, AATI) libraries were pooled and loaded on an Illumina flow cell for cluster generation (HiSeq SR Cluster Kit v4 cBot). Libraries were sequenced SR50 on the HiSeq 2500 system (HiSeq SBS Kit V4) following the manufacturer's protocols.

Single-cell RNA-sequencing

Single cell capture, lysis and cDNA preparation was performed with the Fluidigm C1 system. Cells were loaded on a microfluidic C1 Single Cell Auto Prep Array for mRNA Seq (5-10µm), and capture efficiency evaluated using microscopy. Lysis, reverse transcription and cDNA amplification was performed with the SMARTer Ultra Low RNA Kit for Illumina Sequencing (Clontech/Takara) according to Fluidigm's guidelines for single-cell RNA-seq on the C1 system. cDNA was harvested, profiles checked on the Fragment Analyzer (AATI) and their concentration determined using Quant-iT PicoGreen dsDNA Assay Kit. For subsequent library preparation using Nextera XT DNA library preparation kit (Illumina) following the Fluidigm manual, cDNAs were normalized to 0.3 ng/µl. Libraries were pooled and sequenced SR75 on an Illumina NextSeq 500 system (75 cycles High Output v2 kit).

qPCR validation

Total RNA was isolated from FAC-sorted GFP positive cells from *Hes5::GFP* (E11.5, E15.5 and E18.5*) and Tbr2::GP (*E13.5 BPs, E15.5 BPs and E15.5 NBNs*) transgenic embryos using TRIzol reagent. Independent biological replicates were generated for qPCR validation. Samples were analyzed for their integrity and concentration using Agilent 2100 Bioanalyzer and Quant-IT RiboGreen RNA Assay Kit . DNase treatment was done using Roche DNase kit and cDNA prepared using the PreAmp and Reverse Transcription Master Mix from Fluidigm. Deltagene Assay primers (Fluidigm) and EvaGreen (BioRad) were used for real-time qPCR. Gene expression was assayed using Dynamic Array IFC chips and the BioMark system (Fluidigm). Fluidigm real-time PCR analysis software was used to calculate cycle threshold (Ct) values for each qPCR.

Tissue preparation and immunohistochemistry

Hes5::GFP and *Tbr2::GFP* positive brains at E17.5 were isolated and fixed with 4% PFA in 0.1M phosphate buffer (PBS). Brains were embedded in 3% agarose, sectioned 40μm thick using a Vibrotome. Sections were mounted in mounting media containing diazabicyclo-octane (DABCO; Sigma) as an anti-fading agent on SuperFrost glass slides and visualized using Zeiss Apotome 2 microscope.

Adherent NSC culture *in vitro* and immunocytochemistry

Primary NSCs were isolated from E13.5 dorsal cortices from *Hes5::GFP* transgenic embryos and BPs, NBNs were isolated at E16.5 from *Tbr2::GFP* transgenic embryos. Following FAC-sorting, the cells were seeded in 100 μg/μl Poly L-Lysine pre-coated 8-well Lab-Tek chamber slides and cultured in DMEM/F12 + Glutamax medium (with 2% B27). The cells were incubated for 1h at 37°C, 5% CO_2. The cells were fixed with 4% PFA, at RT for 15minutes and blocked with 5% Normal donkey serum and 0.1% Triton X-100. Primary antibody incubations were performed overnight at 4°C. Secondary antibody incubations were performed at RT, for 1h. The cells were incubated with 1:1000 Dapi for 30 minutes at RT and rinse with PBS. Slides were mounted with DABCO and imaged using Zeiss Apotome 2 microscope.

QUANTIFICATION AND STATISTICAL ANALYSIS

Images taken by Zeiss Apotome 2 were processed with FIJI software. Contrast and image size of IF images were adjusted with Adobe photoshop. Expression profiles of genes of interest were produced in R. Bar graphs were generated by GraphPad Prism 7. All figures were made in Adobe Illustrator CS6.

Sample size is mentioned in the excel sheets for the quantifications. For FACS analysis, for *Hes5::GFP* transgenic embryos, only the bright GFP positive cells were collected. For *Tbr2::GFP* transgenic embryos, both bright and dim GFP positive cells were collected and analyzed. For IF images, three fields of views were analyzed and quantified per sample. Unpaired t-tests were used qPCR validation experiments. The cut-off value for statistical significance were indicated in corresponding figure legend.

DATA AND SOFTWARE AVAILABILITY

The RNA sequencing datasets have been deposited in Gene Expression Omnibus (GEO) with accession number GEO:

Read mapping and data preprocessing

Reads from single cell and cell population mRNA-Seq were mapped to the transcriptome (GENCODE Release M2 GRCm38.p2) with kallisto 0.43.0[*]. The option --pseudobam was used to save the pseudoalignments to transcriptome in BAM file. The reads mapping to multiple transcripts were uniformly distributed. To obtain the expression per transcript, we first divided the number of reads mapping to each transcript by the length of the transcript in nucleotides and then transform the length-normalized read counts in transcript per million (TPM). Gene expression was obtained by summing for each gene the TPM of the transcripts corresponding to the gene. Promoter expression was obtained by summing for each promoter the length-normalized count of the transcripts associated with the promoter and then transformed in TPM. We added a pseudo-count of 0.5 to express transcript, gene and promoter expression in logarithmic space

(log2(TPM+0.5)). For the population mRNA-Seq, we computed replicate averages in log2(TPM+0.5). The method used is adapted from Bray et al, 2016 (Bray et al., 2016a, b).

Differentially expressed genes in different cell types

A pairwise comparison between each two cell types is applied using tximport and Deseq2 packages in R. Next, the first 50 top DEGs (differentially expressed genes) for each cell type has been selected considering fold change of more than 2 and adjusted p-value less than 1e-3. Finally, the common DEGs of each cell type is used for visualization. The complete list of DEGs of each comparison is given in (SI. 1 excel sheet).

The goal of our analysis was to find the most optimal marker genes. That is, if we were to only make gene expression measurements of a few genes (using qPCR for example), those that give us the most information about the sample. When we are only interested in knowing whether the sample belongs to one of two classes (e.g. NSC vs non-NSC), this information content is given by the conditional entropy described below. Hence, we use it as a score to find good marker genes. In the derivation we account for the fact that the empirical expression variance from a few data does not necessarily reflect its true variance by using a prior that makes very small and very large variances unlikely.

Assuming that the probability $P(x|w,\mu)$ to measure log-expression x of a gene follows a Gaussian distribution with mean μ and inverse variance w, and using a uniform prior for μ and a gamma-distribution prior $P(w|\alpha,\beta) = \beta^\alpha w^{\alpha-1} \exp(-\beta w)/\Gamma(\alpha)$ for w, we find the likelihood of getting a set of measurements $D^c = (x_1, x_2, ..., x_{n^c})$ for samples of class c to be

$$P(D^c|\alpha,\beta) = \frac{\beta^\alpha}{(\beta + n^c v^c/2)^{\alpha+(n^c-1)/2}} \frac{\Gamma(\alpha + (n^c - 1)/2)}{\Gamma(\alpha)}$$

where v^c is the empirical variance of D^c. Hence, we numerically find the maximum-likelihood estimates α^*, β^* from maximizing the sum of log-likelihoods across all genes. Finally, the inferred probability distribution of x in class c is:

$$P(x|c) = Z^c \left(1 + \frac{(x - x^c)^2}{V^c}\right)^{-\gamma^c}$$

where $x^c = \langle x \rangle_c$, $V^c = (n^c + 1)(v^c + 2\beta^*/n^c)$, $\gamma^c = \alpha^* + (n^c - 1)/2$ and $Z^c = \frac{\Gamma(\gamma^c)}{\sqrt{\pi V^c}\Gamma(\gamma^c - 1/2)}$. This distribution is approximately Gaussian with variance $\sigma^2 = V^c/(2\gamma^c)$ which provides us with a more accurate estimate of the true variance of a gene rather than simply taking v^c.

Furthermore, we can take the expression of $P(x|c)$ and $P(c) = 1/|c|$ to calculate the conditional entropy $H(c|x) = H(x,c) - H(x)$. While

$$H(x,c) = -\sum_c \int dx \, P(x|c)P(c) \log[P(x|c)P(x)]$$

$$= -\log(Z^c) + \gamma^c\big(\psi(\gamma^c) - \psi(\gamma^c - 1/2)\big),$$

with ψ being the digamma function, has an analytical solution, $H(x) = \int P(x) \log\big(P(x)\big)$ with $P(x) = \sum_c P(x|c)P(c)$ can be calculated through numerical integration.

In an experiment which only measures the expression of a single gene, $H(c|x)$ serves as a measure for how much information the result provides about the class of the sample. With only two classes, we can

write $H(x|c) = -p_e \log p_e - (1 - p_e) \log(1 - p_e)$, which we can numerically invert to find p_e, the probability to falsely classify a sample based on gene expression. The table below summarizes the classes for which we looked for such marker genes:

	Class 2	Number of marke genes $p_e < 0.01$
By cell type		
NSC	Non-NSC	37
BP	Non-BP	0
NBN	Non-NBN	136
NSC	BP	49
NSC	NBN	469
BP	NBN	249
NSC by phase		
Expansion NSC	Non-expansion NSC	222
Neurogenesis NSC	Non-neurogenesis NSC	4
Gliogenesis NSC	Non-gliogenesis NSC	102
Expansion NSC	Neurogenesis NSC	207
Expansion NSC	Gliogenesis NSC	759
Neurogenesis NSC	Gliogenesis NSC	117
Neurogenic (E12.5-16.5) NSC by day		
E12.5	Other days	0
E13.5	Other days	3
E14.5	Other days	0
E15.5	Other days	1
E16.5	Other days	50
E12.5-E13.5	E14.5-E16.5	9
E12.5-E14.5	E15.5-E16.5	16
BP by day		
E12.5	Other days	248
E13.5	Other days	0
E14.5	Other days	29
E15.5	Other days	0
E16.5	Other days	1
E17.5	Other days	3
E18.5	Other days	1
PN	Other days	38
E12.5-E13.5	E14.5-PN	54
E12.5-E14.5	E15.5-PN	83

E12.5-E15.5	E16.5-PN	0
E12.5-E16.5	E17.5-PN	15
E12.5-E17.5	E18.5-PN	4
Other		
BP E12.5-E14.5	NBN	354
BP E15.5-PN	NBN	650

Selection of highly variable genes:

To select the most highly variable genes, we have defined a score for each gene based on the contribution of each gene on each principle component and the variance that each component explains considering the first two components, as following:

$$Score(g_i) = \sqrt{(w_{g_i}(pc_1) * var(pc_1))^2 + (w_{g_i}(pc_2) * var(pc_2))^2}.$$

Where $w_{g_i}(pc_k)$ refers to the weight (contribution) of gene i in pc_k and $var(pc_k)$ denotes the percentage of variance that is covered by pc_k. Next, the first 2000 genes with the highest scores are selected as the highly variable genes, HVGs.

Clustering of single cells

First, single cells at each time point are clustered by applying 500 times k-means clustering to avoid the dependency of k-means clustering on the random initialization number (seed value). To implement k-means clustering, *clustering* package considering Euclidean distance as metric in R is used. Next, the assignment matrix is estimated based on the frequency of observing each two single cells in the same clustering at each iteration. Next, the hierarchal clustering is used to sort the assignment matrix using Euclidean distance as metric and *ward. D2* as method in *hclust* function in R.

Selection of differentially expressed gene in single cells

Kruskal-Wallis non-parametric test is used to select differentially expressed genes and genes with adjusted p-value of less than 1e-3 are considered as significantly differentially expressed genes.

Visualization

PCA is applied using *prcomp* function in R after centering the log transferred data. Heatmap are illustrated using *pheatmap* package in R on log transferred data.

NeuroStemX Data Exploration Web App

The NeuroStemX data exploration web app makes it possible to navigate data produced in the NeuroStemX project. The site supports viewing data by focusing on one of several parameters: gene list, biological sample, or measurement type (single cell vs. population).

The website allows entry of a list of mouse genes (either as gene symbol or Ensembl ID) to focus on the data acquired for those genes. It alternatively allows viewing data on individual samples. When looking at a sample, a list of genes that have been determined to be outliers are shown. A gene is considered an outlier for a sample

if the expression value of the gene either exceeds the 75th percentile + 1.5*iqr or is less than the 25th percentile - 1.5*iqr, where percentiles and inter-quartile range are computed based on the expression values for the given gene over all samples within the measurement type (single cell or population).

When viewing all data for a measurement type, data is displayed using hierarchical clustering. The InCHLib widget displays the clustered data. Clustering is performed using the fastcluster package in python with distance (both row and column) calculated using the Euclidean metric and linkage (both row and column) performed using Ward's method (Mullner, 2013; Skuta et al., 2014).

The site supports performing gene ontology enrichment analysis either locally, using goatools, or with PANTHER. For local enrichment analysis, we use the MGI_Gene_Model_Coord annotations based on the GRCm38 assembly (Mi et al., 2017).

Goatools: https://github.com/tanghaibao/goatools

Haibao Tang *et al*. GOATOOLS: Tools for Gene Ontology. Zenodo. 10.5281/zenodo.31628.

MGI_Gene_Model_Coord.rpt

http://www.informatics.jax.org/downloads/reports/index.html

References

Arlotta, P., Molyneaux, B.J., Chen, J., Inoue, J., Kominami, R., and Macklis, J.D. (2005). Neuronal subtype-specific genes that control corticospinal motor neuron development in vivo. Neuron *45*, 207-221.

Arnold, S.J., Huang, G.J., Cheung, A.F., Era, T., Nishikawa, S., Bikoff, E.K., Molnar, Z., Robertson, E.J., and Groszer, M. (2008). The T-box transcription factor Eomes/Tbr2 regulates neurogenesis in the cortical subventricular zone. Genes Dev *22*, 2479-2484.

Arnold, S.J., Sugnaseelan, J., Groszer, M., Srinivas, S., and Robertson, E.J. (2009). Generation and analysis of a mouse line harboring GFP in the Eomes/Tbr2 locus. Genesis *47*, 775-781.

Artimo, P., Duvaud, S., Pachkov, M., Ioannidis, V., van Nimwegen, E., and Stockinger, H. (2016). The ISMARA client. F1000Res *5*.

Balwierz, P.J., Pachkov, M., Arnold, P., Gruber, A.J., Zavolan, M., and van Nimwegen, E. (2014). ISMARA: automated modeling of genomic signals as a democracy of regulatory motifs. Genome Res *24*, 869-884.

Bansod, S., Kageyama, R., and Ohtsuka, T. (2017). Hes5 regulates the transition timing of neurogenesis and gliogenesis in mammalian neocortical development. Development *144*, 3156-3167.

Basak, O., and Taylor, V. (2007). Identification of self-replicating multipotent progenitors in the embryonic nervous system by high Notch activity and Hes5 expression. Eur J Neurosci *25*, 1006-1022.

Bel-Vialar, S., Itasaki, N., and Krumlauf, R. (2002). Initiating Hox gene expression: in the early chick neural tube differential sensitivity to FGF and RA signaling subdivides the HoxB genes in two distinct groups. Development *129*, 5103-5115.

Blaschuk, K.L., and ffrench-Constant, C. (1998). Developmental neurobiology: Notch is tops in the developing brain. Curr Biol *8*, R334-R337.

Bray, N.L., Pimentel, H., Melsted, P., and Pachter, L. (2016a). Erratum: Near-optimal probabilistic RNA-seq quantification. Nat Biotechnol *34*, 888.

Bray, N.L., Pimentel, H., Melsted, P., and Pachter, L. (2016b). Near-optimal probabilistic RNA-seq quantification. Nat Biotechnol *34*, 525-527.

Bray, S.J. (2006). Notch signalling: a simple pathway becomes complex. Nat Rev Mol Cell Biol *7*, 678-689.

Chuang, J.H., Tung, L.C., and Lin, Y.S. (2015). Neural differentiation from embryonic stem cells in vitro: An overview of the signaling pathways. World J Stem Cells *7*, 437-447.

Custo Greig, L.F., Woodworth, M.B., Galazo, M.J., Padmanabhan, H., and Macklis, J.D. (2013). Molecular logic of neocortical projection neuron specification, development and diversity. Nat Rev Neurosci *14*, 755-769.

Desai, A.R., and McConnell, S.K. (2000). Progressive restriction in fate potential by neural progenitors during cerebral cortical development. Development *127*, 2863-2872.

Ebendal, T., Bengtsson, H., and Soderstrom, S. (1998). Bone morphogenetic proteins and their receptors: Potential functions in the brain. J Neurosci Res *51*, 139-146.

Ecker, J.R., Geschwind, D.H., Kriegstein, A.R., Ngai, J., Osten, P., Polioudakis, D., Regev, A., Sestan, N., Wickersham, I.R., and Zeng, H. (2017). The BRAIN Initiative Cell Census Consortium: Lessons Learned toward Generating a Comprehensive Brain Cell Atlas. Neuron *96*, 542-557.

Englund, C., Fink, A., Lau, C., Pham, D., Daza, R.A., Bulfone, A., Kowalczyk, T., and Hevner, R.F. (2005). Pax6, Tbr2, and Tbr1 are expressed sequentially by radial glia, intermediate progenitor cells, and postmitotic neurons in developing neocortex. J Neurosci *25*, 247-251.

Fode, C., Ma, Q., Casarosa, S., Ang, S.L., Anderson, D.J., and Guillemot, F. (2000). A role for neural determination genes in specifying the dorsoventral identity of telencephalic neurons. Genes Dev *14*, 67-80.

Franco, S.J., Gil-Sanz, C., Martinez-Garay, I., Espinosa, A., Harkins-Perry, S.R., Ramos, C., and Muller, U. (2012). Fate-restricted neural progenitors in the mammalian cerebral cortex. Science *337*, 746-749.

Franco, S.J., and Muller, U. (2013). Shaping Our Minds: Stem and Progenitor Cell Diversity in the Mammalian Neocortex. Neuron *77*, 19-34.

Fukuchi-Shimogori, T., and Grove, E.A. (2001). Neocortex patterning by the secreted signaling molecule FGF8. Science *294*, 1071-1074.

Gaiano, N., and Fishell, G. (2002). The role of notch in promoting glial and neural stem cell fates. Annu Rev Neurosci *25*, 471-490.

Gerstmann, K., Pensold, D., Symmank, J., Khundadze, M., Hubner, C.A., Bolz, J., and Zimmer, G. (2015). Thalamic afferents influence cortical progenitors via ephrin A5-EphA4 interactions. Development *142*, 140-150.

Gil, O.D., Zanazzi, G., Struyk, A.F., and Salzer, J.L. (1998). Neurotrimin mediates bifunctional effects on neurite outgrowth via homophilic and heterophilic interactions. J Neurosci *18*, 9312-9325.

Gil-Sanz, C., Espinosa, A., Fregoso, S.P., Bluske, K.K., Cunningham, C.L., Martinez-Garay, I., Zeng, H.K., Franco, S.J., and Muller, U. (2015). Lineage Tracing Using Cux2-Cre and Cux2-CreERT2 Mice. Neuron *86*, 1091-1099.

Gomes, F.C., Sousa Vde, O., and Romao, L. (2005). Emerging roles for TGF-beta1 in nervous system development. Int J Dev Neurosci *23*, 413-424.

Gotz, M., and Huttner, W.B. (2005). The cell biology of neurogenesis. Nat Rev Mol Cell Biol *6*, 777-788.

Guo, C., Eckler, M.J., McKenna, W.L., McKinsey, G.L., Rubenstein, J.L.R., and Chen, B. (2013). Fezf2 Expression Identifies a Multipotent Progenitor for Neocortical Projection Neurons, Astrocytes, and Oligodendrocytes. Neuron *80*, 1167-1174.

Han, W.Q., and Sestan, N. (2013). Cortical Projection Neurons: Sprung from the Same Root. Neuron *80*, 1103-1105.

Haubensak, W., Attardo, A., Denk, W., and Huttner, W.B. (2004). Neurons arise in the basal neuroepithelium of the early mammalian telencephalon: a major site of neurogenesis. Proc Natl Acad Sci U S A *101*, 3196-3201.

Hevner, R.F., Daza, R.A., Rubenstein, J.L., Stunnenberg, H., Olavarria, J.F., and Englund, C. (2003). Beyond laminar fate: toward a molecular classification of cortical projection/pyramidal neurons. Dev Neurosci *25*, 139-151.

Imayoshi, I., Sakamoto, M., Yamaguchi, M., Mori, K., and Kageyama, R. (2010). Essential roles of Notch signaling in maintenance of neural stem cells in developing and adult brains. J Neurosci *30*, 3489-3498.

Itoh, N., and Ornitz, D.M. (2004). Evolution of the Fgf and Fgfr gene families. Trends Genet *20*, 563-569.

Iwata, T., and Hevner, R.F. (2009). Fibroblast growth factor signaling in development of the cerebral cortex. Dev Growth Differ *51*, 299-323.

Johnson, M.B., and Walsh, C.A. (2017). Cerebral cortical neuron diversity and development at single-cell resolution. Curr Opin Neurobiol *42*, 9-16.

Lai, T., Jabaudon, D., Molyneaux, B.J., Azim, E., Arlotta, P., Menezes, J.R., and Macklis, J.D. (2008). SOX5 controls the sequential generation of distinct corticofugal neuron subtypes. Neuron *57*, 232-247.

Liddelow, S., and Barres, B. (2015). SnapShot: Astrocytes in Health and Disease. Cell *162*, 1170-1170 e1171.

Lipkowitz, S., Gobel, V., Varterasian, M.L., Nakahara, K., Tchorz, K., and Kirsch, I.R. (1992). A comparative structural characterization of the human NSCL-1 and NSCL-2 genes. Two basic helix-loop-helix genes expressed in the developing nervous system. J Biol Chem *267*, 21065-21071.

Liu, S.J., Nowakowski, T.J., Pollen, A.A., Lui, J.H., Horlbeck, M.A., Attenello, F.J., He, D., Weissman, J.S., Kriegstein, A.R., Diaz, A.A.*, et al.* (2016). Single-cell analysis of long non-coding RNAs in the developing human neocortex. Genome Biol *17*, 67.

Lodato, S., and Arlotta, P. (2015). Generating neuronal diversity in the mammalian cerebral cortex. Annu Rev Cell Dev Biol *31*, 699-720.

Louvi, A., and Artavanis-Tsakonas, S. (2006). Notch signalling in vertebrate neural development. Nat Rev Neurosci *7*, 93-102.

Lui, J.H., Hansen, D.V., and Kriegstein, A.R. (2011). Development and evolution of the human neocortex. Cell *146*, 18-36.

Mi, H., Huang, X., Muruganujan, A., Tang, H., Mills, C., Kang, D., and Thomas, P.D. (2017). PANTHER version 11: expanded annotation data from Gene Ontology and Reactome pathways, and data analysis tool enhancements. Nucleic Acids Res *45*, D183-D189.

Molofsky, A.V., Krencik, R., Ullian, E.M., Tsai, H.H., Deneen, B., Richardson, W.D., Barres, B.A., and Rowitch, D.H. (2012). Astrocytes and disease: a neurodevelopmental perspective. Genes Dev *26*, 891-907.

Molyneaux, B.J., Arlotta, P., Menezes, J.R., and Macklis, J.D. (2007). Neuronal subtype specification in the cerebral cortex. Nat Rev Neurosci *8*, 427-437.

Mukhtar, T., and Taylor, V. (2018). Untangling Cortical Complexity During Development. J Exp Neurosci *12*, 1179069518759332.

Mullner, D. (2013). fastcluster: Fast Hierarchical, Agglomerative Clustering Routines for R and Python. J Stat Softw *53*, 1-18.

Nowakowski, T.J., Bhaduri, A., Pollen, A.A., Alvarado, B., Mostajo-Radji, M.A., Di Lullo, E., Haeussler, M., Sandoval-Espinosa, C., Liu, S.J., Velmeshev, D.*, et al.* (2017). Spatiotemporal gene expression trajectories reveal developmental hierarchies of the human cortex. Science *358*, 1318-1323.

Ohtsuka, T., Shimojo, H., Matsunaga, M., Watanabe, N., Kometani, K., Minato, N., and Kageyama, R. (2011). Gene expression profiling of neural stem cells and identification of regulators of neural differentiation during cortical development. Stem Cells *29*, 1817-1828.

Ono, K., Takebayashi, H., Ikeda, K., Furusho, M., Nishizawa, T., Watanabe, K., and Ikenaka, K. (2008). Regional- and temporal-dependent changes in the differentiation of Olig2 progenitors in the forebrain, and the impact on astrocyte development in the dorsal pallium. Dev Biol *320*, 456-468.

Paridaen, J.T., and Huttner, W.B. (2014). Neurogenesis during development of the vertebrate central nervous system. EMBO Rep *15*, 351-364.

Paul, V., Tonchev, A.B., Henningfeld, K.A., Pavlakis, E., Rust, B., Pieler, T., and Stoykova, A. (2014). Scratch2 Modulates Neurogenesis and Cell Migration Through Antagonism of bHLH Proteins in the Developing Neocortex. Cereb Cortex *24*, 754-772.

Pollen, A.A., Nowakowski, T.J., Chen, J., Retallack, H., Sandoval-Espinosa, C., Nicholas, C.R., Shuga, J., Liu, S.J., Oldham, M.C., Diaz, A.*, et al.* (2015). Molecular identity of human outer radial glia during cortical development. Cell *163*, 55-67.

Pourquie, O. (2003). The segmentation clock: Converting embryonic time into spatial pattern. Science *301*, 328-330.

Rash, B.G., Lim, H.D., Breunig, J.J., and Vaccarino, F.M. (2011). FGF signaling expands embryonic cortical surface area by regulating Notch-dependent neurogenesis. J Neurosci *31*, 15604-15617.

Rodriguez-Martinez, G., and Velasco, I. (2012). Activin and TGF-beta effects on brain development and neural stem cells. CNS Neurol Disord Drug Targets *11*, 844-855.

Rosenberg, A.B., Roco, C.M., Muscat, R.A., Kuchina, A., Sample, P., Yao, Z., Graybuck, L.T., Peeler, D.J., Mukherjee, S., Chen, W.*, et al.* (2018). Single-cell profiling of the developing mouse brain and spinal cord with split-pool barcoding. Science *360*, 176-182.

Sahara, S., and O'Leary, D.D. (2009). Fgf10 regulates transition period of cortical stem cell differentiation to radial glia controlling generation of neurons and basal progenitors. Neuron *63*, 48-62.

Sarnat, H.B. (2013). Clinical neuropathology practice guide 5-2013: markers of neuronal maturation. Clin Neuropathol *32*, 340-369.

Sessa, A., Ciabatti, E., Drechsel, D., Massimino, L., Colasante, G., Giannelli, S., Satoh, T., Akira, S., Guillemot, F., and Vania, B. (2017). The Tbr2 Molecular Network Controls Cortical Neuronal Differentiation Through Complementary Genetic and Epigenetic Pathways. Cereb Cortex *27*, 3378-3396.

Shimojo, H., Ohtsuka, T., and Kageyama, R. (2008). Oscillations in notch signaling regulate maintenance of neural progenitors. Neuron *58*, 52-64.

Shimojo, H., Ohtsuka, T., and Kageyama, R. (2011). Dynamic expression of notch signaling genes in neural stem/progenitor cells. Front Neurosci *5*, 78.

Skuta, C., Bartunek, P., and Svozil, D. (2014). InCHlib - interactive cluster heatmap for web applications. J Cheminform *6*, 44.

Stancik, E.K., Navarro-Quiroga, I., Sellke, R., and Haydar, T.F. (2010). Heterogeneity in Ventricular Zone Neural Precursors Contributes to Neuronal Fate Diversity in the Postnatal Neocortex. Journal of Neuroscience *30*, 7028-7036.

Takebayashi, H., and Ikenaka, K. (2015). Oligodendrocyte generation during mouse development. Glia *63*, 1350-1356.

Telley, L., Agirman, G., Prados, J., Amberg, N., Fievre, S., Oberst, P., Bartolini, G., Vitali, I., Cadilhac, C., Hippenmeyer, S.*, et al.* (2019). Temporal patterning of apical progenitors and their daughter neurons in the developing neocortex. Science *364*, 547-+.

Telley, L., Govindan, S., Prados, J., Stevant, I., Nef, S., Dermitzakis, E., Dayer, A., and Jabaudon, D. (2016). Sequential transcriptional waves direct the differentiation of newborn neurons in the mouse neocortex. Science *351*, 1443-1446.

Wang, H., Ge, G.N., Uchida, Y., Luu, B., and Ahn, S. (2011). Gli3 Is Required for Maintenance and Fate Specification of Cortical Progenitors. Journal of Neuroscience *31*, 6440-6448.

Woodworth, M.B., Greig, L.C., Kriegstein, A.R., and Macklis, J.D. (2012). SnapShot: cortical development. Cell *151*, 918-918 e911.

Zhang, C., Tu, H.L., Jia, G., Mukhtar, T., Taylor, V., Rzhetsky, A., and Tay, S. (2019). Ultra-multiplexed analysis of single-cell dynamics reveals logic rules in differentiation. Sci Adv *5*, eaav7959.

Zhang, R., Engler, A., and Taylor, V. (2018). Notch: an interactive player in neurogenesis and disease. Cell Tissue Res *371*, 73-89.

Zhang, Y., and Barres, B.A. (2010). Astrocyte heterogeneity: an underappreciated topic in neurobiology. Curr Opin Neurobiol *20*, 588-594.

Zhou, B., Osinski, J.M., Mateo, J.L., Martynoga, B., Sim, F.J., Campbell, C.E., Guillemot, F., Piper, M., and Gronostajski, R.M. (2015). Loss of NFIX Transcription Factor Biases Postnatal Neural Stem/Progenitor Cells Toward Oligodendrogenesis. Stem Cells Dev *24*, 2114-2126.

Chapter 1

c0001 # Fundamentals of Neurogenesis and Neural Stem Cell Development

Robert Beattie*, Tanzila Mukhtar* and Verdon Taylor
Department of Biomedicine, University of Basel, Mattenstrasse, Basel, Switzerland

s0010 ## 1.1 NEURULATION: FORMATION OF THE CENTRAL NERVOUS SYSTEM ANLAGE
[AU1]

p0010 During the early stages of postgastrulation embryonic development, the ectoderm differentiates to form the epidermis and the neural ectoderm, the primordium of the nervous system (for review see Ref. [1]). In vertebrates, the central nervous system (CNS) begins as the neural plate, an ectodermal-derived structure that folds dorsally to form the neural tube through a process called neurulation. Neurulation is divided into the sequential phases of primary and secondary neurulation initiated through a combination of growth factors and inhibitory signals secreted by the underlying axial mesoderm (notochord), dorsal ectoderm, and Spemann organizer (Figure 1.1). The neural tube then differentiates rostrally into the future brain and caudally to form the spinal cord and most of the peripheral nervous system, which will not be covered here. The rostral part of the neural tube segregates into three swellings, establishing the forebrain, midbrain, and hindbrain. In parallel, the rostro-caudal tube is segmented into modules called neuromeres.

p0015 During neurulation, neural crest cells (NCCs) are formed at the neural plate border, a junction between the surface ectoderm and the most dorsal neurepithelium. NCCs are unique to vertebrates, and induction of NCCs begins in mammals during embryogenesis in the midbrain and continues caudally toward the tail [2,3]. Initially, NCCs are an integral part of the neurepithelium and are morphologically indistinguishable. Upon induction, NCCs delaminate from the lateral neural plate/dorsal neural tube and migrate throughout the embryo. Various classes of NCCs include cranial, cardiac, vagal, trunk, and sacral, all of which have unique migration patterns. NCCs give rise to the majority of the peripheral nervous system and the bone and cartilage of the head; they also generate smooth muscle cells and pigment cells. In avians, fish, and amphibians,

NCC delamination requires cytoskeletal and cytoadhesive changes brought on by key transcription factors from the Snail gene family. Snail1 and Snail2 directly repress E-cadherin, which facilitates cell migration [2]. So far no such correlation has been identified during mammalian embryogenesis. The transcription factor Smad-interacting protein 1 is known to downregulate E-cadherin expression and is required for correct delamination of NCCs [2,6]. Because NCCs have both multipotent and self-renewing capabilities, it is hypothesized that they comprise a heterogeneous population of progenitors, each of which specifies a distinct cell type in the body [7]. Alternatively, NCC differentiation could be guided by intrinsic cues or extrinsic signals emanating from the tissues they interact with during migration [2,6]. For example, the role of extrinsic fibroblast growth factor (FGF) signaling has been demonstrated in determining the specific fate of craniofacial mesenchyme [2]. Because NCCs have many of the hallmarks of early stem cell progenitors, they may be interesting candidates for studying tissue engineering and regenerative medicine in the future. For a detailed review, please refer to [2,3,6].

s0015 ## 1.2 NEURULATION AND NEURAL TUBE FORMATION

p0020 The mammalian brain and most of the spinal cord are formed during the first phase of neurulation, which is commonly divided into four phases. In mice, neurulation begins at around embryonic day (E) 8 with the induction of the neural plate when the inhibitory signals chordin, noggin, and follistatin are secreted by the Spemann organizer. These factors block bone morphogenic protein 4 (BMP4) signaling, inducing dorsal epiblast cells and allowing the anteroposterior midline of the ectoderm to adopt a neuroectodermal fate. These neuroectodermal cells undergo an apicobasal thickening and generate the neural plate along the

---

* Equal contribution.

1
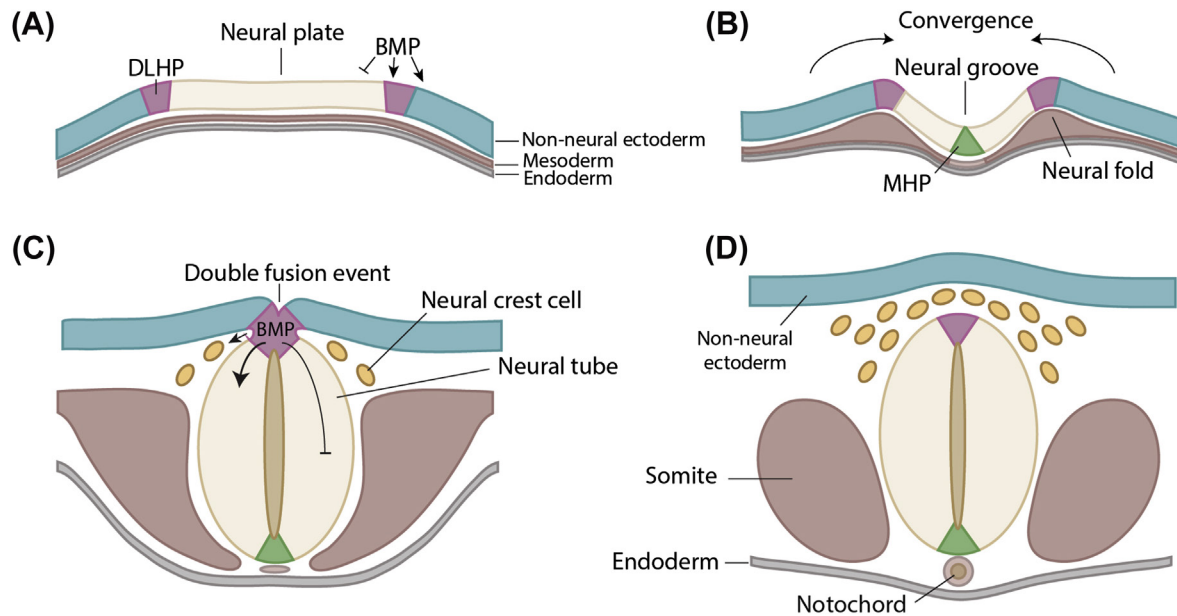
f0010

FIGURE 1.1 **Schemes of central nervous system development.** The brain and most of the spinal cord are formed during primary neurulation, which is commonly divided into four phases. (A) Epiblast cells are induced to a neuroectoderm fate, generating the neural plate. (B) The remodeling phase, in which the neural plate undergoes convergent extension and begins to fold along the median hinge point (MHP) and dorsolateral hinge points. (C) The two neural folds converge at the midpoint and then proceed to fuse, leading to the dorsal closure of the neural tube. During neurulation, neural crest cells (NCCs) are formed at the neural plate border, a junction between the surface ectoderm and the most dorsal neurepithelium. NCCs are unique to vertebrates, and induction of NCCs begins in mammals during embryogenesis in the midbrain and continues caudally toward the tail [2,3]. (D) By embryonic day 9 in the mouse, fusion is complete. BMP—bone morphogenic protein. *Adapted from Refs [4,5].*

dorsal midline of the embryo. Once committed, neuroectodermal cells no longer require inhibitory signals for neural plate formation to proceed (Figure 1.1) [8,9].

p0025   The neural plate undergoes a remodeling phase, whereby convergent extension increases the length (rostrocaudally) and narrows the width (transversely) simultaneously. During these processes, the neural plate continues to thicken apicobasally, generating cellular forces that begin to bend the neural plate and induce neural tube formation. As the lateral folds of the neural plate converge to the midline, the epidermal ectoderm delaminates from the neurepithelium of the neural plate, and fusion of both the ectoderm and the dorsal neural tube proceeds [8,9]. The neural tube zips closed posteriorly from the hindbrain and anteriorly from the midhindbrain junction, while remaining open over the future fourth ventricle posterior to the cerebellum. By E9 in the mouse, fusion is complete and the neural tube is closed, forming the primitive ventricles of the future brain regions.

p0030   Far less is known about secondary neurulation, which is the formation of the posterior region of the neural tube and caudalmost portion of the spinal cord. Secondary neurulation begins from a solid mass of cells forming from the tail bud. These cells form the medullary cord, which then cavitates to form multiple lumina. Finally, these lumina fuse into a single lumen, continuing the central canal of the neural tube in the most rostral aspects. In contrast to primary neurulation, here the process is more a hollowing

out of a mass of cells rather than tube formation from an ectodermal plate of cells [10].

1.3 REGIONALIZATION OF THE MAMMALIAN NEURAL TUBE

s0020

1.3.1 Molecular Basis of Regionalization

s0025

The neurepithelium of the neural tube follows a sequential series of overlapping and competing patterning steps during brain development. Timing is critical, particularly in structures such as the cerebral cortex, where even moderate changes in gene expression pattern can lead to serious developmental, motor, behavioral, psychological, and cognitive disorders. The best characterized morphogens and signaling pathways involved in regional identity include Sonic hedgehog (Shh), retinoic acid (RA), FGF, wingless (Wnt), and BMP signaling (Figure 1.2) [11,12]. Shh is secreted by the notochord (axial mesoderm) beneath the floor plate of the neural tube and controls neuronal cell fate in a concentration-dependent manner [13]. RA is secreted from the mesoderm and defines the posterior CNS, including the hindbrain and spinal cord. RA contributes to segmentation of the hindbrain into eight distinct compartments called rhombomeres, which later give rise to the medulla, pons, and cerebellum. FGF activity along with RA and Wnt leads to the caudalization of the neural tissue [14,15]. Wnt

p0035
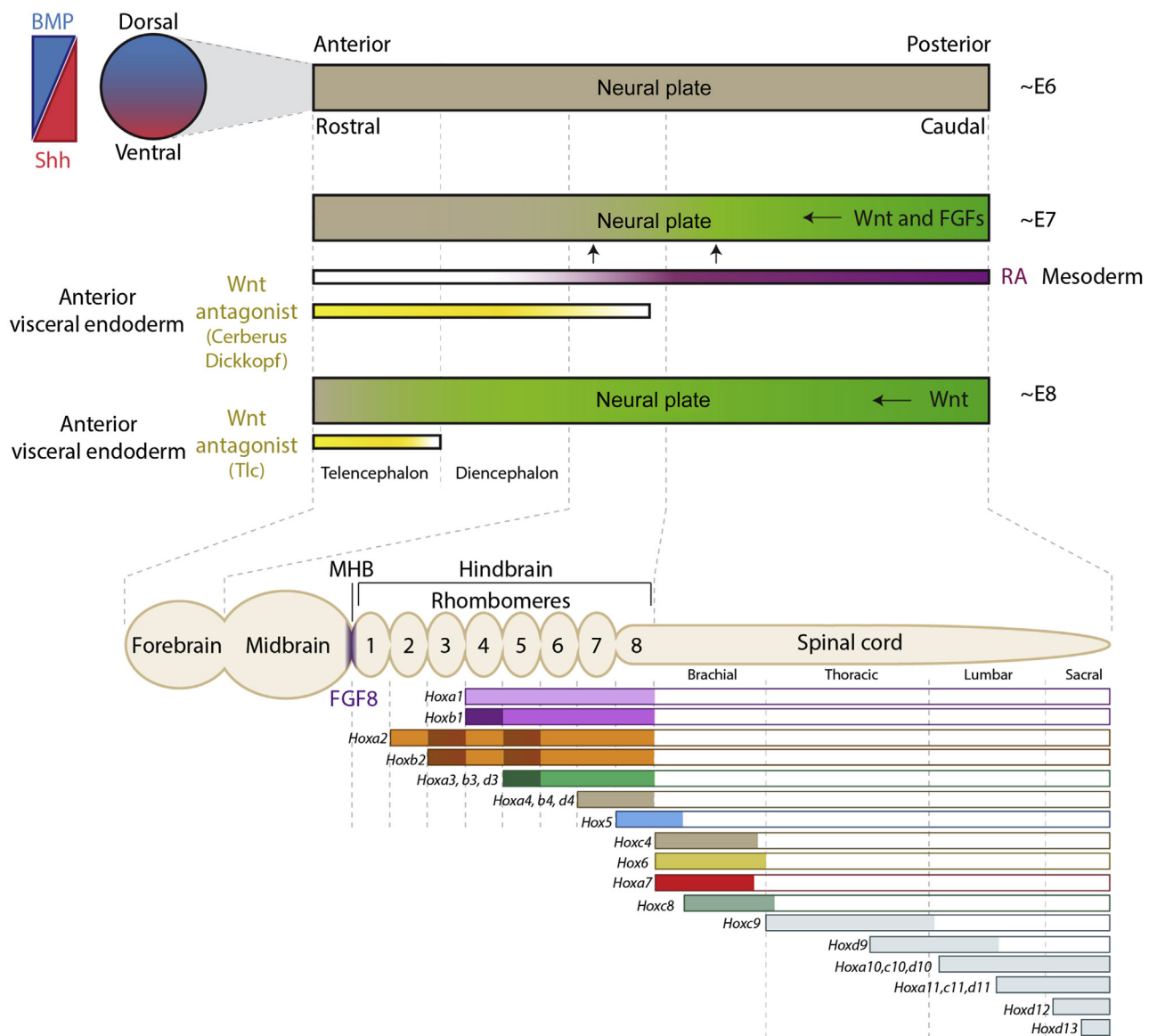
f0015

FIGURE 1.2 Regionalization during neural tube formation is dependent on overlapping agonistic and antagonistic morphogen gradients. Dorsoventral patterning of the neural tube is largely dependent on bone morphogenic protein (BMP) and Sonic hedgehog (Shh) signaling. Some of the key factors involved in patterning the anteroposterior axis include wingless (Wnt) and its antagonists (Cerberus, Dickkopf, Tlc), fibroblast growth factor (FGF), and retinoic acid. Distribution of these factors leads to the eventual segmentation of the neural tube into the forebrain, midbrain, hindbrain, and spinal cord. FGF8 expression delineates the MHB. Additionally, the Hox family of genes, located on four different chromosomes (HoxA, HoxB, HoxC, and HoxD), is crucial in spatiotemporal patterning of the neural tube. *Hox1–Hox5* are responsible for hindbrain segmentation, and *Hox4–Hox11* are involved in patterning of the spinal cord. MHB—midbrain–hindbrain boundary. *Adapted from Refs [11,21–25].*

signaling is crucial in the development of the neural tube, particularly in establishing anteroposterior polarity. Several Wnt antagonists, including Cerberus, Dickkopf, and Tlc, are important in patterning the dorsal telencephalon [16–20]. Diffusion of BMPs and their antagonists along the neural plate creates a gradient of high BMP activity dorsally to low activity ventrally. This leads to the specification of distinct pools of progenitors in the dorsal spinal cord [4,12].

p0040   Additionally, the Hox gene family of homeodomain-containing transcription factors is highly conserved across vertebrates and plays a key role in body patterning [22]. The majority of the 39 Hox genes found throughout vertebrates are expressed in the CNS where they play crucial roles in neuronal specification and selectivity. Hox genes are organized into clusters (HoxA, HoxB, HoxC, and HoxD) on four different chromosomes and exhibit a 3′–5′ gradient of sensitivity to RA. *Hox1–Hox5* (like RA) are involved in hindbrain segmentation into rhombomeres. *Hox4–Hox11* are expressed in the spinal cord and lead to rostrocaudal positioning of neuronal subtypes (Figure 1.2) [23,24].

s0030 ### 1.3.2 Structural Organization of Cellular Compartments and Boundaries in the Developing Neural Tube

p0045 As the neural tube progressively becomes more regionalized, the organization of distinct structural domains arises. Segmentation of the neural tube in the mouse begins initially by assigning anterior–posterior identity along the neuraxis, dividing into the forebrain, midbrain, hindbrain, and spinal cord. The hindbrain (or rhombencephalon) is further divided into rhombomeres which give rise to the metencephalon (the pons and the cerebellum) as well as the myelencephalon (the medulla oblongata). The midbrain (or mesencephalon) is located caudal to the hindbrain and rostral to the forebrain. The forebrain (or prosencephalon) divides into the diencephalon (prethalamus, thalamus, hypothalamus, subthalamus, epithalamus, and pretectum) and the telencephalon (cerebrum) (Figure 1.2). The cerebrum can be further divided into the cerebral cortex, the basal ganglia, and the limbic system (Figure 1.2). For a full review of the cellular compartments and boundaries in vertebrate brain development see Kiecker and Lumsden [25].

s0035 ### 1.4 ONSET OF NEUROGENESIS IN THE TELENCEPHALON

p0050 The mammalian neocortex modulates processing of sensory information and motor activity and mediates cognition. The isocortex formation of the cerebral cortex develops in an inside-out temporal fashion and comprises six histologically distinct neuronal layers. These layers differ in neuronal composition, connectivity, and density. The earliest born neurons populate the deep layers (VI and V), and the later born neurons migrate past the deep layer neurons to form the upper layers (IV, III, and II) of the future cerebral cortex (see later sections). Diverse neuronal subtypes that contribute to the complex neural circuitry are specified by a multitude of factors. Much progress has been made toward understanding the molecular pathways and mechanisms controlling neuronal cell-type diversity in the cortex. However, detailed mechanistic knowledge of the interplay between the transcriptional networks and upstream factors has yet to be elucidated [26].

1.5 THE TRANSITION OF THE NEUREPITHELIUM TO NEURAL STEM CELLS

s0040

p0055 Neurogenesis is composed of an orchestrated series of cellular events that include proliferation, fate commitment, differentiation, maturation, expansion, migration, and functional integration of newborn neurons into neuronal circuits. In the developing mouse CNS there are at least two distinct classes of progenitor cells, the apical progenitors (APs) and the basal progenitors (BPs) (Figure 1.3). The APs include neuroepithelial progenitors (NEPs), which generate radial glial cells (RGCs), and short neural precursors, all of which have stem cell character [27–30]. By E9, the neurepithelium is a single layer of NEPs, which form the pseudo-stratified neurepithelium. Owing to the displacement of the cell body (karyon) of the NEPs during the cell cycle, the ventricular zone resembles a multilayered structure but it is actually a pseudo-stratified single-cell epithelium. The migration of the nucleus (karyon)
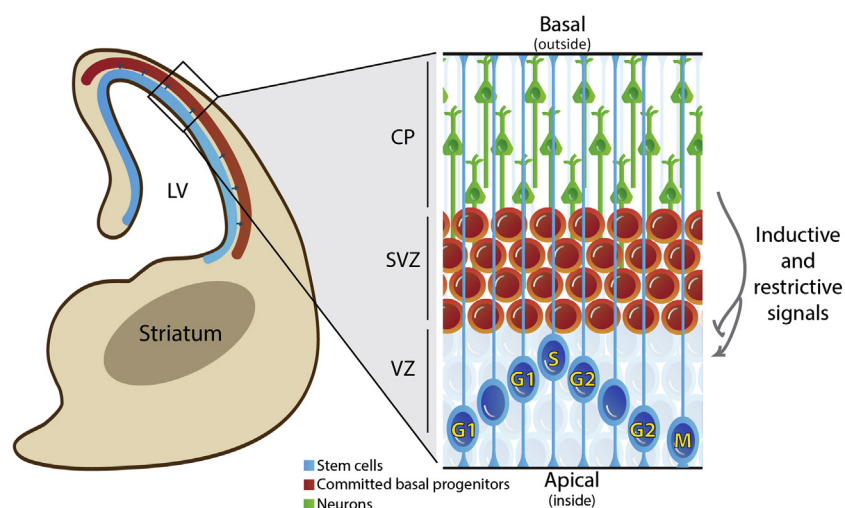
f0030 **FIGURE 1.3** **Scheme of a coronal hemisection of the developing mouse telencephalon and the stem and progenitor populations.** As neurogenesis continues, neural stem cells (NSCs) retain contact with the outside of the neural tube and their apical end feet line the tube, resulting in long polarized processes. NSCs undergo interkinetic nuclear migration during the cell cycle. DNA replication (S phase) always takes place when the cell body reaches the ventricular (VZ)–subventricular zone (SVZ) boundary, mitosis (M) and karyokinesis take place at the luminal surface (apical) of the neural tube. Committed progeny of the NSCs, basal progenitors, migrate to the SVZ where they may divide before differentiating into immature neurons that migrate to the superficial layers of the forming cortical plate (CP) and future cerebral cortex.

along the apicobasal process during the cell cycle is referred to as interkinetic nuclear migration and is cell cycle dependent. Mitosis occurs at the apical side of the cell at the lumen of the neural tube, whereas S phase takes place at the basal boundary of the ventricular zone, and G1 and G2 occur during directed migration of the nucleus (Figure 1.3) [31,32]. As NEPs and RGCs transition from symmetric proliferation to asymmetric neurogenic divisions during neurogenesis their cell cycle lengthens almost entirely due to lengthening of the G1 phase.

p0060   NSCs in the ventricular zone (VZ) of the neural tube connect with one another through tight and adherens junctions at their apical ends. The maintenance of cell polarity is dependent upon the adherens junctions and polarity is critical for NSC function [27,33]. Between E9 and E10 (before the onset of neurogenesis) NEPs maintain their radial morphology, but begin to exhibit astroglial hallmarks and downregulate tight junctions and other epithelial markers, ultimately

transforming into a more restricted distinct cell type called RGCs [28,34]. The nuclei of RGCs continue to migrate along the apical–basal axis during the cell cycle, but interkinetic nuclear movement becomes continually more restricted to the apical end of the extending basal process (Figure 1.3). By the time neurogenesis begins in the forebrain, between E10 and E11 in the mouse, RGCs start to upregulate markers characteristic of astroglia, including glutamate transporter, brain–lipid-binding protein (BLBP), glial fibrillary acidic protein (GFAP), and vimentin. Apical end feet of the RGCs remain anchored to one another through adherens junctions [35,36].

As development continues, a class of intermediate progenitors called BPs is formed. Unlike NEPs and RGCs, BPs do not have apical connections to the lumen of the neural tube but instead undergo a limited number of cell divisions in the subventricular zone (SVZ), a region basal and adjacent to the VZ (Figure 1.4) [37,38]. BPs in the SVZ upregulate   p0065
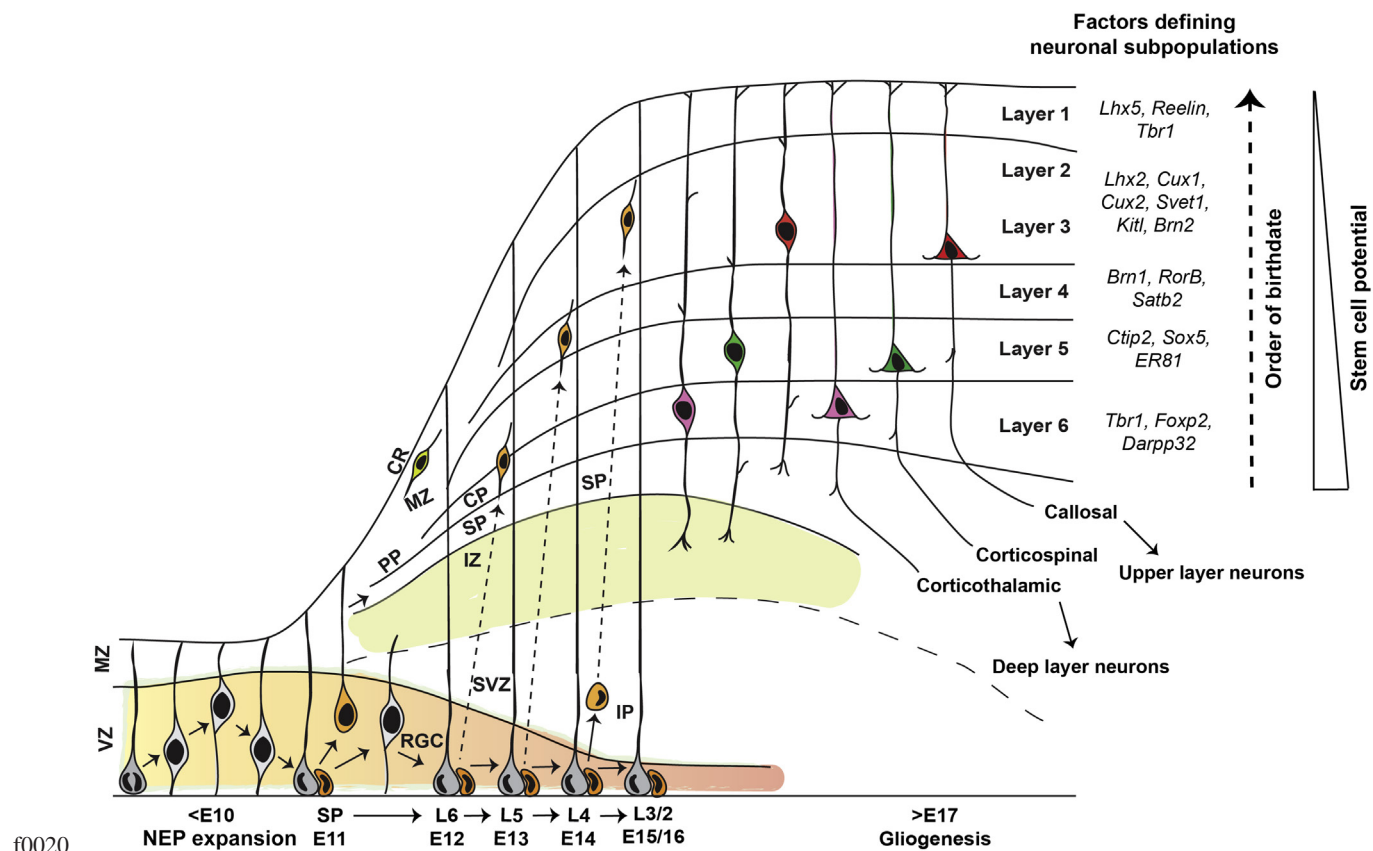
FIGURE 1.4   Neurogenesis and migration of neurons in the mouse cortex. Neural epithelial progenitors (NEPs) in the ventricular zone (VZ) of the developing telencephalon generate the many neuronal subtypes of the six-layered cerebral cortex, potentially starting as a homogeneous multipotent cell population that becomes fate restricted over time during neurogenesis. Before neurogenesis commences, NEPs undergo a series of symmetric divisions in the VZ, expanding the stem cell pool. As neurogenesis proceeds, the VZ NEPs transform into radial glial cells (RGCs) and generate basal progenitors (BPs), which populate the subventricular zone (SVZ). Newly formed neurons derived directly either from NSCs or from the BPs migrate radially outward forming the various cortical layers in an inside-out fashion. The first projection neurons populate the preplate (PP) forming the nascent cortical plate (CP). The CP later becomes layers 2 to 6 of the neocortex. CP neurons split the PP into the marginal zone (MZ) and subplate (SP). Each layer of the cerebral cortex is composed of different neuronal subtypes, which are generated sequentially throughout neurogenesis. Toward the end of neurogenesis the radial scaffolding of the RGCs is dismantled and RGCs become gliogenic, generating cortical and subependymal zone astrocytes and a sheet of ependymal cells lining the ventricles. Some of the key transcription factors used in defining neuronal subtypes are listed adjacent to their respective cortical layer. *Adapted from [42].*

[AU2] the transcription factors cut-like homeobox 1 (Cux1), Cux2, and Tbr2, and although limited self-renewing divisions have been shown, they subsequently undergo symmetric differentiating cell divisions to generate two neurons [39–41].

s0045 1.5.1 Asymmetric versus Symmetric Cell Divisions

p0070 During cortical development, neural progenitors can undergo three modes of cell division. Before neurogenesis begins NEPs divide symmetrically, giving rise to two NEP daughter cells, allowing for rapid expansion of the progenitor pool. Later, NSCs can undergo asymmetric divisions, allowing for both self-renewal of the NSC and generation of a differentiated daughter cell [43,44]. The committed daughter cells are either a single neuron or a BP, which can undergo further cell divisions. RGCs act as a scaffold for the newborn neurons to migrate into the forming cerebral cortex. The third mode of cell division involves an amplification step at the BP stage, increasing the progenitor pool before finally differentiating into neurons. Because a single RGC can give rise to multiple BPs, and a single BP can give rise to two or more neurons, the SVZ is generally recognized as one of the main sites of amplification during neurogenesis [29,45,46]. Regulation of the number of RGCs that divide to give rise directly to neurons or BPs is crucial in controlling neurogenesis. Too many daughter cells differentiating directly into neurons results in overall neurogenesis being severely reduced owing to a lack of BP amplification. Although mitotic spindle orientation is not the only determinant, it has been shown to play a direct role in RGC daughter cell fate.

s0050 1.6 PROGENITOR FATE COMMITMENT AND RESTRICTION

p0075 A detailed understanding of the mechanisms that lead to the formation of multiple neuronal subtypes from a single population of neocortical stem cells is still lacking [47]. Two alternative models have been proposed to explain the process of temporal expansion and differentiation in the cortex. The "common progenitor" model proposes that NSCs restrict their fate temporally as neurogenesis progresses, sequentially generating neurons unique to each layer of the cerebral cortex. Alternatively, the "multiple progenitor" model proposes that NSCs are a heterogeneous pool at the outset, in which each NSC subtype would be guided by intrinsic and extrinsic signals to generate specific neuronal subtypes or astrocytes. Currently, there is evidence supporting both models [48].

s0055 1.6.1 The Common Progenitor Model

p0080 Heterochronic transplantation experiments performed in ferrets by McConnell and colleagues revealed that the potential of NSCs is restricted over time. With age, NSCs become more defined in their fate, eventually losing the ability to generate deep-layer neurons [49,50]. Further supporting the common progenitor model, clonal analysis showed that neocortical NSCs generate deep- and upper-layer neurons in vitro in a sequential and temporal manner [51]. Additionally, retroviral lineage tracing experiments labeling NSCs in vivo support fate restriction of NSCs during development and NSC multipotency [52]. Fezf2, a transcription factor enriched in cortical layer 5 and important in fate specification and connectivity of subcerebral projection neurons, is expressed by NSCs throughout cortical neurogenesis [26,53,54]. Fate mapping experiments demonstrated that these Fezf2$^+$ NSCs could sequentially generate both deep- and upper-layer neurons while becoming fate restricted over time [53]. Ectopic expression of Fezf2 directed the late cortical progenitors to differentiate into deeper-layer projection-like neurons, emphasizing its instructive role. Moreover, Fezf2 is expressed by NSCs as early as E8.5 in the pallial neurepithelium, suggesting its impact on fate determination [42,47,48].

1.6.2 Multiple Progenitor Model s0060

p0085 Early evidence showed that several transcription factors are responsible for the fate determination of various neuronal subtypes. These factors and the onset of their expression during development imply different subsets of progenitors, which are predetermined and committed to generate specific neuronal subtypes [48]. These fate-restricted NSCs in the developing telencephalon express the transcription factors Cux1 and Cux2, both of which have been associated with differentiated and specific neuron subtypes in the cerebral cortex [55]. Cux1 and Cux2 are expressed in the VZ and SVZ abundantly during upper-layer neurogenesis, primarily specifying callosal projection neurons [55]. However, during early development Cux2$^+$ NSCs proliferate and expand without differentiating. Later, when neurons of the superficial cortical layers are being generated, these NSCs and progenitors switch to a neurogenic mode and generate Cux2$^+$ upper-layer neurons. These findings challenged the existing common progenitor model but left many questions unanswered. Subsequent lineage tracing experiments confirmed the presence of Cux2$^+$ NSCs but suggested they generate both upper- and deep-layer neurons as well as interneurons derived from the ventral telencephalon [53]. The presence of multipotent NSCs expressing Fezf2 and Cux2 does not negate the possibility of the existence of fate-restricted progenitors, but additional single-cell analysis of fate and lineage will be required [50,53].

p0090 Other models in the field emphasize the presence of stem cells that are multipotent and switch their fate over the course of sequential rounds of cortical neurogenesis. This would suggest that NSCs would be initially committed to

one fate during development and then switch to an alternate fate as corticogenesis proceeds. Multipotent NSCs could then generate multiple neuronal subtypes while still restricting their potential and eventually becoming unipotent. Further investigation of the mechanisms driving neurogenesis is crucial to understand NSC cell regulation [48].

s0065 1.7 MOLECULAR MECHANISMS OF NEURAL STEM CELL MAINTENANCE

s0070 1.7.1 Notch Signaling as a Key Regulator in Maintenance of NSCs

p0095 To maintain neurogenesis from the developing embryo into adulthood, NSCs must be able to self-renew. One of the best-studied signaling pathways shown to be involved in NSC maintenance, proliferation, quiescence, and survival is the Notch pathway [56–62]. Notch receptors are type 1 transmembrane proteins, which can be activated through extracellular protein–protein interactions with ligands of either the Delta or the Serrate (Delta-like and cluster of differentiation antigen CD339 or Jagged, respectively, in mammals) family on adjacent cells. Upon activation receptors undergo sequential proteolytic cleavage, first by a disintegrin and metalloprotease and then by a presenilin containing γ-secretase, releasing the intracellular domain of Notch (NICD) [63,64]. Canonical Notch signaling is mediated by the interaction of nuclear-translocated NICD with the CSL transcriptional complex (RBP-J in mice) (Figure 1.5). This interaction disrupts the preformed repressor complex and switches it to an activator by recruiting Mastermind and chromatin-modifying agents (i.e., histone acetyltransferase) to induce target gene expression [65–70]. The best-studied targets of the Notch pathway in mammals are the orthologs of hairy/enhancer of split (Hes/Hey). The direct canonical Notch targets, *Hes1* and *Hes5,* are two of these basic helix–loop–helix (bHLH) transcriptional regulators and are critical for neural development [71]. Hes1 and Hes5 directly repress transcription of proneural genes including *Ascl1* (Mash1), *Atoh1* (Math1), and *Neurog2* (Ngn2), thereby maintaining NSCs in a progenitor state [62,71]. Conversely, inactivation of Notch results in upregulation of the proneural genes and neural progenitor differentiation [61,72,73]. Manipulating the Notch signaling pathway using γ-secretase inhibitors, by ablating *RBP-J*, by knocking out individual members of the Notch family, or by expressing an activated NICD showed that Notch is key in modulating progenitor cell proliferation and neurogenesis during embryonic development [61,72,73].

p0100   The classic "lateral inhibition" model of Notch signaling in NSCs proposes that all early progenitors express similar levels of proneural genes and Notch ligands. Then through stochastic variations, the levels of receptors, ligands, and proneural genes fluctuate between adjacent cells, resulting in a "salt-and-pepper" pattern of Notch component gene expression. Cells with slightly higher ligand levels activate receptors in neighboring cells, causing an inhibition of proneural genes in those cells. Differences in the gene expression profiles of neighboring cells continue to be exacerbated and eventually lead to the lineage commitment of the high proneural gene-expressing cell. Real-time imaging in Hes reporter mice showed that negative feed-forward and feedback loops exist, resulting in oscillatory expression of downstream Notch signaling components and their targets over time, which are independent and not linked to cell cycle phases [60,74,75]. Therefore, a cell with high proneural gene expression at one time point may revert to a low proneural gene expression state shortly thereafter. Oscillations of Notch signaling in progenitors of the nervous system are analogous but not identical to the waves of Notch activity seen during somite formation. Oscillations in components of Notch may further alter the ability of NSCs to respond to external differentiation cues and be critical for regulating NSC potential [76]. Notch1 has been proposed to play a role in the maintenance of actively dividing NSCs in the adult neurogenic niche [77–81]. In the SVZ of the lateral ventricle wall and dentate gyrus (DG) of adult mice Notch activity promotes NSC survival and maintenance and stem cell self-renewal [77,78,80,82–84]. However, both the preservation of and the transition from a quiescent NSC state to an activated state appear to be RBP-J dependent [61,79,81,83].

p0105   Great efforts have been made over the years to identify molecular markers that discriminate populations of quiescent and activated NSCs from niche astrocytes; however, none have proven to be ideal [85,86]. Epidermal growth factor receptors have been associated with active SVZ NSCs that maintain astrocytic (BLBP) and glial (GFAP) markers, and Prominin-1 expression associates with NSCs, distinguishing them from parenchymal astrocytes [81,85]. In the adult DG horizontal, nonradial cells with active Notch signaling include a population of actively dividing NSCs [84]. However, there is also a population of quiescent horizontal DG NSCs that currently cannot be discerned based on molecular marker alone [84,87]. New genetic tools will need to be generated and markers identified that allow for independent and simultaneous lineage tracing of these two NSC populations. For an in-depth analysis of the role of Notch in quiescence and active NSC populations see Giachino and Taylor [88].

p0110   In the adult forebrain SVZ niche, NSCs receive inductive cues directing them to specific fates and restrictive signals, which limit their potential and prevent differentiation [89]. Some of these inductive cues most likely work in tandem with Notch [90]. Noncanonical activation of Notch through pigment epithelium-derived factor (PEDF) secreted by vascular endothelial cells within the adult lateral ventricle SVZ can bias cell fate toward RGC-like states. By activating nuclear factor κB, PEDF exports nuclear receptor corepressor, which
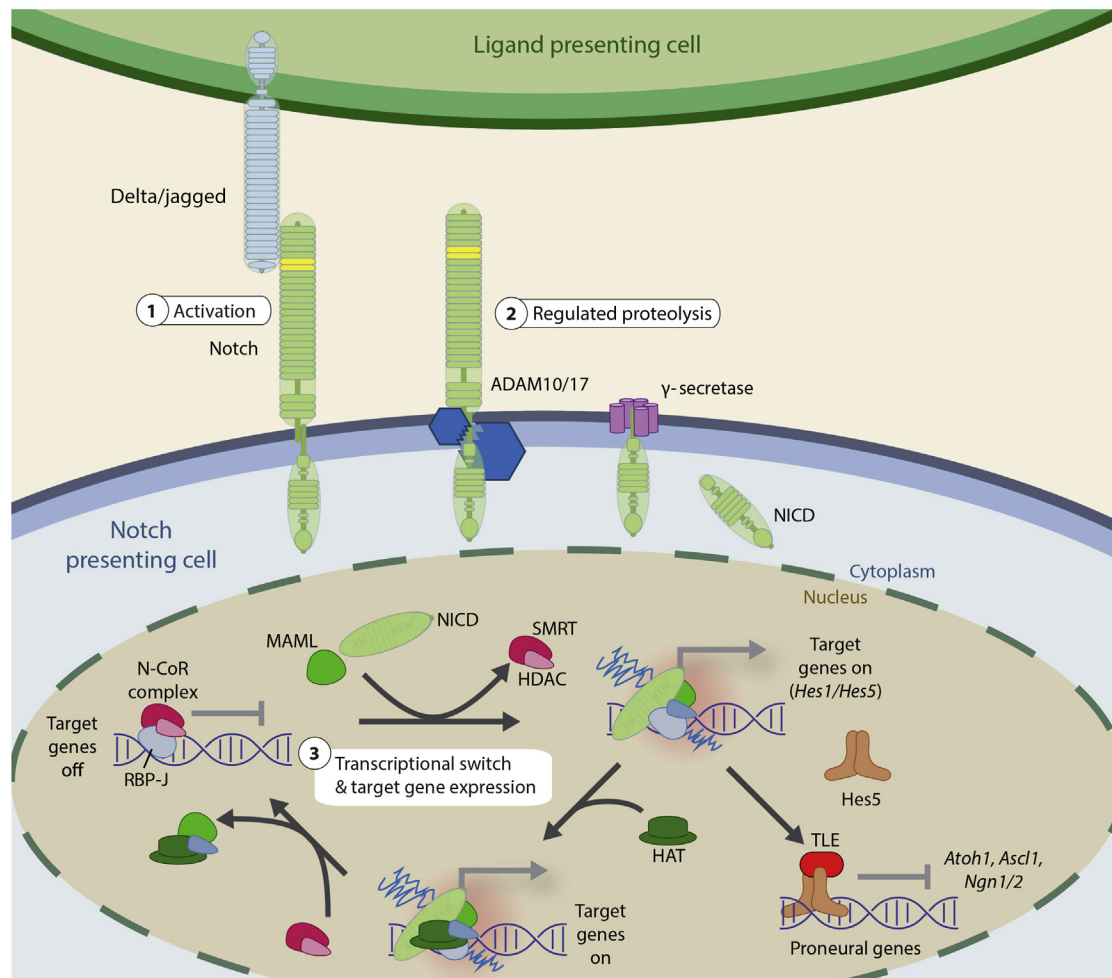
f0035

FIGURE 1.5   **Canonical notch receptor signaling in the control of neurogenesis.** Notch receptors and their ligands are type 1 transmembrane proteins. Notch receptor activation is triggered when either Delta or Jagged presented by neighboring cells binds to the ectodomain, resulting in regulated intramembrane proteolysis in which first a disintegrin and metalloprotease (ADAM10 or 17) and then a presenilin containing γ-secretase cleave the receptor, releasing a soluble intracellular domain (NICD). The NICD translocates to the nucleus where it interacts with the CSL (CBF1, Su(H), and Lag1—RBP-J in mice) protein complex including the DNA-binding protein recombining binding protein suppressor of hairless (RBP-J). The binding of NICD releases the nuclear receptor corepressor complex (*N*-CoR), which includes silencing mediator of retinoid and thyroid receptors (SMRT) and histone deacetylases (HDAC). The NICD-bound CSL complex is a positive regulator of Notch target genes including *Hes1* and *Hes5*. Hes5 is a basic helix–loop–helix transcription factor that, together with a zinc finger protein of the transducing-like enhancer of split (TLE) family, represses the proneural genes (*Atoh1*, *Ascl1*, and *Ngn1/2*) in NSCs and thereby inhibits neuronal differentiation. The NICD complex also interacts with a histone acetyltransferase (HAT), leading to epigenetic marking of target genes and transcriptional activation.

acts as a transcriptional inhibitor of the Notch target genes *Hes1* and *Egfr*, allowing for NSCs to undergo asymmetric, self-renewing divisions [91]. Other inductive cues include hypoxia-inducible factor 1α, which under hypoxic conditions is stabilized and cooperates with Notch signaling to promote expression of target genes by NSCs.

s0075   ## 1.8 INTERNEURON GENERATION FROM THE VENTRAL TELENCEPHALON

p0115   Neuronal subtypes can be defined according to the neurotransmitters they secrete, which include γ-aminobutyric acid (GABA), acetylcholine, dopamine, and glutamine. In the cerebral cortex, the excitatory glutamatergic cortical neurons and the inhibitory interneurons (i.e., GABAergic interneurons) mediate excitation and inhibition, respectively. Alterations in either population of neurons results in neurological and psychiatric disorders. The GABAergic interneurons are morphologically, physiologically, and neurochemically distinct from the glutamatergic excitatory neurons. As embryonic development proceeds, excitatory and inhibitory neurons mature and form synapses with one another to establish a complex cortical network. The distinct properties of the neuronal subtypes also aid in modulating the cortical output and plasticity of the cortex by creating local inhibitory networks. Disruption of the excitatory and inhibitory
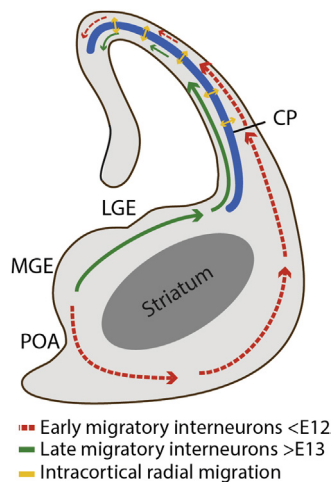
f0025

FIGURE 1.6 Generation of interneurons in the mammalian forebrain. Interneurons (inhibitory neurons) are generated from the ventral telencephalon during embryonic development and migrate tangentially from the subpallium and integrate to the cortex. The subpallian sources of interneurons are the lateral ganglionic eminence (LGE), the medial ganglionic eminence (MGE), and the preoptic area/anterior endopeduncular (POA). Interneurons are divided into the early- and late-born populations, which adopt different tangential migratory pathways to the cerebral cortex. Upon reaching their mediolateral location in the dorsal telencephalon, the migratory interneuron neuroblasts migrate radially into the cortical plate (CP). *Adapted from Ref. [96].*

neuronal balance is implicated in neurological disorders in humans, such as schizophrenia, epilepsy, and autism [92].

p0120   Interneurons in a mouse are produced mainly between E11 and E17 [92]. In mice as well as in primates and humans interneurons originate from the ventral NSCs and progenitors residing in the medial ganglionic eminence (MGE), caudal ganglionic eminence, preoptic area, and anterior entopeduncular area of the subpallium (ventral telencephalon) (Figure 1.6) [92]. Following dorsal migration from the subpallium, the interneurons integrate into the cerebral cortex, in a sequential and temporal order similar to that seen in corticogenesis (Figure 1.6) [42]. The subpallial region expresses the transcription factors Dlx1 and Dlx2, which are essential for interneuron production, migration, and differentiation [92]. Other factors, including Nkx2.1 and Sox6, are expressed in the MGE and affect interneuron differentiation by controlling downstream transcriptional programs in NSCs and postmitotic neurons [92]. For a detailed review please refer to [93–95]. Because of the lack of markers or lineage tracing studies, little is known at the time of this writing about the molecular variations of single interneurons in different functional regions [26,92].

s0080 ## 1.9 FORMATION OF THE CEREBRAL ISOCORTEX AND CORTICAL LAYERING

p0125 Upon induction of neurogenesis, numerous neocortical determinants are expressed along the dorsolateral wall of the telencephalon. Key factors, including LIM homeobox 2, forkhead box G1, empty spiracles homolog 2 (Emx2), and paired box 6 (Pax6), control the neocortical progenitor domains along the dorsal and ventral axis [26]. When the dorsal determinants Pax6 and Emx2 are ablated the ventral domain of the telencephalon is expanded [97]. It is speculated that Pax6 and Tlx regulate cell fate decisions in VZ NSCs, and loss-of-function studies show defects in the thickness of the superficial cortex [98–100]. Fezf2, Satb2, Ctip2, and Tbr1 have been identified as key NSC subtype markers, directing neuronal subtype specification (Figure 1.4) [26,48]. As neurogenesis proceeds, mature deep-layer neurons exhibit progressive postmitotic refinement of subtype identity, with layer-specific patterns of gene expression (Figure 1.4). At E13.5, postmitotic deep-layer neurons coexpress Ctip2 and Satb2. Later, neurons express either Ctip2 or Satb2 and become fate-restricted to subcerebral projection neurons and corticothalamic projection neurons, respectively [101,102]. This may indicate the presence of a more plastic state in which the neuronal cell fate is determined. Also, neuronal diversification and regional specialization result in increased sophistication of neural circuitry and determine functionally distinct areas. As of 2014, data suggest a progressive recruitment of transcription factors during cortical development, leading to a continually restricted neuronal fate [103]. Several inductive and repressive cues that regulate the regimental corticogenesis influence these factors that are expressed dynamically throughout development. In the future, lineage tracing of cell populations facilitated by surface molecular markers and cell-sorting approaches, single-cell analysis, and genome sequencing methods may provide additional insights into cortical patterning and specification. Additionally, assessing cortical plasticity and determining clear boundaries within subtypes during neurogenesis could pave the way for future therapeutic interventions [26].

s0085 ## 1.10 OLIGODENDROGENESIS AND ASTROGENESIS

p0130 Glia cells carry out a diverse range of critical functions in the brain, including ensuring adequate nutrient supplies to neurons, providing scaffolding and support, insulating axons, removing cellular debris, and destroying pathogens. Oligodendrocytes compose one of the major types of glia cells and have the ability not only to provide support, but, when mature, also to myelinate and insulate axons, thereby ensuring proper signal transduction (reviewed in Ref. [104]). Differentiation of oligodendrocytes from early oligodendrocytic precursor cells (OPCs) into mature myelinating cells is a process termed oligodendrogenesis. Much like neurogenesis, oligodendrogenesis requires a complex network of morphogens, transcription factors, and signaling

pathway cross talk for maturation to occur correctly. Some of the key signaling pathways involved include Wnt, Shh, BMP, and Notch [105].

p0135   Oligodendrocytes in the developing forebrain are produced in three sequential and competitive phases beginning in the embryo and continuing into early postnatal development [106]. Interestingly, oligodendrocytes from the first wave of oligodendrogenesis in the forebrain are almost completely absent from the postnatal brain, potentially eliminated or out-competed by later waves [106]. Oligodendrocytes begin in the developing neural tube as multipotent NEPs. Through sequential rounds of asymmetric cell divisions morphogen gradients of BMP and Shh restrict NEPs first to RGCs and then to OPCs [105]. OPCs then proceed to receive chemoattractant and mitogen signals instructing them to proliferate and migrate from the SVZ into the developing forebrain [105]. Once OLPs reach their destination, they proceed to integrate and differentiate, forming myelin and ensheathing axons.

p0140   Depending on the stage of oligodendrocyte maturation, oligodendrocytes express a range of markers. Key markers displayed by OPCs are platelet-derived growth factor receptor α (PDGFRα), Nkx2.2, and NG2, as well as the transcription factors Olig2 and Sox10 [107]. However, a variety of OPC populations exist, with some having limited or no expression of PDGFRα [108,109]. Conversely, all OPCs seem to express Sox10, and therefore Sox10 is generally accepted as an identifier of OPCs [106]. Later, mature myelinating oligodendrocytes express common markers such as myelin basic protein, myelin oligodendrocyte glycoprotein, and 2′,3′-cyclic nucleotide 3′-phosphodiesterase [107].

p0145   Another population of glial cells in the brain is the astrocytes that are important for neuronal function and are generated from the same pool of NSCs that gives rise to the neurons. Astrocytes are not just bystanders in brain function, they are also involved in the synaptic transmission and processing of neural circuits and modulate synapses and synaptic connectivity [110]. Additionally, astrocytes maintain a steady state in the CNS by modulating the ions, pH, neurotransmitter metabolism, and flow of blood [111]. At the onset of astrogliogenesis, stem cells can generate either BPs or astrocytes. BPs require the bHLH factor neurogenin-1 to inhibit the formation of astrocytes, whereas astrogliogenesis is promoted by the JAK/STAT signaling pathway [110].

s0090 1.10.1 Human Neocorticogenesis

p0150 The human cerebral cortex has expanded dramatically during phylogeny. Rodents have a smaller neocortex that lacks folding (lissencephalic), presenting limitations for studying the larger and highly folded (gyrencephalic) human neocortex. Human corticogenesis is characterized by the appearance of an enlarged SVZ that is split into an inner

SVZ (iSVZ) and an outer SVZ (oSVZ) by a thin fiber layer [112]. The increased neocortical surface area and volume in humans is associated with an expanded pool of progenitor cells in the oSVZ [113]. It has been proposed that the developing cerebral cortex has a columnar organization in which the newly born neurons migrate basally on a continuous radial fiber to the superficial layers. This results in the formation of radial columns of cells with related function [31,114]. The "radial unit hypothesis" integrates these concepts of cortical expansion and thalamic cues affecting size and cellular composition with neuronal function [103]. However, other studies have suggested that some lateral dispersion of clonally associated neurons exists, contrasting with the columnar organization model [31,115].

p0155   In the human brain, an increase in the number of neurons is achieved through three stages of extensive cellular expansion. In humans, cortical neuron production begins by gestational week (GW) 6. Subsequently the oSVZ develops, after GW11, and expands dramatically to become the main germinal region of the neocortex [113]. Compared to the NSCs and BPs in the rodent telencephalon, humans have additional progenitor pools including outer radial glia in the oSVZ that are defined by morphology and location. Outer radial glia numbers increase as they undergo multiple cell divisions and add to the BP pool. The cells in the oSVZ, like their VZ counterparts, also express nestin, vimentin, Pax6, and GFAP, with Tbr2 (a marker for BPs) being selective for oSVZ cells [116,117]. The oSVZ in the human dorsal cerebral cortex also contains a class of proliferating cells that express markers relevant to inhibitory neurons, including ASCL1, DLX2, NKX2-1, and calretinin, suggesting an expansion of immature interneurons migrating to their final location in the dorsal cortex [31,113]. Thymidine labeling experiments in primates show a relationship between the proliferation phases within the oSVZ and peaks of corticogenesis. This supports the hypothesis that the oSVZ and not the VZ is the main domain expanding during primate cortical development [103,118]. Experiments in ferrets, cats, and humans also revealed that with an increase in brain gyrification, there are more proliferating cells associated with the oSVZ than there are in the VZ/iSVZ.

p0160   Considering the dramatic differences between humans and rodents, various in vitro methods that recapitulate human brain development have been employed with great success. Birthdating studies by Gaspard et al., 2008, and Eiraku et al., 2008, demonstrated that mouse embryonic stem cells (ESCs) could be induced to undergo neurogenesis in vitro in a fashion similar to what is observed in the developing cerebral cortex [119–121]. These results were recapitulated in human ESCs, although with a slower induction of the neurogenic program, which may reflect the ontogenetic time frame of our species [119,120]. Subsequently, a fully stratified three-dimensional (3D) system for

the generation of retinal tissue from mouse ESCs has been developed, which provides a valuable resource for developing therapeutics in cases of retinal degeneration [122]. With new technologies such as patient-derived iPS cells, the molecular basis and genetic mutations involved in neurodegenerative disorders may begin to be unraveled. Indeed, several studies have been able to model human corticogenesis in vitro using 2D culture systems, although a 3D system still remains a challenge [123–125].

p0165   As great as our advances in understanding the molecular biology of the developing brain have been in recent decades, there is still much that must be addressed before NSCs and iPS cells can be considered for therapeutic intervention. A deeper understanding of population-specific molecular markers, lineage relationships, and transcriptional profiles will contribute to developing new methods for the field of regenerative medicine.

s0100 REFERENCES

[AU3]

[1] Tam PP, Loebel DA. Gene function in mouse embryogenesis: get set for gastrulation. Nat Rev Genet 2007;8(5):368–81.

[2] Bhatt S, Diaz R, Trainor PA. Signals and switches in Mammalian neural crest cell differentiation. Cold Spring Harb Perspect Biol 2013;5(2).

[3] Green SA, Bronner ME. Gene duplications and the early evolution of neural crest development. Semin Cell Dev Biol 2013;24(2):95–100.

[4] Liu A, Niswander LA. Bone morphogenetic protein signalling and vertebrate nervous system development. Nat Rev Neurosci 2005;6(12):945–54.

[5] Jessell TM, Sanes JR. In: Kandel ER, Schwartz JH, Jessell TM, editors. Principles of neural science: the induction and patterning of the nervous system. 4th ed, New York: McGraw-Hill, Health Professions Division; 2000.

[6] Sauka-Spengler T, Bronner M. Snapshot: neural crest. Cell 2010; 143(3):486. 486 e1.

[7] Van de Putte T, et al. Mice lacking Zfhx1b, the gene that codes for Smad- interacting protein-1, reveal a role for multiple neural crest cell defects in the etiology of Hirschsprung disease-mental retardation syndrome. Am J Hum Genet 2003;72(2):465–70.

[8] Copp AJ, Greene ND, Murdoch JN. The genetic basis of mammalian neurulation. Nat Rev Genet 2003;4(10):784–93.

[9] Copp AJ. Neurulation in the cranial region–normal and abnormal. J Anat 2005;207(5):623–35.

[10] Shimokita E, Takahashi Y. Secondary neurulation: fate-mapping and gene manipulation of the neural tube in tail bud. Dev Growth Differ 2011;53(3):401–10.

[11] Rallu M, Corbin JG, Fishell G. Parsing the prosencephalon. Nat Rev Neurosci 2002;3(12):943–51.

[12] Lupo G, Harris WA, Lewis KE. Mechanisms of ventral patterning in the vertebrate nervous system. Nat Rev Neurosci 2006;7(2):103–14.

[13] Cohen M, Briscoe J, Blassberg R. Morphogen interpretation: the transcriptional logic of neural tube patterning. Curr Opin Genet Dev 2013;23(4):423–8.

[14] Tiberi L, Vanderhaeghen P, van den Ameele J. Cortical neurogenesis and morphogens: diversity of cues, sources and functions. Curr Opin Cell Biol 2012;24(2):269–76.

[15] Sansom SN, Livesey FJ. Gradients in the brain: the control of the development of form and function in the cerebral cortex. Cold Spring Harb Perspect Biol 2009;1(2):a002519.

[16] Ciani L, Salinas PC. WNTS in the vertebrate nervous system: from patterning to neuronal connectivity. Nat Rev Neurosci 2005; 6(5):351–62.

[17] Hebert JM, Fishell G. The genetics of early telencephalon patterning: some assembly required. Nat Rev Neurosci 2008;9(9):678–85.

[18] Houart C, et al. Establishment of the telencephalon during gastrulation by local antagonism of wnt signaling. Neuron 2002;35(2):255–65.

[19] Piccolo S, et al. The head inducer Cerberus is a multifunctional antagonist of Nodal, BMP and Wnt signals. Nature 1999;397(6721):707–10.

[20] Bafico A, et al. Novel mechanism of Wnt signalling inhibition mediated by Dickkopf-1 interaction with LRP6/Arrow. Nat Cell biol 2001;3(7):683–6.

[21] Maden M. Retinoic acid in the development, regeneration and maintenance of the nervous system. Nat Rev Neurosci 2007;8(10):755–65.

[22] Pearson JC, Lemons D, McGinnis W. Modulating Hox gene functions during animal body patterning. Nat Rev Genet 2005;6(12): 893–904.

[23] Akin ZN, Nazarali AJ. Hox genes and their candidate downstream targets in the developing central nervous system. Cell Mol Neurobiol 2005;25(3–4):697–741.

[24] Philippidou P, Dasen JS. Hox genes: choreographers in neural development, architects of circuit organization. Neuron 2013;80(1):12–34.

[25] Kiecker C, Lumsden A. Compartments and their boundaries in vertebrate brain development. Nat Rev Neurosci 2005;6(7):553–64.

[26] Molyneaux BJ, et al. Neuronal subtype specification in the cerebral cortex. Nat Rev Neurosci 2007;8(6):427–37.

[27] Gotz M, Huttner WB. The cell biology of neurogenesis. Nat Rev Mol Cell Biol 2005;6(10):777–88.

[28] Kriegstein AR, Gotz M. Radial glia diversity: a matter of cell fate. Glia 2003;43(1):37–43.

[29] Fishell G, Kriegstein AR. Neurons from radial glia: the consequences of asymmetric inheritance. Curr Opin Neurobiol 2003;13(1):34–41.

[30] Gal JS, et al. Molecular and morphological heterogeneity of neural precursors in the mouse neocortical proliferative zones. J Neurosci 2006;26(3):1045–56.

[31] Lui JH, Hansen DV, Kriegstein AR. Development and evolution of the human neocortex. Cell 2011;146(1):18–36.

[32] Taverna E, Huttner WB. Neural progenitor nuclei IN motion. Neuron 2010;67(6):906–14.

[33] Franco SJ, Muller U. Shaping our minds: stem and progenitor cell diversity in the mammalian neocortex. Neuron 2013;77(1):19–34.

[34] Malatesta P, Hartfuss E, Gotz M. Isolation of radial glial cells by fluorescent-activated cell sorting reveals a neuronal lineage. Development 2000;127(24):5253–63.

[35] Rasin MR, et al. Numb and Numbl are required for maintenance of cadherin-based adhesion and polarity of neural progenitors. Nat Neurosci 2007;10(7):819–27.

[36] Kuo CT, et al. Postnatal deletion of numb/numblike reveals repair and remodeling capacity in the subventricular neurogenic niche. Cell 2006;127(6):1253–64.

[37] Haubensak W, et al. Neurons arise in the basal neurepithelium of the early mammalian telencephalon: a major site of neurogenesis. Proc Natl Acad Sci U.S.A 2004;101(9):3196–201.

[38] Noctor SC, et al. Cortical neurons arise in symmetric and asymmetric division zones and migrate through specific phases. Nat Neurosci 2004;7(2):136–44.

[39] Nieto M, et al. Expression of Cux-1 and Cux-2 in the subventricular zone and upper layers II-IV of the cerebral cortex. J Comp Neurol 2004;479(2):168–80.

[40] Cubelos B, et al. Cux-2 controls the proliferation of neuronal intermediate precursors of the cortical subventricular zone. Cereb Cortex 2008;18(8):1758–70.

[41] Englund C, et al. Pax6, Tbr2, and Tbr1 are expressed sequentially by radial glia, intermediate progenitor cells, and postmitotic neurons in developing neocortex. J Neurosci 2005;25(1):247–51.

[42] Kwan KY, Sestan N, Anton ES. Transcriptional co-regulation of neuronal migration and laminar identity in the neocortex. Development 2012;139(9):1535–46.

[43] Noctor SC, et al. Neurons derived from radial glial cells establish radial units in neocortex. Nature 2001;409(6821):714–20.

[44] Miyata T, et al. Asymmetric inheritance of radial glial fibers by cortical neurons. Neuron 2001;31(5):727–41.

[45] Knoblich JA. Mechanisms of asymmetric stem cell division. Cell 2008;132(4):583–97.

[46] Kriegstein A, Alvarez-Buylla A. The glial nature of embryonic and adult neural stem cells. Annu Rev Neurosci 2009;32:149–84.

[47] Leone DP, et al. The determination of projection neuron identity in the developing cerebral cortex. Curr Opin Neurobiol 2008;18(1):28–35.

[48] Greig LC, et al. Molecular logic of neocortical projection neuron specification, development and diversity. Nat Rev Neurosci 2013; 14(11):755–69.

[49] Desai AR, McConnell SK. Progressive restriction in fate potential by neural progenitors during cerebral cortical development. Development 2000;127(13):2863–72.

[50] Han W, Sestan N. Cortical projection neurons: sprung from the same root. Neuron 2013;80(5):1103–5.

[51] Shen Q, et al. The timing of cortical neurogenesis is encoded within lineages of individual progenitor cells. Nat Neurosci 2006;9(6):743–51.

[52] Tan SS, Breen S. Radial mosaicism and tangential cell dispersion both contribute to mouse neocortical development. Nature 1993; 362(6421):638–40.

[53] Guo C, et al. Fezf2 expression identifies a multipotent progenitor for neocortical projection neurons, astrocytes, and oligodendrocytes. Neuron 2013;80(5):1167–74.

[54] Chen B, Schaevitz LR, McConnell SK. Fezl regulates the differentiation and axon targeting of layer 5 subcortical projection neurons in cerebral cortex. Proc Natl Acad Sci U.S.A 2005;102(47):17184–9.

[55] Franco SJ, et al. Fate-restricted neural progenitors in the mammalian cerebral cortex. Science 2012;337(6095):746–9.

[56] Androutsellis-Theotokis A, et al. Notch signalling regulates stem cell numbers in vitro and in vivo. Nature 2006;442(7104):823–6.

[57] Mizutani K, et al. Differential notch signalling distinguishes neural stem cells from intermediate progenitors. Nature 2007;449(7160):351–5.

[58] Ohtsuka T, et al. Hes1 and Hes5 as notch effectors in mammalian neuronal differentiation. EMBO J 1999;18(8):2196–207.

[59] Hitoshi S, et al. Notch pathway molecules are essential for the maintenance, but not the generation, of mammalian neural stem cells. Genes Dev 2002;16(7):846–58.

[60] Basak O, Taylor V. Identification of self-replicating multipotent progenitors in the embryonic nervous system by high notch activity and Hes5 expression. Eur J Neurosci 2007;25(4):1006–22.

[61] Imayoshi I, et al. Essential roles of notch signaling in maintenance of neural stem cells in developing and adult brains. J Neurosci 2010; 30(9):3489–98.

[62] Louvi A, Artavanis-Tsakonas S. Notch signalling in vertebrate neural development. Nat Rev Neurosci 2006;7(2):93–102.

[63] Brou C, et al. A novel proteolytic cleavage involved in notch signaling: the role of the disintegrin-metalloprotease TACE. Mol Cell 2000;5(2):207–16.

[64] Mumm JS, et al. A ligand-induced extracellular cleavage regulates gamma-secretase-like proteolytic activation of Notch1. Mol Cell 2000;5(2):197–206.

[65] Kurooka H, Kuroda K, Honjo T. Roles of the ankyrin repeats and C-terminal region of the mouse notch1 intracellular region. Nucleic Acids Res 1998;26(23):5448–55.

[66] Tamura K, et al. Physical interaction between a novel domain of the receptor notch and the transcription factor RBP-J kappa/Su(H). Curr Biol 1995;5(12):1416–23.

[67] Kato H, et al. Involvement of RBP-J in biological functions of mouse Notch1 and its derivatives. Development 1997;124(20):4133–41.

[68] Hsieh JJ, Hayward SD. Masking of the CBF1/RBPJ kappa transcriptional repression domain by Epstein-Barr virus EBNA2. Science 1995;268(5210):560–3.

[69] Dou S, et al. The recombination signal sequence-binding protein RBP-2N functions as a transcriptional repressor. Mol Cell Biol 1994;14(5):3310–9.

[70] Fiuza UM, Arias AM. Cell and molecular biology of Notch. J Endocrinol 2007;194(3):459–74.

[71] Hatakeyama J, et al. Hes genes regulate size, shape and histogenesis of the nervous system by control of the timing of neural stem cell differentiation. Development 2004;131(22):5539–50.

[72] Lütolf S, et al. Notch1 is required for neuronal and glial differentiation in the cerebellum. Development 2002;129(2):373–85.

[73] Gaiano N, Nye JS, Fishell G. Radial glial identity is promoted by Notch1 signaling in the murine forebrain. Neuron 2000;26(2):395–404.

[74] Kageyama R, Ohtsuka T, Kobayashi T. The Hes gene family: repressors and oscillators that orchestrate embryogenesis. Development 2007;134(7):1243–51.

[75] Shimojo H, Ohtsuka T, Kageyama R. Oscillations in notch signaling regulate maintenance of neural progenitors. Neuron. 58(1):52–64.

[76] Kageyama R, et al. Dynamic notch signaling in neural progenitor cells and a revised view of lateral inhibition. Nat Neurosci 2008; 11(11):1247–51.

[77] Ables JL, et al. Notch1 is required for maintenance of the reservoir of adult hippocampal stem cells. J Neurosci 2010;30(31):10484–92.

[78] Aguirre A, Rubio ME, Gallo V. Notch and EGFR pathway interaction regulates neural stem cell number and self-renewal. Nature 2010;467(7313):323–7.

[79] Basak O, et al. Neurogenic subventricular zone stem/progenitor cells are Notch1-dependent in their active but not quiescent state. J Neurosci 2012;32(16):5654–66.

[80] Nyfeler Y, et al. Jagged1 signals in the postnatal subventricular zone are required for neural stem cell self-renewal. EMBO J 2005;24(19):3504.

[81] Giachino C, et al. Molecular diversity subdivides the adult forebrain neural stem cell population. Stem Cells 2014;32(1):70–84.

[82] Basak O, Taylor V. Stem cells of the adult mammalian brain and their niche. Cell Mol Life Sci 2009;66(6):1057–72.

[83] Ehm O, et al. RBPJkappa-dependent signaling is essential for long-term maintenance of neural stem cells in the adult hippocampus. J Neurosci 2010;30(41):13794–807.

[84] Lugert S, et al. Quiescent and active hippocampal neural stem cells with distinct morphologies respond selectively to physiological and pathological stimuli and aging. Cell Stem Cell 2010;6(5):445–56.

[85] Pastrana E, Cheng LC, Doetsch F. Simultaneous prospective purification of adult subventricular zone neural stem cells and their progeny. Proc Natl Acad Sci U.S.A 2009;106(15):6387–92.

[86] Beckervordersandforth R, et al. In vivo fate mapping and expression analysis reveals molecular hallmarks of prospectively isolated adult neural stem cells. Cell Stem Cell 2010;7(6):744–58.

[87] Suh H, et al. In vivo fate analysis reveals the multipotent and self-renewal capacities of Sox2+ neural stem cells in the adult hippocampus. Cell Stem Cell 2007;1(5):515–28.

[88] Giachino C, Taylor V. Notching up neural stem cell homogeneity in homeostasis and disease. Front Neurosci 2014;8:32.

[89] Doetsch F. A niche for adult neural stem cells. Curr Opin Genet Dev 2003;13(5):543–50.

[90] Shen Q, et al. Endothelial cells stimulate self-renewal and expand neurogenesis of neural stem cells. Science 2004;304(5675):1338–40.

[91] Andreu-Agulló C, et al. Vascular niche factor PEDF modulates notch-dependent stemness in the adult subependymal zone. Nat Neurosci 2009;12(12):1514–23.

[92] Sultan KT, Brown KN, Shi SH. Production and organization of neocortical interneurons. Front Cell Neurosci 2013;7:221.

[93] Bartolini G, Ciceri G, Marin O. Integration of GABAergic interneurons into cortical cell assemblies: lessons from embryos and adults. Neuron 2013;79(5):849–64.

[94] Caputi A, et al. The long and short of GABAergic neurons. Curr Opin Neurobiol 2013;23(2):179–86.

[95] Southwell DG, et al. Interneurons from embryonic development to cell-based therapy. Science 2014;344(6180):1240622.

[96] Gao P, et al. Lineage-dependent circuit assembly in the neocortex. Development 2013;140(13):2645–55.

[97] Muzio L, et al. Conversion of cerebral cortex into basal ganglia in Emx2(-/-) Pax6(Sey/Sey) double-mutant mice. Nat Neurosci 2002;5(8):737–45.

[98] Caric D, et al. Determination of the migratory capacity of embryonic cortical cells lacking the transcription factor Pax-6. Development 1997;124(24):5087–96.

[99] Tarabykin V, et al. Cortical upper layer neurons derive from the subventricular zone as indicated by Svet1 gene expression. Development 2001;128(11):1983–93.

[100] Zimmer C, et al. Dynamics of Cux2 expression suggests that an early pool of SVZ precursors is fated to become upper cortical layer neurons. Cereb Cortex 2004;14(12):1408–20.

[101] Alcamo EA, et al. Satb2 regulates callosal projection neuron identity in the developing cerebral cortex. Neuron 2008;57(3):364–77.

[102] Srinivasan K, et al. A network of genetic repression and derepression specifies projection fates in the developing neocortex. Proc Natl Acad Sci U.S.A 2012;109(47):19071–8.

[103] Rakic P. Evolution of the neocortex: a perspective from developmental biology. Nat Rev Neurosci 2009;10(10):724–35.

[104] Pfeiffer SE, Warrington AE, Bansal R. The oligodendrocyte and its many cellular processes. Trends Cell Biol 1993;3(6):191–7.

[105] Li H, et al. Two-tier transcriptional control of oligodendrocyte differentiation. Curr Opin Neurobiol 2009;19(5):479–85.

[106] Kessaris N, et al. Competing waves of oligodendrocytes in the forebrain and postnatal elimination of an embryonic lineage. Nat Neurosci 2006;9(2):173–9.

[107] Fancy SP, et al. Myelin regeneration: a recapitulation of development? Annu Rev Neurosci 2011;34:21–43.

[108] Spassky N, et al. Sonic hedgehog-dependent emergence of oligodendrocytes in the telencephalon: evidence for a source of oligodendrocytes in the olfactory bulb that is independent of PDGFRα signaling. Development 2001;128(24):4993–5004.

[109] Spassky N, et al. Multiple restricted origin of oligodendrocytes. J Neurosci 1998;18(20):8331–43.

[110] Kanski R, et al. A star is born: new insights into the mechanism of astrogenesis. Cell Mol Life Sci 2014;71(3):433–47.

[111] Sofroniew MV, Vinters HV. Astrocytes: biology and pathology. Acta Neuropathol 2010;119(1):7–35.

[112] Smart IH, et al. Unique morphological features of the proliferative zones and postmitotic compartments of the neural epithelium giving rise to striate and extrastriate cortex in the monkey. Cereb Cortex 2002;12(1):37–53.

[113] Hansen DV, Rubenstein JL, Kriegstein AR. Deriving excitatory neurons of the neocortex from pluripotent stem cells. Neuron 2011;70(4):645–60.

[114] Rakic P. Neurons in rhesus monkey visual cortex: systematic relation between time of origin and eventual disposition. Science 1974;183(4123):425–7.

[115] Kaas JH. The evolution of brains from early mammals to humans. Wiley Interdiscip Rev Cogn Sci 2013;4(1):33–45.

[116] Zecevic N, Chen Y, Filipovic R. Contributions of cortical subventricular zone to the development of the human cerebral cortex. J Comp Neurol 2005;491(2):109–22.

[117] Bayatti N, et al. A molecular neuroanatomical study of the developing human neocortex from 8 to 17 postconceptional weeks revealing the early differentiation of the subplate and subventricular zone. Cereb Cortex 2008;18(7):1536–48.

[118] Lukaszewicz A, et al. G1 phase regulation, area-specific cell cycle control, and cytoarchitectonics in the primate cortex. Neuron 2005;47(3):353–64.

[119] Eiraku M, et al. Self-organized formation of polarized cortical tissues from ESCs and its active manipulation by extrinsic signals. Cell Stem Cell 2008;3(5):519–32.

[120] Gaspard N, et al. An intrinsic mechanism of corticogenesis from embryonic stem cells. Nature 2008;455(7211):351–7.

[121] Eiraku M, Sasai Y. Self-formation of layered neural structures in three-dimensional culture of ES cells. Curr Opin Neurobiol 2012;22(5):768–77.

[122] Eiraku M, Sasai Y. Mouse embryonic stem cell culture for generation of three-dimensional retinal and cortical tissues. Nat Protoc 2012;7(1):69–79.

[123] Espuny-Camacho I, et al. Pyramidal neurons derived from human pluripotent stem cells integrate efficiently into mouse brain circuits in vivo. Neuron 2013;77(3):440–56.

[124] Bershteyn M, Kriegstein AR. Cerebral organoids in a dish: progress and prospects. Cell 2013;155(1):19–20.

[125] Lancaster MA, et al. Cerebral organoids model human brain development and microcephaly. Nature 2013;501(7467):373–9.

[126] Smart IH. Proliferative characteristics of the ependymal layer during the early development of the mouse neocortex: a pilot study based on recording the number, location and plane of cleavage of mitotic figures. J Anat 1973;116(Pt 1):67–91. [AU4]

[127] Tong CK, Alvarez-Buylla A. SnapShot: adult neurogenesis in the V-SVZ. Neuron 2014;81(1):220. 220 e1. [AU5]

[128] Geschwind DH, Rakic P. Cortical evolution: judge the brain by its cover. Neuron 2013;80(3):633–47. [AU6]

[129] Takahashi T, Nowakowski R, Caviness V. Cell cycle parameters and patterns of nuclear movement in the neocortical proliferative zone of the fetal mouse. J Neurosci 1993;13(2):820–33. [AU7]

[130] Takahashi T, Nowakowski RS, Caviness Jr VS. The cell cycle of the pseudostratified ventricular epithelium of the embryonic murine cerebral wall. J Neurosci 1995;15(9):6046–57. [AU8]

[131] McConnell SK. Fates of visual cortical neurons in the ferret after isochronic and heterochronic transplantation. J Neurosci 1988; 8(3):945–74. [AU9]

[132] Dequéant M-L, et al. A complex oscillating network of signaling genes underlies the mouse segmentation clock. Science 2006; 314(5805):1595–8. [AU10]

[133] Bar EE, et al. Hypoxia increases the expression of stem-cell markers and promotes clonogenicity in glioblastoma neurospheres. Am J Patho 2010;177(3):1491–502. [AU11]

[134] Gustafsson MV, et al. Hypoxia requires notch signaling to maintain the undifferentiated cell state. Dev Cell 2005;9(5):617–28. [AU12]

[135] Franklin RJ, et al. Neuroprotection and repair in multiple sclerosis. Nat Rev Neurol 2012;8(11):624–34. [AU13]

[136] Glezer I, Lapointe A, Rivest S. Innate immunity triggers oligodendrocyte progenitor reactivity and confines damages to brain injuries. FASEB J 2006;20(6):750–2. [AU14]

[137] Rhodes K, Raivich G, Fawcett J. The injury response of oligodendrocyte precursor cells is induced by platelets, macrophages and inflammation-associated cytokines. Neuroscience 2006;140(1): 87–100. [AU15]

[138] Wilson HC, Scolding NJ, Raine CS. Co-expression of PDGF α receptor and NG2 by oligodendrocyte precursors in human CNS and multiple sclerosis lesions. J Neuroimmunol 2006;176(1):162–73. [AU16]

[139] Sim FJ, et al. The age-related decrease in CNS remyelination efficiency is attributable to an impairment of both oligodendrocyte progenitor recruitment and differentiation. J Neurosci 2002;22(7):2451–9. [AU17]

[140] Scolding N, et al. Oligodendrocyte progenitors are present in the normal adult human CNS and in the lesions of multiple sclerosis. Brain 1998;121(12):2221–8. [AU18]

Untangling Cortical Complexity During Development

Tanzila Mukhtar and Verdon Taylor [iD]

Department of Biomedicine, University of Basel, Basel, Switzerland.

ABSTRACT: The cerebral cortex is composed of billions of morphologically and functionally distinct neurons. These neurons are produced and organized in a regimental fashion during development. The ability of neurons to encode and elicit complex cognitive and motor functions depends on their precise molecular processes, identity, and connectivity established during development. Elucidating the cellular and molecular mechanisms that regulate development of the neocortex has been a challenge for many years. The cerebral cortical neuronal subtypes are classified based on morphology, function, intrinsic synaptic properties, location, connectivity, and marker gene expression. Development of the neocortex requires an orchestration of a series of processes including the appropriate determination, migration and positioning of the neurons, acquisition of layer-specific transcriptional hallmarks, and formation of precise axonal projections and networks. Historically, fate mapping, genome-wide analysis, and transcriptome profiling have provided many opportunities for the characterization of neuronal subtypes. During the course of this review, we will address the regimental organization of the cerebral cortex, dissect the cellular subtypes that contribute to cortical complexity, and outline their molecular hallmarks to understand cellular diversity in the cerebral cortex with a focus on the excitatory neurons.

KEYWORDS: Brain development, neural stem cells, neurogenesis, cerebral cortex

Neuroepithelium to Neural Stem Cell Transition and Beyond

Early during vertebrate embryonic development, neural fate is induced in the ectoderm.[1] The consequent patterning of the neural plate results in the formation of the central nervous system. The process of neurulation induces formation of the neural tube, a pseudostratified epithelial sheet of neuroepithelial cells (NEPs). It is the NEPs that are the precursors of the central nervous system including cerebral cortex, which is formed over an extended period of development. Important biological questions remain about how the complex structure of the cerebral cortex, which is composed of diverse neuron subtypes, is generated from a simple epithelial sheet of cells to form the most complex tissue of the body. At embryonic day 9 (E9), the neuroepithelium gives rise to neural stem cells (NSCs) that line the luminal surface of the vesicles of the neural tube.[2,3] In mice, NSCs are located in the ventricular zone (VZ) and the ends of their basal processes remain in contact with the outer (pial) surface of the neural tube. This apical-basal polarity, which spans the thickness of the neural tube, requires the integrity of adherens junctions to segregate the apical and basolateral cell membrane and adhere neighboring NSCs to each other. The importance of adherence in NSC polarity is exemplified by the knockdown of the adherens junction–associated protein Afadin (Af6). Af6 depletion leads to a loss of adherens junctions and disturbed cell polarity.[4]

At the onset of neurogenesis, the NEPs generate radial glial cells (RGCs) and short neural precursors.[5,6] The somata of these cells remain within the VZ but migrate radially along the apical-basal process through the zone during cell division in a process referred to as interkinetic nuclear migration (INM).[3,7–9] The location of the soma within the VZ is cell cycle dependent. During M-phase, the cell body is positioned apically at the luminal surface of the neural tube (Figure 1). As the cell progresses through G1-phase of the cell cycle, the cell body moves radially to the VZ boundary with the overlying subventricular zone (SVZ) and forming cerebral cortex. S-phase and DNA replication occur at the basal boundary of the VZ followed by migration of the cell body back to the luminal surface of the neural tube during G2 to initiate mitosis.[7,10,11] Primary cilia in the apical membrane project into the vesicles and detect factors and signals in the fluid filling the neural tube and these support apical-basal polarity. The orientated cell polarity is important for determining the structure of the cerebral cortex. Disruption of the small GTPase, ADP ribosylation factor–like GTPase 13B (Arl13b), results in loss of cell polarity and the cortical wall is generated in an inverted fashion. M-phase of Arl13b-deficient RGCs is no longer restricted to the luminal surface but also occurs at the basal, pial surface and neurons migrate centripetally to the VZ.[12]

During early phases of neurogenesis, embryonic days 10.5 to 11.5 (E10.5-11.5) in mice, NSCs undergo symmetric stem cell divisions, expanding the pool (Figure 1). This is referred to as the "neural expansion" phase of cortical development. Later, NSCs progressively undergo asymmetric cell divisions, allowing for both self-renewal and the generation of committed daughter cells (Figure 1). The transition from symmetric stem cell to asymmetric neurogenic divisions during neurogenesis is
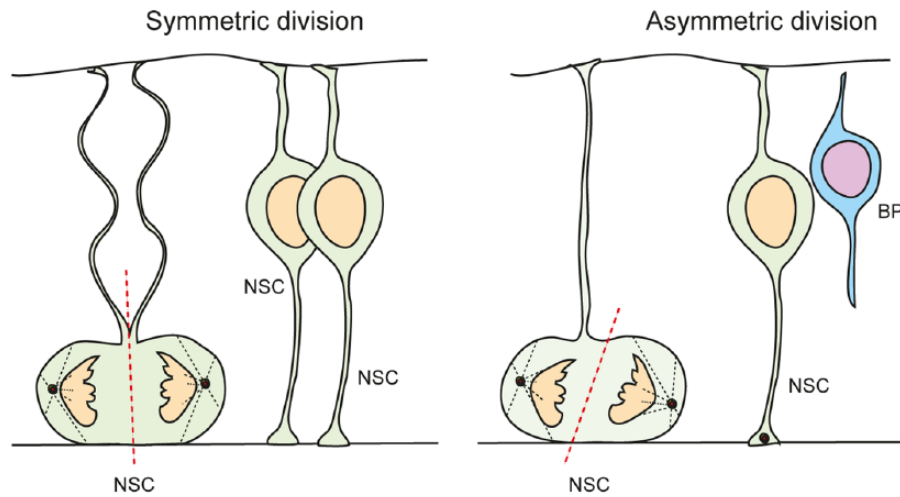
Figure 1. Types of NSC divisions in the ventricular zone are determined by spindle orientation and the inheritance of cell fate determinants. Symmetric divisions generate 2 NSCs, whereas asymmetric division generates 1 NSC and 1 differentiating daughter cell. During neural expansion, most divisions are symmetric, whereas during neurogenesis, most divisions are asymmetric. BP indicates basal progenitor; NSC, neural stem cell.

associated with a lengthening of primarily G1-phase of the cell cycle. However, the S-phase of the NSCs in the symmetric dividing, expansion phase is longer than of those in the asymmetric dividing neurogenic phases.[7,13] Hence, although the precise function of INM and the changing in cell cycle phase length are not understood, it seems that they play an important role on the control of the sequential switching of NSCs from a symmetric self-renewing mode to the asymmetric division mode that drives the production of neurons.

During the neurogenic phase of cortical development, the self-renewal and generation of committed daughter cells have to be tightly controlled. Loss of self-renewing NSC daughter cells would purge the stem cell pool. Conversely, a failure to generate sufficient neuronal-determined precursors would severely affect neuronal composition and cortical layering. During early stages of cortical development, some asymmetric stem cell divisions generate one NSC daughter and a neuron directly. This is referred to as direct neurogenesis. However, as neurogenesis progresses, the daughter cell that is committed to differentiate and leaves the stem cell pool becomes a basal progenitor (BP) and migrates to the forming SVZ (Figure 1).[7,13,14]

Distinct Stem and Progenitor Populations Contribute to Cortical Development

Throughout neurogenesis, another VZ population of dividing cells called the short neural precursors contributes to the progenitor pool. Short neural progenitors have either a short or no basal process at all but retain the apical process and contact to the lumen of the neural tube. These cells are morphologically, ultrastructurally, and molecularly different from the NSCs and have been observed to undergo direct neurogenesis, generating neurons without passing through a BP state.[5]

In higher mammals including ferrets, primates, and humans, additional intermediate progenitor populations have evolved, and although they also reside in the SVZ, they have different morphologies and larger cell fate potentials compared with the classic BPs in mice.[6,15,16] In fact, in primates, some of these intermediate progenitors even display NSC potential and are even referred to as outer RGCs (oRGCs).[16] The oRGCs are morphologically distinct, unipolar, and retain only the basal process with no connection to the VZ and neural tube lumen (Figure 2).[16–18] They also do not express the apical membrane constituents associated with VZ NSCs and RGC including prominin1 (CD133), Par3 family cell polarity regulator (Par3), or atypical protein kinase Cλ (aPKCλ).[15] They have a long basal phospho-Vimentin (pVim)-positive process that extends toward the pia and retain the basal fiber throughout the duration of cell cycle.[10] Similar to VZ RGCs, the soma of oRGCs also moves during cell divisions but this movement is distinct to the INM of VZ NSCs. The soma of oRGCs moves basally and once translocation is complete, they divide mostly by self-renewing, asymmetric divisions, and push the boundary of the outer SVZ (OSVZ) outward expanding the SVZ (Figure 2).[16,19] Self-renewing oRGCs continue to proliferate, whereas the daughter cells differentiate into neurons.

These SVZ progenitors in primates are the major source of expansion and neurogenesis in the cerebral cortex and are responsible for the massive evolutionary expansion of the cortical gray matter, neuron number, and cortical surface. Indirectly, these SVZ progenitors are responsible for the increase in functional capacity of the cerebral cortex in primates.[20] The coexistence of oRGC cells and VZ RGCs demonstrates the distinct germinal zones in higher mammals, highlighting the mechanisms of increased neuron production, relevant for the formation of bigger brains (Figure 2). Here, we will focus on cortical development in the mouse and refer to excellent review focusing on primate and human cortical development.[10]

Basal progenitors are intermediate, transient amplifying cells that undergo 1 or 2 divisions before giving rise to neurons (Figure 2). The BPs are in one of the main zones of amplification
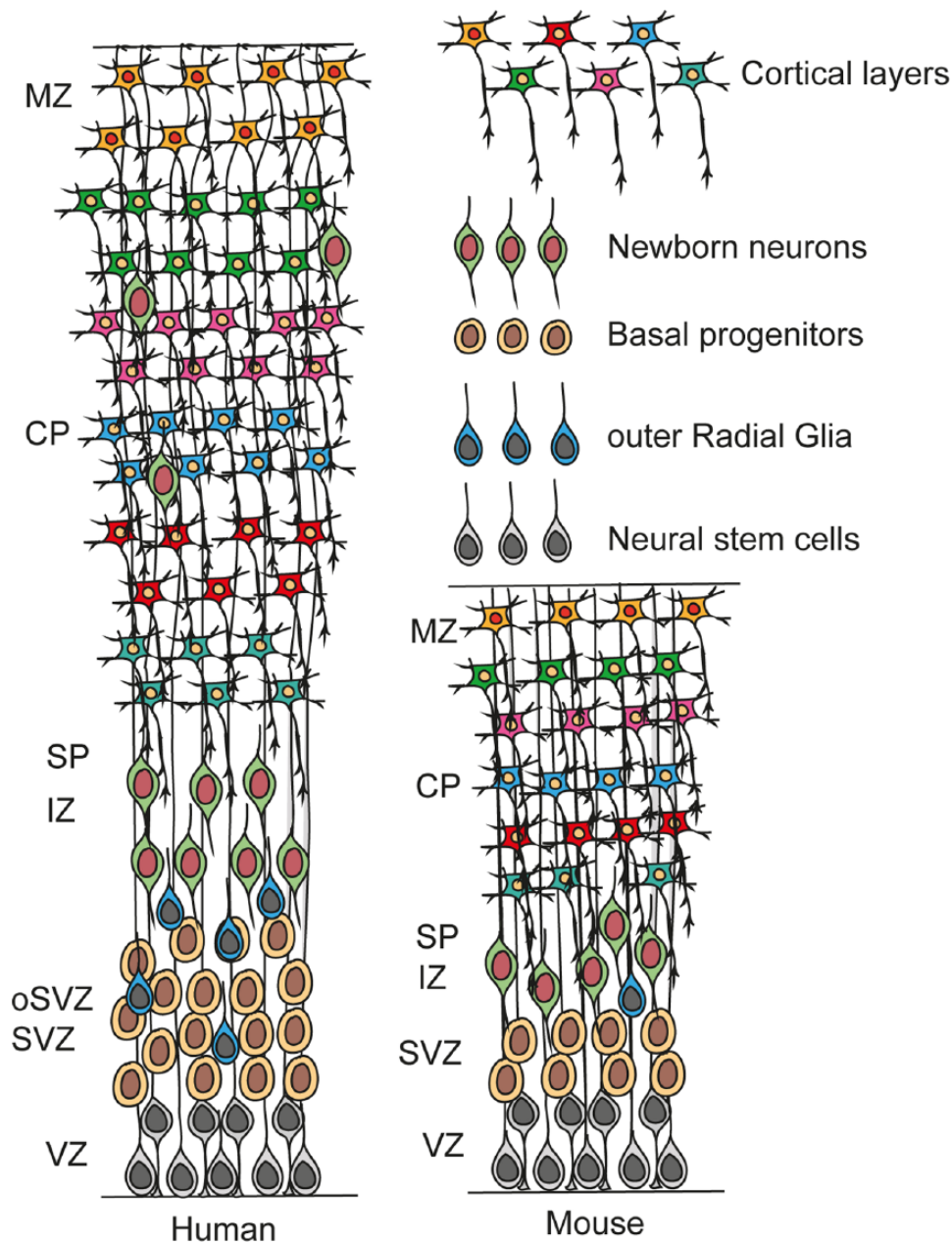
Figure 2. Scheme illustrating the composition and laminar organization of the developing human cortex, in comparison with mouse cortex. The human cerebral cortex develops in a similar fashion to that of the mouse. One exception is the expansion of the subventricular zone (SVZ) to form the outer SVZ (oSVZ). The oSVZ in humans is the main zone of amplification. In addition to the neural stem cells (NSCs) and basal progenitors (BPs) of the developing mouse cerebral cortex, the human has addition progenitors, outer radial glial cells. CP indicates cortical plate; IZ, intermediate zone; MZ, marginal zone; SP, subplate; SVZ, subventricular zone; VZ, ventricular zone.

and neurogenesis in the developing mouse cortex. As neurogenesis reaches completion, the NSCs start to generate other cell lineages, oligodendrocytes, astrocytes, and ependymal cells.[21,22] This is referred to as the "gliogenesis phase" of cortical development. The transition from neurogenesis to gliogenesis is associated with a downregulation of the Golgi-derived apical trafficking and VZ NSCs lose tight junctions while keeping intact the adherens junctions.[23,24] This is followed by the gradual expression of the astroglial hallmarks including glial fibrillary acidic protein (GFAP) in the mouse.[22,24–26] Although the mechanisms of the neurogenic to gliogenic phase transition are

not clearly understood, Notch signaling and its downstream targets, the bHLH (basic helix-loop-helix) transcription factors including the Hes proteins, and the growth factor Fgf10 are necessary for this transition.[27–29]

Because the generation of neurons from BPs results in the expansion of the neuronal progenitor pool enabling the production of many neurons from a restricted population of NSCs, their role is crucial in the expansion of the cortex.[28,30,31] In the mouse, BPs can undergo symmetric divisions and generate 2 neuronal daughter cells.[31] However, evidence suggests that some, if not all, may also undergo 1 or 2 rounds of self-renewing

cell divisions.[28,30,31] Basal progenitors are defined based on their position in the SVZ, their lack of polarized morphology and expression of the transcription factors, Eomesodermin (Eomes or Tbr2), Btg antiproliferation factor 2 (also called Tis21), Cut-like homeobox 1/2 (Cux1/Cux2), and special AT-rich sequence binding protein (Satb2) and the non-coding RNA Svet1.[32–37] Because the different progenitor cell types are localized to different niches and thus likely exposed to different combinations of cues from their microenvironment, it is imperative to study the role of their niche in controlling their proliferation and fate commitment. This cellular heterogeneity requires a deeper understanding of the cell fate identities and commitments.[6]

Symmetric and Asymmetric Cell Divisions

Neural stem cells of the developing cerebral cortex display multiple modes of cell division. Initially, the major form of divisions is symmetric stem cell divisions, generating 2 daughter cells that retain stem cell potential and reenter cell cycle. As development progresses, the stem cell divisions are slowly superseded by asymmetric neurogenic divisions where 1 daughter remains a stem cell and reenters the cell cycle within the VZ, whereas the other is committed to differentiate and will leave the VZ (Figure 1). The third mode is the symmetric neurogenic division where both daughter cells will differentiate thereby depleting the stem cell pool. The balance between these different forms and outcomes of cell division are temporally and spatially regulated which is necessary to control correct cortical development.

The molecular basis of symmetric and asymmetric divisions and the transition from self-renewing to differentiating modes of cell division are not understood. It has become clear that the orientation of the mitotic spindle plays an important role in the type of division and the fate of the respective daughter cells generated (Figure 1). A cleavage plane bisecting the apical membrane of the NSCs, including inheritance of junctional complexes by both daughters, contributes heavily to maintenance of stem cell potential (Figure 1). During symmetric divisions of NSCs, the cleavage plane is oriented perpendicular to the ventricular surface (Figure 1).[38] This spatial organization of the mitotic spindle requires a proper centrosome assembly, duplication and a precise interaction between planar cell polarity components, G protein signaling modulator 2 (Lgn), and Inscuteable (Insc).[13,39–41] The partition of cell components involved in cell polarity, including the Par3 family cell polarity regulator (Par3/Par6), proteins between daughter cells is critical for differential cell fate determination. In symmetric stem cell divisions, the basal process is equally split between the daughter cells (Figure 1).[42,43] The transcription factor empty spiracles homologue 2 (Emx2) is expressed by NSCs of the VZ and promotes perpendicular cleavage plane thereby promoting symmetric expansive cell divisions.[44] Forced Emx2 expression in NSCs during cortical development increases clonal expansion and symmetric cell divisions.[44]

During asymmetric cell divisions, the cleavage plane is orientated parallel to the neural tube luminal surface (Figure 1).

This results in an unequal partition of Par3 into the 2 daughter cells, and the sibling cell receiving less Par3 protein exits cell cycle and differentiates.[42,43] In addition, asymmetric cell division is accompanied by an unequal distribution of fate determinants between the daughter cells. These components include mediators of Notch signaling, the Notch ligand delta-like 1 (Dll1), Mind bomb, and Numb.[45,46] Segregation of Notch components including inhibitors of the pathway leads to differential Notch signaling between daughter cells. Notch signaling plays a critical role in NSC maintenance and differentiation by regulating cell proliferation and fate determination.[45,47,48] Notch activates the expression of *Hes* genes which encode bHLH transcriptional regulators. Hes-related proteins repress expression of the proneurogenic transcription factors including neurogenins (Ngns) and Ascl1.[49,50] Thus, activation of Notch signaling inhibits differentiation of NSCs by suppressing transcription factors required for neurogenesis.[48] In addition, Notch signaling regulates cell cycle progression via regulation of Ascl1 expression. Ascl1 not only controls neurogenic differentiation but is also involved in entry of NSCs into cell cycle.[51,52]

In addition to Notch, some cytoplasmic proteins show differential distribution on asymmetric division. Staufen is a double-stranded RNA–binding protein which is pivotal in asymmetric cell fates in *Drosophila* neural development. Staufen is selectively segregated into the differentiating daughter cells on asymmetric self-renewing cell division.[53] Staufen binds messenger RNAs that encode proteins crucial in cell cycle exit and differentiation. Furthermore, the transcription factor Pax6 promotes asymmetric neurogenic cell division.[54] Pax6-mutant NSCs show a defective cell cycle exit and an increase in self-renewing capacity.[54]

In addition to molecular segregation, the orientation of the mitotic spindle plays an important role in fate determination. In NSCs, the mitotic spindle poles oscillate around their final positions before anaphase is initiated. This dynamic movement of the spindle seems to be important in determining the cleavage plane and then the segregation of intracellular components. Only subtle changes in spindle orientation can cause major shifts in the plane of cytokinesis and thereby the inheritance of membrane compartments and cell fate determinants.[55] Mutations in the abnormal spindle-like microcephaly-associate (*Aspm*) gene severely affect cerebral cortical size and reduce the volume of the cerebral cortex in primates.[56] Aspm is important for spindle orientation and control in the division modes of symmetric versus asymmetric cells.

Inheritance of the apical plasma membrane of NSCs has an influence on cell fate. During symmetric cell divisions, both daughters acquire apical membrane and junctional components. When only 1 daughter cell inherits the apical plasma membrane, for example, when the cleavage plane is parallel to the neural tube luminal surface, that daughter remains as an NSC, whereas the other sibling that does not receive apical
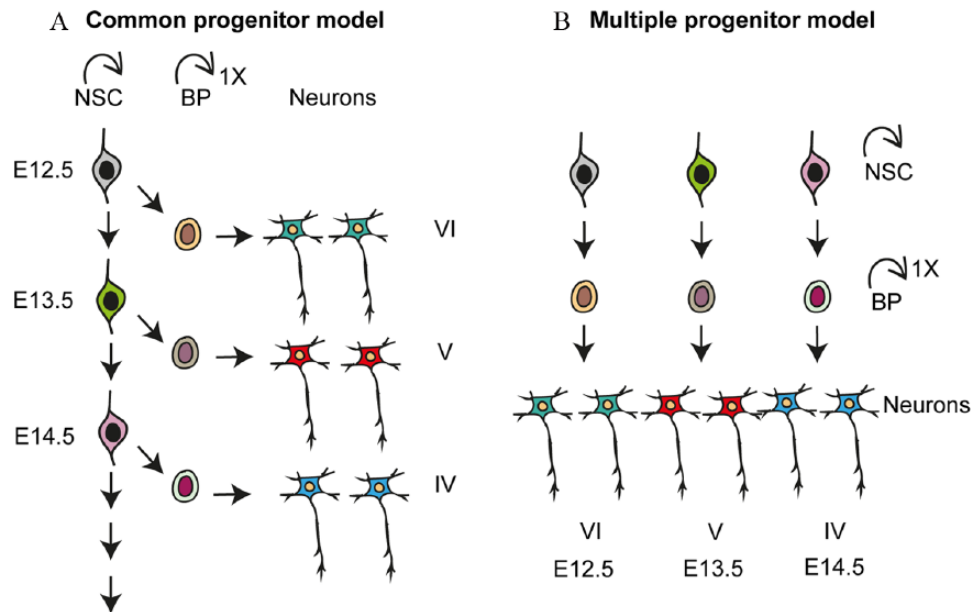
Figure 3. Different models of neuronal subtype specification in developing neocortex. (A) In the common progenitor model, a single type of multipotent NSC sequentially gives rise to all neuronal subtypes during the course of development. Overtime, the fate potential of this NSC becomes increasingly restricted. Fate of the neuron is specified based on its birth date. (B) In the multiple progenitor model, multiple types of NSCs coexist and are, to some degree, predetermined to give rise to specific and restricted neuronal subtypes. Fate of the neuron is specified by the NSC type in this model. BP indicates basal progenitor; NSC, neural stem cell.

membrane and adherens junctions from the mother cell will exit the VZ and commit to differentiation. The SNARE-mediated membrane fusion machinery controls NSC fate specification. A hypomorphic missense mutation in α-SNAP (α-soluble *N*-ethylmaleimide-sensitive fusion protein [NSF] attachment protein) causes NSCs to prematurely switch from symmetric proliferative to asymmetric neurogenic divisions.[57] This is primarily due to an impaired apical protein localization affecting the Golgi-derived membrane traffic necessary for NSC proliferation.[58] In addition, NSCs in these mice show distribution of apical β-catenin along the adherens junctions and phenocopying of conditional β-catenin null mutant mice. Hence, β-catenin plays a role not only in the control of cell cycle but also in the choice between symmetric and asymmetric divisions.[59,60]

Regulation and Cell Fate Commitment

The stem and progenitor cells in the dorsal VZ of the anterior neural tube generate the multiple classes of projection neurons that make up the future cerebral cortex in sequential waves. In the dorsal cerebral cortex, neurogenesis commences around E10.5 in mice.[25,26] The earliest born neurons segregate from the NSCs in the VZ and migrate radially to the pial surface forming the preplate. Later born neurons migrate into the pre-plate, splitting it into the marginal zone and the subplate (Figure 2). Throughout neurogenesis, newborn neurons migrate into the cortical plate (CP), through the preformed layers of earlier born neurons, and as such the early born neurons form the deep layers and the later born neurons form upper layers. The detailed molecular cascade that determines

neuronal cell fate commitment, an excitatory neuron subtype specification, is largely unknown. Different models have been proposed to explain the temporal dynamics of neuronal specification in the dorsal cortex.[61] The "common progenitor model" implies that a single type of NSC sequentially gives rise to the different neuron subtypes overtime during neurogenesis and that neuron fate is determined by time (Figure 3A). According to the "multiple progenitor model," multiple stem cell types coexist and are predetermined to generate specific neuron subtypes.[62] In the multiple progenitor model, the fate of the stem cell and the type of neuron generated are determined by the NSC type (Figure 3B). There is experimental evidence supporting both models.[23,63]

The Common Progenitor Model

McConnell demonstrated that NSC fate becomes restricted over time during development.[64] By performing elegant hetero-chronic transplantation experiments initially in ferrets, they demonstrated that early developmental stage progenitors have a greater potential and can generate early and late neuronal subtypes when grafted into hosts. Conversely, late-stage progenitors have a more restricted potential and a reduced capacity to form early neuronal types in host embryos.[64] This implies that NSCs lose their potential to generate deep layer neurons with time.[64–66] In support of this model, clonal in vitro experiments showed the sequential generation of deep and upper layer neurons from NSCs supporting initial multipotency and subsequent fate restriction over time.[64,67–69] Finally, retroviral labeling and lineage tracing of individual NSCs supported progressive fate restriction in vivo.[70] More recently, genetic labeling
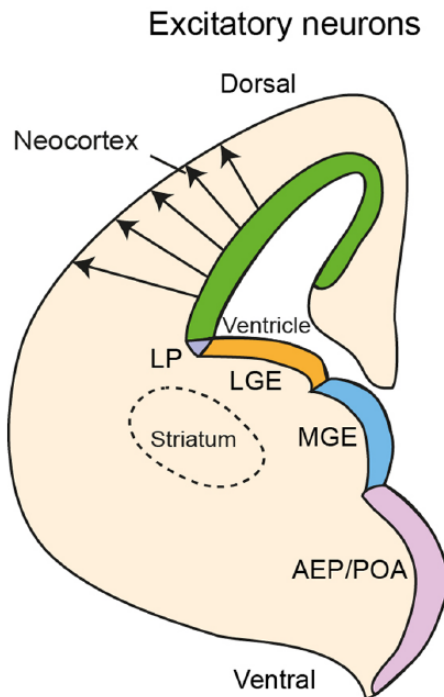
Excitatory neurons

Figure 4. Origin of excitatory projection neurons of the cerebral cortex. Excitatory projection neurons originate from the ventricular zone of the dorsal telencephalon and migrate radially to the cortical plate. Inhibitory interneurons originate from the ventral telencephalon, especially from the MGE, AEP/POA.[76,77] AEP/POA indicates anterior entopeduncular area of the subpallium/preoptic area; LGE, lateral ganglionic eminence; LP, lateral pallium; MGE, medial ganglionic eminence.

in the developing mouse cerebral cortex following expression of the transcription factor Fezf2 (enriched in deep cortical layer V neurons) revealed that Fezf2-expressing NSCs generate deep, upper layer neurons and glial cells.[63,71,72] Instructive roles of factors such as Fezf2 in NSCs can have major implications in cell fate commitment during neurogenesis. Ectopic expression of Fezf2 can direct NSCs to differentiate into deep layer neurons and reverse late fate commitment.[63,73]

The Multiple Progenitor Model

An alternative model for fate specification proposes independent, fate-restricted lineages of NSC that generate specific neuronal subtypes and have limited potentials (Figure 3B). Evidence suggests that many transcription factors expressed during cortical development instruct fate determination.[72] The onset of expression of these transcription factors was proposed to coincide with the developmental time point at which specific neuronal subtypes are determined, indicative of the presence of predetermined NSC subtypes.[62] Analysis of transgenic mice revealed that Cux1 and Cux2 are expressed in VZ and SVZ as early as E10.5, primarily in specific and fate-restricted NSCs. Genetic tracing of Cux1-positive progenitor cells mostly generated upper layer neurons.[23,74] During early development, Cux1- and Cux2-positive NSCs undergo expansion and do not contribute to early layer neuronal

differentiation.[23,74] These seem to be restricted in fate while they undergo neurogenesis and produce only upper layer neurons. Conversely, follow-up experiments analyzing Cux2-positive cells by lineage tracing elucidated their role in generating both deep and upper layer neurons as well as the interneurons from the ventral telencephalon.[63,66]

Other experiments imply the coexistence of multipotent NSCs and their consequent fate restriction through the course of neurogenesis.[23,75] It is possible that cells can be more restricted in their potential and change to alternate fates when subjected to different extrinsic cues. This may explain the switch between multipotent to restricted NSC states. Because the precise structure of the lineage trees for specific neuronal subtypes remains largely unknown in vivo, single-cell clonal analysis to identify markers of clusters of NSCs may contribute to this understanding of cell fate commitment. Both the "common and multiple progenitor models" do not negate the possibility of the other, and future high-resolution experiments are needed at the single-cell level to address NSC heterogeneity and dynamic potential.

Neuronal Diversity and Transcriptional Dynamics in Cortical Layering

The cerebral cortex is an isocortex composed of 6 clearly defined layers. The newborn excitatory neurons migrate out of the VZ along the radial processes of the NSCs (Figures 4 and 5). The immature neurons reach the CP by migrating through their earlier born siblings. On reaching the pial surface, the immature neurons leave the RGC process and differentiate and form neurons of their specific cortical layer. Hence, the isocortex of the cerebrum is formed in an inside-out fashion, with early born neurons forming the deep layers while the later born neurons generating the upper layers (Figure 5). The neuronal type and their location within the isocortex are critical for function. The interneurons of the cerebral cortex originate from the ventral telencephalon and migrate to their final destination in the cerebral cortex (we refer the reader to excellent recent reviews on cortical interneuron development and will not cover the topic here).[76,77]

The major types of cortical projection neurons can be defined by their connectivity and projection patterns depending on whether they project through associative, commissural, and corticofugal projection fibers. Associative projection neurons project their axons within a single cerebral hemisphere connecting local areas or proximal gyri. Commissural, callosal projection neurons are localized primarily in layers II/III, V, and VI of the 6-layered isocortex. They extend their axons from 1 hemisphere to neurons in the contralateral hemisphere. The axons project through the corpus callosum, the major commissural connection between the hemispheres, or through the anterior or posterior commissures. The commissural neurons are further subdivided based on the projection destinations.[72] Corticofugal neurons include the subcerebral neurons,
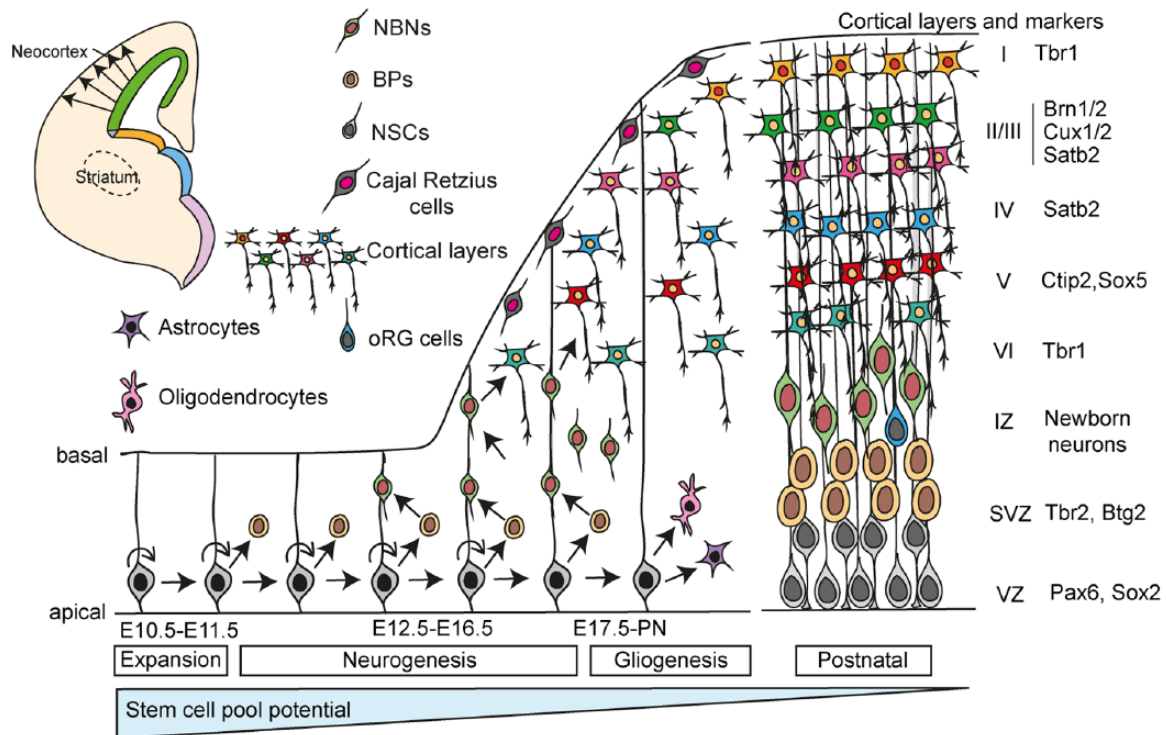
Figure 5. Systematic formation of isocortex layers in the dorsal telencephalon. During early stages of cerebral cortical development (embryonic days E10.5-E11.5), NSCs predominantly undergo symmetric cells divisions to expand the NSC pool. This phase is referred to as the expansion phase. The first neurons to be formed are generated by direct neurogenesis of the NSCs. The Cajal-Retzius cells populate layer I of the isocortex and play important roles in establishing cortical architecture. During late embryogenesis (E12-E16.5), NSCs undergo increasingly more asymmetric divisions to generate 1 NSC (self-renewal) and 1 BP. The BPs generate the neurons. This is the neurogenic phase. Neurons are generated in a sequential, inside-out fashion and are specified by different transcription factors, some of which are shown. At later stages of development, NSCs generate the other cell types of the brain including astrocytes, oligodendrocytes, and ependymal cells (not shown). This is referred to as the gliogenic phase. The potential of the NSC pool reduces over time during development. This does not exclude that multiple restricted stem cells become activated and are lost at different times during cortical development. BPs indicate basal progenitors; IZ, intermediate zone; NBNs, newborn neurons; NSCs, neural stem cells; SVZ, subventricular zone; VZ, ventricular zone.

which are the largest pyramidal neurons and extend projections to subcortical structures including the brainstem and spinal cord. The corticofugal projections include corticopontine, corticospinal, and corticotectal neurons.[78] Another subtype of corticofugal neurons is the corticothalamic neurons, which populate the layer VI of the isocortex with a small population in layer V and extend their projections to different nuclei of the thalamus.[72]

Hence, the regulation of neuron subtype formation and the temporospatial control of neurogenesis are critical for brain function. Numerous neocortical determinants are expressed along the dorsolateral wall of the cortex, on the induction of neurogenesis. Key factors including forkhead box G1 (FoxG1), LIM homeobox 2 (Lhx2), Emx2, and Pax6 define and control the neocortical progenitor domains along the dorsal and ventral axis.[24,72] Ablation of the dorsal progenitor domain determinants Pax6 and Emx2 results in expansion of the ventral domains.[79] Pax6 and T-cell leukemia homeobox (Tlx) regulates the cell fate decisions in the VZ and the loss of function of these factors leads to a thicker superficial cortex. Hence, the NSCs and progenitors of the cerebral cortex are determined by their expression of axial-specifying factors but these fates are

not fixed or restricted as loss of these determinants results in alternate fate acquisition.[72]

The transcription factors Tbr1, Ctip2, Sox5, Fezf2, Satb2, Cux1, Cux2, Brn1, Brn2, and others have been studied extensively and determined to be key determinants of neuronal specification.[7,10,23,32,33,35,62,63,71,73] These transcription factors are often used as markers of specific cortical neuron populations and layers and are expressed in waves during cortical development. Some of these markers are expressed in specific neuronal subtypes within a layer or are expressed in more than one neuronal subtype and layer. For example, the Ets-related protein 81 (Er81/Etv1) is expressed in cortico-cortical and subcerebral projection neurons of layer V.[80] Conversely, LIM domain only 4 (Lmo4) is selectively expressed in callosal neurons of layers II/III.

Some of these fate-determining and defining factors seem to be coexpressed initially and their expression becomes restricted and refined later in neuronal differentiation. For example, in mice, postmitotic deep layer neurons coexpress Ctip2 and Satb2 at E13.5.[35,72,81] As development progresses, these deep layer neurons express either Ctip2 or Satb2 and become fate restricted to form subcerebral projection neurons

or corticothalamic projection neurons, respectively.[35,72,82,83] Ngn1 and Ngn2 are 2 proneural transcription factors and induce neurogenesis; however, Tbr1- and Er81-expressing deep layer neurons are still generated in their absence.[84,85] It is likely that other proneural transcription factors are able to compensate for the loss of Ngns but the exact mechanism remains to be defined.

Epigenetic and Transcriptional Interplay During Neurogenesis

The gene expression in NSCs regulated not only by transcription factors but also by epigenetic mechanisms. DNA methylation and histone modifications are involved in spatial and temporal gene expression during neurogenesis and the switch from neuronal to glial fate.[86–88] New methods for genome-wide methylation mapping facilitates investigation of epigenetic landscapes that control lineage commitments and fate decisions during neuronal specification. Epigenetic regulation of critical transcription factors in NSCs play important roles in the regulation of cell fate and neurogenesis. The expression of epigenetic regulators including the high-mobility group (HMG) proteins during early phases of cortical development regulate chromatin state and methyltransferase activity including enhancer of zeste 2 polycomb repressive complex 2 subunit (Ezh2).[86–88] This suggests that the chromatin in early NSCs is in a more "open" state than that of later NSCs.[87] The transcription factor Tbr2, which is critical for BP generation and differentiation, associates with the histone demethylase Jmjd3 (also called Kdm6b). Tbr2 directs Jmjd3-dependent chromatin remodeling to specific gene loci promoting the removal of H3K27me3 chromatin marks.[89] This emphasizes the additional level of control that Tbr2 has on neuronal specification by regulating the epigenetic marks at specific promoter and enhancer sites.[89]

Hes5 is a pivotal mediator of Notch signaling and inducer of maintenance of NSCs by blocking proneural transcription factor expression. However, the expression of Hes5 also depends on glial cell missing homolog (Gcm) and active DNA demethylation during neurogenesis.[90] Loss of Gcm prevents upregulation of Hes5 and the formation of definitive NSCs between E7.5 and E8.5.[90] Pax6 interacts with BAF155 and BAF170, components of the ATP (adenosine triphosphate)–dependent multi-subunit mSWI/SNF nucleosome remodeling complexes in NSCs. At the onset of neurogenesis, BAF155 and BAF170 compete and modify euchromatin structure.[91,92] This leads to the recruitment of the Pax6/RE1 silencing transcription factor (REST)-corepressor complex to the Pax6 targets, transducin-like enhancer of split 1 (Tle), Eomes, and Cux2, and repressing their expression. This prevents the formation of BPs and late NSCs.

During peak of neurogenesis, the chromatin remodeler sucrose nonfermenting–like protein 1 (Snf2l) represses expression of FoxG1, which leads to the derepression of the cell cycle regulator p21 and promotes neuronal differentiation by inducing cell cycle exit.[91,92] During later stages of neurogenesis, the polycomb proteins repress Ngn1 expression to trigger the NSC fate switch from neurogenesis to astrogliogenesis.[86] The NSC switch to gliogenesis is associated with the expression of the astrocytic protein GFAP. DNA methylation of the *Gfap* promoter prevents its premature activation. Notch signaling induces demethylation of the *Gfap* promoter through the transcription factor nuclear factor I (NFI), by dissociating associated DNA methyltransferases and thereby supports generation of astrocytes.[28,93,94] Further analysis of the interplay between epigenetic and transcriptional dynamics during cortical development may contribute to a greater understanding of novel mechanisms and dysregulation during brain disorders.

Signaling Dynamics During Neurogenesis

Various signaling pathways impinge on downstream effectors and regulate NSC fate decisions during neurogenesis. Among these pathways are Notch, Wnt, Shh, fibroblast growth factors (FGFs), transforming growth factor β (TGF-β), retinoic acid (RA), and Hippo. How the cross talk between these signaling pathways and the integration of their signals on target genes governs complex cell fate choices is unclear.

Notch was first discovered in *Drosophila*, and the signaling pathway is evolutionarily highly conserved.[95] It plays critical roles in NSC maintenance and differentiation. Conditional loss of Notch receptors results in the precocious differentiation, impaired survival, and aberrant migration of NSCs.[45,48] Notch signaling regulates neurogenesis through lateral signaling between neighboring cells. In the presence of Notch ligands, delta-1 (Dll1) and Jagged1 (Jag1), the receptor is cleaved at S2 and S3 sites by ADAM metallopeptidase domain 10 (ADAM10) and γ-secretase, respectively.[96,97] This results in the release of the Notch intracellular domain (NICD). The NICD has nuclear localization signals and mediates the transcription of *Hes* genes via DNA-binding factor recombination signal-binding protein for immunoglobulin kappa J region (RBPJ) complex.[46,98] On interaction of NICD with RBPJ, the preformed repressor complex on target genes is disrupted and replaced by a coactivator complex including mastermind-like protein-1 (Maml) and histone acetyltransferase (HAT, p300). These changes facilitate the recruitment of RNA polymerase II and initiate transcription of target genes including *Hes1* and *Hes5*.[99] The Hes factors in turn downregulate expression of the genes encoding the proneural bHLH factors Ngn and Achaete-Scute family BHLH transcription factor 1b (Ascl).[100,101] Hence, active Notch signaling maintains NSCs in a proliferative state and represses differentiation in the mammalian brain.[49,101,102] The expression of Hes1 and Hes5 oscillates in the VZ due to an auto-inhibitory feedback loop.[28,103] The oscillations in the expression of the Hes factors in turn induce oscillatory expression of proneural factors.[50,97,104] This dynamic expression seems to be critical in modulating the functions of

the proneural transcription factors in controlling proliferation and neurogenic differentiation.[49,101,102] Although the source of Notch ligands is not clear, NSCs, BPs, and newborn neurons express Deltas and Jaggeds as well as the E3 ligase Mind bomb that potentially promote Notch signaling in the NSCs.[105,106]

Wnt signaling is involved in the patterning and development of many tissues including the nervous system.[107,108] Wnt1 and Wnt3a are expressed by cells at the dorsal midline of the developing neural tube. In the absence of Wnt1, midbrain structures fail to form and Wnt3a-mutant mice do not form a hippocampus likely due to the reduced proliferation of hippocampal precursors.[109] Wnt ligands bind the receptor complex Frizzled/LRP5/6 leading to stabilization of cytoplasmic β-catenin. β-catenin translocates to the nucleus and binds to target genes via LEF/TCF factors and recruits histone acetyltransferases.[110] Transgenic overexpression of β-catenin induces enhanced proliferation of cortical neural progenitors leading to an increase in cortical neurons and surface area.[111] During early neurogenesis, Wnts play an active role in symmetric divisions, whereas later, during neurogenesis, Wnts are implicated in neuronal differentiation through expression of N-myc, which in turn represses the Notch signaling.[108] Wnt signaling can also induce the expression of Ngn1 and NeuroD1 thereby counteracting Notch signaling and promoting neuronal differentiation.[86,108] Thus, Wnt and Notch compete to regulate proneural gene expression and the maintenance and differentiation of NSCs. The differential dynamics of signaling pathways impinging on same or different downstream effectors could be cell type or phase specific.

Fibroblast growth factor signaling has been long known to be involved in area specification in the brain.[111] Many Fgfs are expressed in the developing cerebral cortex. Fgf3, 8, 15, 17, and 18 are expressed along the rostral midline of the neocortex in the commissural plate between E9.5 and E12.5, suggesting the presence of a rostral, Fgf-secreting signaling center.[112] The Fgf signals play important roles in anterior-posterior patterning of NSCs and promote proliferation.[113,114] In addition, Fgf signaling can regulate *Hes1* transcription thereby synergizing with and promoting Notch signaling. Fgf18 is expressed in the CP between E13.5 and E16.5, although its role remains unclear.[114] Three of the classical receptor tyrosine kinase Fgf receptors (Fgfr1-3) are expressed by NSCs.[113,115] Fgfr1 is expressed higher by rostral NSCs than caudal NSCs, whereas Fgfr2 and Fgfr3 are expressed higher caudally than rostrally.[116] In mice, loss of Fgfr1 function results in the loss of rostral identity, indicating that Fgf1 acts as a secreted rostral morphogen. Conversely, Fgf2 is expressed higher in the dorsal forebrain than in the ventral, thus contributing to the dorsoventral patterning of the developing brain.[114] Loss of function of Fgf2 changes dorsal cortex specification.[114] Pea3-ETS transcription factors are downstream of the Fgf signaling pathway and ectopic expression of Fgf18 induces their expression with phenotypic changes in neuronal migration.[115] Pea3-ETS

transcription factors are expressed in gradients high rostral to low caudally implying a role in axial patterning in the cerebral cortex.[117]

Transforming growth factor β/bone morphogenetic protein (BMP) signaling pathways play important roles in neurogenesis. Both TGF-β and BMP are expressed in the dorsal cerebral cortex during embryonic neurogenesis and regulate proliferation, survival, differentiation, and migration in the cerebral cortex.[118] The BMP binds to the BMP receptor (BMPR1) on the cell surface and induces phosphorylation of Smad family transcription factors.[119] The BMP signaling inhibits neuronal differentiation and promotes glial differentiation during corticogenesis.[120] Both BMP and Notch may converge on some cellular processes, for example, they could impinge on some similar targets such as Hes3 and inhibitor of DNA-binding factor genes (Ids), as observed during adult neurogenesis.[50]

Retinoic acid, a derivative of vitamin A, is involved in neuronal differentiation.[121,122] Retinoic acid binds nuclear receptors of the RA receptor family (RARs α, β, and γ) that regulate the expression of target genes that contain an RA response element.[121] The interaction of RA with the RAR bound as a repressor complex to target genes releases corepressor proteins and recruits histone acetyltransferases.[123] However, RA can also induce rapid and transient activation of a cascade of kinases including the MAPK and ERK pathways which contribute to coregulation of the RAR target genes by phosphorylation of cofactors and histones.[123,124] Dietary depletion of vitamin A in pregnant mothers results in embryonic defects, including delayed development and reduced cortical hemispheres, with a reduction in neuron-specific class III β tubulin (β-tubulinIII) expression and lower levels of Harvey rat sarcoma viral oncogene (HRas) protein in the intermediate zone and CP regions. The reduction in HRas levels is rescued by supplementing the embryos with RA indicating a stabilization of HRas by RA.[125,126] Retinoic acid deficiency affects neuronal migration to cortical layers V to III during development.[127] This impaired migration also results in neuronal fate switching to layer II neuron subtypes.[127] The RA pathway also cross-talks with Wnt signaling at the level of β-catenin.[128] The Wnt-RA axis is most prominent at the rostral end of the developing cerebral cortex, implying a potential role of RA in arealization of the forebrain.[13]

Hippo signaling regulates size and homeostasis in many organs and tissues.[129] The Hippo signaling pathway is a cascade of kinases that converge onto the control of the transcriptional coregulators Yap and Taz.[130] The Hippo kinases and Yes-associated protein/transcriptional coactivator with PDZ-binding motif (Yap1/Taz) are regulated at different levels by different stimuli including G protein–coupled receptor signaling, cell adhesion, mechanical stress, and changes in cellular energy status.[131] The Hippo kinase cascade can be activated by activation of the macrophage-stimulating 1/2 (Mst1/2) and

large tumor suppressor 1/2 (Lats1/2) kinases. These serine/threonine kinases phosphorylate Yap1 and Taz. Phospho-Yap/Taz is targeted to degradation. If Lats1/2 is inactive, then Yap/Taz is dephosphorylated and translocated to the nucleus where they interact with multiple transcriptional regulators.[130] Yap/Taz interacts with β-catenin and Smads and thus coregulates both the Wnt and TGF-β pathways to regulate gene expression.[130] The TEA domain transcription factors (Tead) are key targets and mediators of the Hippo pathway and critical effectors of Hippo-regulated target gene expression.[125,129] In NSCs, the Hippo pathway plays a niche role and regulates the communication between neighboring cells. The expression of fat tumor suppressor homologue (Fat4) and Dachsous (Dchs), the upstream receptor, and ligand of the pathway increases NSC proliferation and reduces differentiation.[132] However, the targets and the exact mechanism of the Hippo pathway in NSCs and cortical development remain unclear. Hence, future analysis of the Hippo pathway and its control of NSC maintenance, commitment, and differentiation could uncover novel interactions and functions.

Although the origins of many of the factors described above are not clear, the cerebral spinal fluid is an obvious source. Growth factors and morphogens released into the cerebral spinal fluid can influence NSC proliferation and fate. Some of these factors are produced and released by the choroid plexus and their expression is dynamic during cortical development (reviewed by Lehtinen and Walsh[133] and Johansson[134]). In addition, neuronal inputs from subcortical regions of the brain have also been shown to influence neural progenitor proliferation and maintenance.[135,136] This suggests that not only the local environment of the developing cerebral cortex is affecting the production of neurons in the dorsal cortex but more distant brain regions may also play a critical role in the control of cortical NSC fate.

In summary, rather unsurprisingly, development of the brain and particularly the cerebral cortex incorporates many different signaling pathways. Here, we just cover a few but due to the complexity of the cerebral cortex and the need for precise NSC proliferation, fate commitment and differentiation, the balance, and interaction of these pathways will be critical. Hence, a deeper understanding of the signaling pathways and their underlying downstream mechanisms is required to develop a model of how NSCs integrate different signals to regulate development of the brain.

Conclusions

In this review, we have tried to highlight some of the main developmental processes and signaling mechanisms controlling cerebral cortical development. From decades of work, it is clear that transcription factors and signaling are key regulators of NSC generation of the cerebral cortex. However, there remains much to be learnt about how these pathways interact and converge to impose the precise regulation needed to form the complex structure of the cortical isocortex from a simple pseudostratified sheet of NEPs. State-of-the-art technologies employing high-throughput single-cell RNA sequencing platforms have allowed a considerable increase in resolution to the single-cell level. These techniques provide a comprehensive understanding of single cells isolated from the brain, facilitating the extrapolation of intrinsic molecular architecture to function. With the advent of high-throughput single-cell omics and lineage tracing in vivo, the future looks demanding but bright and exciting for elucidating the mechanism of development of the cerebral cortex.

Author Contributions

ORCID iD

Verdon Taylor https://orcid.org/0000-0003-3497-5976

REFERENCES

1. Tam PP, Loebel DA. Gene function in mouse embryogenesis: get set for gastrulation. *Nat Rev Genet*. 2007;8:368–381.
2. Lee HK, Lee HS, Moody SA. Neural transcription factors: from embryos to neural stem cells. *Mol Cells*. 2014;37:705–712.
3. Paridaen JT, Huttner WB. Neurogenesis during development of the vertebrate central nervous system. *EMBO Rep*. 2014;15:351–364.
4. Zhadanov AB, Provance DW Jr, Speer CA, et al. Absence of the tight junctional protein AF-6 disrupts epithelial cell-cell junctions and cell polarity during mouse development. *Curr Biol*. 1999;9:880–888.
5. Gal JS, Morozov YM, Ayoub AE, Chatterjee M, Rakic P, Haydar TF. Molecular and morphological heterogeneity of neural precursors in the mouse neocortical proliferative zones. *J Neurosci*. 2006;26:1045–1056.
6. Stancik EK, Navarro-Quiroga I, Sellke R, Haydar TF. Heterogeneity in ventricular zone neural precursors contributes to neuronal fate diversity in the postnatal neocortex. *J Neurosci*. 2010;30:7028–7036.
7. Tan X, Shi SH. Neocortical neurogenesis and neuronal migration. *Wiley Interdiscip Rev Dev Biol*. 2013;2:443–459.
8. Kosodo Y, Suetsugu T, Suda M, et al. Regulation of interkinetic nuclear migration by cell cycle-coupled active and passive mechanisms in the developing brain. *EMBO J*. 2011;30:1690–1704.
9. Taverna E, Huttner WB. Neural progenitor nuclei IN motion. *Neuron*. 2010;67:906–914.
10. Lui JH, Hansen DV, Kriegstein AR. Development and evolution of the human neocortex. *Cell*. 2011;146:18–36.
11. Takahashi T, Nowakowski RS, Caviness VS Jr. Cell cycle parameters and patterns of nuclear movement in the neocortical proliferative zone of the fetal mouse. *J Neurosci*. 1993;13:820–833.
12. Higginbotham H, Guo J, Yokota Y, et al. Arl13b-regulated cilia activities are essential for polarized radial glial scaffold formation. *Nat Neurosci*. 2013;16:1000–1007.
13. Jiang X, Nardelli J. Cellular and molecular introduction to brain development. *Neurobiol Dis*. 2016;92:3–17.
14. Taverna E, Gotz M, Huttner WB. The cell biology of neurogenesis: toward an understanding of the development and evolution of the neocortex. *Annu Rev Cell Dev Biol*. 2014;30:465–502.
15. Fietz SA, Kelava I, Vogt J, et al. OSVZ progenitors of human and ferret neocortex are epithelial-like and expand by integrin signaling. *Nat Neurosci*. 2010;13:690–699.
16. Hansen DV, Lui JH, Parker PR, Kriegstein AR. Neurogenic radial glia in the outer subventricular zone of human neocortex. *Nature*. 2010;464:554–561.
17. Kelava I, Reillo I, Murayama AY, et al. Abundant occurrence of basal radial glia in the subventricular zone of embryonic neocortex of a lissencephalic primate, the common marmoset Callithrix jacchus. *Cereb Cortex*. 2012;22:469–481.
18. Wang X, Tsai JW, LaMonica B, Kriegstein AR. A new subtype of progenitor cell in the mouse embryonic neocortex. *Nat Neurosci*. 2011;14:555–561.

19. Hansen DV, Rubenstein JL, Kriegstein AR. Deriving excitatory neurons of the neocortex from pluripotent stem cells. *Neuron*. 2011;70:645–660.

20. Shitamukai A, Konno D, Matsuzaki F. Oblique radial glial divisions in the developing mouse neocortex induce self-renewing progenitors outside the germinal zone that resemble primate outer subventricular zone progenitors. *J Neuroscience*. 2011;31:3683–3695.

21. Kriegstein AR, Gotz M. Radial glia diversity: a matter of cell fate. *Glia*. 2003;43:37–43.

22. Malatesta P, Hartfuss E, Gotz M. Isolation of radial glial cells by fluorescent-activated cell sorting reveals a neuronal lineage. *Development*. 2000;127: 5253–5263.

23. Franco SJ, Muller U. Shaping our minds: stem and progenitor cell diversity in the mammalian neocortex. *Neuron*. 2013;77:19–34.

24. Gotz M, Huttner WB. The cell biology of neurogenesis. *Nat Rev Mol Cell Biol*. 2005;6:777–788.

25. Hartfuss E, Galli R, Heins N, Gotz M. Characterization of CNS precursor subtypes and radial glia. *Dev Biol*. 2001;229:15–30.

26. Malatesta P, Hack MA, Hartfuss E, et al. Neuronal or glial progeny: regional differences in radial glia fate. *Neuron*. 2003;37:751–764.

27. Bansod S, Kageyama R, Ohtsuka T. Hes5 regulates the transition timing of neurogenesis and gliogenesis in mammalian neocortical development. *Development*. 2017;144:3156–3167.

28. Haubensak W, Attardo A, Denk W, Huttner WB. Neurons arise in the basal neuroepithelium of the early mammalian telencephalon: a major site of neurogenesis. *Proc Natl Acad Sci U S A*. 2004;101:3196–3201.

29. Sahara S, O'Leary DD. Fgf10 regulates transition period of cortical stem cell differentiation to radial glia controlling generation of neurons and basal progenitors. *Neuron*. 2009;63:48–62.

30. Miyata T, Kawaguchi A, Saito K, Kawano M, Muto T, Ogawa M. Asymmetric production of surface-dividing and non-surface-dividing cortical progenitor cells. *Development*. 2004;131:3133–3145.

31. Noctor SC, Martinez-Cerdeno V, Ivic L, Kriegstein AR. Cortical neurons arise in symmetric and asymmetric division zones and migrate through specific phases. *Nat Neurosci*. 2004;7:136–144.

32. Cubelos B, Sebastian-Serrano A, Kim S, et al. Cux-2 controls the proliferation of neuronal intermediate precursors of the cortical subventricular zone. *Cereb Cortex*. 2008;18:1758–1770.

33. Englund C, Fink A, Lau C, et al. Pax6, Tbr2, and Tbr1 are expressed sequentially by radial glia, intermediate progenitor cells, and postmitotic neurons in developing neocortex. *J Neurosci*. 2005;25:247–251.

34. Nieto M, Monuki ES, Tang H, et al. Expression of Cux-1 and Cux-2 in the subventricular zone and upper layers II-IV of the cerebral cortex. *J Comp Neurol*. 2004;479:168–180.

35. Britanova O, Akopov S, Lukyanov S, Gruss P, Tarabykin V. Novel transcription factor Satb2 interacts with matrix attachment region DNA elements in a tissue-specific manner and demonstrates cell-type-dependent expression in the developing mouse CNS. *Eur J Neurosci*. 2005;21:658–668.

36. Zimmer C, Tiveron MC, Bodmer R, Cremer H. Dynamics of Cux2 expression suggests that an early pool of SVZ precursors is fated to become upper cortical layer neurons. *Cereb Cortex*. 2004;14:1408–1420.

37. Tarabykin V, Stoykova A, Usman N, Gruss P. Cortical upper layer neurons derive from the subventricular zone as indicated by Svet1 gene expression. *Development*. 2001;128:1983–1993.

38. Lancaster MA, Knoblich JA. Spindle orientation in mammalian cerebral cortical development. *Curr Opin Neurobiol*. 2012;22:737–746.

39. Konno D, Shioi G, Shitamukai A, et al. Neuroepithelial progenitors undergo LGN-dependent planar divisions to maintain self-renewability during mammalian neurogenesis. *Nat Cell Biol*. 2008;10:93–101.

40. Peyre E, Jaouen F, Saadaoui M, et al. A lateral belt of cortical LGN and NuMA guides mitotic spindle movements and planar division in neuroepithelial cells. *J Cell Biol*. 2011;193:141–154.

41. Postiglione MP, Juschke C, Xie Y, Haas GA, Charalambous C, Knoblich JA. Mouse inscuteable induces apical-basal spindle orientation to facilitate intermediate progenitor generation in the developing neocortex. *Neuron*. 2011;72: 269–284.

42. Bultje RS, Castaneda-Castellanos DR, Jan LY, Jan YN, Kriegstein AR, Shi SH. Mammalian par3 regulates progenitor cell asymmetric division via notch signaling in the developing neocortex. *Neuron*. 2009;63:189–202.

43. Costa MR, Wen G, Lepier A, Schroeder T, Gotz M. Par-complex proteins promote proliferative progenitor divisions in the developing mouse cerebral cortex. *Development*. 2008;135:11–22.

44. Heins N, Cremisi F, Malatesta P, et al. Emx2 promotes symmetric cell divisions and a multipotential fate in precursors from the cerebral cortex. *Mol Cell Neurosci*. 2001;18:485–502.

45. Gaiano N, Fishell G. The role of notch in promoting glial and neural stem cell fates. *Annu Rev Neurosci*. 2002;25:471–490.

46. Dong Z, Yang N, Yeo SY, Chitnis A, Guo S. Intralineage directional notch signaling regulates self-renewal and differentiation of asymmetrically dividing radial glia. *Neuron*. 2012;74:65–78.

47. Gaiano N, Nye JS, Fishell G. Radial glial identity is promoted by Notch1 signaling in the murine forebrain. *Neuron*. 2000;26:395–404.

48. Lutolf S, Radtke F, Aguet M, Suter U, Taylor V. Notch1 is required for neuronal and glial differentiation in the cerebellum. *Development*. 2002;129:373–385.

49. Imayoshi I, Sakamoto M, Yamaguchi M, Mori K, Kageyama R. Essential roles of notch signaling in maintenance of neural stem cells in developing and adult brains. *J Neurosci*. 2010;30:3489–3498.

50. Imayoshi I, Shimogori T, Ohtsuka T, Kageyama R. Hes genes and neurogenin regulate non-neural versus neural fate specification in the dorsal telencephalic midline. *Development*. 2008;135:2531–2541.

51. Alvarez-Rodriguez R, Pons S. Expression of the proneural gene encoding Mash1 suppresses MYCN mitotic activity. *J Cell Sci*. 2009;122:595–599.

52. Parras CM, Schuurmans C, Scardigli R, Kim J, Anderson DJ, Guillemot F. Divergent functions of the proneural genes Mash1 and Ngn2 in the specification of neuronal subtype identity. *Genes Dev*. 2002;16:324–338.

53. Vessey JP, Amadei G, Burns SE, Kiebler MA, Kaplan DR, Miller FD. An asymmetrically localized Staufen2-dependent RNA complex regulates maintenance of mammalian neural stem cells. *Cell Stem Cell*. 2012;11:517–528.

54. Heins N, Malatesta P, Cecconi F, et al. Glial cells generate neurons: the role of the transcription factor Pax6. *Nat Neurosci*. 2002;5:308–315.

55. Kosodo Y, Roper K, Haubensak W, Marzesco AM, Corbeil D, Huttner WB. Asymmetric distribution of the apical plasma membrane during neurogenic divisions of mammalian neuroepithelial cells. *EMBO J*. 2004;23:2314–2324.

56. Kouprina N, Pavlicek A, Mochida GH, et al. Accelerated evolution of the ASPM gene controlling brain size begins prior to human brain expansion. *PLoS Biol*. 2004;2:E126.

57. Chae TH, Kim S, Marz KE, Hanson PI, Walsh CA. The hyh mutation uncovers roles for alpha Snap in apical protein localization and control of neural cell fate. *Nat Genet*. 2004;36:264–270.

58. Sheen VL, Ganesh VS, Topcu M, et al. Mutations in ARFGEF2 implicate vesicle trafficking in neural progenitor proliferation and migration in the human cerebral cortex. *Nat Genet*. 2004;36:69–76.

59. Zechner D, Fujita Y, Hulsken J, et al. beta-Catenin signals regulate cell growth and the balance between progenitor cell expansion and differentiation in the nervous system. *Dev Biol*. 2003;258:406–418.

60. Chenn A, Walsh CA. Increased neuronal production, enlarged forebrains and cytoarchitectural distortions in beta-catenin overexpressing transgenic mice. *Cereb Cortex*. 2003;13:599–606.

61. Leone DP, Srinivasan K, Chen B, Alcamo E, McConnell SK. The determination of projection neuron identity in the developing cerebral cortex. *Curr Opin Neurobiol*. 2008;18:28–35.

62. Custo Greig LF, Woodworth MB, Galazo MJ, Padmanabhan H, Macklis JD. Molecular logic of neocortical projection neuron specification, development and diversity. *Nat Rev Neurosci*. 2013;14:755–769.

63. Guo C, Eckler MJ, McKenna WL, McKinsey GL, Rubenstein JL, Chen B. Fezf2 expression identifies a multipotent progenitor for neocortical projection neurons, astrocytes, and oligodendrocytes. *Neuron*. 2013;80:1167–1174.

64. McConnell SK. Fates of visual cortical neurons in the ferret after isochronic and heterochronic transplantation. *J Neurosci*. 1988;8:945–974.

65. Desai AR, McConnell SK. Progressive restriction in fate potential by neural progenitors during cerebral cortical development. *Development*. 2000;127:2863–2872.

66. Han W, Sestan N. Cortical projection neurons: sprung from the same root. *Neuron*. 2013;80:1103–1105.

67. Eiraku M, Sasai Y. Mouse embryonic stem cell culture for generation of three-dimensional retinal and cortical tissues. *Nat Protoc*. 2011;7:69–79.

68. Gaspard N, Bouschet T, Hourez R, et al. An intrinsic mechanism of corticogenesis from embryonic stem cells. *Nature*. 2008;455:351–357.

69. Shen Q, Wang Y, Dimos JT, et al. The timing of cortical neurogenesis is encoded within lineages of individual progenitor cells. *Nat Neurosci*. 2006;9:743–751.

70. Tan SS, Breen S. Radial mosaicism and tangential cell dispersion both contribute to mouse neocortical development. *Nature*. 1993;362:638–640.

71. Chen B, Schaevitz LR, McConnell SK. Fezl regulates the differentiation and axon targeting of layer 5 subcortical projection neurons in cerebral cortex. *Proc Nat Acad Sci U S A*. 2005;102:17184–17189.

72. Molyneaux BJ, Arlotta P, Menezes JR, Macklis JD. Neuronal subtype specification in the cerebral cortex. *Nat Rev Neurosci*. 2007;8:427–437.

73. Kwan KY, Sestan N, Anton ES. Transcriptional co-regulation of neuronal migration and laminar identity in the neocortex. *Development*. 2012;139:1535–1546.

74. Franco SJ, Gil-Sanz C, Martinez-Garay I, et al. Fate-restricted neural progenitors in the mammalian cerebral cortex. *Science*. 2012;337:746–749.

75. Gotz M, Williams BP, Bolz J, Price J. The specification of neuronal fate: a common precursor for neurotransmitter subtypes in the rat cerebral cortex in vitro. *Eur J Neurosci*. 1995;7:889–898.

76. Hu JS, Vogt D, Sandberg M, Rubenstein JL. Cortical interneuron development: a tale of time and space. *Development*. 2017;144:3867–3878.

77. Wamsley B, Fishell G. Genetic and activity-dependent mechanisms underlying interneuron diversity. *Nat Rev Neurosci*. 2017;18:299–309.

78. Arlotta P, Molyneaux BJ, Chen J, Inoue J, Kominami R, Macklis JD. Neuronal subtype-specific genes that control corticospinal motor neuron development in vivo. *Neuron*. 2005;45:207–221.

79. Muzio L, DiBenedetto B, Stoykova A, Boncinelli E, Gruss P, Mallamaci A. Conversion of cerebral cortex into basal ganglia in emx2(−/−) pax6(Sey/Sey) double-mutant mice. *Nat Neurosci*. 2002;5:737–745.

80. Hevner RF, Daza RA, Rubenstein JL, Stunnenberg H, Olavarria JF, Englund C. Beyond laminar fate: toward a molecular classification of cortical projection/pyramidal neurons. *Dev Neurosci*. 2003;25:139–151.

81. Di Lullo E, Kriegstein AR. The use of brain organoids to investigate neural development and disease. *Nat Rev Neurosci*. 2017;18:573–584.

82. Alcamo EA, Chirivella L, Dautzenberg M, et al. Satb2 regulates callosal projection neuron identity in the developing cerebral cortex. *Neuron*. 2008;57:364–377.

83. Srinivasan K, Leone DP, Bateson RK, et al. A network of genetic repression and derepression specifies projection fates in the developing neocortex. *Proc Natl Acad Sci U S A*. 2012;109:19071–19078.

84. Schuurmans C, Armant O, Nieto M, et al. Sequential phases of cortical specification involve neurogenin-dependent and -independent pathways. *EMBO J*. 2004;23:2892–2902.

85. Fode C, Ma Q, Casarosa S, Ang SL, Anderson DJ, Guillemot F. A role for neural determination genes in specifying the dorsoventral identity of telencephalic neurons. *Genes Dev*. 2000;14:67–80.

86. Hirabayashi Y, Suzki N, Tsuboi M, et al. Polycomb limits the neurogenic competence of neural precursor cells to promote astrogenic fate transition. *Neuron*. 2009;63:600–613.

87. Kishi Y, Fujii Y, Hirabayashi Y, Gotoh Y. HMGA regulates the global chromatin state and neurogenic potential in neocortical precursor cells. *Nat Neurosci*. 2012;15:1127–1133.

88. Pereira JD, Sansom SN, Smith J, Dobenecker MW, Tarakhovsky A, Livesey FJ. Ezh2, the histone methyltransferase of PRC2, regulates the balance between self-renewal and differentiation in the cerebral cortex. *Proc Natl Acad Sci U S A*. 2010;107:15957–15962.

89. Sessa A, Ciabatti E, Drechsel D, et al. The Tbr2 molecular network controls cortical neuronal differentiation through complementary genetic and epigenetic pathways. *Cereb Cortex*. 2017;27:3378–3396.

90. Hitoshi S, Ishino Y, Kumar A, et al. Mammalian Gcm genes induce Hes5 expression by active DNA demethylation and induce neural stem cells. *Nat Neurosci*. 2011;14:957–964.

91. Tuoc TC, Boretius S, Sansom SN, et al. Chromatin regulation by BAF170 controls cerebral cortical size and thickness. *Dev Cell*. 2013;25:256–269.

92. Yip DJ, Corcoran CP, Alvarez-Saavedra M, et al. Snf2l regulates Foxg1-dependent progenitor cell expansion in the developing brain. *Dev Cell*. 2012;22:871–878.

93. Fan G, Martinowich K, Chin MH, et al. DNA methylation controls the timing of astrogliogenesis through regulation of JAK-STAT signaling. *Development*. 2005;132:3345–3356.

94. Namihira M, Kohyama J, Semi K, et al. Committed neuronal precursors confer astrocytic potential on residual neural precursor cells. Dev Cell. 2009;16:245–255.

95. Blaschuk KL, Ffrench-Constant C. Developmental neurobiology: notch is tops in the developing brain. *Curr Biol*. 1998;8:R334–R337.

96. Brou C, Logeat F, Gupta N, et al. A novel proteolytic cleavage involved in notch signaling: the role of the disintegrin-metalloprotease TACE. *Mol Cell*. 2000;5:207–216.

97. Mumm JS, Schroeter EH, Saxena MT, et al. A ligand-induced extracellular cleavage regulates gamma-secretase-like proteolytic activation of notch1. *Mol Cell*. 2000;5:197–206.

98. Basak O, Taylor V. Identification of self-replicating multipotent progenitors in the embryonic nervous system by high notch activity and Hes5 expression. *Eur J Neurosci*. 2007;25:1006–1022.

99. Zhang R, Engler A, Taylor V. Notch: an interactive player in neurogenesis and disease. *Cell Tissue Res*. 2017;371:73–89.

100. Louvi A, Artavanis-Tsakonas S. Notch signalling in vertebrate neural development. *Nat Rev Neurosci*. 2006;7:93–102.

101. Hatakeyama J, Bessho Y, Katoh K, et al. Hes genes regulate size, shape and histogenesis of the nervous system by control of the timing of neural stem cell differentiation. *Development*. 2004;131:5539–5550.

102. Fiuza UM, Arias AM. Cell and molecular biology of notch. *J Endocrinol*. 2007;194:459–474.

103. Ochiai W, Nakatani S, Takahara T, et al. Periventricular notch activation and asymmetric Ngn2 and Tbr2 expression in pair-generated neocortical daughter cells. *Molec Cell Neurosci*. 2009;40:225–233.

104. Shimojo H, Ohtsuka T, Kageyama R. Oscillations in notch signaling regulate maintenance of neural progenitors. *Neuron*. 2008;58:52–64.

105. Kawaguchi D, Yoshimatsu T, Hozumi K, Gotoh Y. Selection of differentiating cells by different levels of delta-like 1 among neural precursor cells in the developing mouse telencephalon. *Development*. 2008;135:3849–3858.

106. Mizutani K, Yoon K, Dang L, Tokunaga A, Gaiano N. Differential notch signalling distinguishes neural stem cells from intermediate progenitors. *Nature*. 2007;449:351–355.

107. Harrison-Uy SJ, Pleasure SJ. Wnt signaling and forebrain development. *Cold Spring Harb Perspect Biol*. 2012;4:a008094.

108. Kuwahara A, Hirabayashi Y, Knoepfler PS, et al. Wnt signaling and its downstream target N-myc regulate basal progenitors in the developing neocortex. *Development*. 2010;137:1035–1044.

109. Inestrosa NC, Varela-Nallar L. Wnt signalling in neuronal differentiation and development. *Cell Tissue Res*. 2015;359:215–223.

110. Wrobel CN, Mutch CA, Swaminathan S, Taketo MM, Chenn A. Persistent expression of stabilized beta-catenin delays maturation of radial glial cells into intermediate progenitors. *Dev Biol*. 2007;309:285–297.

111. Fukuchi-Shimogori T, Grove EA. Neocortex patterning by the secreted signaling molecule FGF8. *Science*. 2001;294:1071–1074.

112. Bachler M, Neubuser A. Expression of members of the Fgf family and their receptors during midfacial development. *Mech Develop*. 2001;100:313–316.

113. Itoh N, Ornitz DM. Evolution of the Fgf and Fgfr gene families. *Trends Genet*. 2004;20:563–569.

114. Rash BG, Lim HD, Breunig JJ, Vaccarino FM. FGF signaling expands embryonic cortical surface area by regulating notch-dependent neurogenesis. *J Neurosci*. 2011;31:15604–15617.

115. Iwata T, Hevner RF. Fibroblast growth factor signaling in development of the cerebral cortex. *Dev Growth Differ*. 2009;51:299–323.

116. Sansom SN, Livesey FJ. Gradients in the brain: the control of the development of form and function in the cerebral cortex. *Csh Perspect Biol*. 2009;1:a005219.

117. Hasegawa H, Ashigaki S, Takamatsu M, et al. Laminar patterning in the developing neocortex by temporally coordinated fibroblast growth factor signaling. *J Neurosci*. 2004;24:8711–8719.

118. Rodriguez-Martinez G, Velasco I. Activin and TGF- effects on brain development and neural stem cells. *CNS Neurol Disord Drug Targets*. 2012;11:844–855.

119. Ebendal T, Bengtsson H, Soderstrom S. Bone morphogenetic proteins and their receptors: potential functions in the brain. *J Neurosci Res*. 1998;51:139–146.

120. Gomes FC, Sousa Vde O, Romao L. Emerging roles for TGF-beta1 in nervous system development. *Int J Dev Neurosci*. 2005;23:413–424.

121. Gudas LJ, Wagner JA. Retinoids regulate stem cell differentiation. *J Cell Physiol*. 2011;226:322–330.

122. Duester G. Retinoic acid synthesis and signaling during early organogenesis. *Cell*. 2008;134:921–931.

123. Perissi V, Jepsen K, Glass CK, Rosenfeld MG. Deconstructing repression: evolving models of co-repressor action. *Nat Rev Genet*. 2010;11:109–123.

124. Rochette-Egly C. Retinoic acid signaling and mouse embryonic stem cell differentiation: cross talk between genomic and non-genomic effects of RA. *Biochim Biophys Acta*. 2015;1851:66–75.

125. Park JC, Jeong WJ, Kim MY, Min D, Choi KY. Retinoic-acid-mediated hRas stabilization induces neuronal differentiation of neural stem cells during brain development. *J Cell Sci*. 2016;129:2997–3007.

126. Chuang JH, Tung LC, Lin Y. Neural differentiation from embryonic stem cells in vitro: an overview of the signaling pathways. *World J Stem Cells*. 2015;7:437–447.

127. Easwaran V, Pishvaian M, Salimuddin Byers S. Cross-regulation of beta-catenin-LEF/TCF and retinoid signaling pathways. *Curr Biol*. 1999;9:1415–1418.

128. Haushalter C, Asselin L, Fraulob V, Dolle P, Rhinn M. Retinoic acid controls early neurogenesis in the developing mouse cerebral cortex. *Dev Biol*. 2017;430:129–141.

129. Lin KC, Park HW, Guan KL. Regulation of the hippo pathway transcription factor TEAD. *Trends Biochem Sci*. 2017;42:862–872.

130. Panciera T, Azzolin L, Cordenonsi M, Piccolo S. Mechanobiology of YAP and TAZ in physiology and disease. *Nat Rev Mol Cell Biol*. 2017;18:758–770.

131. Zeng Q, Hong W. The emerging role of the hippo pathway in cell contact inhibition, organ size control, and cancer development in mammals. *Cancer Cell*. 2008;13:188–192.

132. Cappello S, Gray MJ, Badouel C, et al. Mutations in genes encoding the cadherin receptor-ligand pair DCHS1 and FAT4 disrupt cerebral cortical development. *Nat Genet*. 2013;45:1300–1308.

133. Lehtinen MK, Walsh CA. Neurogenesis at the brain-cerebrospinal fluid interface. *Annu Rev Cell Dev Biol*. 2011;27:653–679.

134. Johansson PA. The choroid plexuses and their impact on developmental neurogenesis. *Front Neurosci*. 2014;8:340.

135. Gerstmann K, Pensold D, Symmank J, et al. Thalamic afferents influence cortical progenitors via ephrin a5-EphA4 interactions. *Development*. 2015;142:140–150.

136. Dehay C, Savatier P, Cortay V, Kennedy H. Cell-cycle kinetics of neocortical precursors are influenced by embryonic thalamic axons. *J Neurosci*. 2001;21:201–214.

SYSTEMS BIOLOGY

Ultra-multiplexed analysis of single-cell dynamics reveals logic rules in differentiation

Ce Zhang[1,2,3], Hsiung-Lin Tu[1,2,4], Gengjie Jia[2], Tanzila Mukhtar[5], Verdon Taylor[5], Andrey Rzhetsky[2], Savaş Tay[1,2]*

Dynamical control of cellular microenvironments is highly desirable to study complex processes such as stem cell differentiation and immune signaling. We present an ultra-multiplexed microfluidic system for high-throughput single-cell analysis in precisely defined dynamic signaling environments. Our system delivers combinatorial and time-varying signals to 1500 independently programmable culture chambers in week-long live-cell experiments by performing nearly 10^6 pipetting steps, where single cells, two-dimensional (2D) populations, or 3D neurospheres are chemically stimulated and tracked. Using our system and statistical analysis, we investigated the signaling landscape of neural stem cell differentiation and discovered "cellular logic rules" that revealed the critical role of signal timing and sequence in cell fate decisions. We find synergistic and antagonistic signal interactions and show that differentiation pathways are highly redundant. Our system allows dissection of hidden aspects of cellular dynamics and enables accelerated biological discovery.

INTRODUCTION

Cells operate in dynamic microenvironments where the type and concentration of signaling molecules are ever changing. The stem cell niche presents a range of signaling molecules and growth factors to maintain the stem cell pool. During development or injury, the chemical composition of the niche changes to allow differentiation into defined cell lineages. Signals received at different cell fate decision points determine differentiation trajectories (1). It is highly desirable to recapitulate these dynamic signaling environments in experiments to study stem cell behavior quantitatively, as well as in tissue regeneration applications.

Current live-cell analysis techniques are severely limited in creating and controlling complex dynamical microenvironments. Microfluidic cell culture has been proposed to improve time-consuming and labor-intensive tasks by automating operations (2–8) and to realize previously intractable experiments in dynamic cell culture (6). Individual devices for sorting, culturing, dynamically stimulating, imaging, tracking, and retrieving cells have been demonstrated; however, none of the current systems combine these capabilities. Further, the number of individual dynamic culture conditions created in previous microfluidic devices has been limited to less than 100 (7), limiting their utility in screening a large number of conditions in exploratory signaling and drug studies. In addition, maintaining long-term viable cultures of sensitive primary mammalian cells in microfluidic devices was so far elusive (8–11).

To address all these limitations and to build a universal system for dynamical cell control and analysis, we developed an ultra-multiplexed microfluidic system that combines multimode cell culture [single cell, two-dimensional (2D) monolayer, and 3D neurosphere], generation of dynamic chemical inputs, and 1500 individually addressable cell culture units on a single device (Fig. 1). Each of the 1500 culture chambers can be programmed to receive a different set of signaling molecules, growth factors, or drugs, whose composition and concentration can be automatically changed on-demand. Culture conditions including cell type, cell density, and support matrices can be predetermined for each

independent chamber. Coupled with custom software for chip control and computational data processing, the system can perform programmed delivery of thousands of formulated fluidic inputs to designate on-chip culture units while monitoring and analyzing cellular responses via live-cell microscopy and end-point biochemical analysis methods (Fig. 1D). In a typical 1-week-long experiment, this system tracks ~30,000 individual cells cultured under 1500 dynamic individual conditions by performing ~10^6 pipetting steps with nanoliter precision, and creates millions of single-cell data points. These are capabilities well beyond manual, robotic, or other microfluidic systems in terms of labor, cost, and time.

RESULTS

Cultivating a broad range of cells in dynamic microenvironments requires precise control of cell density, surface properties, support matrices, gas and fluidic exchange, media and growth factor delivery, and humidity. To realize this, we designed a simple two-layer culture chamber that creates a consistent microenvironment for long-term cellular studies (Fig. 1, B and C). The 3D culture chamber can deliver media and ligands to cells via diffusion, preventing cells from undesirable shear stress and displacement in live-cell tracking experiments (Fig. 1, C to E; fig. S1, A to F; and movies S1, S2, and S5). The use of diffusion-based media delivery is flow free and gentle and creates minimal mechanical disturbance to the cellular microenvironment (section S1). The culture chamber can be loaded with gels and other support matrices to enable 3D cell organization (Fig. 1, C and E, and fig. S1, G and H). Furthermore, on-demand cell retrieval from designated chambers is possible by automatic switching to flow-based media delivery (Fig. 1C; fig. S1, A to E; and movies S1 and S3). To formulate complex and dynamic chemical inputs on chip, we designed and integrated a new microfluidic chemical formulator. A wide range of time-varying chemical inputs with distinct characteristics (i.e., pulsed and sinusoidal inputs) can be generated from a few previously prepared fluid vials connected to the chip and can be delivered to live cells with subminute temporal resolution by diffusion or with subsecond resolution by regulated flow (Fig. 1A and movie S4).

The Achilles' heel for microfluidic cell culture has been poor cell viability, which has been especially severe for sensitive primary mammalian

[1]Institute for Molecular Engineering, The University of Chicago, Chicago, IL 60637, USA. [2]Institute for Genomics and Systems Biology, The University of Chicago, Chicago, IL 60637, USA. [3]Institute of Photonics and Photon-Technology, Northwest University, Xi'an 710069, China. [4]Institute of Chemistry, Academia Sinica, Taipei 11529, Taiwan. [5]Department of Biomedicine, University of Basel, 4058 Basel, Switzerland.
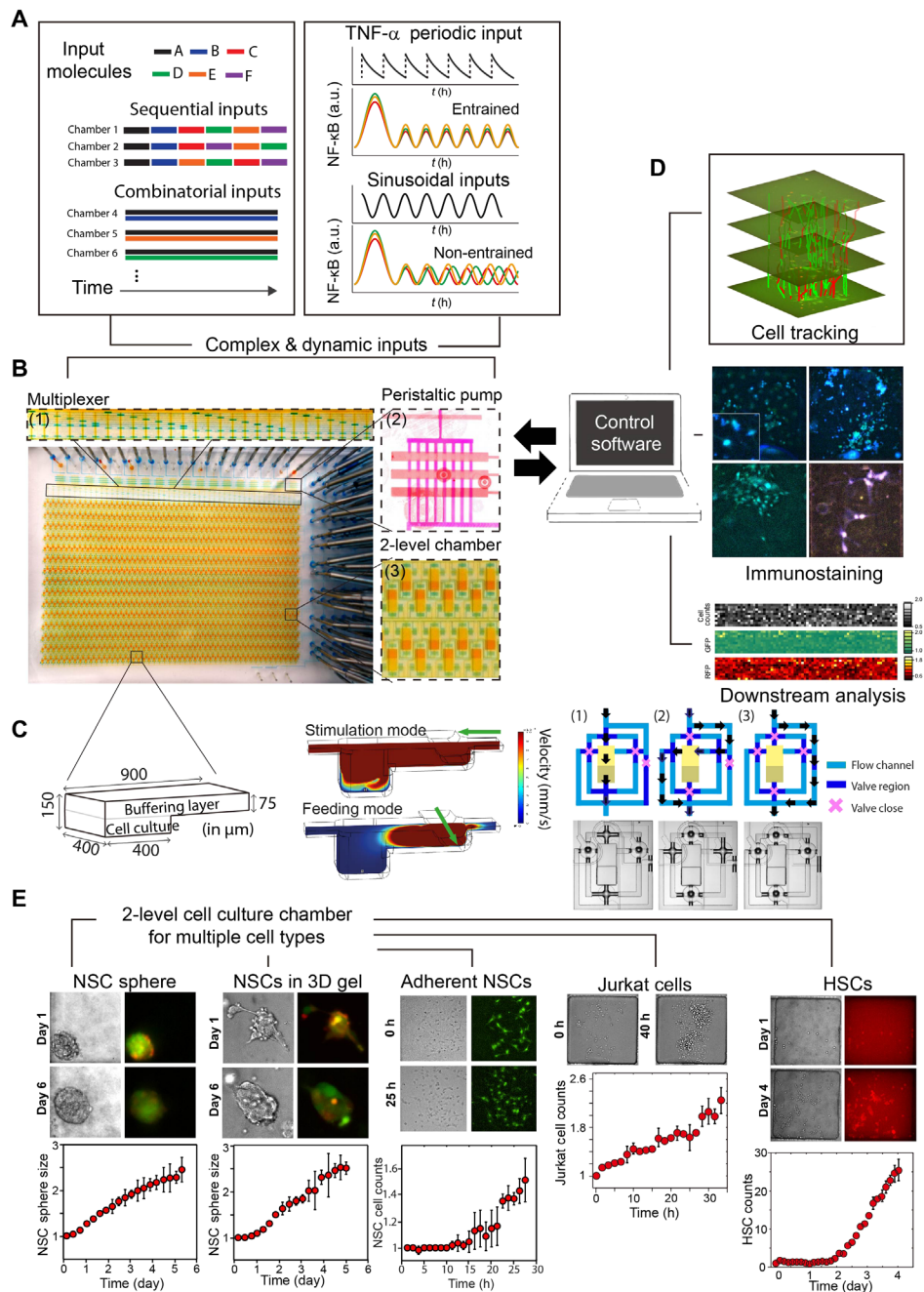*Corresponding author. Email: tays@uchicago.edu

Fig. 1. Ultra-multiplexed, automated cell culture system for dynamical live-cell analysis. The microfluidic device contains 1500 independently programmable culture chambers. During a 1-week experiment, the device performs nearly 10^6 pipetting steps to create and maintain distinct culture conditions in each of the chambers. (**A**) Each chamber can execute a distinct dynamic culture program (combinations, timed sequences, sine waves, etc.) where the fluidic composition can be changed when desired, and dynamic processes (i.e., NF-κB localization or *Hes5* expression) are tracked with single-cell resolution. An on-chip nanoliter multiplexer measures several fluids and mixes them at predetermined ratios to create complex chemical inputs. A peristaltic pump delivers inputs to any given chamber. For the combinatorial input scenario, several chemicals are mixed and delivered to the cells continuously. In sequential inputs, signaling molecules are changed with a programmed time interval ($\Delta t = 1$ day). a.u., arbitrary units. (**B**) The system can culture adherent or nonadherent cells in either suspension mode, monolayer populations, or 3D format using hydrogels. The novel two-layer geometry of the culture chambers allows diffusion-based media delivery to create a stable environment for cells, and provides the additional ability of single-cell tracking of even nonadherent cells during dynamical stimulation. (**C**) Left: Two-layer cell chamber design allows diffusion- or flow-based media delivery, 3D cell culture, immobilization of nonadherent cells by gravity, and automated cell retrieval. Middle: Fluid mechanical simulations indicate the flow rates for diffusion-based media delivery and cell retrieval via direct flow. Right: Each chamber is controlled by a network of dedicated channels and membrane valves that automate various cell culture procedures. (**D**) Cells can be immunostained in the chip. The system is integrated to a fluorescent microscope and can automatically track individual cells in time-lapse experiments. Single cells or populations of interest can be automatically retrieved from individual chambers for off-chip analysis or expansion. GFP, green fluorescent protein; RFP, red fluorescent protein. (**E**) Primary cells (e.g., mouse NSCs and human HSCs) and cell lines (e.g., Jurkat T cells and mouse fibroblasts) are viably cultured and maintained on chip for weeks. Growth rates equal or better than the well plate culture are achieved through frequent diffusion-based media delivery while maintaining an unperturbed microenvironment.

cells (8, 9). To demonstrate general cell viability in our system, we first cultured mouse fibroblast cells and primary human hematopoietic stem cells (HSCs) in adherent and suspension culture modes, respectively, and stimulated them with either constant, pulsed, or sinusoidal formulations of the inflammatory cytokine tumor necrosis factor (TNF) to induce nuclear factor κB (NF-κB) signaling (Fig. 1A and figs. S2 and S3) (15). Dynamic stimulation and indexed tracking of nonadherent cells such as HSCs were not feasible before our study because of flow-based stimulation displacing cells and preventing single-cell tracking. We stimulated human HSCs with different concentrations of TNF as well as in combination with other cytokines [interferon-γ (IFNγ), interleukin-6 (IL-6), interferon gamma-induced protein 10 (IP10), and monocyte chemoattractant protein-1 (MCP-1)] and with dynamic (time-dependent) variations of selected cytokines. Viability for various cell types was further demonstrated by culturing suspension cells including the Jurkat T cell line and mouse HSCs (Fig. 1E and fig. S3C). In both cases, cells proliferated at similar, if not higher, rates than those in bulk experiments in traditional culture dishes.

We cultured primary mouse embryonic neural stem cells (NSCs) and stimulated them on our chip for weeks under three distinct modes: suspension as single cell or as neurosphere, adherent monolayer, and 3D in hydrogels (Figs. 1E and 2 and fig. S1, G and H). The number of adherent NSCs increases by 50% after 24 hours, comparable to traditional well plate culture. Meanwhile, the diameter of NSC spheres in suspension and 3D gel culture both doubled after 4 days of on-chip culture (Fig. 1E and movie S5). Notably, we observe that NSC spheres are often unresponsive to dynamic environmental changes as compared to monolayer cultured cells, suggesting that NSCs self-organize into a protective layered structure during suspension culture (figs. S1G and S4, A to E, and section S4). Thus, NSC differentiation and self-maintenance are assessed at the single-cell level during monolayer culture by tracking Hes5-GFP expression (indicative of self-renewing NSCs) and Dcx-RFP to label neuroblasts (indicating progress toward differentiation) (12, 13, 14, 16–19). NSC growth rate is another key feature we quantified to statistically assess NSC self-renewal.

To study early signaling events during mammalian forebrain development in vitro, we dynamically analyzed NSCs under combinatorial and time-varying signaling inputs in our system (Figs. 2 and 3). The six selected signaling molecules were identified through RNA sequencing of NSCs isolated from embryonic mouse brain tissue, whose receptors are highly expressed during mouse forebrain development. These factors were Jagged1, DLL1, EGF, PACAP, CXCL, and PDGF (20). The effect of these ligands on NSC differentiation and self-maintenance is not well understood. We hypothesized that the different combinations and temporal ordering of these ligands will lead to distinct cell fate outcomes (section S6). We therefore generated thousands of combinations and temporal sequences of these ligands on the chip and delivered them to NSCs cultured in different chambers while monitoring their differentiation and growth at the single-cell level by time-lapse microscopy (Fig. 2). Millions of single-cell data points were generated and quantified in these experiments. The stimulation input conditions are summarized in table S1. Control experiments in traditional 96-well plates under selected dynamic conditions were used to verify results obtained on the microfluidic device (figs. S4, F to H, and S5, A to E, and section S5).

High Hes5 expression in NSCs indicates maintenance of the stem cell state, while reduced Hes5 indicates progression toward differentiation (fig. S6, A to C and G to I, and section S7) (12, 21–26). Through on-chip immunostaining, we found that most NSCs that were stimulated

with a single ligand did not fully differentiate to any distinct lineage within 6 days; however, combined stimulation with all six ligands made NSCs differentiate into neurons during this time period (fig. S5, F to J, and section S8). By evaluating NSC proliferation, Hes5 expression, and cell morphology, we found many culture conditions where the entire population progressed toward differentiation (Fig. 2, A to C, and fig. S6, D to F). Nevertheless, we also found substantial variability at the single-cell level in a given culture condition (Fig. 2, C to E; fig. S7, A and B; and section S10). Distinct proliferation patterns were observed despite similar Hes5-GFP levels (Fig. 2, D and E). Overall, NSCs proliferate at different rates depending on initial cell density, with higher densities leading to higher proliferation rates (Fig. 2E). Mean Hes5 expression levels and single-cell heterogeneity strongly depended on the signaling inputs received by each NSC culture.

To investigate the role of combinatorial or temporal ordering of signals in NSC maintenance or differentiation, we cultured and monitored NSCs under combinatorial and sequential applications of the six regulatory ligands (Fig. 3A; fig. S7, C to F; and table S1). For each independent NSC culture on the chip, we introduced either one ligand each day (sequential inputs) or a combination of the selected ligands over a 6-day period (combinatorial inputs). We measured the ratio of the ligand-treated cells to untreated controls to quantify changes in cell numbers, and Hes5-GFP and Dcx-RFP expression intensities. Each chip experiment consisted of 63 combinatorial and 720 sequential stimulation experiments, and experiments were repeated at least three times, resulting in nearly 3000 dynamic cultures (Fig. 3B). Each of the six ligands are used in various contexts repeatedly, and their effect on stem cell fate is measured directly in individual experiments and also by statistical analysis of all experiments that contain these ligands. Figure 3B shows raw data from a single experiment, which contains single ligand, combinatorial, and sequential stimulation conditions where cell numbers and Hes5 and Dcx expression are quantified in time-lapse measurements in single cells. In Fig. 3C, we show two example experiments: PACAP stimulation induces an increase in cell numbers and a decrease in Hes5 and Dcx levels over 10-day measurements. PDGF stimulation, however, increases both cell numbers and Hes5 levels but decreases Dcx levels in NSCs. In the lower panels of Fig. 3C, we plot the effect of platelet-derived growth factor (PDGF) on cell growth and Hes5 changes in different experiments that use PDGF along with other ligands. Each bar in the histogram shows the effect of PDGF in an individual experiment; in some experiments, PDGF increases the measured quantities, while in others, it leads to a decrease. These changes vary in a wide range, from negative to positive, indicating that the role of a ligand can be highly context dependent (27–30), which we further discuss in the following sections.

DISCUSSION

Our live-cell tracking measurements resulted in an extremely large, multidimensional dataset. To understand the effect of various stimulation conditions on NSC fate in such an experimental landscape, we subjected all experimental outputs to statistical analysis, i.e., Wilcoxon rank-sum test (see Materials and Methods). The effect size (i.e., percentage change in cell numbers and Hes5 and Dcx expression) and adjusted P values associated with each ligand input condition can be visualized using bubble plots (Fig. 3D). Several selected inputs that resulted in high significance or large effect size are annotated in lower tables in Fig. 3D and fig. S8. For example, the condition PACAP-day1 (annotated sequence no. 4) in the leftmost table overall increases cell numbers by
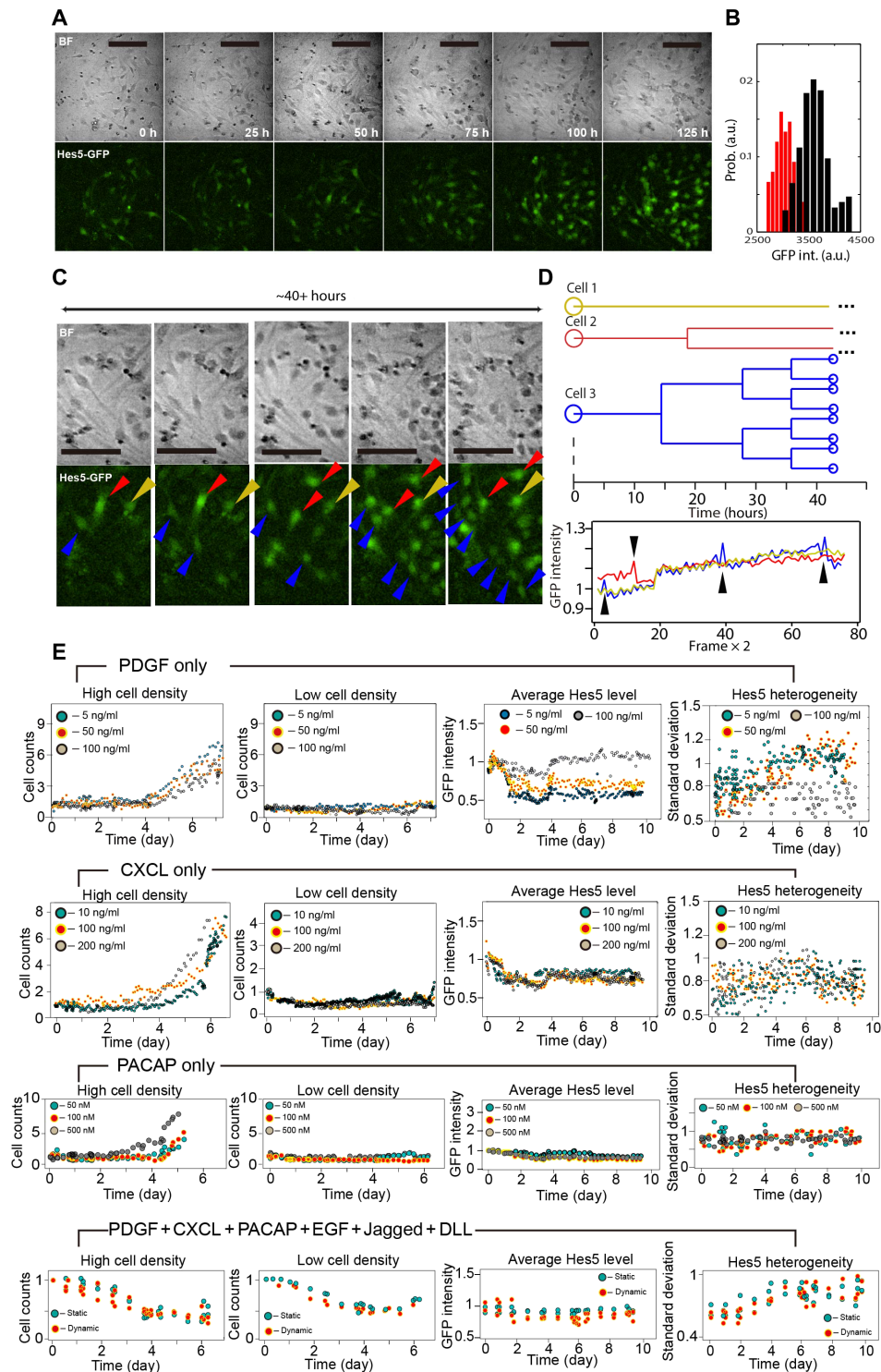
Fig. 2. High-throughput dynamical analysis of NSC differentiation. Millions of single-cell images are generated and automatically analyzed in live-cell signaling factor stimulation measurements, and few example datasets are shown here. (**A**) Time-lapse bright-field (BF) (top) and epifluorescence (bottom) images of NSCs cultured with *PDGF* (100 ng/ml). Scale bars, 100 μm. (**B**) Histogram of *Hes5-GFP* expression in NSCs before (red) and after (black) 1-week culture with *PDGF* (100 ng/ml). High levels of *Hes5* in NSCs indicate maintenance of stem cell state, while reduced *Hes5* indicates progress toward differentiation. (**C**) Enlarged bright-field (top) and corresponding epifluorescence (bottom) images of NSCs shown in (A), cultured on chip with *PDGF* (100 ng/ml). Selected cells were indicated by arrows and individually tracked over 40 hours during on-chip culture. (**D**) Lineage tracing (top) and *Hes5-GFP* expression level (bottom) for the three selected cells in (C). Distinct proliferation patterns were observed despite similar *Hes5-GFP* level. (**E**) We show examples of quantitative analysis of mouse NSC growth and *Hes5* expression in different culture conditions. Each culture contains either a single ligand or a mixture of ligands that are highly expressed in developing mouse brain, including *PDGF*, *CXCL*, *PACAP*, *EGF*, *Jagged*, or *DLL*. *Hes5* expression rate and variability significantly depend on signaling molecules present in culture chambers.
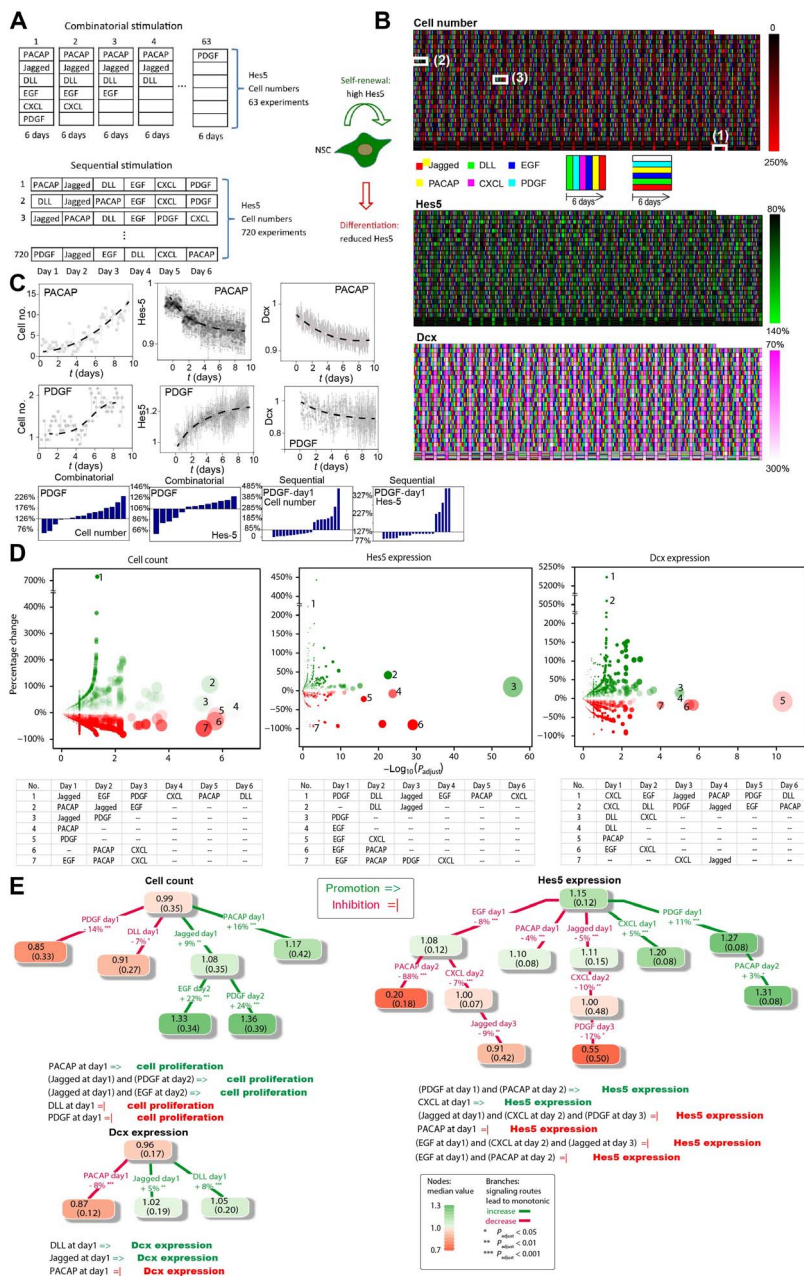
Fig. 3. High-throughput analysis of NSC dynamics reveals signaling logic rules in differentiation. (**A**) NSCs were stimulated in two types of experiments: combinatorial stimulation and sequential stimulation. During combinatorial stimulation, the microfluidic device delivered all possible combinations of *DLL*, *EGF*, *Jagged*, *PACAP*, *CXCL*, and *PDGF* to distinct culture chambers and maintained these conditions for 6 days. During sequential stimulation, the environmental ligands were replaced daily during the 6-day experiments. Cell numbers and single-cell *Hes5-GFP* and *Dcx-RFP* expressions were recorded in each chamber over time. (**B**) Example datasets from one experiment. Signal-induced changes in NSC cell count (top), *Hes5-GFP* expression (middle), and *Dcx* expression (bottom) at day 6 are plotted as heat maps, together with the color-coded bars indicating the combinatorial and sequential signal inputs. The white squares show input conditions with the following ligand combinations and sequences: (1) *DLL + EGF*, (2) *Jagged ≫ CXCL ≫ PDGF ≫ PACAP ≫ EGF ≫ DLL*, and (3) *CXCL ≫ PDGF ≫ PACAP ≫ EGF ≫ DLL ≫ Jagged*. (**C**) Single-cell tracking reveals the dynamic variations in cell numbers and *Hes5* and *Dcx* levels during 6 days of single ligand treatment, with *PACAP* or *PDGF*. The bottom row histograms show results of statistical analyses indicating the influence of *PDGF* on cell growth or *Hes5* level in different experiments that also contain other ligands. Each bar represents a distinct culture experiment. (**D**) Statistical analysis of cell count and *Hes5* and *Dcx* expression using all 720 sequential experiments via Wilcoxon rank-sum test. Y axes show the percentage change of cell numbers and *Hes5* and *Dcx* expression compared to controls (i.e., the effect size) for each ligand input, and the x axes show the corresponding adjusted *P* value. The data are presented with colored bubbles, where the bubble's diameter is proportional to the negative logarithm of adjusted *P* value, and Bubble's color encodes percentage change (green for increase, red for decrease; stronger effect shown in more opaque color). Few selected inputs with high significance or large effect size are annotated with numbers 1 to 7 and are described in lower tables. (**E**) Decision trees are used to visualize the signaling paths toward NSC differentiation or self-maintenance, each of which shows a statistically significant monotonic increase (green paths) or monotonic decrease (red paths) in cell counts and *Hes5* and *Dcx* expression. Each decision tree node includes a median value (color-coded as above) and median absolute deviation (in brackets) of measured values. On the connecting path between nodes, we show the decision attribute to be satisfied for splitting the tree, and the percentage change in cell count and *Hes5* expression or *Dcx* expression (adjusted *P* value indicated by asterisks). Signaling logic rules resulting from the decision trees are listed below. Notations of "=>" and "=|" denote "promote" and "prohibit," respectively.
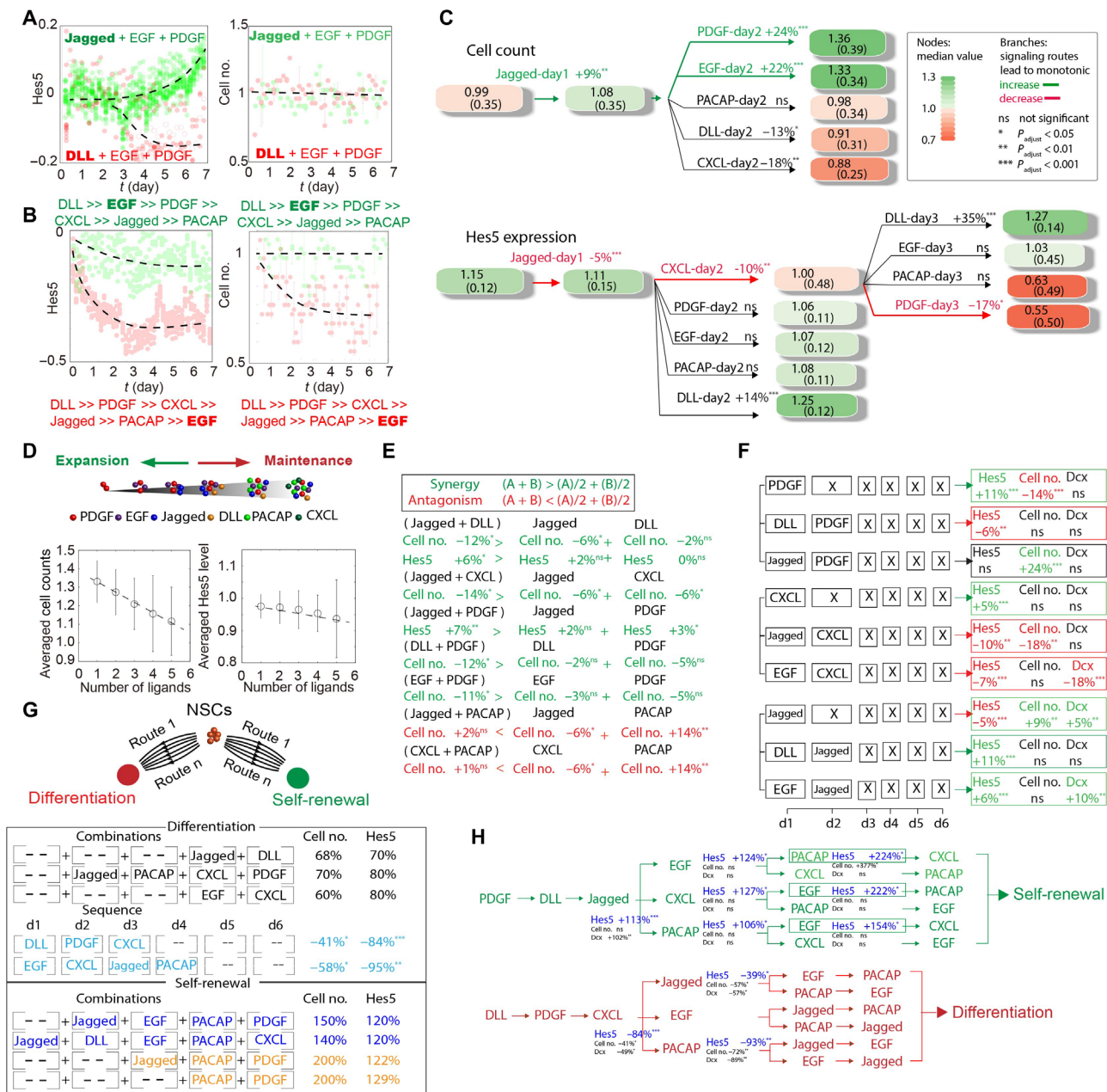
Fig. 4. Statistical analysis of dynamic stimulation experiments uncovers signaling principles in NSC differentiation and self-maintenance. (**A**) Dynamic changes in cell number and *Hes5* level plotted for two ligand combinations containing (*DLL*, *EGF*, *PDGF*) or (*Jagged*, *EGF*, *PDGF*). Dots are single-cell values, and dashed lines indicate population mean. The change in *Hes5* expression can be directed from increase to decrease by only changing one ligand in the combination. (**B**) Comparison of two distinct sequential inputs highlights the importance of input sequence and timing. In both experiments, cells received the same six ligands, but in different orders. Changing the order of a single ligand (e.g., *EGF* from day 2 to day 6) directs NSCs to different cell fate. (**C**) Comparison of optimal and nonoptimal input ligand sequences that lead to monotonic changes in cell counts or *Hes5* expression. Numbers in boxes indicate median value (color-coded) and median absolute deviation (in brackets) of cell count or *Hes5* expression. ns, nonsignificant changes. Optimal paths are highlighted in green (increase) or red (decrease), while the alternatives paths are highlighted in black. (**D**) Increasing number of ligands in a stimulation experiment overall suppresses NSC proliferation, whereas reducing the ligand numbers enhances the stem cell pool. Including more ligands in experiments led to a reduction of the proliferation rate, while the *Hes5* level remained relatively unchanged. Error bars indicate variability of individual experiments from the mean. (**E**) Synergy and antagonism between signaling molecules. The combination of two ligands may lead to enhanced (synergistic) or reduced (antagonistic) effect compared to experiments that use these molecules in isolation. At the top, synergy and antagonism for NSC ligands are defined. Rows at the bottom show actual molecules that are synergistic (green) or antagonistic (red) toward cell proliferation or *Hes5* expression. Measured percent changes from controls are also indicated. (**F**) In sequential stimulation experiments, certain ligands assume context-dependent roles determined by timing of their introduction or the preconditions before use of that ligand. Boxes indicate the identity of ligands used in each day. X in brackets indicate that the exact identity of the ligand in that day does not change the outcome. (**G**) Multiple input conditions lead to similar change in cell numbers and *Hes5* levels, suggesting redundancy in NSC signaling pathways. Example redundant pathways are color-coded. Numbers indicate percent change resulting from stimulation with ligands. (**H**) Cell fate toward differentiation or self-renewal may be decided by certain early signals, indicating early commitment toward self-renewal (*PDGF-day1* ≫ *DLL-day2* ≫ *Jagged-day3*) or differentiation (*DLL-day1* ≫ *PDGF-day2* ≫ *CXCL-day3*) (see table S2 for percentage change and *P* values associated with each condition).

16% (adjusted $P = 4.21 \times 10^{-7}$). This result is achieved by our statistical test that analyzed all experiments that included the *PACAP* in day 1 of the stimulation protocol. Complete test results can be seen in table S2. Furthermore, we used multibranch decision trees to highlight the optimal signaling routes leading to a statistically significant monotonic increase/decrease in the measured cellular parameters (false discovery rate, 0.05). This led us to discover several nontrivial "cellular logic rules" describing the effect of various ligands on cell fate (Fig. 3E). For example, the condition *Jagged-day1* increases cell numbers overall by 9% (adjusted $P = 6.58 \times 10^{-3}$), giving rise to a subgroup of experiments in which the median of normalized cell count is 1.08 (median absolute deviation, 0.35). If *EGF* is added on the following day, the median value increases to 1.33 (absolute deviation, 0.34; adjusted $P = 5.37 \times 10^{-4}$).

We further evaluated the results of our statistical analyses to understand the role of signaling molecules on NSC fate and uncovered several "signaling principles" that highlighted the importance of environmental context and signal timing in NSC differentiation and self-maintenance (Fig. 4 and fig. S7, F to H).

First, dynamic single-cell tracking in combinatorial experiments shows that *Hes5* expression can be directed from increase to decrease by only changing one ligand in the ligand combination (i.e., changing *Jagged* to *DLL*, in Fig. 4A). In sequential experiments where ligands were replaced on a daily basis, changing the temporal order of a single ligand can direct NSCs to different cell fates despite the fact that cells were overall exposed to the same set of ligands through the course of 6 days. For instance, delivering *EGF* on day 2 resulted in relatively higher *Hes5* expression levels and unchanged cell numbers, indicating maintenance of the stem cell pool, whereas moving *EGF* to day 6 led to a significant reduction in *Hes5* expression and cell number, indicative of differentiation (Fig. 4B).

Decision tree analysis found certain optimal routes for signal input sequences to achieve different outcomes. For example, one optimal route leading to NSC proliferation is *Jagged-day1* ≫ *EGF* (or *PDGF*)-*day2*, increasing cell numbers by 9% (adjusted $P = 6.58 \times 10^{-3}$) in day 1 and by 24% in day 2 (adjusted $P = 7.26 \times 10^{-4}$). Any deviation from these routes (i.e., altering the applied ligands) is nonoptimal, resulting in either a decrease or no significant change of cell numbers. An example for *Hes5* expression is the optimal route that reduces its expression by 17% by day 3 (adjusted $P = 2.57 \times 10^{-2}$) (Fig. 4C).

In addition, we found that increasing environmental complexity (i.e., increasing the number of ligands used in cultures) generally suppressed NSC proliferation; however, reducing the input complexity enhanced the stem cell pool. As Fig. 4D shows, including more ligands either in combination or sequentially led to an overall reduction of the proliferation rate compared to controls, while the *Hes5* expression levels remained relatively unchanged.

We found that the combination of two ligands may induce enhanced (synergistic) or reduced (antagonistic) effects compared to experiments that use these ligands in isolation. Examples of these synergy and antagonism between ligands are shown in Fig. 4E. For instance, *Jagged* and *DLL* are synergistic toward reducing NSC numbers: The reduction of cell numbers under combined *Jagged* + *DLL* stimulation (−12%, adjusted $P = 4.53 \times 10^{-2}$) is larger at absolute scale than the sum of reductions under individual stimulation with either molecule (−6%; adjusted $P = 4.40 \times 10^{-2}$; nonsignificant, −2%). Other examples are also shown in Fig. 4E. On the other hand, *Jagged* and *PACAP* are antagonistic pairs in affecting cell proliferation, because combined stimulation with these molecules leads to a lesser reduction in cell numbers

compared to the changes brought by their individual application (−6% for *Jagged*, adjusted $P = 4.40 \times 10^{-2}$; +14% for *PACAP*, adjusted $P = 1.52 \times 10^{-3}$).

Figure 4F shows the context-dependent role of several individual ligands, which is determined by the timing of its introduction or by the preconditions before the use of that ligand. For example, although *PDGF* on day 1 predominantly increases *Hes5* expression by 11% (adjusted $P = 2.94 \times 10^{-56}$), using *DLL* before *PDGF* can revert this change to a 6% reduction (adjusted $P = 4.44 \times 10^{-3}$). If *Jagged* is applied before *PDGF*, the change of *Hes5* expression is nonsignificant, although cell numbers increase. These context-dependent roles can be found in *CXCL* and *Jagged* (lower rows in Fig. 4F).

Another principle emerging from our analysis is the redundancy in NSC signaling pathways, reflecting the intrinsic flexibility of stem cells to respond to their dynamic environment and niche at the early times we measured. Figure 4G shows several examples of signaling routes leading to similar quantitative changes and cell fates. For example, the combinatorial inputs *Jagged* + *DLL* and *Jagged* + *PACAP* + *CXCL* + *PDGF* lead to very similar increases in cell numbers and *Hes5* expression. Similarly, the sequential inputs *DLL-day1* ≫ *PDGF-day2* ≫ *CXCL-day3* and *EGF-day1* ≫ *CXXL-day2* ≫ *Jagged-Day3* ≫ *PACAP-day4* lead to similar reduction in cell numbers and *Hes5* expression. Similar redundant pathways are seen for both differentiation and self-renewal directions.

Last, our analyses show signs of early cellular commitment. Cells at certain early decision points can commit toward differentiation or self-renewal directions and tend to ignore subsequent signals they received. Figure 4H shows two examples: After cells received *PDGF-day1* ≫ *DLL-day2* ≫ *Jagged-day3* in a row, signals that come after do not reverse the increase in cell numbers or *Hes5* level, indicating self-renewal of stem cells. On the other hand, ligand sequence *DLL-day1* ≫ *PDGF-day2* ≫ *CXCL-day3* initiates a strong decrease of cell number and *Hes5* expression, regardless of many other signals that come after this sequence.

In this study, we presented an ultra-multiplexed microfluidic technology with unprecedented capabilities for high-throughput live-cell analysis under complex and dynamic signals. In record-breaking fashion, our microfluidic system mapped the signaling landscape of NSC differentiation in 3000 distinct microenvironments that mimic the dynamical stem cell niche. By statistical analysis and modeling of thousands of live-cell experiments, we identified cellular decision points and differentiation trajectories. Our microfluidic system greatly shortens the time span and improves the reproducibility of high-throughput screening processes with live cells. This technology allows the analysis of unprecedented combinatorial complexity, which may have relevance for the dynamic and regulated microenvironment of the tissue during homeostasis and regeneration.

MATERIALS AND METHODS
Design and fabrication of microfluidic chips
We designed and fabricated the microfluidic device according to the standard protocol, which is reported elsewhere (*2*). Briefly, we designed our two-layer device using AutoCAD (Autodesk Inc., San Rafael, CA, USA) and then printed the sketch on transparencies at 40-kdpi resolution (Fine Line Imaging, MN, USA). Molds for polydimethylsiloxane (PDMS) casting were produced using standard soft lithography. The channel network of the control layer, as well as the flow channels for the flow layer and culture chambers, was produced with either SU-8

3025 or SU-8 3075 (MicroChem, Westborough, MA, USA) on silicon wafers. For the flow layer, we additionally used AZ-50X (AZ Electronic Materials, Luxembourg) at valve positions. Photoresists were spun to a height of 25 μm for channels and 150 μm for culture chambers. To fabricate the chip, 72 g of PDMS (10:1 of monomer/catalyst ratio) was mixed, debubbled, and poured over the trimethylchlorosilane-treated patterned silicon wafer. The PDMS was then cured for 60 min at 80°C. Following plasma and alignment between flow and control layer, inlet holes were then punched after 2-hour thermal bonding. The chip was bonded to a PDMS-coated coverslip and cured for at least 12 hours at 80°C before use.

Chip setup, operation, and control
The glass slide carrying the microfluidic chip was cleaned and taped on a slide holder. Control channels were connected to miniature pneumatic solenoid valves (Festo, Switzerland) that were controlled with a custom MATLAB (MathWorks, USA) through graphical user interface (2). Optimal closing pressures of push-up PDMS membrane valves were determined individually for each chip, typically ranging from 25 to 30 psi. The cell culture chambers were treated with either fibronectin (0.25 mg/ml; Millipore, Austria) for 3T3 cell culture or polylysine (0.01%, Sigma-Aldrich) followed by laminin (1 to 2 mg/ml, Sigma-Aldrich) for adherent NSC culture. The remaining coating solution was flushed off from the chip using either phosphate-buffered saline or cell culture medium. Cell culture medium was prewarmed on chip for at least 1 hour before cell loading.

Cell culture and loading
For standard cell lines, we used Jurkat cells, RAW 264.7 macrophages p65$^{-/-}$ with p65-GFP and H2B-dsRed, as well as NIH 3T3 p65$^{-/-}$ cells with p65-dsRed and H2B-GFP for tracking and analysis of NF-κB activation. These cells were cultured according to the established protocols (31). To seed cells into the chip, adherent cells were harvested at 80% confluence with trypsin, resuspended, and loaded into chips through semiautomated loading program at cell densities from 10^4 to 10^6/ml depending on the desired cell density.

Murine HSCs were isolated with a FACSAria III flow cytometer (BD Biosciences) as Lin$^-$/c-Kit$^+$/Sca-1$^+$/CD48$^-$/CD150$^+$/CD34$^-$ [lineage (Lin): CD3e/CD11b/CD19/CD41/B220/Gr-1/Ter^{119}], which are approximately 50% pure HSCs. Macrophage colony-stimulating factor (M-CSF), a myeloid cytokine released during infection and inflammation, was used to induce HSC differentiation. Human CD34$^+$ cells were isolated from mononuclear cells using the EasySep Human CD34 Positive Selection Kit (STEMCELL Technologies, Vancouver, BC, Canada). CD34$^+$CD38$^-$CD45RA$^-$CD90$^+$CD49f$^+$ HSCs were sorted using a FACSAria III flow cytometer (BD Biosciences). Pro- and anti-inflammatory cytokines, including TNF, IFNγ, IL-6, IP10, and MCP-1, were introduced into the cellular environment as single ligand and in combination. Embryonic NSCs with Hes5-GFP and Dcx-RFP reporters were isolated at embryonic day 13.5 from a transgenic mouse carrying Hes5-GFP and Dcx-RFP using established protocol (14, 17, 18). The resulting primary cells were verified to carry both Hes5-GFP and Dcx-RFP after isolation and allowed to grow for few passages before use in the experiments (19). NSCs were cultured as neurospheres in culture media [Dulbecco's Modified Eagle medium/Nutrient Mixture F-12 + GlutaMAX (Gibco, no. 31331-028); penicillin (10 U/ml); streptomycin (10 μg/ml); B-27 supplement (1:50); and fibroblast growth factor (0.02 μg/ml)]. As NSCs are sensitive to environmental variations, cell handling protocol before loading into the chip was examined systematically (including dis-

sociation conditions and fluorescence-activated cell sorting). To obtain the optimal results, NSC spheres were collected and loaded into the chip 24 hours after fresh dissociation, where each sphere contains ~7 to 10 cells. To avoid potential artifacts due to prolonged in vitro culture, only NSCs within 10 passages were used in the study. In control experiments, transferring chip-cultured NSCs to a well plate showed the sphere-forming ability of Hes5-positive cells, validating Hes5 as a self-maintenance marker in our experiments (fig. S6, H and I) (12).

The environmental conditions were maintained using temperature control and incubator system (Live Cell Imaging Service GmbH, Basel, Switzerland) to strictly 37°C and >98% humidity and 5% CO$_2$ during the experiment, and the PDMS chip was covered with a stage top incubator connected to a humidifier and a gas exchanger.

Live-cell fluorescence microscopy and data analysis
For image acquisition, a Nikon Ti-ECLIPSE microscope with an automated translational stage and a digital complementary metal-oxide semiconductor (CMOS) camera (ORCA-Flash4.0, Hamamatsu, Japan) was used. The stage and image acquisition was controlled via the NIS-Elements software (Nikon, Japan). Bright-field and fluorescence images were acquired and analyzed using a customized MATLAB program. The algorithm extracts single-cell traces including position, nuclear, and cytoplasm fluorescence level. For example, the 3T3 cell nuclear area in each image was identified via the fluorescent nuclear marker H2B-GFP, and then the mean value of the nuclear intensity of the p65-DsRed marker was measured and plotted as a function of time.

Wilcoxon rank-sum test and multiple-test correction
Experiments of sequential and combinatorial ligand additions consisted of 720 and 56 different conditions, respectively. Experiments for each individual treatment condition were repeated for three times. All datasets generated in this way were subjected to the statistical test described as follows. Denote a sequential condition as S_{ij} = {ligand i is added on day j} and a combinatorial condition as C_i = {ligand i is present}, where ligand i = Jagged, DLL, EGF, PACAP, CXCL, PDGF and j = 1, 2, 3, 4, 5, 6. We were interested in investigating the ligands' conditional effects by applying multiple treatments in specific order one after another, $S_{i_m,m}|S_{i_1,1}, S_{i_2,2}, \cdots, S_{i_m,m-1}$ for sequential inputs (starting from day 1), and $C_n|C_i, \cdots, C_k$ for combinatorial inputs. The controls are their negated counterparts $\bar{S}_{i_m,m}|S_{i_1,1}, S_{i_2,2}, \cdots, S_{i_m,m-1}$ or $\overline{C_n}|C_i, \cdots, C_k$. We used the Wilcoxon rank-sum approach to examine whether the distributions of cell counts, Hes5 expression values, or Dcx expression values between these treatment/control comparisons are significantly different. No assumption about normality of the underlying distribution was used (32–34). The detailed steps for both sets of tests are as follows:

1. Pick a ligand condition for investigation and split measured group **U** accordingly into two subgroups: subgroup **A** that satisfies the condition and subgroup $\overline{\textbf{A}}$ that does not.

2. Test whether the distributions of cell counts, Hes5 expression, or Dcx expression in these two subgroups are significantly different. The difference can be quantified by the median of the distribution of individual differences between randomly selected samples from subgroups **A** and $\overline{\textbf{A}}$. The effect size is defined as percentage change, i.e., $\frac{\text{median}(a_i - u_j)}{\text{median}(u_j)} \times 100\%$, where $a_i \in \textbf{A}$, $u_j \in \textbf{U}$ [all medians were computed using Hodge-Lehmann estimator (35)].

3. Repeat steps 1 and 2 for all investigated sample treatment sequences. Here, we controlled the false discovery rate and adjust P values of all tests using Benjamini-Hochberg procedure (36, 37).

SUPPLEMENTARY MATERIALS

Supplementary material for this article is available at http://advances.sciencemag.org/cgi/content/full/5/4/eaav7959/DC1

REFERENCES AND NOTES

1. M. Hemberger, W. Dean, W. Reik, Epigenetic dynamics of stem cells and cell lineage commitment: Digging Waddington's canal. *Nat. Rev. Mol. Cell Biol.* **10**, 526–537 (2009).
2. M. A. Unger, H.-P. Chou, T. Thorsen, A. Scherer, S. R. Quake, Monolithic microfabricated valves and pumps by multilayer soft lithography. *Science* **288**, 113–116 (2000).
3. L. J. Millet, M. U. Gillette, New perspectives on neuronal development via microfluidic environments. *Trends Neurosci.* **35**, 752–761 (2012).
4. V. Lecault, M. VanInsberghe, S. Sekulovic, D. J. H. F. Knapp, S. Wohrer, W. Bowden, F. Viel, T. McLaughlin, A. Jarandehei, M. Miller, D. Falconnet, A. K. White, D. G. Kent, M. R. Copley, F. Taghipour, C. J. Eaves, R. Keith Humphries, J. M. Piret, C. L. Hansen, High-throughput analysis of single hematopoietic stem cell proliferation in microfluidic cell culture arrays. *Nat. Methods* **8**, 581–586 (2011).
5. E. K. Sackmann, A. L. Fulton, D. J. Beebe, The present and future role of microfluidics in biomedical research. *Nature* **507**, 181–189 (2014).
6. J. W. Jeong, J. G. McCall, G. Shin, Y. Zhang, R. Al-Hasani, M. Kim, S. Li, J. Yong Sim, K.-I. Jang, Y. Shi, D. Y. Hong, Y. Liu, G. P. Schmitz, L. Xia, Z. He, P. Gamble, W. Z. Ray, Y. Huang, M. R. Bruchas, J. A. Rogers, Wireless optofluidic systems for programmable in vivo pharmacology and optogenetics. *Cell* **162**, 662–674 (2015).
7. R. Gómez-Sjöberg, A. A. Leyrat, D. M. Pirone, C. S. Chen, S. R. Quake, Versatile, fully automated, microfluidic cell culture system. *Anal. Chem.* **79**, 8557–8563 (2007).
8. M. Mehling, S. Tay, Microfluidic cell culture. *Curr. Opin. Biotechnol.* **25**, 95–102 (2014).
9. L. J. Millet, M. E. Stewart, J. V. Sweedler, R. G. Nuzzo, M. U. Gillette, Microfluidic devices for culturing primary mammalian neurons at low densities. *Lab Chip* **7**, 987–994 (2007).
10. S. Wu, R. O'Lexy, M. Xu, Y. Sang, X. Chen, Q. Yu, K. L. Gallagher, Symplastic signaling instructs cell division, cell expansion, and cell polarity in the ground tissue of *Arabidopsis thaliana* roots. *Proc. Natl. Acad. Sci. U.S.A.* **113**, 11621–11626 (2016).
11. G. G. Giobbe, F. Michielin, C. Luni, S. Giulitti, S. Martewicz, S. Dupont, A. Floreani, N. Elvassore, Functional differentiation of human pluripotent stem cells on a chip. *Nat. Methods* **12**, 637–640 (2015).
12. O. Basak, V. Taylor, Identification of self-replicating multipotent progenitors in the embryonic nervous system by high Notch activity and *Hes5* expression. *Eur. J. Neurosci.* **25**, 1006–1022 (2007).
13. O. Basak, C. Giachino, E. Fiorini, H. R. MacDonald, V. Taylor, Neurogenic subventricular zone stem/progenitor cells are notch1-dependent in their active but not quiescent state. *J. Neurosci.* **32**, 5654–5666 (2012).
14. C. Giachino, O. Basak, V. Taylor, Isolation and manipulation of mammalian neural stem cells in vitro. *Methods Mol. Biol.* **482**, 143–158 (2009).
15. R. A. Kellogg, S. Tay, Noise facilitates transcriptional control under dynamic inputs. *Cell* **160**, 381–392 (2015).
16. S. Lugert, O. Basak, P. Knuckles, U. Haussler, K. Fabel, M. Götz, C. A. Haas, G. Kempermann, V. Taylor, C. Giachino, Quiescent and active hippocampal neural stem cells with distinct morphologies respond selectively to physiological and pathological stimuli and aging. *Cell Stem Cell* **6**, 445–456 (2010).
17. E. Sykova, S. Forostyak, Stem cells in regenerative medicine. *Laser Ther.* **22**, 87–92 (2013).
18. J. Behnan, Z. Grieg, M. Joel, I. Ramsness, B. Stangeland, Neuroepigenetics Gene knockdown of CENPA reduces sphere forming ability and stemness of glioblastoma initiating cells. *Neuroepigenetics* **7**, 6–18 (2016).
19. S. Couillard-Despres, B. Winner, C. Karl, G. Lindemann, P. Schmid, R. Aigner, J. Laemke, U. Bogdahn, J. Winkler, J. Bischofberger, L. Aigner, Targeted transgene expression in neuronal precursors: Watching young neurons in the old brain. *Eur. J. Neurosci.* **24**, 1535–1545 (2006).
20. Allen Institute for Brain Science, *Allen Brain Atlas* (Allen Institute for Brain Science, 2017).
21. O. Basak, J. Beumer, K. Wiebrands, H. Seno, A. van Oudenaarden, H. Clevers, Induced quiescence of Lgr5+ stem cells in intestinal organoids enables differentiation of hormone-producing enteroendocrine cells. *Cell Stem Cell* **20**, 177–190.e4 (2017).
22. S. Lugert, M. Vogt, J. S. Tchorz, M. Müller, C. Giachino, V. Taylor, Homeostatic neurogenesis in the adult hippocampus does not involve amplification of Ascl1^high intermediate progenitors. *Nat. Commun.* **3**, 670 (2012).
23. O. Ehm, C. Göritz, M. Covic, I. Schäffner, T. J. Schwarz, E. Karaca, B. Kempkes, E. Kremmer, F. W. Pfrieger, L. Espinosa, A. Bigas, C. Giachino, V. Taylor, J. Frisén, D. Chichung Lie, RBPJκ-dependent signaling is essential for long-term maintenance of neural stem cells in the adult hippocampus. *J. Neurosci.* **30**, 13794–13807 (2010).
24. C. Giachino, O. Basak, S. Lugert, P. Knuckles, K. Obernier, R. Fiorelli, S. Frank, O. Raineteau, A. Alvarez-Buylla, V. Taylor, Molecular diversity subdivides the adult forebrain neural stem cell population. *Stem Cells* **32**, 70–84 (2014).
25. H. Mori, K. Ninomiya, M. Kino-oka, T. Shofuda, M. Omedul Islam, M. Yamasaki, H. Okano, M. Taya, Y. Kanemura, Effect of neurosphere size on the growth rate of human neural stem/progenitor cells. *J. Neurosci.* **84**, 1682–1691 (2006).
26. E. Pastrana, V. Silva-Vargas, F. Doetsch, Eyes wide open: A critical review of sphere-formation as an assay for stem cells. *Cell Stem Cell* **8**, 486–498 (2011).
27. P. R. Mangan, L. E. Harrington, D. B. O'Quinn, W. S. Helms, D. C. Bullard, C. O. Elson, R. D. Hatton, S. M. Wahl, T. R. Schoeb, C. T. Weaver, Transforming growth factor-ß induces development of the T_H17 lineage. *Nature* **441**, 231–234 (2006).
28. E. Bettelli, Y. Carrier, W. Gao, T. Korn, T. B. Strom, M. Oukka, H. L. Weiner, V. K. Kuchroo, Reciprocal developmental pathways for the generation of pathogenic effector T_H17 and regulatory T cells. *Nature* **441**, 235–238 (2006).
29. G. V. Flores, H. Duan, H. Yan, R. Nagaraj, W. Fu, Y. Zou, M. Noll, U. Banerjee, Combinatorial signaling in the specification of unique cell fates. *Cell* **103**, 75–85 (2000).
30. N. Urbán, F. Guillemot, Neurogenesis in the embryonic and adult brain: Same regulators, different roles. *Front. Cell. Neurosci.* **8**, 396 (2014).
31. S. Tay, J. J. Hughey, T. K. Lee, T. Lipniacki, S. R. Quake, M. W. Covert, Single-cell NF-κB dynamics reveal digital activation and analogue information processing. *Nature* **466**, 267–271 (2010).
32. M. Hollander, D. A. Wolfe, Nonparametric statistical methods, in *Wiley Series in Probability and Mathematical Statistics* (Wiley, 1973).
33. H. B. Mann, D. R. Whitney, On a test of whether one of 2 random variables is stochastically larger than the other. *Ann. Math. Stat.* **18**, 50–60 (1947).
34. F. Wilcoxon, Individual comparisons by ranking methods. *Biometrics Bull.* **1**, 80–83 (1945).
35. E. L. Lehmann, H. J. M. D'Abrera, *Nonparametrics: Statistical Methods Based on Ranks* (Springer, ed. 1, 2006).
36. Y. Benjamini, Y. Hochberg, Controlling the false discovery rate—A practical and powerful approach to multiple testing. *J. R. Stat. Soc. Ser. B* **57**, 289–300 (1995).
37. Y. Benjamini, D. Yekutieli, The control of the false discovery rate in multiple testing under dependency. *Ann. Stat.* **29**, 1165–1188 (2001).

Citation: C. Zhang, H.-L. Tu, G. Jia, T. Mukhtar, V. Taylor, A. Rzhetsky, S. Tay, Ultra-multiplexed analysis of single-cell dynamics reveals logic rules in differentiation. *Sci. Adv.* **5**, eaav7959 (2019).

Science Advances

Ultra-multiplexed analysis of single-cell dynamics reveals logic rules in differentiation

Ce Zhang, Hsiung-Lin Tu, Gengjie Jia, Tanzila Mukhtar, Verdon Taylor, Andrey Rzhetsky and Savas Tay

ARTICLE TOOLS	http://advances.sciencemag.org/content/5/4/eaav7959
SUPPLEMENTARY MATERIALS	http://advances.sciencemag.org/content/suppl/2019/04/01/5.4.eaav7959.DC1
REFERENCES	This article cites 34 articles, 4 of which you can access for free http://advances.sciencemag.org/content/5/4/eaav7959#BIBL
PERMISSIONS	http://www.sciencemag.org/help/reprints-and-permissions

Use of this article is subject to the Terms of Service

Contributions to the Projects

1) I performed all the experiments for Hippo signalling project, analyzed the data, compiled the figures and wrote the manuscript.

2) For the main NeuroStemX resource, all the samples for NSCs, BPs and NBNs populations that were sequenced and analyzed were generated by me.

3) For the main NeuroStemX resource, all the samples for NSCs, BPs and NBNs for Single cell sequencing were generated by me (both C1 and 10X genomics).

4) Experimental validation of RNA-sequencing data and signature genes, done by qPCR done by me and Katja Eschbach, Group Beisel.

5) Figures for the main paper compiled by me, along with other members of the NeuroStemX consortium.

6) Contributed to Dr. Marcelo Boareto's project to understand the role of Jagged1 in neurogenesis. Performed experimental validation for the same.

7) Contributed to Dr. Ce Zhang's project 'Ultra-Multiplexed Analysis of Single Cell Dynamics' and did the biological validation *in vivo*, generated neurospheres from *Hes5::GFP* and *Hes5::GFP; Dcx::dsRed*. Performed qPCR for receptors to test the expression in NSCs, before they could start their experiments.

8) Actively discussed the data and analyses with other members of the NeuroStemX consortium.
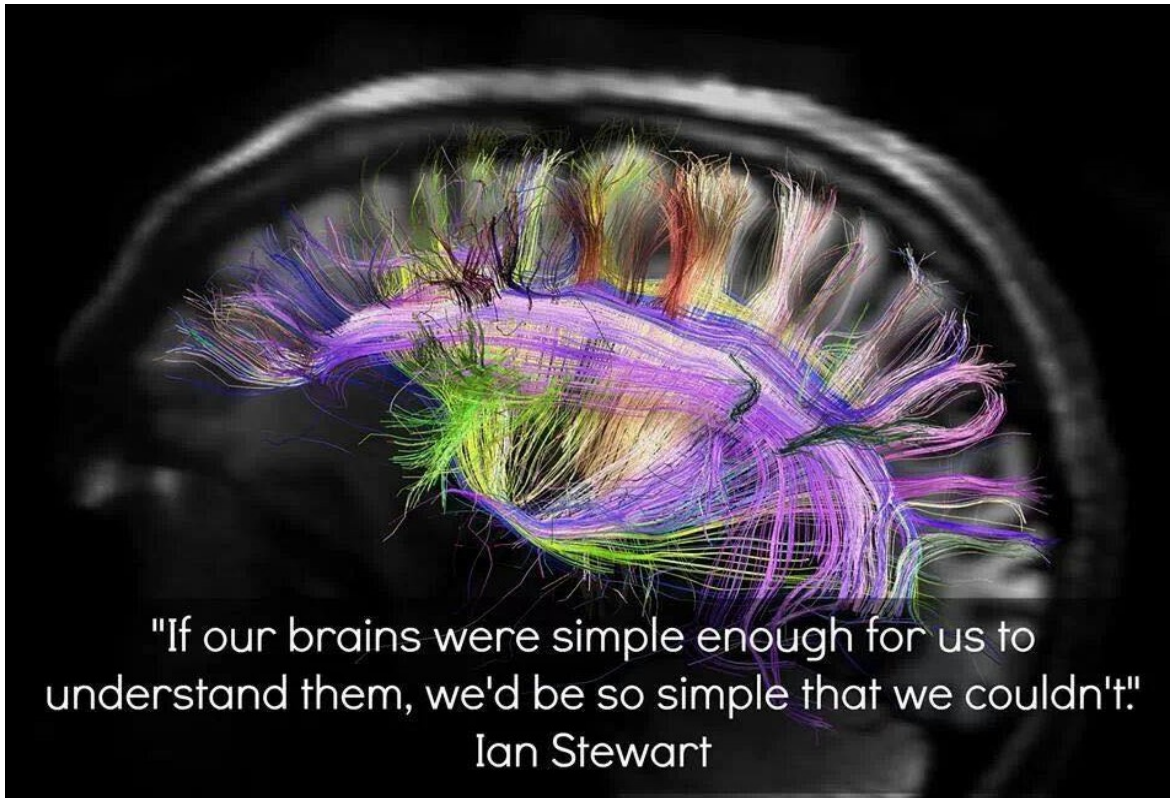
"If our brains were simple enough for us to understand them, we'd be so simple that we couldn't."
Ian Stewart